

ORGANOID TECHNOLOGY AS AN EMERGING TOOL FOR GYNECOLOGICAL ONCOLOGY RESEARCH



Kadi Lõhmussaar

**ORGANOID TECHNOLOGY AS AN EMERGING TOOL FOR
GYNECOLOGICAL ONCOLOGY RESEARCH**

Dawn of precision medicine in cancer research

Kadi Lõhmussaar

ISBN: 978-94-93197-33-6

Author: Kadi Lõhmusaar

Cover: Kristi Luht

Layout and printing by: Off Page, Amsterdam

The research described in this thesis was performed at the Hubrecht Institute, Utrecht, The Netherlands in the lab of Prof. Dr. Hans Clevers.

© All rights reserved. No part of this thesis may be reproduced, stored or transmitted in any form by any means without prior permission of the author. The copyright of the publication remains with the publishers.

**ORGANOID TECHNOLOGY AS AN EMERGING TOOL FOR
GYNECOLOGICAL ONCOLOGY RESEARCH**

Dawn of precision medicine in cancer research

**ORGANOÏDEN ALS EEN NIEUW MODEL VOOR
GYNAECOLOGISCHE ONCOLOGISCH ONDERZOEK**

Dageraad van precisiegeneeskunde in kankeronderzoek

(met een samenvatting in het Nederlands)

Proefschrift

ter verkrijging van de graad van doctor aan de
Universiteit Utrecht
op gezag van de
rector magnificus, prof.dr. H.R.B.M. Kummeling,
ingevolge het besluit van het college voor promoties
in het openbaar te verdedigen op

dinsdag 17 november 2020 des ochtends te 9.15 uur

door

Kadi Lõhmussaar

geboren op 30 juni 1991
te Pärnu, Estland

PROMOTOR

Prof. dr. J.C. Clevers

TABLE OF CONTENTS

Scope of the thesis	7	
Chapter 1	Human-derived model systems in gynecological cancer research	13
Chapter 2	Assessing the origin of high-grade serous ovarian cancer using CRISPR-modification of mouse organoids	37
Chapter 3	An organoid platform for ovarian cancer captures intra- and interpatient heterogeneity	77
Chapter 4	Patient-derived organoids as a novel tool to study cervical cancer	121
Chapter 5	Summarizing discussion	161
Addendum	English summary	173
	Nederlandse samenvatting	177
	Eestikeelne kokkuvõte	180
	List of publications	183
	Acknowledgements	185
	Curriculum Vitae	208

SCOPE OF THE THESIS



SCOPE OF THE THESIS

Organoid technology is an emerging new model system that enables to closely capture and study the physiology and properties of the epithelial tissues “in a dish”. The model relies on the presence of stem cell pools within the tissue of interest and their intrinsic patterning capacity. Under defined niche factors and support from extracellular membrane-like scaffolds, these cells are able to self-organize into three-dimensional structures that closely resemble the architecture and properties of source tissue, creating unparalleled opportunities. Since the invention in intestine, organoid technology has been applied to many additional epithelial tissues, helping to gain valuable insight into their biology both in homeostatic and diseased conditions. More recently, the model has also been adapted to study the female reproductive tract (FRT) and associated disorders. In this thesis we describe the establishment and characterization of a broad panel of 3D organoid cultures from a variety of epithelial gynecological cancers and respective healthy tissues of origin with the purpose to better understand the heterogeneity and the individual characteristics of these tumors.

Gynecological cancers can arise from distinct regions of FRT giving rise to a heterogeneous set of malignancies with distinct clinicopathological characteristics. In order to advance the knowledge and management of these cancers, researchers often rely on different *in vitro* and *in vivo* experimental models. **Chapter 1** reviews the currently available patient-derived model systems to study gynecological cancers, including xenografts, cell lines and more advanced 3D organotypic models. Particular focus is given to the newly emerging organoid systems that have revolutionized our cancer research toolboxes.

In regards to cancer initiation studies, the exact cell type of origin is often a key to accurately model the disease. In the case of the most aggressive form of ovarian cancer – high-grade serous ovarian cancer – the identity of the originating cell has not been conclusively resolved.

Chapter 2 introduces a murine organoid-based approach combined with state-of-the-art CRISPR-Cas9 genome editing tool to investigate the origin of this disease from the two of the suspected tissues of origin in parallel, i.e. either oviduct (equivalent to human fallopian tube) or ovarian surface epithelium. The intersection of these technologies illustrates how genome editing can take organoid research to the next level.

Over time, researchers have started to acknowledge that cancer biology is often more complex than a simplistic pathway scheme and relies heavily on inter- and intra-patient molecular heterogeneity, ideally requiring personalized management to tailor care for each individual patient. The innovation of organoid technology has opened a new promising direction in preclinical studies, allowing to create customized models for individual disease and allow personalized drug screenings. In **chapters 3 and 4** we describe novel protocols that allow establishment of organoid cultures from the main types of ovarian and cervical cancer (and from the healthy source tissue), respectively. The resulting organoid lines closely recapitulate the histology and molecular properties of

the healthy tissues and the tumors of which they were derived, and the platforms offer a great promise in validating personalized therapeutic approaches.

Chapter 5 summarizes all the previous chapters of the thesis and discusses these in light of current literature. We highlight implications and future perspectives of the organoid technology in the field of gynecological oncology.



CHAPTER

1

HUMAN-DERIVED MODEL SYSTEMS IN GYNECOLOGICAL CANCER RESEARCH

Kadi Löhmußaar^{1,2}, Matteo Boretto^{1,2}, Hans Clevers^{1,2}

¹Hubrecht Institute, Royal Netherlands Academy of Art and
Sciences and University Medical Center Utrecht,
Uppsalalaan 8, 3584CM Utrecht, the Netherlands

²Cancer Genomics Netherlands, OncoCode Institute,
3584CG Utrecht, the Netherlands

ABSTRACT

The human female reproductive tract (FRT) is a complex system that combines series of organs, including ovaries, fallopian tubes, uterus, cervix, vagina, and vulva; each of which possesses unique cellular characteristics and functions. This versatility, in turn, allows for the development of a wide range of epithelial gynecological cancers with distinct features. Thus, reliable model systems are required to better understand the diverse mechanisms involved in the regional pathogenesis of the reproductive tract and improve treatment strategies. Here, we review the current human-derived model systems available to study the multitude of gynecological cancers, including ovarian, endometrial, cervical, vaginal, and vulvar cancer, and the recent advances in the push towards personalized therapy.

HIGHLIGHTS

Tumors of the FRT represent a major gynecological burden, with high-grade serous ovarian cancer incurring the highest mortality rate.

Recent advances in sequencing technology and data mining have started to uncover the complex heterogeneity of gynecological cancers, reshaping our modeling approach.

Clinical management and overall 5-year survival rate have not substantially improved, due to decades of unsatisfactory models.

Tumor-derived organoids have emerged as an optimal compromise between *in vitro* and *in vivo* models, maintaining the flexibility of the former while capturing the complexity of the latter.

INTRODUCTION

During human embryogenesis, the FRT arises from a common precursor, coelomic epithelium (also known as mesothelium)¹. Despite the mutual origin, the adult FRT displays regional specification with distinct lineage-committed somatic **stem cells** (see Glossary) that self-renew the organ throughout life². The proper functioning of each organ is required to ensure the overall reproductive capacity of the FRT; exemplified by the collective phase-dependent changes of the menstrual cycle^{3,4}. This reflects the vast plasticity and proliferation capacity of the FRT. Consequential to such a continuous remodeling is the propagation of mutations in cells, which may lead to the development of cancers of the reproductive tract later in life. Indeed, the majority of gynecological cancers are commonly diagnosed in postmenopausal and elderly women⁵. In fact, imbalance in the levels of the primary female sex hormone, estrogen, and its receptors is associated with the etiology of many diseases, including but not limited to the cancers of reproductive organs, wherein estrogen influences cancer initiation and progression^{6,7}. Dependent on the exact location of origin, the FRT epithelium can give rise to a plethora of different cancer types with distinct genomic landscapes; most frequently to ovarian, endometrial, and cervical, but also, to a lesser extent, vaginal and vulvar cancers (Figure 1). To study different epithelial gynecological cancers, transgenic mice have historically provided the opportunity to probe the effect of genetic hits on oncogenes and tumor suppressor genes towards cancer development in a near physiological environment⁸. However, in our pursuit of a representative model, we have to consider fundamental species-specific differences in the FRT, which raise questions about the extent of reliability that animal models can offer. For instance, female mice fail to spontaneously develop relevant gynecological tumors often observed in women with lack of intra-**tumor heterogeneity** and superior aggressiveness. To overcome such differences, alternative human-relevant models have been developed (Figure 2, Key Figure).

IMMORTALIZED CELL LINES

Primary cultures derived from gynecological cancers offer an *in vitro* model system for cancer research at a low maintenance cost, and have been invaluable tools for translational science, allowing genomic manipulation, cell biology studies, and high-throughput screenings beyond what would be feasible in clinical trials or animal models. Such cell lines are generated from patient-derived tissues through immortalization; however, the success rate to establish a new line is often low and unpredictable⁹. When successful, these cell lines are regularly a product of long-term clonal selection and comprise a largely homogeneous cell population that no longer captures the cellular heterogeneity originally present. Importantly, key aspects of tumor metabolism such as nutrient and oxygen consumption are lost in a 2D environment and, even though they can generate tumors easily upon engraftment into immunocompromised hosts, the developed tumors still lack clinical relevance.

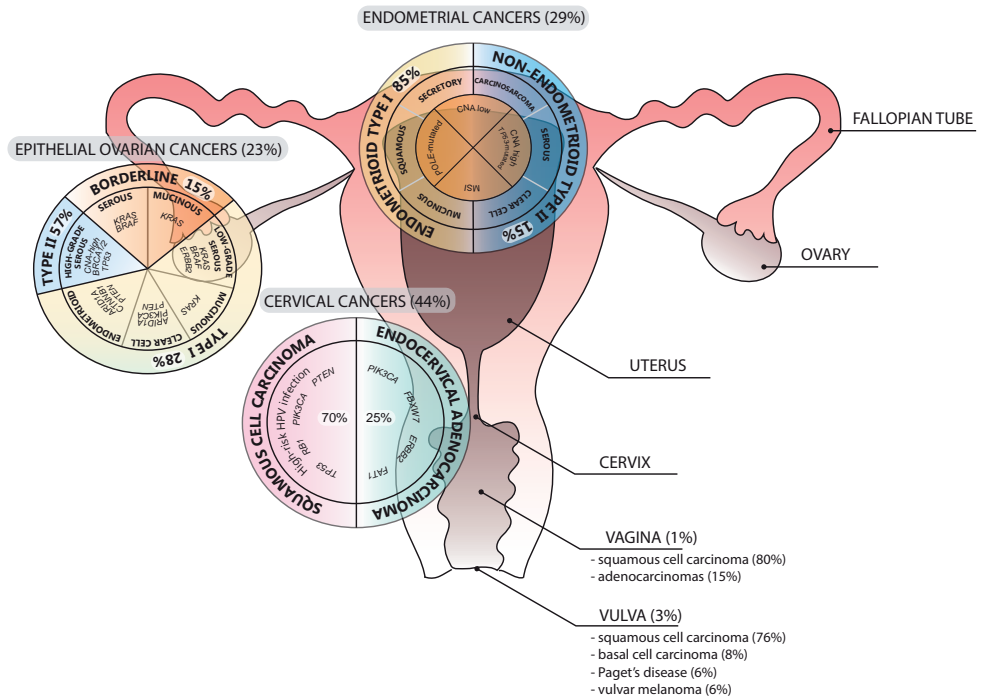


Figure 1. Representation of the Main Tumor Types across the Female Reproductive Tract (FRT). Epithelial malignancies of the FRT affect mainly the ovaries, endometrium, and cervix. Each tumor type is represented with the appropriate clinical incidence and specific features such as histopathological spectrum and genetic alterations. Ovarian cancers are generally classified into borderline, type I (low-grade) and type II (high-grade) subgroups, with the latter covering most of the clinical cases. The more genomically stable low-grade and borderline tumors involve frequent alterations in *KRAS* and *PTEN*, while high-grade serous ovarian cancer is predominantly *TP53*-mutated and carry high CNA burdens. Mutations in *BRCA* genes predispose to ovarian cancer. Endometrial cancer is divided into two main subtypes. While the endometrioid type I is the more abundant, the nonendometrioid type II accounts for most deaths and recurrences. From a genetic standpoint, the serous type II endometrial cancer and most of the carcinosarcomas fall into the CNA high, *TP53*-mutated group, while the endometrioid subtype can be equally categorized into MSI and CNA low. Finally, a subcategory, marked by *POLE* mutations and displaying an ultramutator phenotype has better prognosis. Cervical cancers present as endocervical adenocarcinoma or squamous cell carcinoma. The adenocarcinomas are less common and are characterized by recurrent alterations in *PIK3CA*, *ERBB2*, *FBXW7*, and *FAT1* genes. The latter type accounts for 70% of diagnoses and is mainly caused by high-risk human papillomavirus infection. Mutations in *TP53*, *RB1*, *PIK3CA*, and *PTEN* are common in this type. Vulvar and vaginal cancers, typically diagnosed as squamous cell carcinomas, account for approximately 4% of malignancies in the FRT. Abbreviations: CNA, copy number alteration; MSI, microsatellite instability.

Many conventional 2D epithelial ovarian cancer (EOC) cell lines were established decades ago, when limitation in technology did not allow for their proper validation. Notoriously, an in-depth analysis of a panel of ovarian cancer cultures revealed a shocking

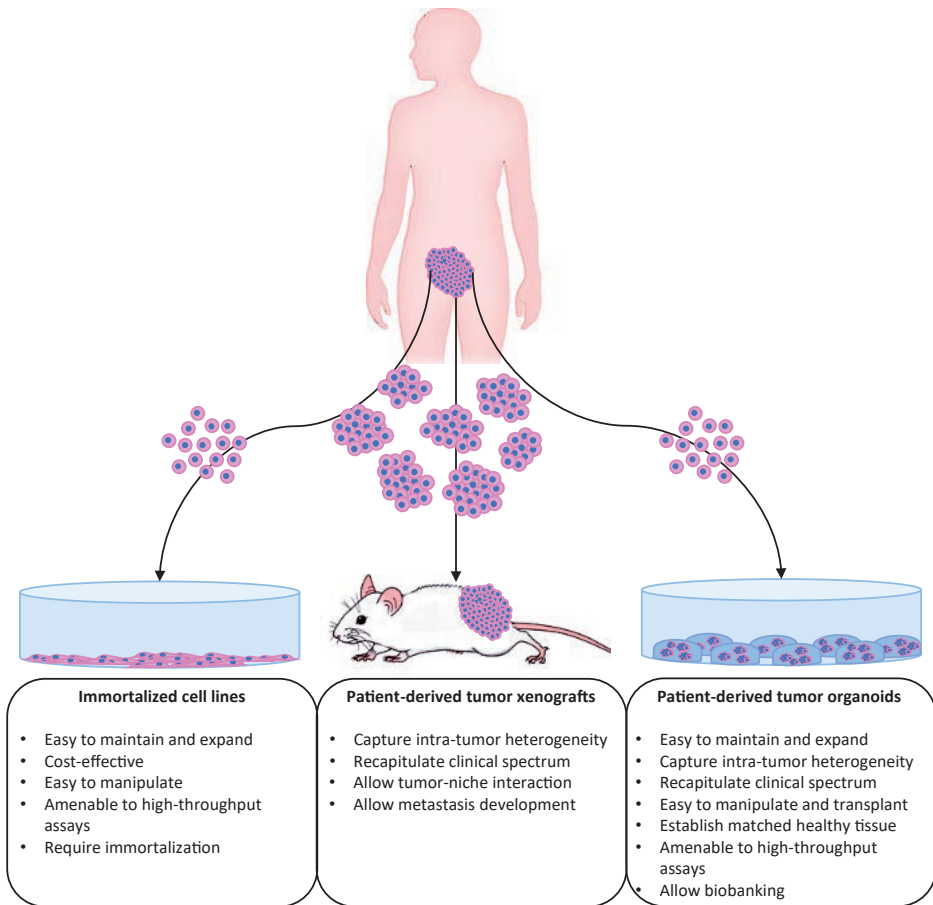
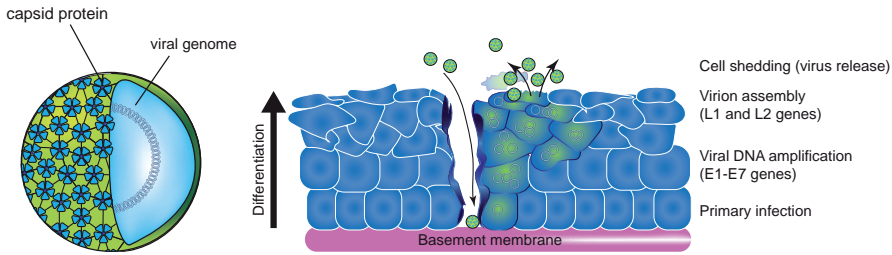


Figure 2, Key Figure. Human-Derived Models for Gynecological Cancers. Flowchart depicting the main models to study the tumors of the female reproductive tract. Tumor cells isolated from the resected specimen can be cultured indefinitely in 2D upon immortalization. Immortalized cell lines can be easily manipulated and subjected to high-throughput techniques such as drug screenings and genome editing. Despite being a cost-effective model, cell lines poorly recapitulate intra-tumor heterogeneity, the phenotypic diversity, and complex hierarchy of a tumor. Patient-derived xenografts (PDXs) are generated by heterotopic or orthotopic transplantation of tumor cells, isolated from biopsies, into immunocompromised mice. Despite the suboptimal establishment efficiency, PDXs preserve the heterogeneity of the primary tumor and allow tumor-niche interaction studies. PDXs can be amplified by sequential transplantation of tumor material over multiple generations. Finally, tumor cells can be embedded in extracellular-matrix-mimicking scaffolds (such as Matrigel, and BME, or more chemically defined synthetic hydrogel systems, e.g. polyethylene glycol hydrogels) and, under appropriate medium conditions, cultured as 3D tumor organoids. Organoids capture features of the primary tumor and do not require immortalization for long-term propagation. These models are suitable for high-throughput applications, while their ease of manipulation is compatible with techniques across disciplines such as immunology and gene editing. The possibility of deriving matched healthy and tumor organoid pairs from the same donor is guiding the design of tumor-specific therapies. Living biobanks of patient-derived tumor organoids have been already generated for ovarian and endometrial cancer, recapitulating the subtype diversity of the diseases.

truth that two of the most commonly used cell lines (SK-OV-3 and A2780) lack the main hallmarks of the high-grade serous ovarian cancer (HG-SOC) subtype they were originally believed to be derived from, including *TP53* mutations and extensive genomic instability, forcing a proper re-evaluation of many previous studies¹⁰. However, genome sequencing has made it possible to perform in-depth analysis of available EOC cell lines to better characterize their histological and molecular features, facilitating more intelligent selection of appropriate lines for subtype-focused studies¹⁰⁻¹³. Additionally, improved culture conditions have recently supported more successful derivation and maintenance of new EOC cell lines, which are thoroughly characterized and seem to better capture tumor heterogeneity than those established before^{14, 15}. A large proportion of EOC cell lines have been derived from malignant peritoneal ascites of neoadjuvant pretreated patients, and are resistant to platinum compounds among other drugs¹⁶, providing a useful tool to study mechanisms by which cells acquire drug resistance. For example, the emerging role of miRNAs, such as miR-130 and miR-29 families, in regulating EOC chemoresistance has received increasing attention in recent years¹⁷. Additionally, intelligent attempts to integrate DNA, mRNA, and methylation alteration data gathered from EOC cell lines have started to reveal novel routes to achieve drug sensitivity¹³.

For decades, cell lines established from endometrial adenocarcinomas have represented the cornerstone of endometrial cancer (EC) research. Molecular mechanisms fueling tumor growth, metastasis, and therapy response have been extensively studied using EC cell lines^{18, 19}. Genomic characterization of the most common commercially available EC cell lines detected **copy number alterations** (CNAs) and **single nucleotide variants** (SNVs) in top EC-mutated genes like *PTEN*, *PIK3CA*, *PIK3RI*, *CTNNB*, and *KRAS*^{20, 21}. Such representative characteristics have made EC cell lines widely used to explore novel therapeutic approaches to target the PI3K/AKT pathway, uncovering a beneficial combination of PI3K and poly (ADP-ribose) polymerase (PARP) inhibitors towards *PTEN*-mutant lines²². Few EC cell lines retain hormone receptor expression; accordingly, its signaling has been investigated *in vitro*, highlighting the pivotal role of the transcriptional activator ETV4 in EC cell growth by controlling estrogen receptor genomic binding, which is particularly interesting for type I EC²³. HEC1A and HEC1B are two EC cell lines derived from the same donor that differ in their microsatellite instability (MSI) status and have proved useful to outline the role of PMS2 in preserving EC genomic stability²⁴. Chemoresistance remains a major hurdle in EC, and cell lines have been used to exploit its driving mechanisms, uncovering possible targets among non-coding RNAs and epigenetic regulators²⁵⁻²⁷. Nevertheless, EC cell lines harbor important shortcomings that limit their potential as valuable surrogates. Most of the commercially available lines are *TP53*-mutant and their phenotype is comparable with that of adenocarcinoma, covering only a minority of EC subtypes, leaving the majority of clinical cases under-represented.

Immortalized cancer cell lines have also been instrumental in cervical cancer research and drug discovery. In fact, the oldest and most commonly used human cell line in cancer



Box 1. HPVs in Cervical Cancer Oncogenesis. HPVs are a small group of non-enveloped icosahedral viruses with double-stranded circular DNA, coding for eight genes: E1-E7 (early genes) and L1 and L2 (late capsid-encoding genes) (Figure I). HPVs belong to the *Papillomaviridae* family and can be further divided into three genera: alpha, beta, and gamma. While the alpha genus is mostly restricted to mucosal epithelial tissues such as anogenital tract and oral cavity, the cutaneous HPV types are represented mainly by the beta and gamma genera and are widely present in the skin of normal individuals. Alpha-HPVs are among the most commonly sexually transmitted infections and the majority of them is naturally cleared within 6-10 months. However, persistent infections with high-risk HPV types, such as HPV16 and HPV18, are known to be the etiological agents of mucosal cancers, including cervical cancer and its precursor lesions.

HPVs are extremely human species-specific and tissue-restricted viruses, showing high tropism towards stratified squamous epithelia, such as the ectocervix. HPVs can enter the targeted tissue via microabrasions in the genital epithelium and the viral infection is only productive when infecting the basal cells at the bottom of the stratified epithelium (Figure I). HPV entry is mediated by initial binding to primary cell surface receptor, namely heparan sulfate proteoglycans¹⁰², but it is also thought to involve secondary receptors, the identity of which is still debated. The subsequent conformational change in capsid proteins allows for virus internalization¹⁰³; however, the exact mechanism is still poorly understood. Following endocytosis, the viral genome is transported to the nucleus for transcription and replication. Viral gene expression is strictly dependent on host cell differentiation, dynamically changing along the keratinocyte squamous differentiation trajectory. The new capsids are formed only at the most superficial layer of the epithelium, where cells die and shed off from the surface; at the same time releasing the progeny of new virions that enable to spread the infection (Figure I). During the persistent infection, high-risk HPV DNA often integrates in the host genome, which causes changes in viral genome. Indeed, during integration viral E2 gene reading frame often gets disrupted, allowing for abrogation of E2-mediated transcriptional repression of the E6/E7 viral oncogene promoters¹⁰⁴. Viral oncogenes (E6 and E7) directly interact with and inhibit the activities of two important tumor suppressor proteins, TP53 and RB1, respectively, targeting them for rapid proteasome-mediated degradation^{105, 106}. Taken together, such events promote HPV-associated carcinogenesis.

research, HeLa, was derived from a patient presenting with a particularly aggressive form of cervical adenocarcinoma²⁸. Subsequently, additional cervical cancer cell lines emerged; however, new analyses have revealed several concerning findings that discourage the use of the conventional cancer cell lines due to evident divergences from the original

tumor^{29,30}. In regards to the tumor modeling, cervical cancer is a unique type, as the majority of them are caused by oncogenic human papillomavirus (HPV) infections³¹ (Box 1). Both conventional immortalized and primary cervical cell cultures, however, fail to recapitulate the squamous differentiation of the ectocervix and thus do not support the stratification-dependent viral life cycle, rendering them largely unsuitable for cancer development studies. In order to generate models that permit squamous differentiation *in vitro*, more advanced organotypic raft cultures have been established. Raft cultures, where primary or immortalized human keratinocytes are seeded onto a gel and differentiated at the air-liquid interface, offered the first breakthrough in achieving keratinocyte differentiation *in vitro*, and supported the reproduction of the complete viral life cycle³². Still, these models do not support direct virus-host interaction and have short lifespans, hindering the studies on viral entry and the effects of long-term infection.

Vaginal and vulvar cancers are rare types of malignancies that together represent about 4% of all FRT cancers³³. Due to their rarity, only a limited number of cytogenetically characterized cell lines for these cancer types have been reported³⁴⁻³⁶, and most of the insight about relevant prognostic biomarkers for this cancer type has been simply gained by immunohistochemical or tissue microarray analysis of the resected specimens. Studies on vulvar cancer cell lines have demonstrated that these tumors are cytogenetically complex with multiple recurrent chromosome rearrangements³⁷. Similar to cervical cancers, a proportion of vaginal and vulvar cancers is caused by infection with high-risk HPV, which is difficult to study in conventional culture systems.

In vitro human cell line models are commonly used for cancer pharmacogenomic and clinical response prediction studies. For example, NCI-60 is a traditional cell line panel that constitutes of a set of 60 cancer cell lines from nine different tumor types, and has been widely used for screening of anticancer compounds. However, among gynecological cancers, only ovarian cancer cell lines are represented in this panel. More recently, additional panels have emerged, such as GlaxoSmithKline (GSK)³⁸ and the Cancer Cell Line Encyclopedia (CCLE)³⁹, that combine larger set of cancer lines for chemical screening and omics data, also expanding the representation of gynecological tumors by inclusion of a number of endometrial and vaginal cancer cell lines. Cell lines with well-defined subtype-specific molecular alterations, such as BRCA1/2 or PI3K mutations, may be valuable tools for preclinical drug discovery, providing an opportunity to perform gene-drug association studies for specific patient populations. In this regard, the discovery of the efficiency of PARP inhibitors in the management of BRCA-deficient EOC was first realized in BRCA1/2-deficient cell lines^{40, 41}. Therefore, such models are useful for initial screening but the results always require proper validation.

XENOGRAFTS

Patient-derived **xenografts** (PDXs), in which cells or intact fragments from fresh human tumor tissue are transplanted into immunocompromised mice, have been instrumental

in studies of *in vivo* chemotherapeutic responses and screening for novel compounds of clinical interest. Indeed, PDXs have been shown to recapitulate histopathological features of the primary tumor and maintain its molecular heterogeneity, even after propagation across multiple generations⁴²⁻⁴⁵. Furthermore, novel tools and methodologies seem to be emerging to facilitate the robustness of the PDX assays⁴⁶⁻⁴⁸. However, the genomic stability of the PDXs over serial passaging has been recently questioned on breast cancer models as **clonal selection** and rapid mouse-specific tumor evolution have been noted in two independent studies^{49, 50}. Such concerns have not been reported in the FRT PDXs to date. Although encouraging, this platform is not suitable for **high-throughput** screenings due to low rates of engraftment, slow tumor growth, and high costs. Additionally, PDX models cannot be genetically modified and rely entirely on the use of immunocompromised mice, precluding experimentation with novel immunomodulatory compounds. Pioneering work with establishing humanized mice that possess functional human immune systems might represent an alternative, despite challenging, solution.

PDX models have been developed from all the major EOC subtypes, with HG-SOC tumors showing the highest success rate^{46, 51}. Additionally, orthotopic PDXs have been shown to closely recapitulate EOC tumor progression, ascites formation, and metastasis as observed in human disease⁵². Given their ability to maintain the original tumor heterogeneity, these models have been successfully exploited for platinum-based chemotherapy whose response seems to highly correlate with that of patients^{53, 54}. Targeted therapies have been applied as well, including PARP inhibitors on *BRCA1/2*-deficient xenografts⁵⁵ or HER2-targeted monoclonal antibodies on HER2-positive ovarian cancer PDXs⁵⁶. Ovarian cancer PDXs have also been utilized to explore biomarkers and molecular mechanisms of chemoresistance. As an example, both CDK12 mRNA expression⁵⁷ and active Wnt signaling⁵⁸ in ovarian cancer PDXs have been linked to disease resistance to platinum therapy. Such features make PDXs a relevant model in EOC research.

Despite low engraftment rate, significantly more efficient for metastatic samples⁴², EC PDX models have been developed and molecularly investigated to screen for a potential application of mammalian target of rapamycin (mTOR) and MEK inhibitors on tumors harboring *PTEN*, *KRAS*, and *PIK3CA* mutations^{42, 59}. Also, inhibition of AKT has been successfully exploited to restrain growth and invasion in a PDX model of EC^{59, 60}. An emerging strategy to address MSI tumors, particularly relevant for EC, is through the modulation of the immune system with immune checkpoint inhibitors directed against the programmed death (PD)-1 and PD-ligand 1 proteins such as pembrolizumab, dostarlimab, avelumab, and durvalumab, which have shown success rates between 27 and 57% in clinical trials⁶¹. In this regard, PDXs in humanized mice might prove relevant preclinical models to address MMR-deficient and POLE-mutated ECs with novel combinatorial therapies, despite being a technical challenge.

PDX models have also been successfully developed from the two main subtypes of cervical cancer^{62, 63}. The tumor-take of these models has been reported between 48 and

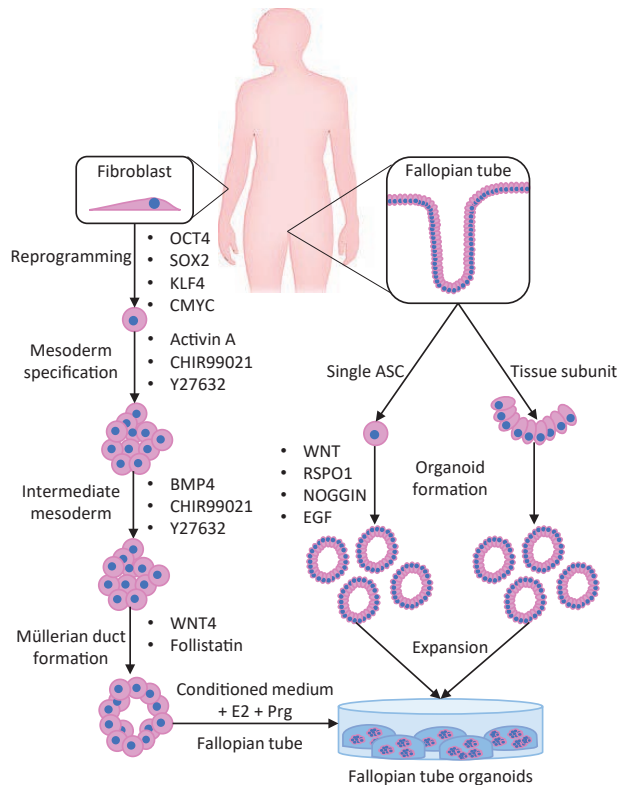
70%^{64,65}. Orthotopic cervical cancer PDXs show huge promise as they have demonstrated good correlation in transcriptomic landscapes as well as similar histological, metastatic, and stromal patterns when compared with the donor tissue⁶³. These models also sustain causative high-risk HPV infection⁶⁴, which might be helpful in unravelling the viral gene expression dynamics in the already transformed cells, providing good opportunities for discovering novel therapeutic targets. In preclinical settings, HER2-amplified cervical cancer PDXs have shown promising results in terms of response to combined treatment with two clinically approved HER2 inhibitors, trastuzumab and lapatinib⁶⁶.

Compared with the aforementioned cancer types, no primary PDX models have been reported for neither vulvar and vaginal cancers to date.

ORGANOIDS

Throughout the last decade, human-derived cell culture models have rapidly evolved towards more advanced 3D organotypic cultures that hold promise in preclinical research. Stem cells-derived **organoids** are *in vitro* 3D cell cultures that closely recapitulate the biology and pathology of the primary tissue (Box 2). These mini-replicas of organs or tumors do not require transformation for survival and allow for long-term expansion, while maintaining the genomic landscape of donor cells. As these systems support the growth of healthy epithelial cells, it gives the organoid models a considerable edge that no other human-derived model system has had before – suitability to study the early stages of tumor development in human-relevant settings⁶⁷. Importantly, tumor organoids have been shown to capture inter- and intratumor heterogeneity and, as such, have potential in preclinical screenings.

Novel organoid cultures for EOC research have been steadily emerging throughout the last couple of years. Normal fallopian tube and ovarian-surface-epithelium-derived organoids that capture the transcriptomic and morphological features of the respective human tissues have been successfully established and offer a platform for studying cancer initiation from these potential origins^{68, 69}. To that end, human-derived fallopian-tube organoids have been shown to be susceptible to CRISPR/Cas9 genome editing by introducing knock-outs of *TP53* and *RB1* genes⁶⁹, paving the way towards better characterization of ovarian cancer initiation and progression. In addition to the healthy organoid lines, both short- and long-term organoid cultures from a panel of solid ovarian cancer tissues, as well as from ascitic and pleural fluids, have been established, including all major subtypes of EOC⁶⁹⁻⁷³. Utilizing a novel single-cell DNA sequencing analysis, it has been confirmed that the organoids reliably maintain the tumor heterogeneity in culture, even after prolonged passaging⁶⁹. A promising preprint on single-cell transcriptomic analysis of high-grade ovarian cancer organoids further supports the preservation of tumor heterogeneity in culture⁷⁴. These recent studies have shown that tumor organoids recapitulate the histological and genomic features of original tumor subtypes and capture intra- and interpatient heterogeneity. Furthermore, the EOC organoids are suitable for



Box 2. Stem-Cell-Derived Organoids. Organoids, in their simplest definition, are 3D near-physiological structures that recapitulate key biological aspects of the original tissue. Two different stem cell types can support *in vitro* organoid formation: embryonic pluripotent stem cells (ESCs) or their *in vitro* artificial counterpart, the induced pluripotent stem cells (iPSCs), and tissue-committed adult stem cells (ASCs) (Figure 1). Through the activation of developmental programs that lead to tissue specification, ESCs and iPSCs self-organize into organotypic structures that contain both epithelial and mesenchymal progenies. This is achieved by the sequential modulation of relevant pathways to induce lineage commitment towards anticipated fate. As for fallopian tubes, WNT, BMP, and TGF- signaling activation is essential in the process of lineage specification towards Müllerian fate¹⁰⁷. ESCs and iPSCs are routinely used to investigate the contribution of specific pathways to tissue development and how genetic defects interfere with it. At convenience, they serve as an alternative to more conventional patient-specific models in case of limitation in source tissue availability.

In adult tissues, there is a small population of ASCs with self-renewing and differentiation capacities located in a tightly regulated compartment termed the **stem cell niche**. This environment provides essential factors for stem cell maintenance, ensuring healthy tissue homeostasis throughout life. These cells can form organoids once embedded into an extracellular-matrix-mimicking scaffold and cultured in the presence of a cocktail of essential niche factors that promote proper mitosis, inhibit epithelial-to-mesenchymal transition, and prevent anoikis (a form of cell death of single cells). Commonly used

niche factors in organoid cultures include WNT pathway activators (such as WNT3A and RSPO1) to retain stemness, NOGGIN to inhibit BMP-driven differentiation, and epidermal growth factor or fibroblast growth factors to induce proper mitosis. Among other tissues, these factors also enable the establishment of organoids from human fallopian tubes⁶⁸. Under these serum-free culture conditions, single ASCs or tissue fragments, will undergo self-organization and morphogenesis to form miniature tissue replicas on the dish. Furthermore, upon tumor resection, or isolation of circulating tumor cells, organoids can also be established from malignant tissues. To avoid contamination with healthy epithelium, tumor cells can be positively selected by manipulation of culture media. As an example, this could be achieved by removing signaling factors such as WNT3A and RSPO1 or adding selection agents, such as Nutlin-3a, which negatively affects healthy cells and positively selects tumor clones due to mutations in core genes of the WNT or TP53 pathway, respectively.

Abbreviations: CHIR99021, GSK-3 inhibitor; E2, 17 β -estradiol; Prg, progesterone; Y27632, Rho kinase inhibitor.

medium-throughput drug screening assays^{69, 71-73, 75} and have been shown to accurately predict clinical response of HG-SOC patients to DNA repair inhibitors⁷⁰. These advantages highlight the potential of tumor organoids to guide precision medicine, particularly in predicting patient-specific responses in preclinical drug screening.

Despite the first organotypic model of human endometrium being reported in 1988⁷⁶, progresses in the field has been stalling for more than two decades due to inappropriate culture conditions. Recently, 3D adult stem-cell-derived endometrial organoids have been established and shown to recapitulate important aspects of endometrial biology, while maintaining genomic stability after extensive *in vitro* expansion^{77, 78}. Consequently, it was possible to establish patient-derived tumor organoids from both endometrioid and nonendometrioid subtypes that captured histopathological features of the primary tumor, such as hormone receptor status, preserved upon *in vivo* engraftment⁷⁹. CNAs and SNVs were also conserved between primary tumor and organoids, covering the top mutated genes and genetic aberrations found in EC, such as *PTEN*, *PIK3CA*, *FBXW7*, *CTNNB1*, and *ARID1A* hotspot mutations^{79, 80}. Medium-based selection can be successfully used to confirm the association between genetic background of the organoids and niche factors independency. For instance, only *CTNNB1*-mutant lines expand in the absence of R-spondin (RSPO)-1⁷⁹, as shown previously in other tumor organoids⁸¹⁻⁸³, demonstrating how niche composition shapes clonal selection in a tumor microenvironment. Encouragingly, the organoids have proved amenable to drug screening both as short- and long-term cultures showing line-dependent sensitivity to PI3K, mTOR, MEK, and histone deacetylase inhibitors, as well as common therapeutic drugs like paclitaxel and cisplatin^{79, 80, 84}. Nevertheless, the preclinical predictive power of the organoids to guide

individual therapies remains to be validated and no ongoing co-clinical trial has been reported so far.

Although reported for a single case of rare cervical clear-cell carcinoma⁸⁵, organoid cultures have not been published to date for the healthy cervix nor for the two most common cervical tumor subtypes, that is, squamous cell and adenocarcinomas. However, a promising preprint has been recently deposited to bioRxiv open repository that reports on establishment of human-derived normal ecto- and endocervical organoids that closely recapitulate the tissues of origin⁸⁶. In our laboratory, we have made similar findings and, according to our unpublished data, long-term organoids could be also grown from cervical squamous cell and adenocarcinomas. These emerging hints will hopefully open up novel directions for the future of cervical cancer research, holding particular promise in advancing natural virus-host interaction studies.

There are currently no organoid cultures reported for vaginal nor vulvar cancers, or respective human normal epithelial counterparts.

CONCLUDING REMARKS

Over the past few decades, human-derived model systems for gynecological cancer research have made much progress. The systems have advanced from primary monolayer cultures to more advanced 3D models that better meet the demands of recapitulating the morphological features and the heterogeneity of donor tissues (see Outstanding Questions). In particular, 3D organoid cultures have emerged and quickly became a particular focus in cancer research, including in gynecological oncology. Indeed, tumor-derived organoids are rewiring our approach to address treatment strategies and improve therapy decision-making for individual patients. Although the amount of data collected on organoids derived from gynecological tumors so far is not as exhaustive as shown for other tumors⁸⁷⁻⁹⁰, it supports their potential use in personalized cancer medicine, addressing type-specific features such as PTEN/PI3K pathway mutations for EC or use of PARP inhibitors for EOC. Moreover, as recently explored for other tumor types^{87, 90, 91}, organoids may serve as a companion diagnostic tool for clinical trials when screened in parallel with the same treatment option selected for the patient. Eventually, therapy response may be monitored in real-time in *in vitro* settings. In this particular scenario, combining multiomics analysis might help predict eventual drug resistance that can be targeted with a more specific second-line intervention. Applying similar concepts for the most aggressive forms of gynecological cancers such as serous EC and carcinosarcomas, as well as HG-SOC, could help increase the therapeutic window and provide more specific options⁷⁵.

MSI and POLE mutations are recurrent features in EC⁹². The heavy mutational burden of these tumors confers high sensitivity to immune checkpoint inhibitors such as pembrolizumab and dostarlimab⁶¹. While the reconstruction of a human immune system in the host is challenging, the recombination of tumor-derived organoids with tumor-

1

2

3

4

5

&

infiltrating T-cells isolated from the same biopsy is easier⁹³. Despite being still unproven for gynecological cancers, MMR-deficient patient-derived organoids and peripheral blood lymphocytes have already been cocultured for other tumor types and have shown promise to enrich for tumor-reactive T-cells, successfully probed for tumor-cell-killing activity *in vitro*^{94, 95}. In the field of cervical, vaginal, and vulvar cancer, studies about causative high-risk HPV infection have been hampered due to the difficulty of naturally infecting and completing the viral life cycle in conventional cell cultures, as well as due to the inability to track the infection-related events in the long term. The first hints about the emergence of cervical organoids that recapitulate the squamous differentiation and that can be expanded indefinitely will potentially offer a new tool to directly address questions about cervical oncogenesis that were not possible before. Similar models are demanded for rarer vaginal and vulvar cancers in the years to come.

The arrival of the sequencing era considerably increased the amount of data generated. In particular, integrated multiomics approaches improved our knowledge of the molecular basis of individual tumor types^{92, 95-99}. Such systematic analyses have already been applied to primary tumors of the reproductive system and enhanced our understanding of intratumor heterogeneity, which is now being harnessed at a single cell level^{69, 100, 101}. In this regard, the organoids offer the potential to combine unlimited expansion with the requirements of a multiomics approach.

To conclude, with the rapid pace of technological advancements, cancer research has been offered a multitude of promising models whose full capacity should be thoroughly explored and benefited from to improve the treatment and prevention strategies for gynecological cancers in years to come.

OUTSTANDING QUESTIONS

How can we improve gynecological cancer models to better understand mechanisms of tumor initiation, progression and metastasis?

How do we exploit the knowledge to start detecting the gynecological tumors at the early stage?

What is the predictive value of gynecological cancer models and can they feasibly assist in preclinical treatment decisions (are they compatible with clinical workflow)?

Could different tumor subtypes carrying identical aberrations benefit from the same treatment strategies?

Would it be feasible to build personalized cancer models for each patient or do we learn faster from the cohort studies to guide precision medicine?

ACKNOWLEDGEMENTS

This work is part of the OncoCode Institute, which is partly financed by the Dutch Cancer Society and was funded by the gravitation program CancerGenomics.nl from the Netherlands Organisation for Scientific Research (NWO). K.L. is a PhD student supported by a grant from Gieskes-Strijbis Foundation (1816199). M.B. is a postdoctoral researcher supported by a long-term fellowship of the European Organization for Molecular Biology (EMBO, ALTF 765-2019). H.C. is a Principal Investigator at the Hubrecht Institute and pioneer of the organoid technology.

1

2

3

4

5

&

GLOSSARY

Clonal selection: biological process upon which mutational events confer a growth advantage to a single cell and its progeny which can therefore escape niche control.

Copy number alteration: aberration in chromosome structure that leads to a gain or a loss in DNA copies.

High-throughput: an experimental method that uses automated equipment designed for the simultaneous analysis of a large number of samples, impractical for conventional techniques.

Organoids: adult stem-cell-derived organotypic structures capable of long-term self-renewal *in vitro* in chemically defined media. Organoids recapitulate key biological features of the original tissue including morphology, function, gene expression, and differentiation dynamics.

Single nucleotide variant: variation in a single nucleotide of the coding sequence of a gene that can either result in a silent, missense, or nonsense mutation.

Stem cell: undifferentiated cell with the unique capacity of unlimited proliferative potential and the ability to generate more specialized cells in each tissue.

Stem cell niche: specific area of a tissue with specialized cells directly interacting with stem cells by providing factors that induce either their self-renewal or their differentiation towards more functional cells. The presence of certain growth factors is geographically restricted within the niche creating a selective pressure towards mutations in tumor cells.

Tumor heterogeneity: it refers to the presence of tumor cells with distinct profiles like cell morphology, gene expression, genetic mutations, and metabolism, as a consequence of clonal expansion of divergent clones.

Xenograft: transplantation of donor tissue into a host of a different species.

REFERENCES

1. Kurman, R.J., Ellenson, L.H. & Ronnett, B.M. *Blaustein's pathology of the female genital tract*, Edn. 6th. (Springer, New York; 2011).
2. Patterson, A.L. & Pru, J.K. Long-term label retaining cells localize to distinct regions within the female reproductive epithelium. *Cell Cycle* **12**, 2888-2898 (2013).
3. Kangawa, A., Otake, M., Enya, S., Yoshida, T. & Shibata, M. Normal Developmental and Estrous Cycle-dependent Histological Features of the Female Reproductive Organs in Microminipigs. *Toxicol Pathol* **45**, 551-573 (2017).
4. Xiao, S. *et al.* A microfluidic culture model of the human reproductive tract and 28-day menstrual cycle. *Nat Commun* **8**, 14584 (2017).
5. Mirhashemi, R., Nieves-Neira, W. & Averette, H.E. Gynecologic malignancies in older women. *Oncology (Williston Park)* **15**, 580-586; discussion 592-584, 597-588 (2001).
6. Brown, S.B. & Hankinson, S.E. Endogenous estrogens and the risk of breast, endometrial, and ovarian cancers. *Steroids* **99**, 8-10 (2015).
7. Deroo, B.J. & Korach, K.S. Estrogen receptors and human disease. *J Clin Invest* **116**, 561-570 (2006).
8. Sharpless, N.E. & Depinho, R.A. The mighty mouse: genetically engineered mouse models in cancer drug development. *Nat Rev Drug Discov* **5**, 741-754 (2006).
9. Verschraegen, C.F. *et al.* Establishment and characterization of cancer cell cultures and xenografts derived from primary or metastatic Mullerian cancers. *Clin Cancer Res* **9**, 845-852 (2003).
10. Domcke, S., Sinha, R., Levine, D.A., Sander, C. & Schultz, N. Evaluating cell lines as tumour models by comparison of genomic profiles. *Nat Commun* **4**, 2126 (2013).
11. Beaufort, C.M. *et al.* Ovarian cancer cell line panel (OCCP): clinical importance of in vitro morphological subtypes. *PLoS One* **9**, e103988 (2014).
12. Anglesio, M.S. *et al.* Type-specific cell line models for type-specific ovarian cancer research. *PLoS One* **8**, e72162 (2013).
13. Papp, E. *et al.* Integrated Genomic, Epigenomic, and Expression Analyses of Ovarian Cancer Cell Lines. *Cell Rep* **25**, 2617-2633 (2018).
14. Ince, T.A. *et al.* Characterization of twenty-five ovarian tumour cell lines that phenocopy primary tumours. *Nat Commun* **6**, 7419 (2015).
15. Nelson, L. *et al.* A living biobank of ovarian cancer ex vivo models reveals profound mitotic heterogeneity. *Nat Commun* **11**, 822 (2020).
16. Langdon, S.P. Isolation and culture of ovarian cancer cell lines. *Methods Mol Med* **88**, 133-139 (2004).
17. Mihanfar, A., Fattahi, A. & Nejabati, H.R. MicroRNA-mediated drug resistance in ovarian cancer. *J Cell Physiol* **234**, 3180-3191 (2019).
18. Gordon, L.K. *et al.* EMP2 regulates angiogenesis in endometrial cancer cells through induction of VEGF. *Oncogene* **32**, 5369-5376 (2013).
19. Jiang, T. *et al.* High levels of Nrf2 determine chemoresistance in type II endometrial cancer. *Cancer Res* **70**, 5486-5496 (2010).

20. Cheung, L.W. *et al.* High frequency of PIK3R1 and PIK3R2 mutations in endometrial cancer elucidates a novel mechanism for regulation of PTEN protein stability. *Cancer Discov* **1**, 170-185 (2011).
21. Wang, Y. *et al.* Genomic characterization of gene copy-number aberrations in endometrial carcinoma cell lines derived from endometrioid-type endometrial adenocarcinoma. *Technol Cancer Res Treat* **9**, 179-189 (2010).
22. Philip, C.A. *et al.* Inhibition of PI3K-AKT-mTOR pathway sensitizes endometrial cancer cell lines to PARP inhibitors. *BMC Cancer* **17**, 638 (2017).
23. Rodriguez, A.C. *et al.* ETV4 Is Necessary for Estrogen Signaling and Growth in Endometrial Cancer Cells. *Cancer Res* **80**, 1234-1245 (2020).
24. Glaab, W.E. *et al.* Characterization of distinct human endometrial carcinoma cell lines deficient in mismatch repair that originated from a single tumor. *J Biol Chem* **273**, 26662-26669 (1998).
25. Dedes, K.J., Wetterskog, D., Ashworth, A., Kaye, S.B. & Reis-Filho, J.S. Emerging therapeutic targets in endometrial cancer. *Nat Rev Clin Oncol* **8**, 261-271 (2011).
26. Oki, S. *et al.* Oncogenic histone methyltransferase EZH2: A novel prognostic marker with therapeutic potential in endometrial cancer. *Oncotarget* **8**, 40402-40411 (2017).
27. Zhuo, Z. & Yu, H. miR-205 inhibits cell growth by targeting AKT-mTOR signaling in progesterone-resistant endometrial cancer Ishikawa cells. *Oncotarget* **8**, 28042-28051 (2017).
28. Gey, G.O., Coffmann, W.D. & Kubicek, M.T. Tissue culture studies of the proliferative capacity of cervical carcinoma and normal epithelium. *Cancer Res* **12**, 264-265 (1952).
29. Sandberg, R. & Ernberg, I. Assessment of tumor characteristic gene expression in cell lines using a tissue similarity index (TSI). *Proc Natl Acad Sci U S A* **102**, 2052-2057 (2005).
30. Carlson, M.W., Iyer, V.R. & Marcotte, E.M. Quantitative gene expression assessment identifies appropriate cell line models for individual cervical cancer pathways. *BMC Genomics* **8**, 117 (2007).
31. zur Hausen, H., Gissmann, L., Steiner, W., Dippold, W. & Dreger, I. Human papilloma viruses and cancer. *Bibl Haematol*, 569-571 (1975).
32. Cheng, S., Schmidt-Grimminger, D.C., Murant, T., Broker, T.R. & Chow, L.T. Differentiation-dependent up-regulation of the human papillomavirus E7 gene reactivates cellular DNA replication in suprabasal differentiated keratinocytes. *Genes Dev* **9**, 2335-2349 (1995).
33. Bray, F. *et al.* Global cancer statistics 2018: GLOBOCAN estimates of incidence and mortality worldwide for 36 cancers in 185 countries. *CA Cancer J Clin* **68**, 394-424 (2018).
34. Raitanen, M. *et al.* Characterization of 10 vulvar carcinoma cell lines by karyotyping, comparative genomic hybridization and flow cytometry. *Gynecol Oncol* **93**, 155-163 (2004).
35. Dongre, H. *et al.* Establishment of a novel cancer cell line derived from vulvar carcinoma associated with lichen sclerosus exhibiting a fibroblast-dependent tumorigenic potential. *Exp Cell Res* **386**, 111684 (2020).
36. Hietanen, S. *et al.* Human papillomavirus in vulvar and vaginal carcinoma cell lines. *Br J Cancer* **72**, 134-139 (1995).
37. Worsham, M.J. *et al.* Consistent chromosome abnormalities in squamous cell carcinoma of the vulva. *Genes Chromosomes Cancer* **3**, 420-432 (1991).

38. Greshock, J. *et al.* Molecular target class is predictive of in vitro response profile. *Cancer Res* **70**, 3677-3686 (2010).
39. Barretina, J. *et al.* The Cancer Cell Line Encyclopedia enables predictive modelling of anticancer drug sensitivity. *Nature* **483**, 603-607 (2012).
40. Farmer, H. *et al.* Targeting the DNA repair defect in BRCA mutant cells as a therapeutic strategy. *Nature* **434**, 917-921 (2005).
41. Fong, P.C. *et al.* Inhibition of poly(ADP-ribose) polymerase in tumors from BRCA mutation carriers. *N Engl J Med* **361**, 123-134 (2009).
42. Depreeuw, J. *et al.* Characterization of patient-derived tumor xenograft models of endometrial cancer for preclinical evaluation of targeted therapies. *Gynecol Oncol* **139**, 118-126 (2015).
43. Siolas, D. & Hannon, G.J. Patient-derived tumor xenografts: transforming clinical samples into mouse models. *Cancer Res* **73**, 5315-5319 (2013).
44. Hubbard, S.A. *et al.* Evidence for cancer stem cells in human endometrial carcinoma. *Cancer Res* **69**, 8241-8248 (2009).
45. Aparicio, S., Hidalgo, M. & Kung, A.L. Examining the utility of patient-derived xenograft mouse models. *Nat Rev Cancer* **15**, 311-316 (2015).
46. Liu, J.F. *et al.* Establishment of Patient-Derived Tumor Xenograft Models of Epithelial Ovarian Cancer for Preclinical Evaluation of Novel Therapeutics. *Clin Cancer Res* **23**, 1263-1273 (2017).
47. Liu, Y. *et al.* Gene expression differences between matched pairs of ovarian cancer patient tumors and patient-derived xenografts. *Sci Rep* **9**, 6314 (2019).
48. Rajaram, S. *et al.* A multi-modal data resource for investigating topographic heterogeneity in patient-derived xenograft tumors. *Sci Data* **6**, 253 (2019).
49. Eirew, P. *et al.* Dynamics of genomic clones in breast cancer patient xenografts at single-cell resolution. *Nature* **518**, 422-426 (2015).
50. Ben-David, U. *et al.* Patient-derived xenografts undergo mouse-specific tumor evolution. *Nat Genet* **49**, 1567-1575 (2017).
51. Heo, E.J. *et al.* Patient-Derived Xenograft Models of Epithelial Ovarian Cancer for Preclinical Studies. *Cancer Res Treat* **49**, 915-926 (2017).
52. Bankert, R.B. *et al.* Humanized mouse model of ovarian cancer recapitulates patient solid tumor progression, ascites formation, and metastasis. *PLoS One* **6**, e24420 (2011).
53. Ricci, F. *et al.* Patient-derived ovarian tumor xenografts recapitulate human clinicopathology and genetic alterations. *Cancer Res* **74**, 6980-6990 (2014).
54. Topp, M.D. *et al.* Molecular correlates of platinum response in human high-grade serous ovarian cancer patient-derived xenografts. *Mol Oncol* **8**, 656-668 (2014).
55. George, E. *et al.* A patient-derived-xenograft platform to study BRCA-deficient ovarian cancers. *JCI Insight* **2**, e89760 (2017).
56. Harris, F.R. *et al.* Targeting HER2 in patient-derived xenograft ovarian cancer models sensitizes tumors to chemotherapy. *Mol Oncol* **13**, 132-152 (2019).
57. Guffanti, F. *et al.* Platinum sensitivity and DNA repair in a recently established panel of patient-derived ovarian carcinoma xenografts. *Oncotarget* **9**, 24707-24717 (2018).

58. Nagaraj, A.B. *et al.* Critical role of Wnt/beta-catenin signaling in driving epithelial ovarian cancer platinum resistance. *Oncotarget* **6**, 23720-23734 (2015).
59. Bradford, L.S. *et al.* Assessing the efficacy of targeting the phosphatidylinositol 3-kinase/AKT/mTOR signaling pathway in endometrial cancer. *Gynecol Oncol* **133**, 346-352 (2014).
60. Winder, A., Unno, K., Yu, Y., Lurain, J. & Kim, J.J. The allosteric AKT inhibitor, MK2206, decreases tumor growth and invasion in patient derived xenografts of endometrial cancer. *Cancer Biol Ther* **18**, 958-964 (2017).
61. Green, A.K., Feinberg, J. & Makker, V. A Review of Immune Checkpoint Blockade Therapy in Endometrial Cancer. *Am Soc Clin Oncol Educ Book* **40**, 1-7 (2020).
62. Press, J.Z. *et al.* Xenografts of primary human gynecological tumors grown under the renal capsule of NOD/SCID mice show genetic stability during serial transplantation and respond to cytotoxic chemotherapy. *Gynecol Oncol* **110**, 256-264 (2008).
63. Chaudary, N., Jaluba, K., Pintilie, M. & Hill, R.P. Establishment of orthotopic primary cervix cancer xenografts. *Methods Mol Biol* **1249**, 381-391 (2015).
64. Hoffmann, C. *et al.* Creation and characterization of a xenograft model for human cervical cancer. *Gynecol Oncol* **118**, 76-80 (2010).
65. Scott, C.L., Mackay, H.J. & Haluska, P., Jr. Patient-derived xenograft models in gynecologic malignancies. *Am Soc Clin Oncol Educ Book*, e258-266 (2014).
66. Oh, D.Y. *et al.* HER2 as a novel therapeutic target for cervical cancer. *Oncotarget* **6**, 36219-36230 (2015).
67. Drost, J. *et al.* Use of CRISPR-modified human stem cell organoids to study the origin of mutational signatures in cancer. *Science* **358**, 234-238 (2017).
68. Kessler, M. *et al.* The Notch and Wnt pathways regulate stemness and differentiation in human fallopian tube organoids. *Nat Commun* **6**, 8989 (2015).
69. Kopper, O. *et al.* An organoid platform for ovarian cancer captures intra- and interpatient heterogeneity. *Nat Med* **25**, 838-849 (2019).
70. Hill, S.J. *et al.* Prediction of DNA Repair Inhibitor Response in Short-Term Patient-Derived Ovarian Cancer Organoids. *Cancer Discov* **8**, 1404-1421 (2018).
71. Maru, Y., Tanaka, N., Itami, M. & Hippo, Y. Efficient use of patient-derived organoids as a preclinical model for gynecologic tumors. *Gynecol Oncol* **154**, 189-198 (2019).
72. Jabs, J. *et al.* Screening drug effects in patient-derived cancer cells links organoid responses to genome alterations. *Mol Syst Biol* **13**, 955 (2017).
73. Maenhoudt, N. *et al.* Developing Organoids from Ovarian Cancer as Experimental and Preclinical Models. *Stem Cell Reports* **14**, 717-729 (2020).
74. Velletri, T. *et al.* Single cell derived organoids capture the self-renewing subpopulations of metastatic ovarian cancer. *bioRxiv* **484121** (2018).
75. de Witte, C.J. *et al.* Patient-Derived Ovarian Cancer Organoids Mimic Clinical Response and Exhibit Heterogeneous Inter- and Inpatient Drug Responses. *Cell Rep* **31**, 107762 (2020).
76. Rinehart, C.A., Jr., Lyn-Cook, B.D. & Kaufman, D.G. Gland formation from human endometrial epithelial cells in vitro. *In Vitro Cell Dev Biol* **24**, 1037-1041 (1988).

77. Boretto, M. *et al.* Development of organoids from mouse and human endometrium showing endometrial epithelium physiology and long-term expandability. *Development* **144**, 1775-1786 (2017).
78. Turco, M.Y. *et al.* Long-term, hormone-responsive organoid cultures of human endometrium in a chemically defined medium. *Nat Cell Biol* **19**, 568-577 (2017).
79. Boretto, M. *et al.* Patient-derived organoids from endometrial disease capture clinical heterogeneity and are amenable to drug screening. *Nat Cell Biol* **21**, 1041-1051 (2019).
80. Pauli, C. *et al.* Personalized In Vitro and In Vivo Cancer Models to Guide Precision Medicine. *Cancer Discov* **7**, 462-477 (2017).
81. Nanki, K. *et al.* Divergent Routes toward Wnt and R-spondin Niche Independency during Human Gastric Carcinogenesis. *Cell* **174**, 856-869 e817 (2018).
82. Seino, T. *et al.* Human Pancreatic Tumor Organoids Reveal Loss of Stem Cell Niche Factor Dependence during Disease Progression. *Cell Stem Cell* **22**, 454-467 e456 (2018).
83. Drost, J. *et al.* Sequential cancer mutations in cultured human intestinal stem cells. *Nature* **521**, 43-47 (2015).
84. Girda, E., Huang, E.C., Leiserowitz, G.S. & Smith, L.H. The Use of Endometrial Cancer Patient-Derived Organoid Culture for Drug Sensitivity Testing Is Feasible. *Int J Gynecol Cancer* **27**, 1701-1707 (2017).
85. Maru, Y. *et al.* Establishment and characterization of patient-derived organoids from a young patient with cervical clear cell carcinoma. *Cancer Sci* **110**, 2992-3005 (2019).
86. Chumduri, C., Gurumurthy, R.K., Berger, H., Koster, S., Brinkmann, V., Klemm, U., Mollenkopf, H.-J., Herbst, H., Mangler, M., and Meyer, T.F. Transition of Wnt signaling microenvironment delineates the squamo-columnar junction and emergence of squamous metaplasia of the cervix. *bioRxiv* **443770** (2018).
87. Driehuis, E. *et al.* Pancreatic cancer organoids recapitulate disease and allow personalized drug screening. *Proc Natl Acad Sci U S A* (2019).
88. Yao, Y. *et al.* Patient-Derived Organoids Predict Chemoradiation Responses of Locally Advanced Rectal Cancer. *Cell Stem Cell* **26**, 17-26 e16 (2020).
89. Ganesh, K. *et al.* A rectal cancer organoid platform to study individual responses to chemoradiation. *Nat Med* **25**, 1607-1614 (2019).
90. Driehuis, E. *et al.* Oral Mucosal Organoids as a Potential Platform for Personalized Cancer Therapy. *Cancer Discov* **9**, 852-871 (2019).
91. Ooft, S.N. *et al.* Patient-derived organoids can predict response to chemotherapy in metastatic colorectal cancer patients. *Sci Transl Med* **11** (2019).
92. Cancer Genome Atlas Research, N. *et al.* Integrated genomic characterization of endometrial carcinoma. *Nature* **497**, 67-73 (2013).
93. Neal, J.T. *et al.* Organoid Modeling of the Tumor Immune Microenvironment. *Cell* **175**, 1972-1988 e1916 (2018).
94. Dijkstra, K.K. *et al.* Generation of Tumor-Reactive T Cells by Co-culture of Peripheral Blood Lymphocytes and Tumor Organoids. *Cell* **174**, 1586-1598 e1512 (2018).

95. Salvesen, H.B. *et al.* Integrated genomic profiling of endometrial carcinoma associates aggressive tumors with indicators of PI3 kinase activation. *Proc Natl Acad Sci U S A* **106**, 4834-4839 (2009).
96. Cherniack, A.D. *et al.* Integrated Molecular Characterization of Uterine Carcinosarcoma. *Cancer Cell* **31**, 411-423 (2017).
97. Ducie, J. *et al.* Molecular analysis of high-grade serous ovarian carcinoma with and without associated serous tubal intra-epithelial carcinoma. *Nat Commun* **8**, 990 (2017).
98. Dou, Y. *et al.* Proteogenomic Characterization of Endometrial Carcinoma. *Cell* **180**, 729-748 e726 (2020).
99. Bailey, M.H. *et al.* Comprehensive Characterization of Cancer Driver Genes and Mutations. *Cell* **174**, 1034-1035 (2018).
100. Hashimoto, S. *et al.* Comprehensive single-cell transcriptome analysis reveals heterogeneity in endometrioid adenocarcinoma tissues. *Sci Rep* **7**, 14225 (2017).
101. Roerink, S.F. *et al.* Intra-tumour diversification in colorectal cancer at the single-cell level. *Nature* **556**, 457-462 (2018).
102. Richards, K.F., Bienkowska-Haba, M., Dasgupta, J., Chen, X.S. & Sapp, M. Multiple heparan sulfate binding site engagements are required for the infectious entry of human papillomavirus type 16. *J Virol* **87**, 11426-11437 (2013).
103. Richards, R.M., Lowy, D.R., Schiller, J.T. & Day, P.M. Cleavage of the papillomavirus minor capsid protein, L2, at a furin consensus site is necessary for infection. *Proc Natl Acad Sci U S A* **103**, 1522-1527 (2006).
104. Bernard, B.A. *et al.* The human papillomavirus type 18 (HPV18) E2 gene product is a repressor of the HPV18 regulatory region in human keratinocytes. *J Virol* **63**, 4317-4324 (1989).
105. Gonzalez, S.L., Stremlau, M., He, X., Basile, J.R. & Munger, K. Degradation of the retinoblastoma tumor suppressor by the human papillomavirus type 16 E7 oncoprotein is important for functional inactivation and is separable from proteasomal degradation of E7. *J Virol* **75**, 7583-7591 (2001).
106. Scheffner, M., Werness, B.A., Huibregtse, J.M., Levine, A.J. & Howley, P.M. The E6 oncoprotein encoded by human papillomavirus types 16 and 18 promotes the degradation of p53. *Cell* **63**, 1129-1136 (1990).
107. Yucer, N. *et al.* Directed Differentiation of Human Induced Pluripotent Stem Cells into Fallopian Tube Epithelium. *Sci Rep* **7**, 10741 (2017).



CHAPTER

2

ASSESSING THE ORIGIN OF HIGH- GRADE SEROUS OVARIAN CANCER USING CRISPR-MODIFICATION OF MOUSE ORGANIDS

Kadi Löhmuusaar^{1,2,*}, Oded Kopper^{1,2,*}, Jeroen Korving^{1,2},
Harry Begthel^{1,2}, Celien P. H. Vreuls³,
Johan H. van Es^{1,2}, Hans Clevers^{1,2}

¹Hubrecht Institute, Royal Netherlands Academy of Arts and Sciences
and UMC Utrecht, Utrecht, The Netherlands

²Oncode Institute, Utrecht, The Netherlands

³Department of Pathology, UMC Utrecht, Utrecht, The Netherlands.

*These authors contributed equally to this work

ABSTRACT

High-grade serous ovarian cancer (HG-SOC) – often referred to as a “silent killer” – is the most lethal gynaecological malignancy. The fallopian tube (murine oviduct) and ovarian surface epithelium (OSE) are considered the main candidate tissues of origin of this cancer. However, the relative contribution of each tissue to HG-SOC is not yet clear. Here, we establish organoid-based tumor progression models of HG-SOC from murine oviductal and OSE tissues. We use CRISPR-Cas9 genome editing to introduce mutations into genes commonly found mutated in HG-SOC, such as *Trp53*, *Brca1*, *Nf1* and *Pten*. Our results support the dual origin hypothesis of HG-SOC, as we demonstrate that both epithelia can give rise to ovarian tumors with high-grade pathology. However, the mutated oviductal organoids expand much faster *in vitro* and more readily form malignant tumors upon transplantation. Furthermore, *in vitro* drug testing reveals distinct lineage-dependent sensitivities to the common drugs used to treat HG-SOC in patients.

INTRODUCTION

High-grade serous ovarian cancer (HG-SOC) is the most prevalent and aggressive gynecological malignancy that accounts for 70-80% of ovarian cancer mortalities¹. Most ovarian cancer patients are diagnosed at a late stage, when the tumor has already metastasized throughout the abdominal cavity. As a result, the early stages of tumor development are not well characterized.

For years, it was believed that HG-SOC originates from the ovarian surface epithelium (OSE), which actively participates in the cyclical ovulatory rupture and repair processes². It was assumed that the inflammatory environment induced by these processes exposed the OSE cells to oxidative stress and caused cell damage that could consequently lead to the accumulation of deleterious somatic mutations³. However, failure to identify HG-SOC precursor lesions in the OSE has led to the hypothesis that these carcinomas either arise *de novo*, without an intermediary lesion from epithelial inclusion cysts, or derive from an extra-ovarian source altogether.

Accumulating findings have shifted the focus away from the OSE towards the fimbria of the fallopian tube (FT). One of the first indications that suggested the FT as a possible origin of ovarian cancer were the lesions that were identified in the FT of high-risk patients carrying BRCA1/2 germline mutations⁴⁻⁶. These lesions, that are now referred to as serous tubal intraepithelial carcinomas (STICs), were found to carry mutations in the *TP53* gene, as present in almost all cases of HG-SOC (96%)^{7, 8}.

To study the potential of the OSE and FT to transform into HG-SOC, several models have been established. Studies with immortalized OSE cell lines as well as intrabursally administered viral particles that induce site-specific mutagenesis have been used to show the capability of OSE cells to generate different types of ovarian tumors in mice⁹⁻¹³. Mouse models that enable targeted mutagenesis in oviduct epithelium (the equivalent of human FT) via the use of tissue-specific gene promoters (such as *Pax8* or *Ovgp1*) have shown the ability of oviductal cells to transform into ovarian tumors¹⁴⁻¹⁶. Additionally, several transcriptomic and proteomic analyses of human HG-SOC tissue support the dual origin of HG-SOC¹⁷⁻²². Yet, until now a direct comparison between the relative potential of oviduct and OSE to contribute to HG-SOC development has not been performed. Understanding the early stages of HG-SOC development and its tissue of origin is crucial for the design of early diagnosis and preventive strategies, especially for high risk individuals such as women with *BRCA1* and *BRAC2* germline mutations.

Comparable HG-SOC models to study the tumor origin of OSE and FT in parallel have not been developed. In this study, we apply an organoid platform that enables a direct comparison of the two tissues of interest and, through *in vitro* engineering approach, elucidate their respective susceptibility to the disease.

1

2

3

4

5

&

RESULTS

Derivation of organoids from murine oviduct and OSE

To derive long-term organoid cultures, mouse oviduct and OSE tissues were dissected, subjected to different enzymatic treatments, embedded in basement membrane extract (BME) and cultured in appropriate media (Figure 1a and Supplementary Data 1). Using this protocol, oviduct and OSE cystic organoid formation was observed within 1-2 weeks following isolation (Figure 1a).

It was previously shown that *Lgr5*, a key player in the WNT signaling pathway, marks stem cells of the murine OSE^{23, 24}, and that estrogen plays a stimulatory effect on OSE growth and proliferation²⁵. In line with these observations, we found that OSE organoid growth is dependent on the addition of WNT protein to the medium, while oviduct organoids are not (Figure 1b). The fact that oviductal cultures were not dependent on the addition of exogenous WNT suggests that these organoids either do not need active WNT signaling to grow or they produce their own WNT and, thus, are able to maintain growth through paracrine or autocrine WNT signaling. To rule out the latter, we exposed oviductal organoids to the IWP2 porcupine inhibitor which inhibits WNT O-acylation and secretion. IWP2 did not exert an inhibitory effect on oviductal organoid growth, confirming their WNT-independence (Figure 1b). To avoid introducing additional variability to the analysis by culturing the lines in different media, oviductal and OSE organoids were both cultured in WNT- and Estrogen-containing medium, unless stated otherwise. Oviductal and OSE organoid lines can both be expanded long-term (> 1 year) while maintaining normal numbers of chromosomes, as demonstrated by metaphase spread analysis (Figure 1c).

Oviductal and OSE organoids show distinct characteristics

The endogenous oviduct is a monolayered epithelium that contains two main cell types, namely secretory and ciliated cells. In contrast, the OSE has no ciliated cells and is comprised of a monolayer of squamous-to-cuboidal epithelial cells²⁶. Both oviductal and OSE organoids show cystic monolayered organoid growth, recapitulating the epithelium of tissues they were derived from (Figure 1a-b). In order to compare the oviductal and OSE organoid lines more thoroughly, we performed RNA-sequencing (RNA-seq) analysis of parental tissues and organoid lines. Hierarchical clustering of the 500 most significantly differentially expressed genes between the oviductal and OSE organoid groups shows that oviductal organoids cluster together with the oviduct tissue and separate from the OSE organoids, which cluster with the OSE tissue (Figure 2a). Importantly, our RNA-seq analysis allowed us to confirm the expression of several genes known to be specifically expressed in oviductal secretory (*Pax2*, *Pax8*, *Ovgp1*) and ciliated cells (*Dnali1*, *Foxj1*) in our oviductal organoids and tissues (Figure 2b). These genes were largely absent in the OSE counterpart with the exception of oviductal secretory cell marker *Pax8* which was also found to be expressed in OSE organoids but not in the OSE tissue (Figure 2b). Significant enrichment

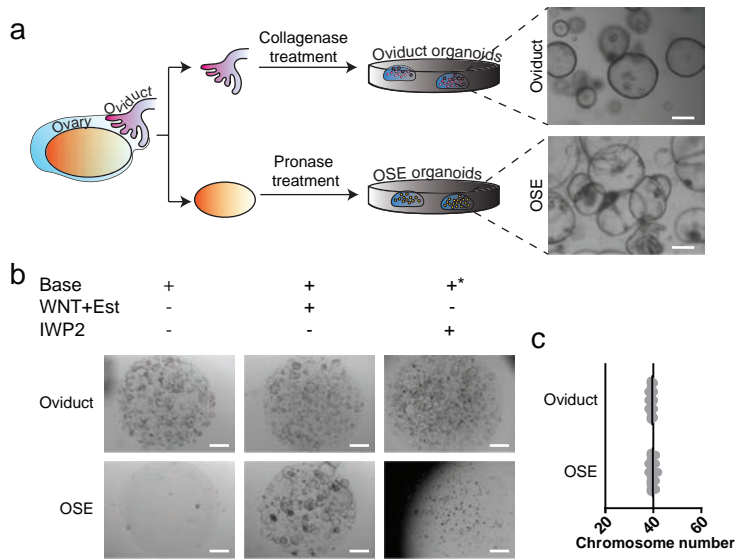


Figure 1. Derivation of organoids from murine oviduct and OSE. (a) For organoid derivation oviducts and ovaries were separated and subjected to collagenase or pronase treatment, respectively. The representative brightfield images of both organoid cultures are shown. Scale bar, 200 μ m. The organoid derivation was reproducible over 4 independent experiments. (b) Basic medium requirement of oviductal and OSE organoids. OSE organoids are WNT-dependent. Representative images from n=3 independent experiments. Est – Estrogen, IWP2 – inhibitor of WNT protein 2, asterisk - in the WNT inhibitor conditions Rspo1 is withdrawn from the base medium. Scale bar, 2 mm. (c) Scatter plot presenting chromosome number distribution and mean of 3 independent lines, based on organoid metaphase spreads (20 spreads per line, 3 biological replicates, n=60). Both wild-type organoid lines sustain healthy karyotype during culturing.

of motile cilium assembly genes in oviductal organoids was also confirmed by Gene Set Enrichment Analysis (GSEA) (Figure 2c).

Previously, it has been established that *Pax8*-expressing secretory cells can serve as progenitor cells for ciliated cells and inhibition of NOTCH pathway has been shown to play a role in inducing ciliogenesis^{27, 28}. To assess the differentiation potential of the *Pax8*-expressing cells in our organoids, we treated both organoid lineages with the gamma-secretase complex inhibitor (DAPT). Consistent with their origin, oviductal organoids showed increased expression of ciliated cell markers upon NOTCH inhibition (Figure 2d). Furthermore, the ciliated cells in oviductal organoids possessed beating cilia, confirming their functionality (Supplementary Video 1). In contrast, OSE organoids treated with DAPT did not form ciliated cells (Figure 2d).

To characterize the oviductal and OSE organoids at the cell level, we performed immunohistochemical stainings for the epithelial marker, CK8, the secretory cell marker, PAX8, and the ciliated cell marker, acetylated α -tubulin (Figure 2e-f). Both oviductal and OSE organoids were uniformly positive for CK8, confirming their epithelial origin

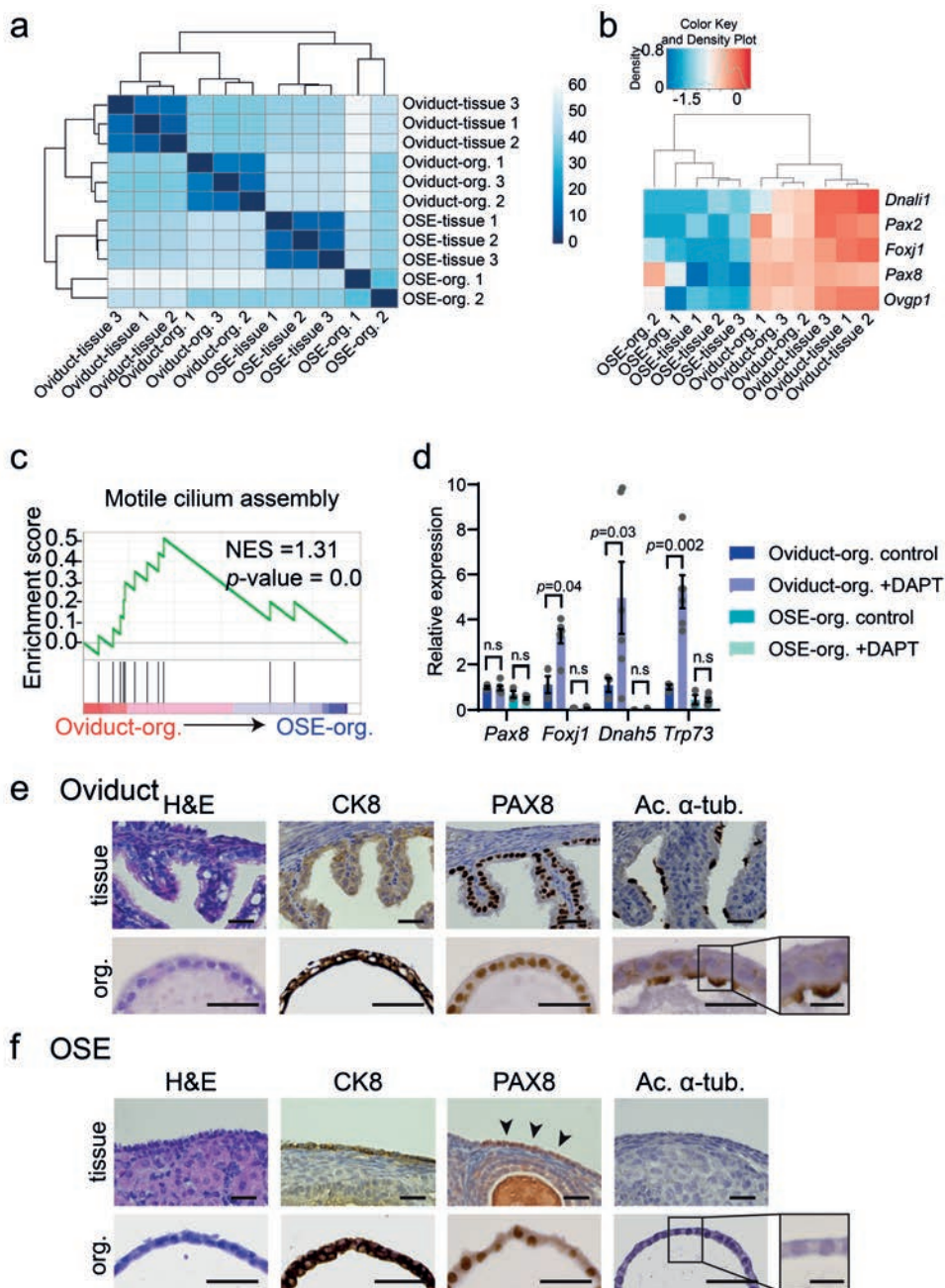


Figure 2. Characterization of healthy oviductal and OSE organoids. (a) Sample-to-sample heatmap showing the Euclidean distances between the organoids and parental bulk tissues as calculated from the regularized log transformation. Correlation is based on the top 500 differentially expressed genes between the organoid lines and the pseudocolor scale shows hierarchical distance from minimum (0, dark blue) to maximum (60, white). (b) Heatmap depicting known oviductal marker genes and their expression in the oviductal and OSE organoids and tissues. (c) Gene set

- enrichment analysis (GSEA) showing strong enrichment of genes involved in motile cilium assembly in oviductal organoids compared to OSE organoids. NES: normalized enrichment score, *p*-value is a permutation-based *p*-value that is computed and corrected for multiple testing (n=3 oviductal and n=2 OSE biologically independent organoid lines for each group). (d) qPCR results showing upregulation of selected genes (*Foxj1*, *Dnah5*, *Trp73*) involved in ciliogenesis in oviductal organoids upon treatment with NOTCH pathway inhibitor (DAPT) for 2 weeks. Assay was performed in n=3 biologically independent replicates over three independent experiments. Error bars represent \pm SEM. Statistical significance was calculated by two-tailed Student's t-test, n.s – not significant. (e) Histological stainings of oviduct tissue and corresponding organoids (n=4 independent experiments). The organoids are positive for epithelial marker CK8 and show presence of both PAX8-positive secretory and acetylated α -tubulin-positive ciliated cells. Scale bar, 25 μ m; scale bar of inset, 10 μ m. (f) Histological stainings of OSE tissue and corresponding organoids (n=4 independent experiments). OSE-derived organoids are positive for CK8 and PAX8, but lack ciliated cells. Scale bar, 25 μ m; scale bar of inset, 10 μ m. (a-f) Org. – organoids.

(Figure 2e-f). The presence of both secretory and ciliated cell types in oviductal organoids and tissues were confirmed by positive stainings for PAX8 and cilia (Figure 2e). As revealed from RNA-seq analysis, OSE organoids also express the well-acknowledged oviductal secretory cell marker PAX8 (Figure 2b, 2f). OSE tissue is largely PAX8-negative, however, rare PAX8-positive areas can be found in OSE lining and have been reported before (Figure 2f, arrow heads)^{29, 30}. Altogether, characterization of oviductal and OSE organoids revealed distinct gene expression patterns that were consistent with their respective tissue of origin.

Generating murine organoid models for HG-SOC development

According to the current tubal HG-SOC development model³¹, mutations in the *TP53* gene, which are found in about 96% of cases, are considered an early event in tumor development, and can lead to “p53 signature” lesions, i.e. a linear stretch of cells that stain for mutant p53^{31, 32}. Upon accumulation of additional mutations, these lesions can gain proliferative capacity and generate serous tubal intraepithelial carcinomas^{33, 34}, also known as STICs, which then progress to invasive carcinoma. In addition to p53, the PI3K/RAS and homologous recombination (HR) pathways are commonly altered in HG-SOC (45% and 51% of cases, respectively)⁷. To establish *in vitro* oviduct and OSE tumor development models, we utilized CRISPR-Cas9 technology to target the murine *Trp53* gene alone or in combination with *Brca1*, *Pten*, and *Nf1* (Figure 3a-b). These genes are recurrently mutated in human HG-SOC^{7, 35}.

We derived oviductal and OSE organoids from mice carrying a *Cas9-P2A-EGFP* expression cassette knocked into the ROSA26 locus, such that Cas9 and enhanced green fluorescent protein (EGFP) are expressed ubiquitously (Figure 3a)³⁶. Organoids were transfected with up to 3 different sgRNAs targeting the aforementioned genes, and then cultured for two weeks in the presence of Nutlin-3a to select for mutated *Trp53* cells³⁷ (Figure 3a). Surviving organoids were picked, clonally expanded, and their mutation

1

2

3

4

5

&

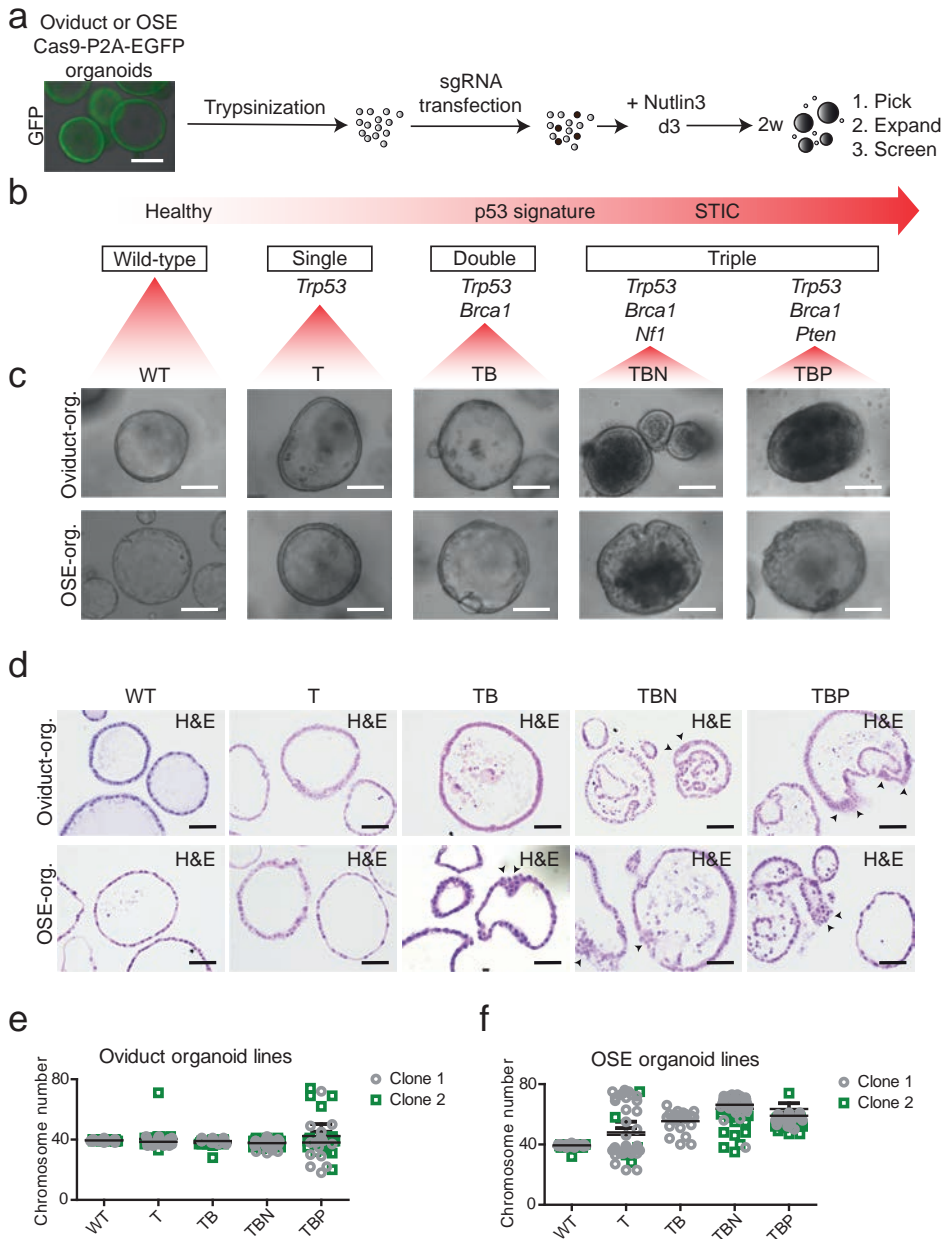


Figure 3. CRISPR-modification of oviductal and OSE organoids. (a) Strategy to generate the mutant lines using CRISPR-Cas9. The lines were trypsinized to single-cell suspension followed by sgRNA transfection. Three days after transfection Nutlin-3a was added to the medium to allow mutant *Trp53* organoid outgrowth. In 2 weeks emerging clonal organoids were picked, expanded and screened. Scale bar, 200 μ m. (b) Hypothesized tumor progression model of HG-SOC and chosen genes to build comparable progression models. STIC – serous tubal intraepithelial carcinoma. (c) Brightfield images of comparable clones with different set of mutations from both oviductal and OSE organoid. Scale bar, 100 μ m. (d) Immunohistochemical stainings for H&E to visualize the more detailed

- phenotype of oviductal and OSE clones. Arrow heads point to the cellular stratification. Scale bar, 50 μ m. (c-d) Org. – organoids. (e-f) Scatter plots presenting chromosome number distribution and mean of (e) oviduct wild-type and mutant clones or (f) OSE wild-type and mutant clones, based on organoid metaphase spreads (n=20 spreads per biologically independent clones). (c-e) WT – wild-type, T – *Trp53* mutant; TB – *Trp53*, *Brca1* mutant; TBN – *Trp53*, *Brca1*, *Nf1* mutant; TBP – *Trp53*, *Brca1*, *Pten* mutant.

composition was analysed by targeted sequencing. We established clonal oviductal and OSE organoid lines containing single (*Trp53*; T), double (*Trp53/Brca1*; TB) and triple (*Trp53/Brca1/Pten*; TBP or *Trp53/Brca1/Nf1*; TBN) gene knockouts (Figure 3b-c, Supplementary Figure 1a-b). *Trp53* loss in single and double mutants was confirmed by Western blot analysis (Supplementary Figure 1c) and all the mutants were resistant towards Nutlin-3a treatment compared to the respective wild-types (WT) (Supplementary Figure 1d).

To achieve loss of function mutations, sgRNAs were designed to target promoter-proximal exons of the genes of interest (Supplementary Figure 1a) and, with the exception of *Brca1* sgRNAs, all the sgRNAs exhibited $\geq 50\%$ targeting efficiency in organoids as calculated by the number of targeted clones that survived in Nutlin-3a selection (Supplementary Figure 1a). *Brca1* sgRNAs showed a much lower efficiency, as only 15% of screened clones had been targeted by the sgRNA (Supplementary Figure 1a). Not only was the *Brca1* gene difficult to target, but we could also never obtain clones in which both alleles of *Brca1* carried out-of-frame mutations (i.e. completely knocked out), even on the background of *Trp53* mutation. Statistically, the observed targeting frequencies for *Brca1* locus do not fit with the expected frequencies as calculated based on our knowledge as to how the single allele is targeted (Supplementary Data 2). This suggests homozygous lethality of *Brca1*-null mutations in our rapidly dividing organoid systems. We performed a double-strand break (DSB) assay to test whether mutating a single allele of *Brca1* is sufficient to sensitize the cells to double-strand breaks. The heterozygous *Brca1*-mutants displayed significantly higher number of phosphorylated histone γ H2A.X-positive cells upon treatment with the genotoxic agent Mitomycin C, confirming the presence of DSB repair defect in those clones (Supplementary Figures 2a-c) and supporting haploinsufficiency of *Brca1* as previously reported³⁸. We were successful in targeting all remaining genes of interest and created complete knock-outs of these genes. Genetically modified organoids were derived from both oviductal and OSE origins with two independent clones for each combination of mutations. All the clones and their mutations are summarized in the tables under the Supplementary Figure 1b.

Next, we characterized the lines more thoroughly by examining the differences in the histological, proliferative and apoptotic properties of the clones. Single (T) and double (TB) mutant organoids from both origins did not show any apparent morphological change in culture, whereas the triple mutants (TBN and TBP) from both origins displayed a denser and folded appearance (Figure 3c). This morphological difference was confirmed by hematoxylin and eosin (H&E) stainings where the triple mutants exhibited more

1

2

3

4

5

&

irregular shapes and cellular stratification (Figure 3d). In order to study the effect of different mutations on organoid growth speed, we closely monitored the expansion of the organoids by measuring the size of the organoids daily for a week (Supplementary Figure 2d-e). In the oviductal lineage, we observed that all the mutation combinations induced significantly faster growth rate of the clones compared to the corresponding WT organoids (Supplementary Figure 2d). In contrast, the growth rate of the OSE clones was largely unaffected upon introduction of mutations, with an exception of OSE-TBN and OSE-TBP lines that showed slightly higher or lower growth rate compared to the WT, respectively (Supplementary Figure 2e). We also evaluated whether the levels of apoptosis differed between the lineages and the individual mutants. In oviduct-derived organoids, we observed a decrease in apoptosis upon introduction of mutations with the triple mutants possessing the least amount of apoptotic cells (Supplementary Figure 2f). In contrast, in the OSE-derived organoids the effect appeared to be reversed as the triple mutants displayed more apoptotic cells than the single or double mutants (Supplementary Figure 2f).

One of the hallmarks of HG-SOC is extensive chromosomal instability^{7, 8}. To evaluate the genomic stability of the mutant organoids, we performed metaphase spread analysis approximately 8 weeks after clonal selection of the single, double, and triple mutant clones (Figure 3e-f). As expected, WT organoids from both origins displayed normal chromosome numbers (Figure 3e-f). Aberrant chromosome numbers in genetically modified oviduct organoids were observed only in the TBP triple mutants (Figure 3e), demonstrating the differential effect of the distinct mutated gene sets. Strikingly, in genetically modified OSE organoids, chromosomal abnormalities were already evident following a single knockout of the *Trp53* gene and were observed in double and triple mutant organoids as well, suggesting tissue-specific effects of *Trp53* mutation (Figure 3f). Similarly to the OSE organoids, induction of extensive chromosomal abnormalities upon a single *Trp53* mutation has been observed before in human intestinal organoids³⁹.

Oviductal and OSE organoids show differential drug responses

We evaluated the drug sensitivity of our mutants to a set of chemotherapy regimens commonly used for HG-SOC treatment in patients, including cisplatin, paclitaxel and niraparib (PARP-inhibitor). Both, paclitaxel and niraparib revealed differential sensitivities between the various mutant organoid sets derived from the two lineages (Figure 4a-d). In the oviductal lineage, the lines were generally more sensitive to paclitaxel (Figure 4a) and niraparib (Figure 4c) upon acquiring more mutations. In contrast, in OSE lineage, the mutant lines were less sensitive to paclitaxel (Figure 4b) and niraparib (Figure 4d) compared to the WT line. As an exception, in the case of niraparib treatment, we noticed that the TBP triple mutants from both lineages behave differently from other mutants, showing the least sensitivity to the drug (Figure 4c-d). It has been reported before that *Pten* mutation in the combination with *Brca1* mutation induces reversion in PARP-inhibitor

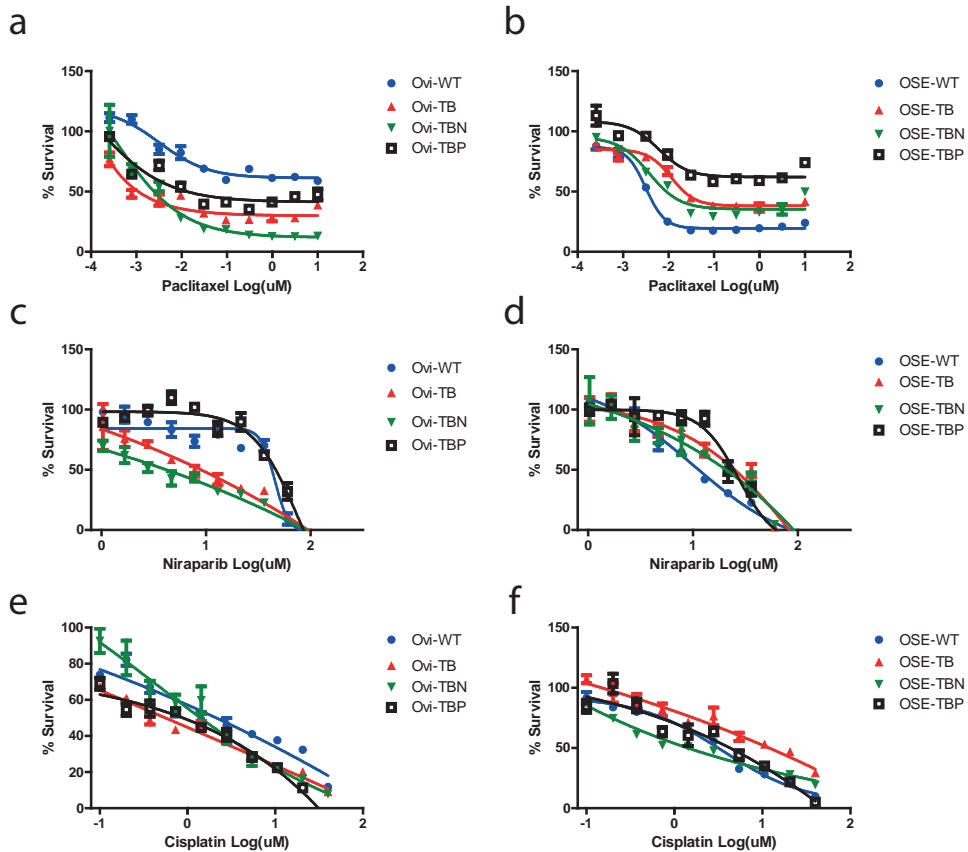


Figure 4. *In vitro* drug sensitivity of oviductal and OSE lines. (a-b) Representative dose response curves of paclitaxel-treated (a) oviductal and (b) OSE clones. (c-d) Representative dose response curves of niraparib-treated (c) oviductal and (d) OSE clones. (e-f) Representative dose response curves of cisplatin treated (e) oviductal and (f) OSE clones. (a-f) Error bars represent \pm SEM of quadruplicates ($n=4$) over 2 independent experiments. Ovi – oviduct; WT – wild-type; TB – *Trp53*, *Brca1* mutant; TBN – *Trp53*, *Brca1*, *Nf1* mutant; TBP – *Trp53*, *Brca1*, *Pten* mutant.

sensitivity⁴⁰. Our data supports the finding. We did not observe distinct effects within mutants with the exposure to the common platinum-based drug, cisplatin (Figure 4e-f).

Taken together, our data suggests that, dependent on their origin, the mutants show differential response to the two commonly used chemotherapeutic agents, which further substantiates the need to study the different sites of origin for HG-SOC more thoroughly.

Tumorigenic potential of oviduct- and OSE-derived organoids

To assess their tumorigenic capacity, the genetically modified and WT organoids were orthotopically or subcutaneously transplanted into immunodeficient mice (Figure 5a and Supplementary Data 3-4). As expected, none of the subcutaneously or orthotopically transplanted WT or *Trp53* single mutant organoids gave rise to tumors in either lineage

1

2

3

4

5

&

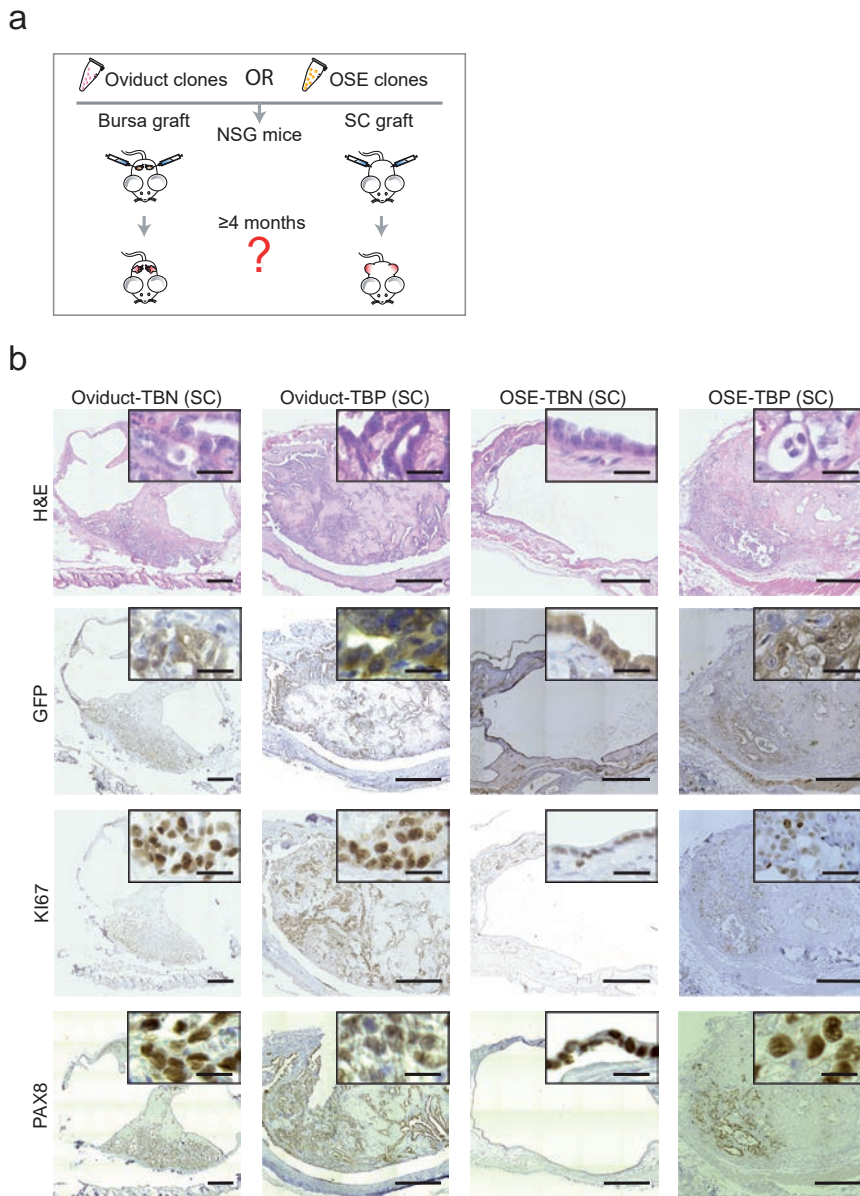


Figure 5. Both origins are able to give rise to HG-SOC-like tumors. (a) Transplantation strategy. The clones were transplanted either subcutaneously or orthotopically into the bursa of immunodeficient mice and tumor formation was assessed up to 4 months after organoid injections. Each mouse received two injections with the same clone into the opposite flanks or bursal cavities (n=2 injections/mouse). **(b)** Representative histological overview and close-up images of subcutaneous tumors derived from transplantations with different triple mutant oviductal (n=12 tumors) and OSE (n=7 tumors) clones. H&E, GFP, Ki67 and PAX8 stainings are shown. Scale bar, 25 μ m. SC – subcutaneous; TBN – *Trp53*, *Brca1*, *Nf1* mutant; TBP – *Trp53*, *Brca1*, *Pten* mutant.

Table 1. Summary table of transplantation outcomes with oviductal and OSE organoids.

Origin	Clone	No. of injected cells	Orthotopic tumor take	Subcutaneous tumor take
Oviduct	WT	ca 100 000	0/6 (0%)	0/2 (0%)
OSE	WT	ca 100 000	0/6 (0%)	0/2 (0%)
Oviduct	T	ca 100 000	0/8 (0%)	0/4 (0%)
OSE	T	ca 100 000	0/8 (0%)	0/4 (0%)
Oviduct	TB	ca 100 000	0/8 (0%)	2/4 (50%)
OSE	TB	ca 100 000	0/6 (0%)	0/4 (0%)
Oviduct	TBN	ca 100 000	11/12 (92%)	6/6 (100%)
OSE	TBN	ca 100 000	0/8 (0%)	5/8 (63%)
Oviduct	TBP	ca 100 000	12/12 (100%)	6/6 (100%)
OSE	TBP	ca 100 000	0/8 (0%)	2/4 (50%)

Footnotes: WT – wild-type, T – *Trp53* mutant; TB – *Trp53, Brca1* mutant; TBN – *Trp53, Brca1, Nf1* mutant; TBP – *Trp53, Brca1, Pten* mutant.

(Table 1). In two cases (50% success rate, n=4) tumor growth was observed following the subcutaneous oviduct-TB organoid transplantations, showing the potential of double mutants to acquire tumorigenic potential *in vivo* (Table 1). However, no tumor growth was observed with comparable OSE-TB organoids, irrespective of the transplantation method. Next, when genetically modified triple mutant organoids were orthotopically transplanted, both TBN and TBP oviduct triple mutant organoids formed tumors (92% success rate, n=12 and 100% success rate, n=12, respectively) (Table 1). In contrast, despite carrying the same oncogenic mutations, none of the orthotopically transplanted OSE organoids gave rise to tumors, including the TBN and TBP triple mutants (Table 1).

When the genetically modified organoids were subcutaneously transplanted, both TBN and TBP oviduct triple mutant organoids developed into tumors (100% success rate, n=6 and 100% success rate, n=6, respectively) (Table 1). Surprisingly, although TBN and TBP OSE-derived triple mutants were not able to form tumors following orthotopic transplantations, they did form tumors after subcutaneous transplantations with 63% (n=8) and 50% (n=4) success rate, respectively (Table 1). Taken together, these results indicate that both oviductal epithelium as well as OSE can give rise to ovarian tumors. However, the inability for the OSE lineage to do so at the orthotopic site in the given time frame (4 months) suggests that tumors from OSE arise with slower kinetics.

Further analysis of the mice that were injected with WT, single (T), double (TB) or triple (TBN/TBP) mutant organoids that did not develop tumors revealed minute non-proliferative cystic remnants of the transplantations (Supplementary Figure 3a), confirming the success of the organoid transplantations and highlighting their benign nature. Taken together, although both oviduct and OSE organoids can give rise to ovarian tumors, oviduct-derived organoids appear to hold considerably higher tumorigenic potential.

1

2

3

4

5

&

Next, tumors were isolated and their histological properties were analysed. H&E staining analysis revealed two distinct phenotypes: cystic (n=18) and solid tumors (n=26) (Figure 5b, Supplementary Figure 3b-c, Supplementary Data 3-4). These phenotypes had no apparent correlation with the tissue of origin nor transplantation site. To distinguish organoid-derived tumor cells from the recipient normal mouse cells, tumors were stained with an anti-GFP antibody which confirmed that the tumors originated from the transplanted clones (Figure 5b, Supplementary Figure 3b-c). Interestingly, in a subset of solid tumors this staining revealed a population of GFP-positive cells with mesenchymal features that surrounded glandular tumor structures (Supplementary Figure 3b), indicating the occurrence of an epithelial-to-mesenchymal transition (EMT).

All tumors from either origin ubiquitously stained for PAX8 (Figure 5b) – a well-known marker for HG-SOC, with the exception of solid tumors that consisted of both glandular and mesenchymal like tumor cells (Supplementary Figure 3b). In these tumors only the glandular structures were positively stained for PAX8, and were surrounded by PAX8-negative mesenchymal-like cells, suggestive of involvement of EMT in *Pax8* downregulation (Supplementary Figure 3b). Mesenchymal features and EMT are often associated with tumor metastasis. Indeed, all oviduct-derived orthotopic tumors displayed abdominal wall metastases (Supplementary Figure 3d).

Oviduct-derived tumors were generally more proliferative as shown by bigger tumor sizes (Supplementary Figure 3e) and higher KI67 labeling index (Supplementary Figure 3f, Figure 5b). As a result of the more proliferative tumor growth, the oviductal tumors also displayed significantly higher number of apoptotic cells as quantified from the cleaved Caspase-3 stainings in the tumors (Supplementary Figure 3g). As determined by a certified pathologist, solid tumors from both oviductal and OSE origins displayed histologically human HG-SOC-like features, including glandular growth and serous papillary structures. However, the cystic tumor histology we observed was atypical to HG-SOCs (Figure 5b, Supplementary Figure 4a). Nevertheless, the cystic tumors showed no mucinous architecture or presence of conspicuous cilia, excluding the diagnosis of benign mucinous borderline tumor or serous borderline cystadenoma, respectively, and displayed malignant features such as abundant mitotic figures, pleomorphism and nuclear atypia suggestive of malignant type of ovarian carcinoma (Figure 5b, Supplementary Figure 4a-c).

Oviduct tumor-derived organoids recapitulate tumor evolution

As described previously, we occasionally observed that the oviductal solid tumors displayed two distinct morphologies: glandular epithelial (epi) or mixed epithelial-mesenchymal-like (mes) phenotype. However, the tumor morphology was not a clone-dependent feature as the same triple mutant oviductal clone could give rise to both histopathological appearances at adjacent locations. As an example, we injected oviduct-TBP mutant organoids subcutaneously into the left and right flanks of the immunodeficient mice (Figure 6a). Visible tumors grew on both sides of the mice and subsequent

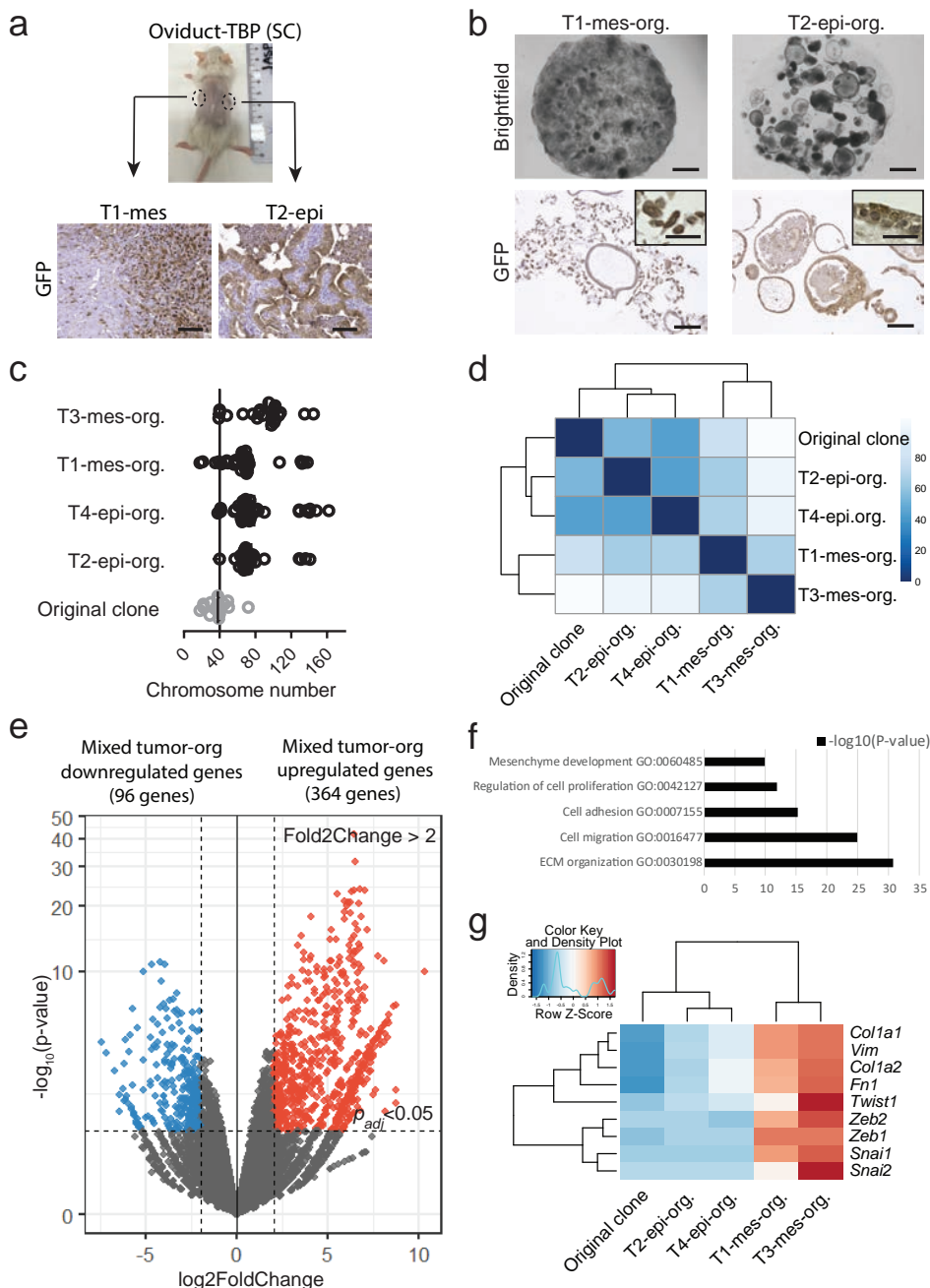


Figure 6. Oviduct tumor-derived organoids recapitulate tumor evolution. (a) Representative image of a mouse showing left and right side subcutaneous tumors derived from oviduct-TBP clone injection. Distinct histological phenotype of two adjacent subcutaneous tumors (labelled as T1-mes and T2-epi according to the histological phenotype) injected with the same oviduct-TBP clone. GFP stainings are shown (n=4 tumors observed). Scale bar, 100 μm . (b) Brightfield images (top) as well as GFP-stainings (bottom) of T1- mes and T2-epi tumor-derived organoid cultures ▶

► (labelled as T1-mes-org. and T2-epi-org., org. – organoids). Brightfield image scale bar, 2 mm. GFP-stained image scale bar, 100 μm ; inset scale bar, 25 μm). (c) Scatter plot presenting chromosome number distribution and mean of oviduct-TBP original clone and resulting 4 independent tumor-derived organoid lines (labelled as T1-mes-org., T2-epi-org., T3-mes-org. and T4-epi-org., org. – organoids), n=20 spreads per biologically independent clone. (d) Sample-to-sample heatmap showing the Euclidean distances between the original oviduct-TBP clone and the resulting tumor-derived organoids as calculated from the regularized log transformation. Correlation is based on all the differentially expressed genes in the dataset and the pseudocolor scale shows hierarchical distance from minimum (0, dark blue) to maximum (100, white). (e) Volcano plot of RNA expression comparison between the organoids derived from epithelial (n=2) and epithelial-mesenchymal tumors (n=2). Red: significantly upregulated genes ($\log_2\text{FoldChange} > 2$, $p_{\text{adj}} < 0.05$) in organoids with mixed epithelial-mesenchymal phenotype. Blue: significantly downregulated genes ($\log_2\text{FoldChange} < -2$, $p_{\text{adj}} < 0.05$) in organoids with mixed epithelial-mesenchymal phenotype. (f) Significantly enriched biological processes in mixed epithelial-mesenchymal cultures. (g) Heatmap showing up-regulation of selected EMT-related genes in organoids that were derived from tumors displaying mesenchymal phenotype.

histopathological examination revealed that some mice developed tumors that displayed distinct morphologies at adjacent subcutaneous injection sites (Figure 6a).

To determine whether these morphological differences could be recapitulated in the culture system, we derived independent organoid lines from four distinct-looking oviductal tumors (2 epi- and 2 mes-like tumors). To specifically select for the growth of the tumor-derived cells, organoids were derived and grown in Nutlin-3a supplemented medium (Figure 6b). Consistent with the differential tumor histotypes we observed *in vivo*, we found remarkable differences between the organoids derived from these tumors (Figure 6b). The mesenchymal-like tumors gave rise to the mixed-like organoid cultures (T1-mes-org. and T3-mes-org.) that contained both cystic epithelial organoids as well as fibroblast-like cells (Figure 6b). All cells expressed GFP, confirming that they were derived from the same original oviductal TBP clone (Figure 6b). In contrast, the organoid cultures (T2-epi-org. and T4-epi-org.) derived from the glandular subcutaneous tumors resulted in the GFP-positive organoids that were uniformly epithelial and had no detectable fibroblast-like component, recapitulating the parental tumors (Figure 6b). Subsequent metaphase spread analysis revealed that all the four tumor-derived organoid lines had acquired more widespread chromosomal abnormalities compared to the original clone, likely reflecting the tumor cell evolution *in vivo* (Figure 6c).

Next, we analysed gene expression patterns of these four independent organoid lines that were derived from mesenchymal- and epithelial-like tumors (Figure 6d). Gene expression analysis revealed that the cultures that displayed uniform epithelial phenotype (T2-epi-org. and T4-epi-org.) clustered together with the original oviductal TBP clone, whereas the mixed tumor-derived cultures (T1-mes-org. and T3-mes-org.) formed a separate group (Figure 6d).

To determine biological pathways and patterns enriched in the mixed-type tumor-derived organoids, we performed comparison between the organoids derived from

the distinct types of tumors (Figure 6e). Among the 364 genes upregulated in the mixed-type organoids (Figure 6e), there was a significant enrichment for the biological processes related to the extracellular matrix (ECM) organization, cell migration, cell adhesion, cell proliferation and mesenchyme development (Figure 6f). More detailed gene expression analysis revealed that, in compliance with the epithelial-mesenchymal phenotype, the mixed-type organoid cultures showed upregulation of several EMT-related genes (e.g. *Vim*, *Twist1* and *Zeb1/2*) compared to the original clone, while non-mesenchymal tumor derivatives largely lacked the expression of such genes (Figure 6g).

Oviductal tumors resemble the molecular subtypes of HG-SOC

Four molecular subtypes of human HG-SOC – mesenchymal, immunoreactive, differentiated and proliferative – have been previously identified^{7, 41}. We therefore sought to analyse to what extent our tumors resembled human molecular subtypes. As the majority of the OSE-derived tumors were too small for saving a material for anything beyond histological analysis, we performed RNA-sequencing on 6 of the oviductal TBP clone-derived tumors (labelled as Tumor 1-6) to assess whether these tumors, originating from the same genetic background (i.e. TBP mutants), show a resemblance to any of the previously identified molecular subtypes of HG-SOC. Hierarchical clustering analysis including oviductal WT organoids, TBP mutants and the 6 independent oviductal TBP clone-derived tumors assigned the organoids and the tumor tissues into two separate clusters (Figure 7a). Interestingly, the 6 tumors mapped to a single branch, but were then further divided into two main clusters (clusters I and II) with the cluster II splitting into two additional subclusters (IIa and IIb) (Figure 7a). Based on this clustering, we performed gene set enrichment analysis with the known signature genes upregulated in all the four human molecular subtypes previously identified⁴². The analysis revealed that while the tumors in cluster I had significant enrichment for the differentiated-like subtype (NES = 1.11, $p = 0.018$), the tumors in clusters IIa and IIb were most similar to the immunoreactive-like subset of HG-SOCs (NES = 1.49, $p = 0.02$ and NES = 1.86, $p = 0.0$, respectively) (Figure 7b). Taken together, this data suggests that murine oviduct organoid-derived tumors are able to give rise to a varied set of human HG-SOC-like tumors as shown by their resemblance to different molecular subtypes.

DISCUSSION

In this study, we employ organoid technology to study the origin of HG-SOC. The current consensus in the field states that the fallopian tube is the main origin for HG-SOC. However, accumulating evidence indicates that ovarian surface epithelium might also give rise to a smaller subset of tumors¹⁷⁻²². To document the possible relative contributions of both hypothesized origins to HG-SOC, we have established 3D murine organoid cultures from both lineages to model the disease. Organoids derived from oviduct and OSE show evident differences in their gene expression. Surprisingly, OSE organoids express *Pax8*,

1

2

3

4

5

&

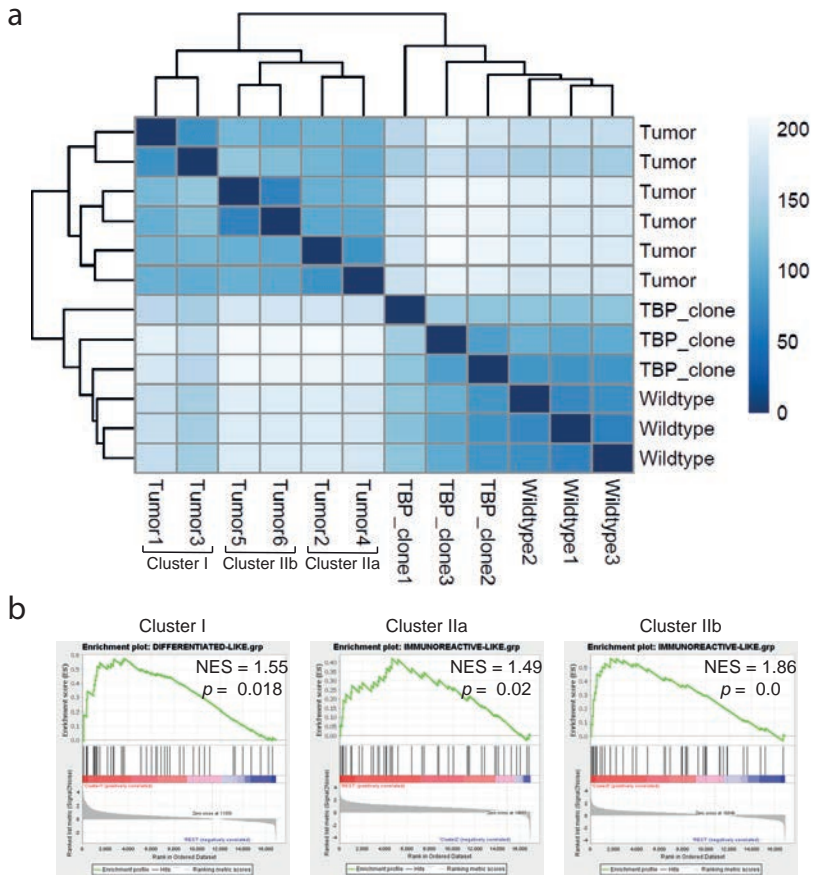


Figure 7. Oviductal tumors resemble the molecular subtypes of HG-SOC. (a) Sample-to-sample heatmap showing the Euclidean distances between the oviductal wild-type organoids, TBP-clones and 6 independent TBP-clone-derived tumor tissues as calculated from the regularized log transformation. Correlation is based on all the differentially expressed genes between the samples and the pseudocolor scale shows hierarchical distance from minimum (0, dark blue) to maximum (200, white). Clustering assigns the tumors into 3 distinct clusters (Cluster I, IIa and IIb). TBP – *Trp53*, *Brca1*, *Pten* mutant. **(b)** GSEA showing strong enrichment for genes characteristic to human differentiated- and immunoreactive-like HG-SOCs in different tumor clusters. NES: normalized enrichment score, p -value is a permutation based p -value that is computed and corrected for multiple testing.

a well-known oviductal secretory cell marker commonly used for the diagnosis of HG-SOCs. This finding suggests that *Pax8* might not serve as straightforward marker for oviduct-derived HG-SOCs as previously thought. Instead, both tissues as well as their organoid-derivatives can express *Pax8*.

Previously, it has been shown that organoid cultures can serve as reliable systems for studying tissues in health^{28, 43, 44} and disease⁴⁵⁻⁴⁷, and for modeling cancer development^{39, 48-51}. During revision of our manuscript, a parallel study was published where

organoids were used to investigate HG-SOC. However, the introduced mutations and targeting constructs were limited to only two genes, *Rb* and *Trp53*⁵². Here, we introduced common HG-SOC mutations into oviductal and OSE organoid cultures, including *Trp53*, *Brca1*, *Nf1* and *Pten*. Surprisingly, we could never obtain a homozygous *Brca1* knock-out in our organoids, yet all the relevant *Brca1* heterozygous mutants displayed deficiency in the homologous recombination pathway. Homozygous knockout of *Brca1* is embryonically lethal^{53, 54}, yet possible in tissue-targeted transgenic models¹⁵. However, the number of targeted cells *in vivo* is much higher compared to our *in vitro* engineering approach which might support the survival of homozygous mutations. Alternatively, the *in vitro* growth medium environment might not support genomically destabilizing mutations such as those in the *Brca1* gene. The mutant clones from the two lineages showed differential genomic stability as well as differential changes in proliferation and apoptosis upon acquiring more mutations. Additionally, distinct lineage-specific response was observed with two common HG-SOC drugs, paclitaxel and niraparib, substantiating the importance of studying the possible dual origin of human HG-SOC.

The contribution of the mutant clones derived from either of the two origins to tumor development was assessed by subcutaneous and orthotopic transplantation assays. Our results demonstrate that both tissues are able to give rise to tumors that recapitulate the histopathology of human HG-SOCs. However, oviductal tumors outperform the OSE tumors by several aspects, such as more successful tumor-derivation and higher proliferation rate. Interestingly, OSE-derived clones were not able to grow as orthotopic tumors, suggesting the presence of regulatory cues that specifically inhibit the survival or proliferation of the OSE, but not the oviductal derivatives, in the bursal environment, despite the similar mutation background. Additionally, our data suggests that the tumors arising from murine oviductal origin are able to genetically resemble distinct molecular subtypes previously identified in human HG-SOCs^{7, 41}.

In conclusion, our model supports the prevalent standpoint in the field that the majority of HG-SOCs arise from the fallopian tube. Albeit, to a lesser extent, OSE is also capable of giving rise to HG-SOC-like tumors. Further research may substantiate these results in a human organoid setting, help identifying novel biomarkers to distinguish OSE- from FT-derived HG-SOCs, and uncover the possible differential clinical behaviors of the tumors from these two origins.

METHODS

Mice

Wild-type *C57BL/6* and *B6J.129(B6N)-Gt(ROSA)26Sor^{tm1(CAG-cas9*,-EGFP)FzhlJ}* (JAX stock #026175)³⁶ mice strains were used for derivation of wild-type and *Cas9/GFP*-expressing organoids, respectively. For mutant organoid transplantations, NOD scid gamma (*NSG; NOD.Cg-Prkdc^{scid} Il2rg^{tm1Wjl}/SzJ*) mice were used. Transplantation experiments were performed after institutional review by the Animal Ethics Committee of the Royal

1

2

3

4

5

&

Netherlands Academy of Arts and Sciences (KNAW) with project license of AVD8010020151 and research protocol HI17.1001.

Human specimens

The patient tumor material was collected from consenting patients undergoing surgical resection at the University Medical Centre (UMC) Utrecht Hospital. Tissue collection was approved by the medical ethical committee UMC Utrecht under the biobanking protocol: 14-472 HUB-OVI. All patients participating in this study signed the informed consent forms.

Derivation of oviductal organoids

For organoid derivation, ovaries and oviducts were dissected from mice and carefully separated under the stereo microscope. Oviducts were first placed into a collagenase solution (1 mg/mL of collagenase from *Clostridium histolyticum*, Sigma, C9407) in AdDF+++ (Advanced DMEM/F12 supplemented with 1x Glutamax, 10 mM HEPES and penicillin-streptomycin, all from Invitrogen) with ROCK inhibitor (Y-27632, 10 μ M). The tissue was incubated at 37°C for 2h while shaking followed by vigorous mechanical sharing using a fire-polished glass pipette and centrifugation for 5 min at 450 xg. The material was further digested with TrypLE (Gibco, Cat. 12605-010) for 5 min at 37°C, washed several times with ice cold AdDF+++ and embedded in Basement Membrane Extract (Cultrex® BME RGF type 2, Amsbio, Cat. 3533-005-02). The cell-BME suspension was plated on a pre-warmed suspension culture plate (Greiner) and allowed to solidify at 37°C for 30 min before addition of medium. Basal culture medium for oviductal organoids includes 20% R-spondin conditioned medium (made in-house), 1% Noggin conditioned medium (U Protein Express), 1x B27 (Gibco), 1.25 mM n-Acetylcystein (Sigma), 50 ng/ml EGF (Peprotech) and 500 nM A83-01 (Tocris). WNT inhibitor IWP2 (3 μ M, Stemgent) was used for showing WNT-independency of oviductal organoids. For induction of ciliogenesis, DAPT (10 μ M, Tocris) was added to the WNT-deprived culture medium and analysis was performed 2 weeks after the start of the treatment. The organoids could be reproducibly derived from over 4 independent isolations.

Derivation of OSE organoids

Ovaries were subjected to more gentle treatment with pronase solution (1 mg/ml of Pronase E, Sigma) in AdDF+++ with ROCK inhibitor at 37°C for 30 min while shaking. This method allows removal of OSE cells from the surface of the ovaries while leaving the rest of the tissue intact. After digestion the ovaries were gently sheared a few hundred times by using an adjusted 1 ml pipette tip (tip hole needs to be cut large enough for the ovaries to enter without breaking them) to detach the loosened OSE sheets from the surface of the ovaries. Next, the supernatant containing epithelial fragments was transferred to another tube, pelleted by centrifugation for 5 min at 450 xg and further digested with TrypLE for 5 min at 37°C. After several washes with ice cold AdDF+++

the cells were embedded in BME and plated on pre-warmed culture plates as described above. The minimal required medium for OSE organoids contains all the factors present in the oviductal organoid medium (see above), but is additionally supplemented with 50% conditioned WNT3a (made in-house) and 0.1 μM β -Estradiol (Sigma). Addition of FGF2 during initial passages can improve the organoid outgrowth. WNT inhibitor IWP2 was used for demonstrating WNT-dependency of OSE organoids. For ciliogenesis assay, cultures were grown in the presence of DAPT for 2 weeks until analysis. The organoids could be reproducibly derived from over 4 independent isolations.

Organoid growth assay

Organoids were removed from BME and trypsinized with TrypLE. Cells were washed in medium and passed through a 40 μm cell strainer to ensure a single-cell suspension. Cells were diluted in trypan blue to exclude dead cells and counted using a haemocytometer. 1000 cells were plated into 5 μl BME drops into 48-well plates (Greiner Bio-One, 677102) and overlaid with 250 μl medium. Images of the organoids were taken every day for a week, organoid sizes were measured (12 organoids per line) using ImageJ software (version 1.51j8). Subsequently, from the resulting data, the growth curves were constructed in Microsoft Excel 2019. Experiment was repeated twice.

Flow cytometry

To assess the apoptosis in organoids, the cells were stained and analysed by flow cytometry. Organoids were collected and dissociated into single-cell suspension via trypsinization. The cells were stained with Annexin V Apoptosis Detection Kit (88-8007-72, eBioscience) according to the manufacturer's instructions. A BD FACSCanto II system was used to analyse the samples. The assay was performed twice. The gating strategy is provided in the Supplementary Figure 5.

Immunohistochemistry

Tissues were fixed overnight in 4% paraformaldehyde at 4 $^{\circ}\text{C}$ followed by dehydration and paraffin embedding. To prepare organoids for histological stainings, intact BME-drops containing organoids were collected from the culture plates and incubated in Cell Recovery Solution (Corning, Cat. 354253) on ice for 30 min, occasionally inverting the tube, to dissolve BME. Organoids were then allowed to settle to the bottom of the tube by free gravitation, supernatant removed and the material fixed in 4% paraformaldehyde at room temperature for 1 hour. After fixation, the organoids were washed in PBS, and embedded into paraffin blocks. Sections were cut and hydrated before staining. Sections were subjected to H&E staining or immunohistochemistry by using antibodies listed in the Table 2. The images were acquired on Leica DM4000 microscope and processed using Leica LAS X software.

1

2

3

4

5

&

Table 2. Antibody specifications.

Antibody	Company, Cat#	Dilution	Incubation	Antibody retrieval
PAX8	Proteintech, 10336-1-AP	1:2000	Overnight, RT	Citrate buffer, pH 6.0
Ac-alpha-Tubulin	Santa Cruz, sc-23950	1:2000	Overnight, RT	Citrate buffer, pH 6.0
KI67	Monosan, MONX10283	1:2000	Overnight, RT	Citrate buffer, pH 6.0
Cytokeratin-8	Santa Cruz, sc-101459	1:50	Overnight, RT	Citrate buffer, pH 6.0
GFP	Life Technologies, A11122	1:1000	Overnight, RT	Citrate buffer, pH 6.0
Cleaved Caspase-3 (D175)	Cell Signaling Technology, #9661L	1:500	Overnight, RT	Citrate buffer, pH 6.0

Double strand break repair assay

Organoids were treated overnight with 15 μ M Mitomycin C (Sigma, M4287). About 16 hours later, organoids were harvested and fixed in 4% formalin overnight at 4°C. Prior to the whole-mount staining, the fixed organoids were permeabilized with 0.5% Triton-X (Sigma), 2% donkey serum (BioRad) in PBS for 30 minutes at 4°C and blocked with 0.1% Tween-20 (Sigma) and 2% donkey serum in PBS for 15 minutes at room temperature. Subsequently, organoids were stained with mouse anti- H2A.X primary antibody (1:500, Millipore, clone JBW301) overnight at 4°C, followed by 4 washes with PBS and incubation with secondary goat anti-mouse AF-647 antibody (1:250, Thermo Fisher, catalog number A-21235) for 2 hours at room temperature in the dark and washed again with PBS. DAPI was used to counterstain nuclei. Organoids were mounted and imaged on an SP8 confocal microscope (Leica). Fluorescent microscopic images of H2A.X were quantified as follows: Based on the staining, the nuclei were classified as H2A.X-positive or -negative. The fraction of positively stained nuclei over all nuclei is displayed as one datapoint per organoid. At least 10 organoids were quantified per line over two independent experiments.

Karyotyping

About 2-3 days after splitting of the organoids, the cultures were treated with 0.1 μ g/mL colcemid (Gibco, Cat. 15210-040) added to the culture media for 6 hours. Organoids were then collected and dissociated into single-cells using TrypLE. Single cells were swollen by addition of pre-warmed 75 mM KCl and incubated at 37 C for 10 min. Cells were fixed by slow drop-wise addition of ice-cold methanol:acetic acid (3:1) while gently tapping the cell suspension. Slides were mounted with DAPI-containing Vectashield, imaged on a DM6000 Leica microscope with a 100x objective, and quantified by manual chromosome counting. At least 15 spreads per clone were analysed.

Organoid transfection and genotyping

For generating mutant organoid lines for selected genes (*Trp53*, *Brca1*, *Nf1* and *Pten*), the CRISPR-Cas9-mediated genome editing was used. The single-guide RNAs (sgRNAs)

Table 3. Sequences targeted by designed sgRNAs.

Gene	Exon (F – forward, R – reverse)	Targeted sequence
<i>Trp53</i>	Exon 3, F	AAGTCACAGCACATGACGG
<i>Brca1</i>	Exon 6, F	GCGTCGATCATCCAGAGCGT
<i>Nf1</i>	Exon 8, F	CCAGGACATCTCCAAGGATG
<i>Pten</i>	Exon 6, R	ATATACATAGCGCCTCTGAC

were designed by using the CRISPR Design tool (Zhang Lab, MIT). For all the genes two separate sgRNAs were designed, and, based on the *in vitro* screening assay, the better performing sgRNA was chosen for each gene for the following organoid experiments. The sequences of the final sgRNAs are shown in the Table 3.

For organoid transfection experiments about 640 μ l of BME with Cas9-expressing oviductal or OSE organoids were collected from the plate (about 4/12-wells) and dissociated into single-cells using TrypLE, washed with AdDF++ (without antibiotics), resuspended in high-density in 500 μ l of growth medium with 10 μ M ROCK inhibitor (without antibiotics) and transferred to a well on a 24-well culture plate. The sgRNA transfection was performed by using the Stemfect RNA Transfection Kit (Stemgent) according to the manufacturer's instructions. Briefly, 12.5 μ l of transfection buffer was mixed together with 1 μ l of transfection reagent and incubated at room temperature for 10 min followed by addition of the sgRNA mixture containing 12.5 μ l of transfection buffer and 5 μ g of appropriate sgRNAs. The total volume of transfection mixture (ca 25 μ l) was incubated at room temperature for 15 min before adding it to the cell-suspension and the plate was placed in a humidified incubator at 37 C for 4-5 hours. After incubation, cells were collected and plated according to the standard protocol and covered with full medium containing 10 μ M ROCK inhibitor. Around 2-3 days post transfection, the medium was exchanged with the growth medium containing 10 μ M Nutlin-3a (Cayman Chemical) to select for p53 mutant organoids. Within two weeks clonal organoid outgrowth could be readily observed, the organoids were picked, expanded and screened for mutations in targeted genes. If the triple mutants were not obtained after the first round of transfection, an additional transfection was performed.

For genotyping, genomic DNA was isolated using DirectPCR lysis reagent (Viagen). Primers for the PCR amplification using GoTaq Flexi DNA polymerase (Promega) were as follows: *Trp53_for*, 5'-CAGGAAGCCAAAGGGTGAAGA-3', *Trp53_rev*, 5'-CCCATCTACAGTCCCCCTTG-3'; *Brca1_for*, 5'-TGGAGTGCAAGTAAAGCCT-3', *Brca1_rev*, 5'-ACCGACAATTAAGATGGAGTGCT-3'; *Nf1_for*, 5'-CCCGGGAACTATCAGCCTT-3', *Nf1_rev*, 5'-CTGTTTGACCTAGCATGGACA-3'; *Pten_for*, 5'-TGCAGTACAGAGACCATTGACT-3', *Pten_rev*, 5'-CGACACACAGACAGCTAAGAA-3'. Products were cloned into pGEM-T Easy vector system I (Promega) and subsequently Sanger sequenced by MacroGen Europe (Amsterdam, The Netherlands) using universal T7 sequencing primer.

1

2

3

4

5

&

Western blot

Organoids were treated with 10 μ M Nutlin-3a to activate p53 pathway 24 hours prior to the harvesting. Samples were lysed using RIPA buffer (50 mM Tris-HCl pH 8.0, 150 mM NaCl, 0.1% SDS, 0.5% Na-Deoxycholate, 1% NP-40) containing Complete protease inhibitors (Roche). Protein content was quantified using standard Bradford assay (BioRad) and equal amounts of protein (a' 20 μ g) were run on gradient polyacrylamide gel (4-15%; Biorad) and transferred to PVDF membranes (Millipore). Membranes were blocked and probed with antibodies directed against p53 (sc-6243, 1:250, Santa Cruz Biotechnology) and GAPDH (LN2100751, 1:1000, Labned). Uncropped versions of the Western blots are provided in the Supplementary Figure 6. The results were confirmed twice.

RNA isolation, cDNA preparation and qRT-PCR

For qPCR analysis, RNA was isolated from organoids and tissues using the RNeasy Mini Kit (Qiagen, Cat. 74104) following the manufacturer's instructions including DNaseI treatment. For qPCR, RNA was reverse transcribed from 500 ng of total RNA using GoScript and random primer (both Promega). qPCR was performed with three biological replicates in duplicates using the indicated primers, SYBR Green Mixture (BioRad) and BioRad CFX Manager Version 3.1. Gene expression was quantified using the delta-delta-Ct method and normalized against β -Actin housekeeping gene. qPCR primers used in this study were as follows: β -Actin_for, 5'-GTCGAGTCGCGTCCACC-3', β -Actin_rev, 5'-GTCATCCATGGCGAACTGGT-3'; Pax8_for, 5'-GATGCCTCACAACCTCGATCA-3', Pax8_rev, 5'-AAGGATCTTGCTTACACAGC-3'; Foxj1_for, 5'-ACCAAGATCACTCTGTCCGG-3', Foxj1_rev, 5'-GATGGAATTCTGCCAGGTG-3'; Dnah5_for, 5'-ATGGACTGACTTCTCGCCTC-3', Dnah5_rev, 5'-GTCGTTGCGTCAGAACTCG-3'; Trp73_for, 5'-GGGAGCAACAGGCTCTGAAT-3'; Trp73_rev, 5'-GCTCTGCTTGAATGCACGTT-3'.

Library preparation and RNA-seq analysis

For RNA-seq analysis, RNA was isolated from the organoids and tissues using the RNeasy Mini Kit (Qiagen) following the manufacturer's instructions or standard Trizol extraction protocol, respectively. In both cases DNaseI treatment was included. *In vitro* transcription was performed using 1-5 ng cDNA as template and RNA was reverse transcribed into a sequencing library. After preparation, the quality and quantity of the libraries were checked with Bioanalyzer2100 DNA High Sensitivity chips (Cat. 5067-4626) and Qubit (Qubit® dsDNA HS Assay Kit, Cat. Q32854); all samples had a RIN value of 10. Sequencing was performed on an Illumina NextSeq500 by using 75-bp paired-end sequencing. Paired-end reads from Illumina sequencing were aligned to the mouse genome (GRCm38 assembly) with BWA⁵⁵. The raw data file consists of a total number of reads for each gene (without UMI correction) that were uniquely mapped to the transcriptome (with a mapping quality above 60), and that had the appropriate transcription direction. DESeq2 (v1.18.0) package was used to normalize count data and for differential gene expression

analysis in program R (R version 3.5.1, Bioconductor version 3.8 (BiocManager 1.30.4)). Gene set enrichment analysis (GSEA) was performed using GSEA software v3.0 beta2.

***In vitro* drug screen**

Two days prior to the start of the assay, organoids were disrupted into single cells using TrypLE and filtered using a 70 µm nylon cell strainer (BD Falcon). The cells were subsequently counted, and resuspended in 5% BME/growth medium (25,000 cells/mL) prior plating in 40 µl volume (Multi-drop Combi Reagent Dispenser, Thermo Scientific, catalog no. 5840300) in 384-well plates (Corning, catalog no. 4588). The drugs were added 2 days after plating the cells using the Tecan D300e Digital Dispenser (Tecan). Nutlin-3a (Cayman Chemical, catalog no. 10004372) and niraparib (Selleckchem, catalog no. S2741) and paclitaxel (Sigma, catalog no. T7402) were dissolved in DMSO. Cisplatin (Sigma, catalog no. C2210000) was dissolved in PBS containing 0.3% Tween-20, which was required to dispense the drug using the HP printer. All wells were normalized for solvent used. DMSO percentage never exceeded 1% and PBS/Tween-20 percentage never exceeded 2%. Drug exposure was performed in quadruplicates for each concentration shown. Five days (120 hours) after the addition of the drugs, ATP levels were measured using the CellTiter-Glo 3-D Reagent (Promega, catalog no. G9681) according to the manufacturer's instructions, and luminescence was measured using a Spark multimode microplate reader (Tecan). Results were normalized to vehicle (100%) and baseline control (Staurosporine 1 µmol/L; 0%). Data was analysed using GraphPad Prism software (version 7.04) and lines were fitted using the option "log(inhibitor) vs normalized response - variable slope". Drug screening results were confirmed in quadruplicates (n=4) over two independent experiments.

***In vivo* transplantation assays**

Before transplantations, wild-type or mutant oviductal and OSE organoids were harvested and broken into smaller injectable fragments via mechanical shearing with a fire-polished glass pipette. Cells were then resuspended in 10% BME in PBS and approximately 100 000 cells were injected per location. Both subcutaneous and orthotopic injections were performed. For each mutation combination, two separate clones were transplanted. At least two mice were used for orthotopic and one mouse for subcutaneous transplantations per clone. Ear clipping was used for animal recognition. The mice were sacrificed up to 4 months (ca 120 days) after injections. Tumor volumes were measured and estimated by formula: Tumor volume = (length x width²)/2, where length represents the largest tumor diameter and width the perpendicular tumor diameter. Tumor volume was measured on all the OSE-derived tumors and randomly selected oviductal-derived tumors. All the tumors were subjected to immunohistochemical analysis. KI67- and cleaved Caspase-3-positive cells were quantified using ImageJ software. From n=4 tumors also organoids were derived.

1

2

3

4

5

&

Establishment of tumor-derived organoids

A small piece of a tumor tissue was dissected, mechanically dissociated and cells were extracted by collagenase treatment as described in the Methods above (same protocol as under Derivation of oviductal organoids). Cultures were grown under Nutlin-3a selection to specifically promote the outgrowth of the tumor cells and inhibit the growth of host cells.

Data availability

The RNA-sequencing data have been deposited in the GEO database under the accession code GSE147882. The gene signature lists for different molecular subtypes of HG-SOC referenced during the study are available under Konecny et al. (2014) supplementary data at doi: 10.1093/jnci/dju249. The source data underlying Figures 1-3, 5 and Supplementary Figures 1-4, 6 are provided as a Source Data file. All the other data supporting the findings of this study are available within the article and its supplementary information files and from the corresponding author upon reasonable request. A reporting summary for this article is available as a Supplementary Information file.

ACKNOWLEDGEMENTS

We thank B. Artegiani and T. Dayton for critically reading the manuscript. We acknowledge Anko de Graaff and Stefan van der Elst from the Hubrecht Imaging Centre (HIC) and Flow Cytometry Core Facility, respectively.

AUTHOR CONTRIBUTIONS

H.C., O.K. and K.L. designed the project and wrote the manuscript. O.K. established the wild-type organoid cultures. K.L. characterized the wild-type/mutant organoid cultures and engineered all the mutant organoid lines. K.L. performed mRNA bulk sequencing analysis. J.K. performed *in vivo* transplantation assays. H.B. and J.K. performed immunohistochemistry. C.P.H.V. evaluated and classified the tumors. J.H.v.E. arranged the mice. H.C. and O.K. supervised the study.

COMPETING INTERESTS

H.C. is an inventor on several patents involving the adult stem cell-based organoid technology. The remaining authors declare no competing interests.

REFERENCES

1. Gershenson, D.M. *et al.* Clinical behavior of stage II-IV low-grade serous carcinoma of the ovary. *Obstet Gynecol* **108**, 361-368 (2006).
2. Scully, R.E. Pathology of ovarian cancer precursors. *J Cell Biochem Suppl* **23**, 208-218 (1995).
3. Fathalla, M.F. Incessant ovulation--a factor in ovarian neoplasia? *Lancet* **2**, 163 (1971).
4. Carcangiu, M.L. *et al.* Incidental carcinomas in prophylactic specimens in BRCA1 and BRCA2 germ-line mutation carriers, with emphasis on fallopian tube lesions: report of 6 cases and review of the literature. *Am J Surg Pathol* **30**, 1222-1230 (2006).
5. Powell, C.B. *et al.* Risk-reducing salpingo-oophorectomy in BRCA mutation carriers: role of serial sectioning in the detection of occult malignancy. *J Clin Oncol* **23**, 127-132 (2005).
6. Callahan, M.J. *et al.* Primary fallopian tube malignancies in BRCA-positive women undergoing surgery for ovarian cancer risk reduction. *J Clin Oncol* **25**, 3985-3990 (2007).
7. Cancer Genome Atlas Research, N. Integrated genomic analyses of ovarian carcinoma. *Nature* **474**, 609-615 (2011).
8. Ciriello, G. *et al.* Emerging landscape of oncogenic signatures across human cancers. *Nat Genet* **45**, 1127-1133 (2013).
9. Sasaki, R. *et al.* Oncogenic transformation of human ovarian surface epithelial cells with defined cellular oncogenes. *Carcinogenesis* **30**, 423-431 (2009).
10. Wu, J. *et al.* HMGA2 overexpression-induced ovarian surface epithelial transformation is mediated through regulation of EMT genes. *Cancer Res* **71**, 349-359 (2011).
11. Clark-Knowles, K.V., Senterman, M.K., Collins, O. & Vanderhyden, B.C. Conditional inactivation of Brca1, p53 and Rb in mouse ovaries results in the development of leiomyosarcomas. *PLoS One* **4**, e8534 (2009).
12. Xing, D. & Orsulic, S. A mouse model for the molecular characterization of brca1-associated ovarian carcinoma. *Cancer Res* **66**, 8949-8953 (2006).
13. Szabova, L. *et al.* Perturbation of Rb, p53, and Brca1 or Brca2 cooperate in inducing metastatic serous epithelial ovarian cancer. *Cancer Res* **72**, 4141-4153 (2012).
14. Sherman-Baust, C.A. *et al.* A genetically engineered ovarian cancer mouse model based on fallopian tube transformation mimics human high-grade serous carcinoma development. *J Pathol* **233**, 228-237 (2014).
15. Perets, R. *et al.* Transformation of the fallopian tube secretory epithelium leads to high-grade serous ovarian cancer in Brca;Tp53;Pten models. *Cancer Cell* **24**, 751-765 (2013).
16. Zhai, Y. *et al.* High-grade serous carcinomas arise in the mouse oviduct via defects linked to the human disease. *J Pathol* **243**, 16-25 (2017).
17. Ducie, J. *et al.* Molecular analysis of high-grade serous ovarian carcinoma with and without associated serous tubal intra-epithelial carcinoma. *Nat Commun* **8**, 990 (2017).
18. Lawrenson, K. *et al.* A Study of High-Grade Serous Ovarian Cancer Origins Implicates the SOX18 Transcription Factor in Tumor Development. *Cell Rep* **29**, 3726-3735 e3724 (2019).
19. Hao, D. *et al.* Integrated Analysis Reveals Tubal- and Ovarian-Originated Serous Ovarian Cancer and Predicts Differential Therapeutic Responses. *Clin Cancer Res* **23**, 7400-7411 (2017).

1

2

3

4

5

&

20. Coscia, F. *et al.* Integrative proteomic profiling of ovarian cancer cell lines reveals precursor cell associated proteins and functional status. *Nat Commun* **7**, 12645 (2016).
21. Eckert, M.A. *et al.* Genomics of Ovarian Cancer Progression Reveals Diverse Metastatic Trajectories Including Intraepithelial Metastasis to the Fallopian Tube. *Cancer Discov* **6**, 1342-1351 (2016).
22. McDaniel, A.S. *et al.* Next-Generation Sequencing of Tubal Intraepithelial Carcinomas. *JAMA Oncol* **1**, 1128-1132 (2015).
23. Flesken-Nikitin, A. *et al.* Ovarian surface epithelium at the junction area contains a cancer-prone stem cell niche. *Nature* **495**, 241-245 (2013).
24. Ng, A. *et al.* Lgr5 marks stem/progenitor cells in ovary and tubal epithelia. *Nat Cell Biol* **16**, 745-757 (2014).
25. Bai, W., Oliveros-Saunders, B., Wang, Q., Acevedo-Duncan, M.E. & Nicosia, S.V. Estrogen stimulation of ovarian surface epithelial cell proliferation. *In Vitro Cell Dev Biol Anim* **36**, 657-666 (2000).
26. Auersperg, N., Wong, A.S., Choi, K.C., Kang, S.K. & Leung, P.C. Ovarian surface epithelium: biology, endocrinology, and pathology. *Endocr Rev* **22**, 255-288 (2001).
27. Ghosh, A., Syed, S.M. & Tanwar, P.S. In vivo genetic cell lineage tracing reveals that oviductal secretory cells self-renew and give rise to ciliated cells. *Development* **144**, 3031-3041 (2017).
28. Kessler, M. *et al.* The Notch and Wnt pathways regulate stemness and differentiation in human fallopian tube organoids. *Nat Commun* **6**, 8989 (2015).
29. Adler, E., Mhawech-Fauceglia, P., Gayther, S.A. & Lawrenson, K. PAX8 expression in ovarian surface epithelial cells. *Hum Pathol* **46**, 948-956 (2015).
30. McCloskey, C.W. *et al.* A new spontaneously transformed syngeneic model of high-grade serous ovarian cancer with a tumor-initiating cell population. *Front Oncol* **4**, 53 (2014).
31. Lee, Y. *et al.* A candidate precursor to serous carcinoma that originates in the distal fallopian tube. *J Pathol* **211**, 26-35 (2007).
32. Piek, J.M. *et al.* Dysplastic changes in prophylactically removed Fallopian tubes of women predisposed to developing ovarian cancer. *J Pathol* **195**, 451-456 (2001).
33. Kuhn, E. *et al.* TP53 mutations in serous tubal intraepithelial carcinoma and concurrent pelvic high-grade serous carcinoma--evidence supporting the clonal relationship of the two lesions. *J Pathol* **226**, 421-426 (2012).
34. Kindelberger, D.W. *et al.* Intraepithelial carcinoma of the fimbria and pelvic serous carcinoma: Evidence for a causal relationship. *Am J Surg Pathol* **31**, 161-169 (2007).
35. Patch, A.M. *et al.* Whole-genome characterization of chemoresistant ovarian cancer. *Nature* **521**, 489-494 (2015).
36. Platt, R.J. *et al.* CRISPR-Cas9 knockin mice for genome editing and cancer modeling. *Cell* **159**, 440-455 (2014).
37. Vassilev, L.T. *et al.* In vivo activation of the p53 pathway by small-molecule antagonists of MDM2. *Science* **303**, 844-848 (2004).
38. Sedic, M. *et al.* Haploinsufficiency for BRCA1 leads to cell-type-specific genomic instability and premature senescence. *Nat Commun* **6**, 7505 (2015).

39. Drost, J. *et al.* Sequential cancer mutations in cultured human intestinal stem cells. *Nature* **521**, 43-47 (2015).
40. Peng, G. *et al.* Genome-wide transcriptome profiling of homologous recombination DNA repair. *Nat Commun* **5**, 3361 (2014).
41. Tothill, R.W. *et al.* Novel molecular subtypes of serous and endometrioid ovarian cancer linked to clinical outcome. *Clin Cancer Res* **14**, 5198-5208 (2008).
42. Konecny, G.E. *et al.* Prognostic and therapeutic relevance of molecular subtypes in high-grade serous ovarian cancer. *J Natl Cancer Inst* **106** (2014).
43. Hu, H. *et al.* Long-Term Expansion of Functional Mouse and Human Hepatocytes as 3D Organoids. *Cell* **175**, 1591-1606 e1519 (2018).
44. Basak, O. *et al.* Induced Quiescence of Lgr5+ Stem Cells in Intestinal Organoids Enables Differentiation of Hormone-Producing Enteroendocrine Cells. *Cell Stem Cell* **20**, 177-190 e174 (2017).
45. Kopper, O. *et al.* An organoid platform for ovarian cancer captures intra- and interpatient heterogeneity. *Nat Med* **25**, 838-849 (2019).
46. Sachs, N. *et al.* A Living Biobank of Breast Cancer Organoids Captures Disease Heterogeneity. *Cell* **172**, 373-386 e310 (2018).
47. van de Wetering, M. *et al.* Prospective derivation of a living organoid biobank of colorectal cancer patients. *Cell* **161**, 933-945 (2015).
48. Matano, M. *et al.* Modeling colorectal cancer using CRISPR-Cas9-mediated engineering of human intestinal organoids. *Nat Med* **21**, 256-262 (2015).
49. Boj, S.F. *et al.* Organoid models of human and mouse ductal pancreatic cancer. *Cell* **160**, 324-338 (2015).
50. Artegiani, B. *et al.* Probing the Tumor Suppressor Function of BAP1 in CRISPR-Engineered Human Liver Organoids. *Cell Stem Cell* **24**, 927-943 e926 (2019).
51. Tuveson, D. & Clevers, H. Cancer modeling meets human organoid technology. *Science* **364**, 952-955 (2019).
52. Zhang, S. *et al.* Both fallopian tube and ovarian surface epithelium are cells-of-origin for high-grade serous ovarian carcinoma. *Nat Commun* **10**, 5367 (2019).
53. Hakem, R. *et al.* The tumor suppressor gene Brca1 is required for embryonic cellular proliferation in the mouse. *Cell* **85**, 1009-1023 (1996).
54. Gowen, L.C., Johnson, B.L., Latour, A.M., Sulik, K.K. & Koller, B.H. Brca1 deficiency results in early embryonic lethality characterized by neuroepithelial abnormalities. *Nat Genet* **12**, 191-194 (1996).
55. Li, H. & Durbin, R. Fast and accurate short read alignment with Burrows-Wheeler transform. *Bioinformatics* **25**, 1754-1760 (2009).

1

2

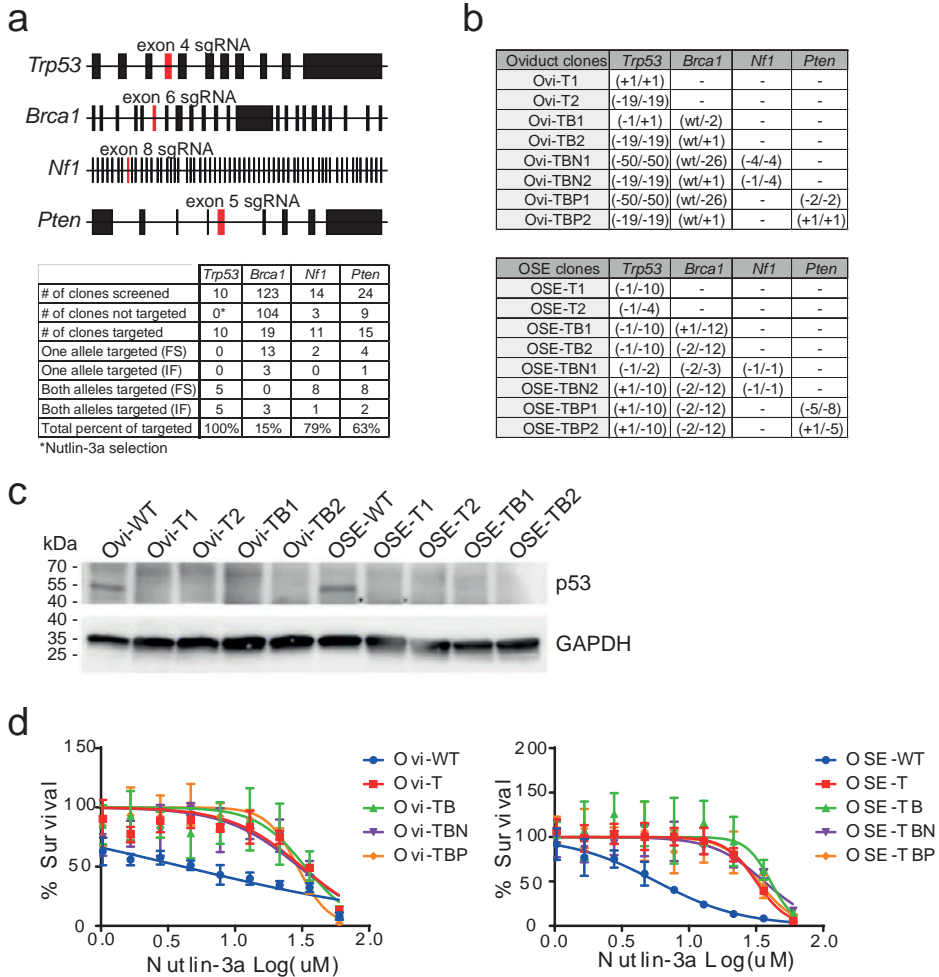
3

4

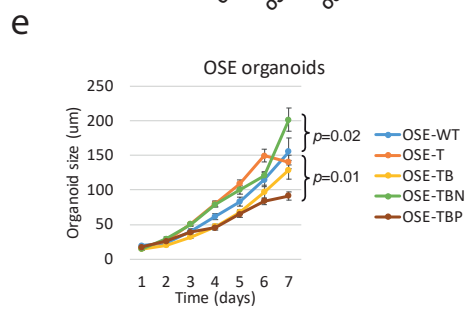
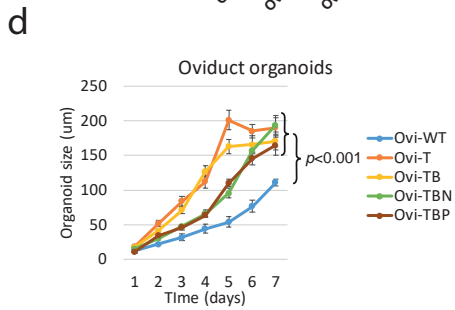
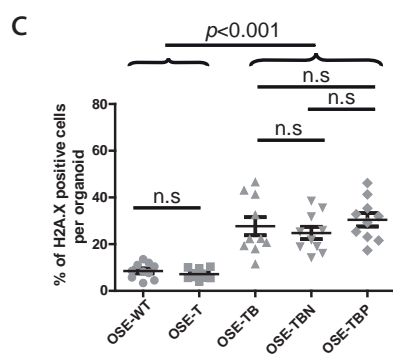
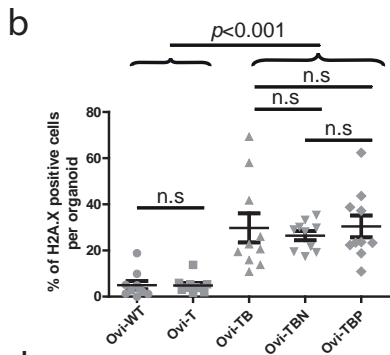
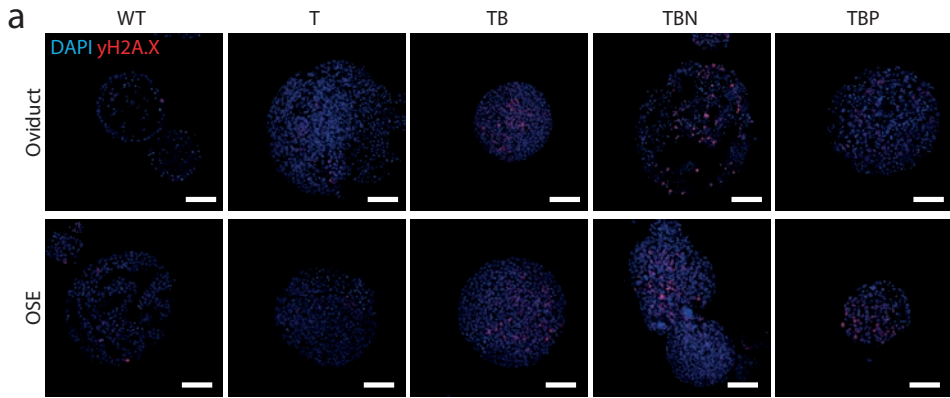
5

&

SUPPLEMENTARY INFORMATION



Supplementary Figure 1. Derivation of mutant clones via CRISPR-Cas9. (a) The sgRNA targeting exons and their targeting efficiency in the indicated genes. Asterisk – followed by Nutlin-3a selection 100% of the clones were targeted in *Trp53* gene. **(b)** Summary tables of all the established clones and their exact mutations from oviductal (top) and OSE (bottom) origin. **(c)** Western blot analysis of p53 expression in wild-type, T- and TB-mutant organoids from both lineages. GAPDH is shown as a loading control. Representative from n=2 independent experiments. Uncropped images of the blots are provided in the Supplementary Figure 6. **(d)** Nutlin-3a sensitivity assay of mutants and respective wild-types from oviductal (left graph) and OSE (right graph) lineages. Dots and error bars represent the mean and \pm SEM of technical quadruplicates (n=4), respectively, over two independent experiments. **(c-d)** Ovi – oviduct; WT – wild-type; T – *Trp53* mutant; TB – *Trp53*, *Brca1* mutant; TBN – *Trp53*, *Brca1*, *Nf1* mutant; TBP – *Trp53*, *Brca1*, *Pten* mutant.

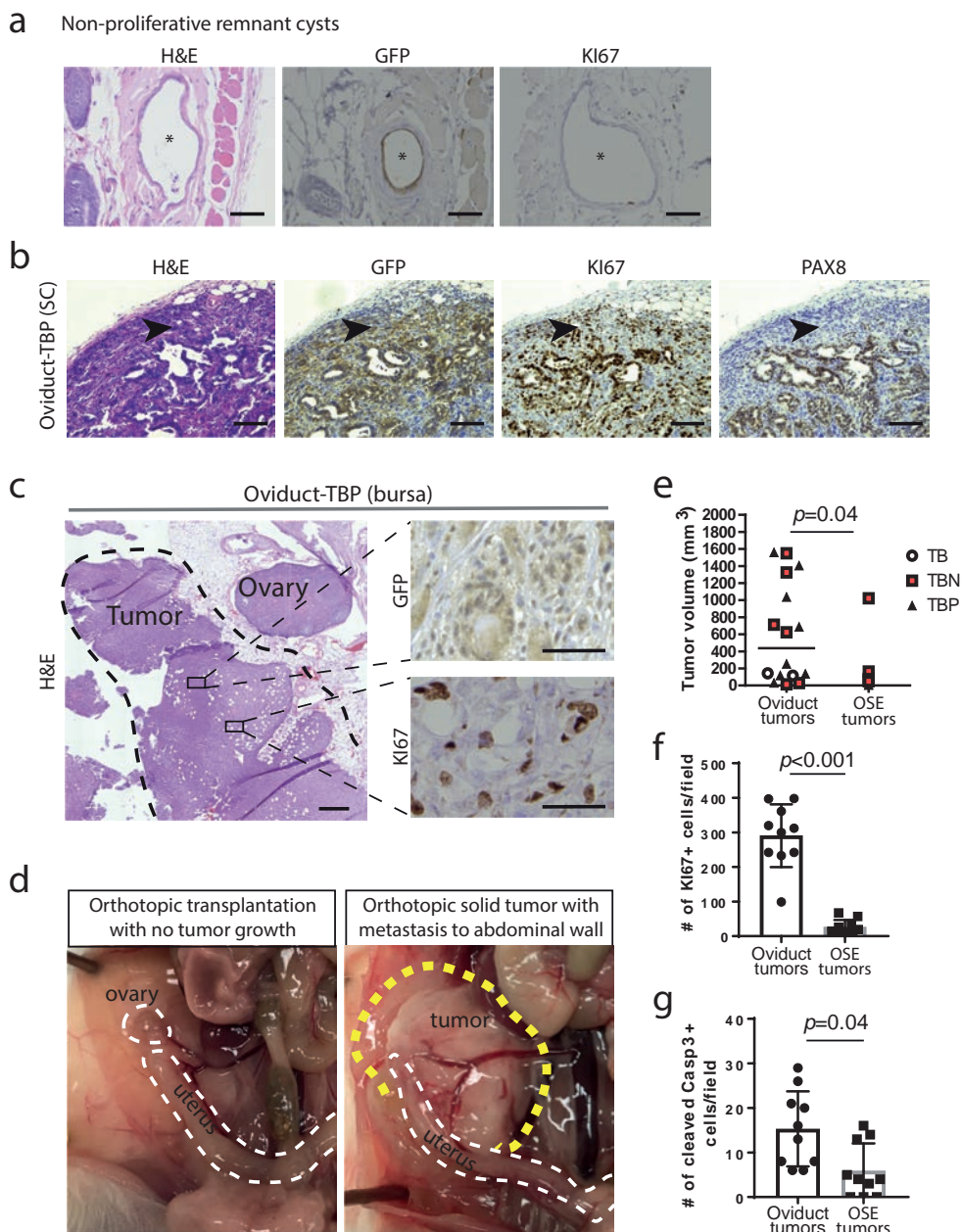


f

Clone	Live	Early apoptotic	Late apoptotic
	(Annexin V-/PI-)	(Annexin V+/PI-)	(Annexin V+/PI+)
Ovi-WT	53.4%	38.2%	4.2%
Ovi-T	70.2%	24.4%	2.3%
Ovi-TB	66.7%	27.3%	2.8%
Ovi-TBN	79.8%	16.7%	1.3%
Ovi-TBP	80.1%	16.2%	1.2%
OSE-WT	53.7%	27.6%	8.9%
OSE-T	87.1%	7.3%	1.0%
OSE-TB	76.7%	17.6%	1.7%
OSE-TBN	71.8%	21.7%	2.9%
OSE-TBP	43.6%	48.1%	6.3%

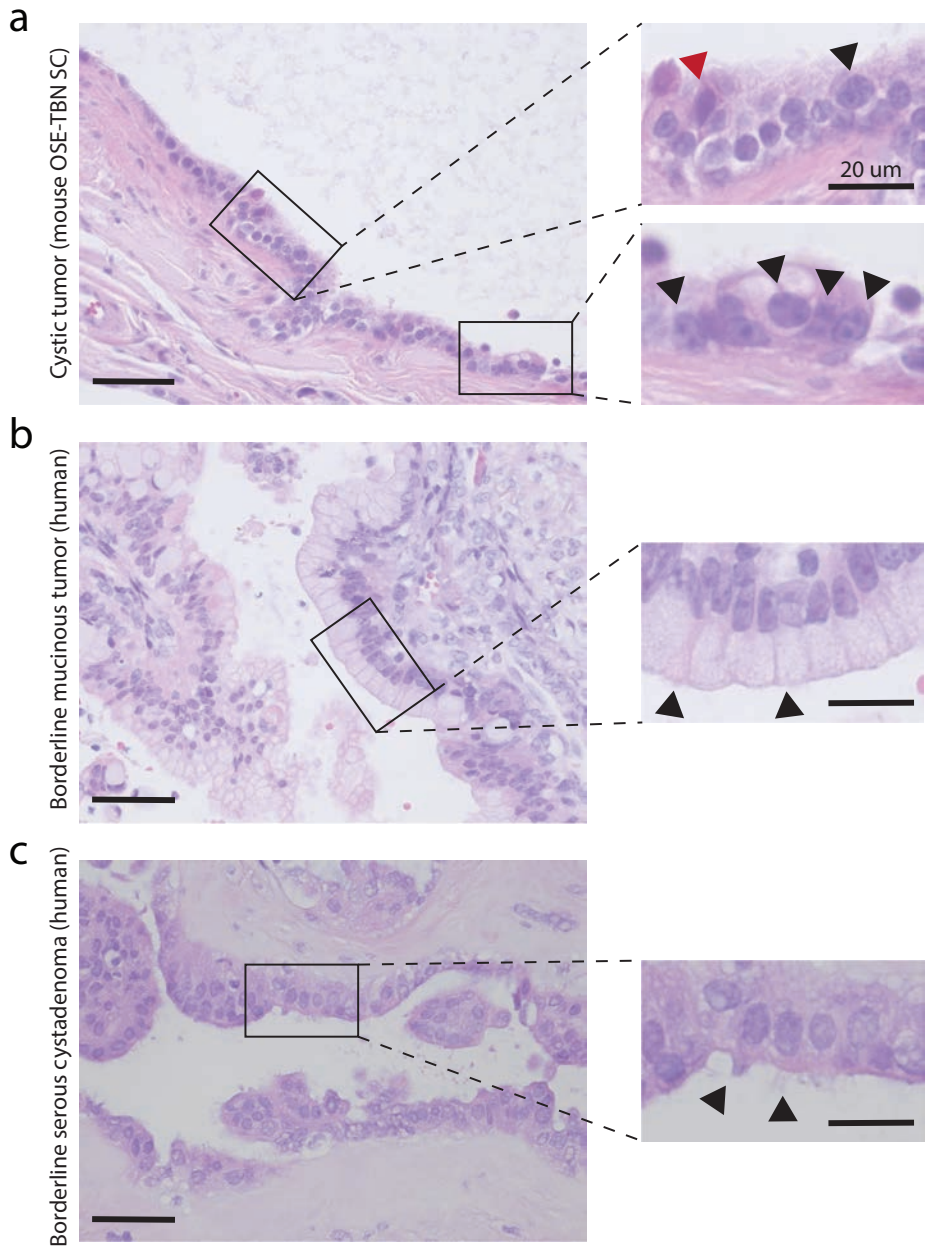
Supplementary Figure 2. Additional characterization of mutant clones. (a) Representative images of DNA damage induction in clones from both lineages after overnight treatment with Mitomycin C, measured by γ H2A.X immunofluorescence (n=2 independent experiments). Scale bar, 100 μ m. (b-c) Quantification of (a): Percentage of nuclei positive for γ H2A.X in Mitomycin

► C-treated organoids. Error bars represent \pm SEM (n=10 organoids/line). Statistical significance was calculated by two-tailed Student's t-test, *p*-values were not adjusted for multiple comparisons, n.s - not significant. **(d-e)** Organoid growth assay measured by daily increase in organoid sizes in oviductal **(d)** and OSE **(e)** lineages for a week (n=2 independent experiments). Statistical significance was calculated by two-tailed Student's t-test, *p*-values were not adjusted for multiple comparisons. Error bars represent \pm SEM (n=12 organoids/line). **(f)** Percentages of cells stained for Annexin V and PI and analysed by flow cytometry to evaluate apoptosis in all clones (n=2 independent experiments). **(a-f)** Ovi - oviduct; WT – wild-type, T – *Trp53* mutant; TB – *Trp53*, *Brca1* mutant; TBN – *Trp53*, *Brca1*, *Nf1* mutant; TBP – *Trp53*, *Brca1*, *Pten* mutant.



Supplementary Figure 3. Additional characterization of organoid-derived tumors. (a) Representative histological stainings of non-proliferative remnant cysts (asterisks) observed in subcutaneous transplantation with the wild-type organoids (n=4 injections). Scale bar, 50 μ m. (b) Histological example of an oviduct-TBP clone-derived subcutaneous tumor showing epithelio-mesenchymal phenotype. H&E, GFP, Ki67 and PAX8 stainings are shown (n=4 mice observed). Arrow heads point to the GFP-positive mesenchymal-like cells that have lost the expression of PAX8. Scale bar 100 μ m. (c) Representative histological stainings of orthotopic solid tumor derived from oviductal

► TBP clone (n=8 tumors). H&E, GFP and KI67 stainings are shown. H&E staining scale bar, 500 μm ; GFP/KI67 image scale bar, 50 μm . **(d)** Representative images of orthotopic transplantations with oviductal clones which yielded no tumor (left, n=23 injections) or solid tumor (right, n=15 injections) growth with abdominal wall metastases. Uterus horn and ovary – white dashed line, tumor – yellow dashed line. **(e)** The distribution and mean of the tumor volumes derived from oviduct (n=16) and OSE (n=7). Statistical significance was calculated by one-sided unpaired Student's t-test. **(f)** Number of KI67-positive cells per 20x magnification image fields in oviduct- and OSE-derived tumors (5 fields per tumor, 2 tumors/origin, n=10). Error bars represent $\pm\text{SEM}$. Statistical significance was calculated by two-tailed Student's t-test. **(g)** Number of cleaved Caspase-3 positive cells per 20x magnification image fields in oviduct- and OSE-derived tumors (5 fields per tumor, 2 tumors/origin, n=10). Error bars represent $\pm\text{SEM}$. Statistical significance was calculated by two-tailed Student's t-test.



Supplementary Figure 4. Comparative histological properties of a murine organoid-derived cystic tumor and two distinct human benign ovarian tumors. **(a)** Representative image of a murine organoid-derived cystic tumor (n=9 mice observed). As an example, OSE-TBN (*Trp53*, *Brca1*, *Nf1* mutant) clone-derived subcutaneous (SC) tumor is shown. Upper inset: multiple nucleoli (black arrowhead) and nuclear atypia (red arrowhead). Bottom inset: abundant mitotic figures (black arrowheads). **(b)** Human borderline mucinous tumor from a patient. Inset: mucinous glands (arrowheads). **(c)** Human borderline serous cystadenoma from a patient. Inset: cilium (arrowheads). **(a-c)** Large image scale bar, 50 μ m; inset scale bar, 20 μ m.

1

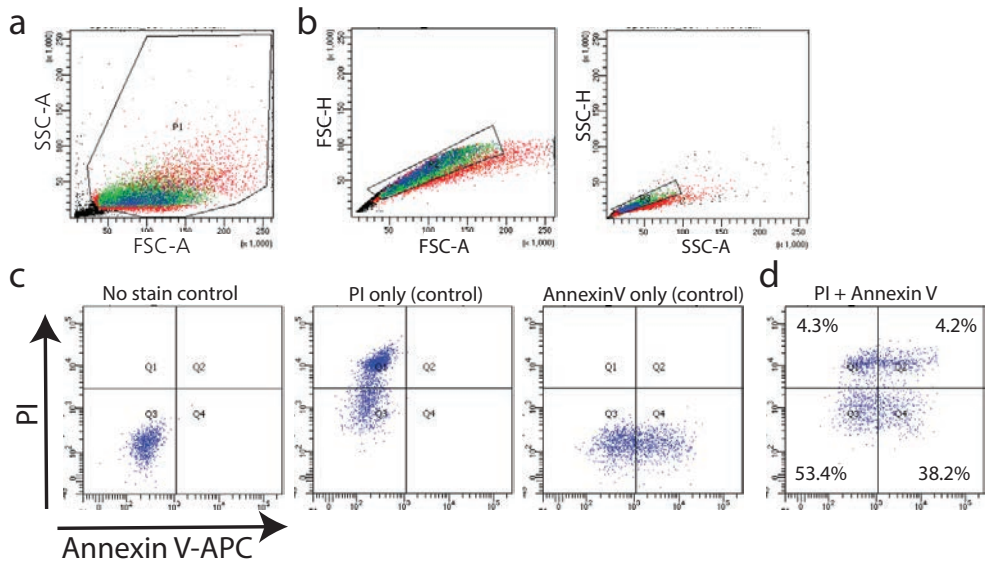
2

3

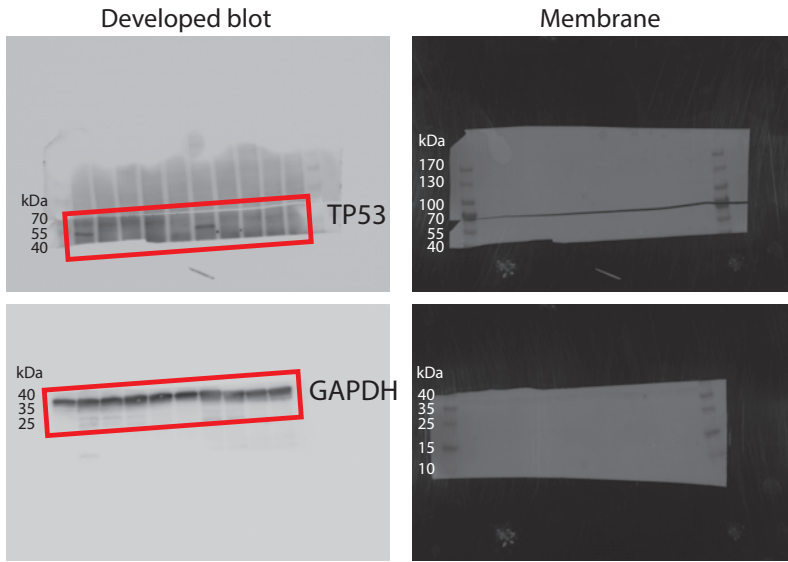
4

5

&



Supplementary Figure 5. FACS gating strategy. (a) In this sample gating, the cells were first gated for forward- and side-scatter area (FSC-A vs SSC-A) to select the cell population of interest and exclude the debris. (b) Next, a sequential gating was performed to obtain single cells. The cells were first gated for forward-scatter area and height (FSC-A vs FSC-H) followed by gating for side-scatter area and height (SSC-A vs SSC-H), which allows for higher sensitivity in doublet exclusion. (c) No stain, “PI only” and “Annexin V only” samples were used to set up the gates for the assay. (d) Subsequently, PI and Annexin V-APC double-stained clones were analysed for apoptotic events. Q1: PI-positive and Annexin V-negative necrotic cell fraction, Q2: PI and Annexin V double-positive late apoptotic cell fraction; Q3: PI- and Annexin V-negative live cell fraction; Q4: PI-negative and Annexin V-positive early apoptotic cells. The main results are shown in the Supplementary Figure 2f.



Supplementary Figure 6. Uncropped images of Western blots. The panels circled with red rectangles are displayed in the Supplementary Figure 1c.

1

2

3

4

5

&

LIST OF SUPPLEMENTARY FILES

Supplementary Data 1* Medium recipes of mouse oviductal and OSE organoids

Supplementary Data 2* Statistical analysis of targeting odds on Brca1 and Pten locuses

Supplementary Data 3* Transplantation outcomes with oviduct-derived clones

Supplementary Data 4* Transplantation outcomes with OSE-derived clones

Supplementary Video 1* High speed time-lapse imaging of normal oviductal organoid line with beating cilia.

*Supplementary Data files/Video are available online at doi: [10.1038/s41467-020-16432-0](https://doi.org/10.1038/s41467-020-16432-0).



CHAPTER

AN ORGANOID PLATFORM FOR OVARIAN CANCER CAPTURES INTRA- AND INTERPATIENT HETEROGENEITY

3

Oded Kopper^{1,2}, Chris J. De Witte^{3,14}, Kadi Löhmuusaar^{1,2,14},
Jose Espejo Valle-Inclan^{3,14}, Nizar Hami^{2,4}, Lennart Kester^{1,2},
Anjali Vanita Balgobind^{1,2}, Jeroen Korving^{1,2}, Natalie Proost⁵,
Harry Begthel^{1,2}, Lise M. van Wijk⁶, Sonia Arístin Revilla^{1,2},
Rebecca Theeuwssen⁵, Marieke Van De Ven⁵,
Markus J. van Roosmalen³, Bas Ponsioen^{2,4}, Victor WH Ho⁷,
Benjamin G. Neel⁷, Tjalling Bosse⁸, Katja N. Gaarenstroom⁹,
Harry Vrieling⁶, Maaïke P.G. Vreeswijk⁶, Paul J. Van Diest¹⁰,
Petronella O. Witteveen¹¹, Trudy Jonges¹⁰, Johannes L. Bos^{2,4},
Alexander van Oudenaarden^{1,2}, Ronald P. Zweemer¹²,
Hugo J.G. Snippert^{2,4}, Wigard P. Kloosterman³, Hans Clevers^{1,2,13}

¹ Hubrecht Institute, Royal Netherlands Academy of Arts and Sciences
and UMC Utrecht, Utrecht, The Netherlands

² Oncode Institute

³ Center for Molecular Medicine, University Medical Center Utrecht,
Utrecht University, Utrecht, The Netherlands

⁴ Molecular Cancer Research, Center for Molecular Medicine, University
Medical Center Utrecht, Utrecht University, Utrecht, The Netherlands

⁵ Preclinical Intervention Unit of the Mouse Clinic for Cancer and Ageing
(MCCA) at the NKI, Amsterdam, The Netherlands

⁶ Department of Human Genetics, Leiden University Medical Center,
Leiden, The Netherlands

⁷ Princess Margaret Cancer Center, University Health Network,
Toronto, ON Canada

⁸ Department of Pathology, Leiden University Medical Center, Leiden,
The Netherlands

⁹ Department of Gynecology, Leiden University Medical Center, Leiden,
The Netherlands

¹⁰ Department of Pathology, University Medical Center Utrecht, Utrecht
University, Utrecht, The Netherlands

¹¹ Department of Medical Oncology, Cancer Center, University Medical
Center Utrecht, Utrecht University, Utrecht, The Netherlands

¹² Department of Gynaecological Oncology, Cancer Center, University
Medical Center Utrecht, Utrecht University, Utrecht, The Netherlands

¹³ The Netherlands Princess Máxima Center for Pediatric Oncology,
Utrecht, The Netherlands

¹⁴ These authors contributed equally

ABSTRACT

Ovarian cancer (OC) is a heterogeneous disease usually diagnosed at a late stage. Experimental *in vitro* models that faithfully capture the hallmarks and tumor heterogeneity of OC are limited and hard to establish. We present a novel protocol that enables efficient derivation and long-term expansion of OC organoids. Utilizing this protocol, we have established 56 organoid lines from 32 patients, representing all main subtypes of OC. OC organoids recapitulate histological and genomic features of the pertinent lesion from which they were derived, illustrating intra- and interpatient heterogeneity, and can be genetically modified. We show that OC organoids can be used for drug screening assays and capture different tumor subtype responses to the gold standard platinum-based chemotherapy, including acquisition of chemoresistance in recurrent disease. Finally, OC organoids can be xenografted, enabling *in vivo* drug sensitivity assays. Taken together, this demonstrates their potential application for research and personalized medicine.

INTRODUCTION

Over the past decade, the field of epithelial ovarian cancer research has gone through a dramatic shift led by a series of recent discoveries^{1, 2}. It has become clear that OC is a heterogeneous disease consisting of a wide spectrum of distinct molecular and clinical entities. Epithelial ovarian neoplasms can be divided into three main groups: borderline tumors (non-carcinoma), Type-I and Type-II tumors (carcinomas)^{3, 4}. Borderline tumors (BTs) account for 15% of OC malignancies and consist primarily of serous BT (SBT) and mucinous BT (MBT) subtypes. BTs are frequently found adjacent to Type-I tumors and share many of their characteristics. It is therefore believed that they can transform into Type-I tumors³. Type-I tumors are genetically stable, and carry a distinct set of frequently mutated genes, including, *KRAS*, *BRAF*, *PTEN* and *CTNNB1*⁴. There are four main Type-I subtypes: low-grade serous (LGS), mucinous (MC), endometrioid (END) and clear cell carcinomas (CCC)⁴. Type-II tumors are comprised of high-grade serous (HGS) tumors, which are the most common type of OC and account for 70-80% of mortalities². HGS tumors frequently carry mutations in *TP53* (96%), *BRCA1* and *BRCA2* genes (20%), and are an extreme example of chromosomally unstable cancer^{5, 6}. HGS tumors are believed to develop either from the fimbria of the fallopian tube (FT)⁷ or from the ovarian surface epithelium (OSE). However, the relative contribution of these tissues to tumor development is still under debate⁸.

Tumor cell lines and patient-derived tumor xenografts are the most commonly used human model systems for the study of OC⁹⁻¹³. Despite their contribution to cancer research, these models have a number of drawbacks¹⁴. Establishing a new cell line is a challenging and time-consuming process that involves a long period of fibroblast contamination reduction and has a low success rate. Thus, in many cases the resulting cell lines are the product of a strong *in vitro* selection, which inevitably leads to the loss of tumor molecular characteristics, including copy number variations (CNVs), mutations, and intra-patient heterogeneity¹⁵. In contrast to 2D cell lines, xenografts reliably recapitulate components of the tumor environment, such as the 3D structure and the interaction of cancer cells with stroma and blood vessel infiltration¹⁶. Nevertheless, xenografts involve significant investments in resources for their maintenance, are poorly suited for large scale drug screening or for genetic manipulation and undergo rapid mouse-specific tumor evolution¹⁷. To overcome these drawbacks and to allow personalized approaches to cancer treatment, novel OC research platforms are needed^{1, 2, 16}.

As first shown for colorectal cancer¹⁸, tumor organoid cultures represent robust 3D *in vitro* systems that faithfully recapitulate the tumor from which they are derived¹⁹⁻²². Organoid technology is based on the definition of a cocktail of growth factors and small molecules (used in conjunction with the basement membrane mimic Matrigel) to recreate the niche requirements for long-term growth of cells. Organoid cultures can be clonally established from single cells derived from tumor tissue allowing the study of tumor heterogeneity²³. Organoids allow rapid assaying of phenotype-genotype correlations and

1

2

3

4

5

&

drug sensitivity, while recapitulating patient response^{22, 24-26}. The potential of organoid platforms for OC research was illustrated in a recent paper in which short-term cultured HGS organoids (7-10 days) were genomically characterized and then used in various assays to study DNA repair inhibitor response²⁷.

Here, we present and characterize an OC research platform that supports the efficient derivation and long-term expansion of OC organoids corresponding to non-malignant borderline tumors, as well as mucinous, clear-cell, endometrioid, low- and high-grade serous carcinomas.

RESULTS

Derivation of OC organoids

OC tissue and blood were obtained from consenting patients who underwent tumor resection and/or drainage of ascites/pleural effusion, either before or after (neoadjuvant) chemotherapy (Table S1). For each cancer case, the available tissue was used for organoid derivation, DNA isolation and histological analysis. Tumor pieces designated for organoid derivation, were further dissociated and the isolated tumor cells were suspended in BME, plated and supplemented with medium (Extended Data Figure 1a).

We used a recently described Fallopian Tube (FT) organoid medium²⁸ as our starting point for OC medium optimization. To improve organoid derivation rate, compounds that follow two main guiding criteria were tested as additives to the FT baseline medium: 1) Compounds previously reported to be highly expressed in ovarian tumors and therefore hypothesized to support OC growth^{29, 30}, 2) Factors used to support OC cell growth^{31, 32} and other types of tumor organoids^{21, 25}. We noted that addition of hydrocortisone, Forskolin and Heregulin -1 to FT medium improved the efficiency of OC organoid derivation. We also observed that WNT conditioned medium, an essential component of the FT medium, was not essential for all tumor organoid lines. Moreover, it had a negative effect on some of the lines, presumably due to the presence of serum in the conditioned medium and not WNT itself. Therefore, we used two types of OC medium for organoid derivation: with ('OCwnt medium') or without ('OC medium') WNT conditioned medium (Table S2). Typically, it became obvious after 2-3 passages which of the two media was optimal for individual OC cultures. OC organoid growth rates showed significant variability between cases, with passaging intervals varying from one to four weeks and split ratios ranging from 1:1.5 to 1:4 (Table S3). Organoids could be expanded long-term, i.e. at the time of final submission, 22 lines had been passaged for >15 times and 4 lines for >30 times without slowing down (Extended Data Figure 2, Table S3). Organoids could be cryopreserved and efficiently recovered (85% success rate, N=33, Table S3).

OC is often diagnosed after the tumor has already metastasized. In some cases, we were able to obtain both the primary tumor and the different metastatic lesions. We were therefore able to derive multiple organoid lines from individual patients. In one case, we established primary and recurrent tumor organoids from the same patient. In total, we

established 56 organoid lines, derived from 32 different patients. Organoids were derived with a success rate of 65%, representing both pre-malignant and malignant neoplasms covering the spectrum of OC, including MBT, SBT, MC, LGS, CCC, END and HGS (Figure 1a, Table S4). OC organoid nomenclature is based on their histopathological subtype and a number that refers to patient and tumor location. Patient clinical data is presented in Table S1.

Derivation of normal FT and OSE organoids from *BRCA* germline mutation carriers

Women with germline mutations in the *BRCA1/BRCA2* genes are at high risk of developing OC^{33, 34}. Therefore, organoids from normal FT and OSE of these individuals, in addition to non-carriers, should provide a valuable resource for research on the early stages of tumor development. We obtained FT and ovarian tissue from women undergoing prophylactic bilateral salpingo-oophorectomy (pBSO). As previously reported for FT organoids²⁸, pBSO-derived FT organoids were visible within 3-4 days after isolation, displayed a rounded, cystic phenotype and could be maintained long-term. Consistent with their tissue of origin, FT organoids expressed markers of both secretory and ciliated cells (PAX8 and acetylated- α -tubulin, respectively), and contained beating ciliated cells (Extended Data Figure 3a-c, Movie S1).

OSE organoids displayed a slower growth rate compared to FT organoids. They were usually visible 1-2 weeks after plating, and could be passaged once every 2-3 weeks for extended periods of time. OSE organoids displayed a cystic phenotype and expressed cytokeratin 8, demonstrating their epithelial origin (Extended Data Figure 3d).

In total, we were able to derive (success rate >90%) FT organoids from 10 pBSO-patients and OSE organoids from 6 pBSO-patients. In addition, we derived 2 FT lines from non-carriers. Normal organoid nomenclature and patient information data for each line is presented in Table S5.

Morphological and histological characterization of OC organoids

Normal FT and OSE organoid lines consistently displayed a cystic morphology with some epithelium folds and invaginations, that appeared upon organoid maturation (Extended Data Figure 3). In contrast, OC organoids show wide morphological variation between and within distinct histological subtype groups (Extended Data Figure 1b, c). Most BT organoids were cystic, whereas MC, LGS, END and CCC organoids formed denser organoid structures harboring multiple lumens. HGS organoids presented a wide morphological spectrum, varying from cystic to dense with different degrees of circularity and cellular cohesiveness (Extended Data Figure 1c, d). Scanning electron microscopy (SEM) revealed that morphological heterogeneity was not restricted to organoid shape, but also occurred at the cellular level (Extended Data Figure 1c). Moreover, SEM showed different degrees of cellular organization, as evidenced by cellular cohesiveness and microvilli alignment.

1

2

3

4

5

&

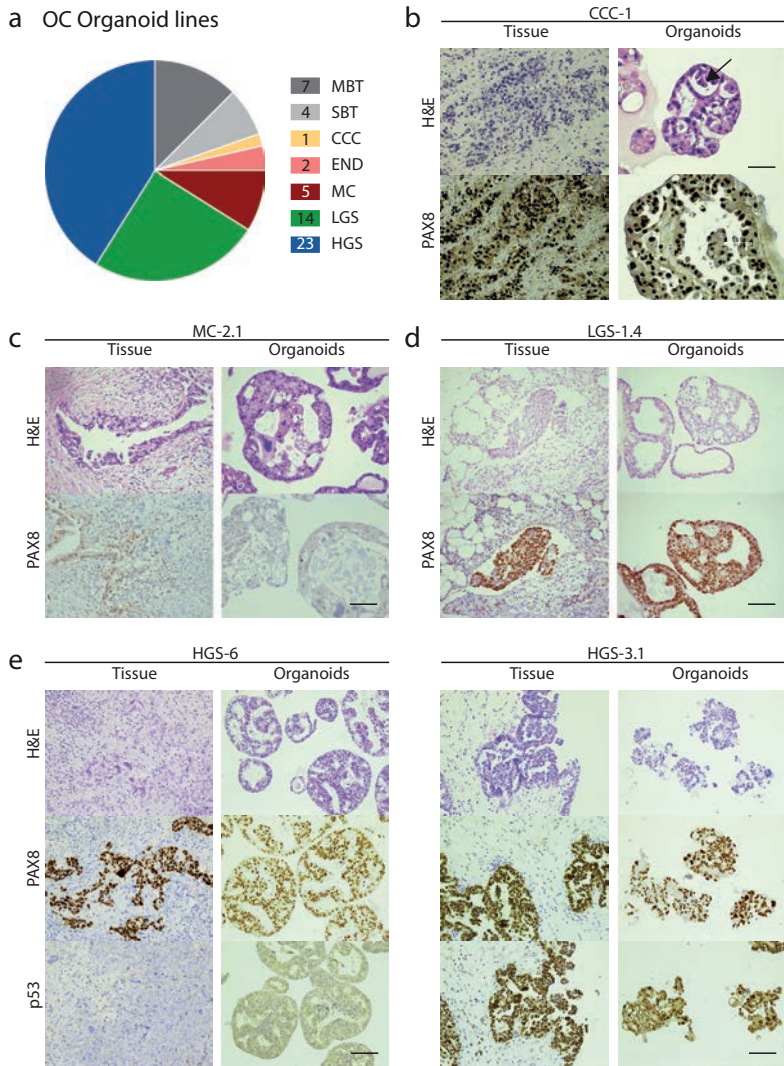


Figure 1. Subtype diversity and histological characterization of OC organoids. (a) An overview of established OC organoid lines according to their subtype distribution. Numbers in the legend represent the amount of lines established from each subtype. (b) Histological comparison of CCC organoids and their corresponding tumor tissue. Upper and lower panels show H&E and PAX8 staining, respectively. Arrow indicates hobnail cells, which characterize CCC. Scale bar, 100µm. (c) Histological comparison of representative MC organoids and their corresponding tumor tissue. Upper and lower panels show H&E and PAX8 staining, respectively. Tumor and organoids are negatively stained for PAX8, a marker of the serous subtype. Scale bar, 100µm. (d) Histological comparison of representative LGS organoids and their corresponding tumor tissue. Upper and lower panels show H&E and PAX8 staining, respectively. Organoids maintain positive PAX8 staining. Scale bar, 100µm. (e) Histological comparison of HGS organoids and their corresponding tumors (HGS-6 on the left, and HGS-3.1 on the right). H&E staining of HGS-6 organoid line displays papillary-like structures growing into the lumen, forming a dense phenotype. HGS-3.1 organoids are characterized with ▶

- ▶ disorganized morphology, which is evident by loss of organoid circularity and cellular cohesiveness. PAX8 positively stains both organoids and the tumor cells within the tissue. Mutations in the *TP53* gene can lead to protein loss as presented by HGS-6 organoid/tumor pair, or strong nuclear staining, presented by HGS-3.1 organoid/tumor pair. Histological characterization across the different organoid lines is presented in Extended Data Figure 2e and Table S6. Scale bar, 100µm.

To compare organoids to their corresponding tumor tissue, we performed hematoxylin and eosin (H&E) staining and evaluated expression of OC biomarkers, such as PAX8 and p53. Of note, the tumor organoids consist of the transformed epithelial cells of a tumor, but do not contain immune-, vessel- or connective tissue-elements. Histological analysis of the primary tumor tissue used for organoid derivation revealed different degrees of normal cell contamination as indicated by H&E and p53 staining (Extended Data Figure 2c). This stressed the need for histological analysis of the primary tissue used for organoid derivation, as low tumor purity can influence organoid derivation efficiency, and genomic correlation between organoids and tissue.

H&E staining of OC organoids revealed multiple tumor characteristics, such as the presence of papillary-like structures, nuclear and cellular atypia, and features of hobnail cells (Figure 1, Extended Data Figure 1d). These characteristics were not detected in normal FT- and OSE-organoids, which, in contrast, displayed well-organized epithelium (Extended Data Figure 3). Moreover, in an H&E based blinded test conducted by a certified pathologist on samples from normal FT and OSE organoids (N=5) as well as OC organoids (N=18), only FT and OSE organoids were classified as “normal”. OC organoids were either classified as “non-definitive” (N=5, 28%) or malignant (N=13, 72%). OC organoids that were classified as “non-definitive” correspond to borderline and LGS tumors (N=4, N=1, respectively). In agreement with their histological classification, most MBT and MC organoid lines were positive for periodic acid–Schiff (PAS) (9 out of 11) and negative for PAX8 (7 out of 11) staining, the latter a hallmark that distinguishes ovarian mucinous and serous tumors (Figure 1c, Table S6)³⁵. Ovarian serous organoids that were tested retained PAX8 and p53 expression status as observed for their corresponding tumor tissue (Figure 1d, E, Extended Data Figure 2e, Table S6). Mutations in the *TP53* gene can lead to diverse patterns of p53 staining, such as protein loss or strong nuclear staining. Such patterns were observed in different HGS organoid lines and their corresponding tumor tissue and were in agreement with their sequencing data (Figure 1e, Table S7). Organoids displayed a high percentage of Ki67-positive cells (Extended Data Figure 2b). Thus, histological analysis of OC organoids demonstrated their similarity to the carcinoma fields within the corresponding primary tumors, and their distinction from non-malignant FT and OSE organoids.

Organoids faithfully recapitulate OC at the genomic level

To further validate that OC organoids are composed of malignant cells, we performed metaphase spread analysis. The majority of tested organoid lines were aneuploid, a well-

1

2

3

4

5

&

characterized hallmark of most solid tumors³⁶. Interestingly, in some cases, a significant variation in average chromosome number was observed for different organoid lines derived from the same patient (Figure 2a).

To determine whether OC organoids faithfully recapitulate the genomic landscape of the primary tumors from which they were derived, we next performed WGS analysis. In total, we sequenced 40 organoid lines from 22 different patients. The corresponding tumor and normal blood samples for 35 of these lines were also sequenced and used as a reference (Table S7). We first used WGS data to estimate the percentage of malignant cells in both organoid and tumor samples³⁷. As predicted from histological analysis, in most cases, cancer cell content of organoids was considerably higher than that of the corresponding tumor (tumor organoids: $88.1 \pm 23\%$ versus tumor tissue: $45.1 \pm 9.2\%$ (mean \pm Standard deviation) across all samples) (Extended Data Figure 2d, Table S7). CNV analysis revealed similar patterns between organoid / tumor pairs (Figure 2b, Extended Data Figure 4a). Moreover, comparing the genomic landscape from early and late passage HGS organoids revealed that CNVs were well maintained even after prolonged passaging (HGS-1, passage 8 vs. 32; HGS-2, passage 6 vs. 15; HGS-3.1, passage 4 vs. 32; HGS-3.2, passage 4 vs. 25; HGS-6, passage 8 vs. 21; HGS-1-R2, passage 4 vs. 17) (Figure 2c, Extended Data Figure 4a). Most organoids derived from HGS tumors displayed many CNVs, whereas organoids derived from Type-I and BTs revealed a relatively subtle number of CNVs (Figure 2b, Extended Data Figure 4a). Thus, OC organoids recapitulate the genomic characteristics of the different OC subtypes from which they are derived^{4, 38}. To further quantify genetic correlation between organoids and corresponding tumors, we analyzed somatic single nucleotide variants (SNVs) and structural variants (SVs). Most SNVs and SVs present in the original tumor were maintained in the organoids derived thereof, and *vice versa* (Extended Data Figure 4b, Extended Data Figure 5a). Shared mutations were also maintained after extended passaging (Extended Data Figure 4b). Some organoid lines, such as HGS-19, HGS-3.1 and MC-2.1, presented marked differences with their corresponding tumor sample (Extended Data Figure 5a). We believe that these differences result from low tumor cell content within the original tumor samples as evident from their low number of SNVs, SVs and the lack of obvious CNVs (Extended Data Figure 4).

Next, we tested whether organoids displayed known OC-associated somatic mutations, amplifications and deletions. Somatic mutations in *KRAS* and *BRAF* genes, which are frequently found in MC and LGS tumors^{39, 40}, were identified in the corresponding organoid subtypes (MC-1, MC-2 (*KRAS*), LGS-5 (*BRAF*) Figure 3, Table S7). Moreover, all organoids derived from HGS tumors showed non-silent mutations including missense, stop gain and frameshifts in the *TP53* gene, in some cases accompanied by the loss of the second allele (Figure 3, Table S7). Amplifications of *MYC* and *CCNE1* as well as loss of *RB1*, *PTEN* and *CDKN2A/B* genes (frequent in HGS tumors^{5, 41}), were observed (Figure 3). These oncogenic modifications were mostly conserved between organoids and corresponding tumors (Figure 3, Table S7).

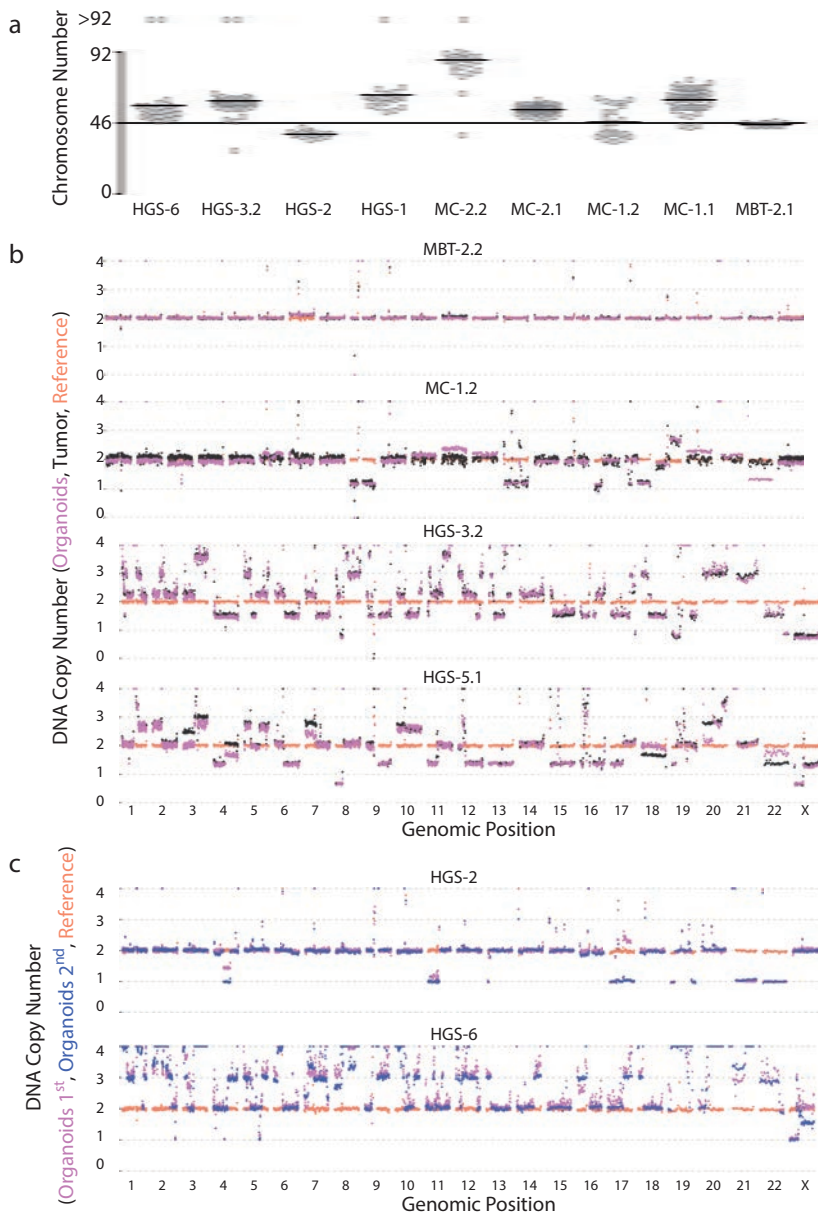


Figure 2. Organoids maintain genomic landscape of corresponding tumors. (a) Scatter plot, presenting chromosome number distribution and mean, based on organoid metaphase spreads. All the lines display aneuploidy except for the borderline tumor sample (MBT-2.1). Some of the organoid lines present a relatively narrow chromosome number distribution (MBT-2.1, MC-2.1, HGS-2), whereas others show a wide distribution (MC-1.1, MC-1.2), an indication for tumor heterogeneity. Differences between organoid lines that were derived from a single patient (MC-1.1/ MC-1.2 and MC-2.1/ MC2.2) implies intra-patient heterogeneity. n= number of analyzed metaphase spread from left to right: 24, 33, 14, 20, 24, 40, 22, 48, and 14. **(b)** Genome-wide CNV analysis of tumor and organoid pairs. For each sample, CNV profile of blood germline reference (orange), tumor ▶

1

2

3

4

5

&

- ▶ (black) and organoids (pink) are displayed. CNVs observed in original tumor samples are maintained in organoid lines. MBT-2.2 organoid line displays a relative flat CNV pattern in accordance with MBT-2.1 that was derived from the same patient, and shows normal metaphase spreads (in Figure 2a). HGS lines display extreme CNV abnormalities (see also Extended Data Figure 4). (c) Genome-wide CNV analysis of early (Organoids 1st) and late (Organoids 2nd) passage organoid pairs (HGS-2, passage 6 vs. passage 15; HGS-6, passage 8 vs. passage 21). A ploidy of 3 was assumed for this sample). For each sample, CNV profile of blood germline reference (orange), early (pink) and late (blue) passaged organoid are displayed. CNV profiles observed in organoid samples are maintained.

DNA methylation analysis was performed on a subset of organoids at early and late time points, using Illumina Infinium methylationEPIC 850K BeadChip. Clustering of these organoid samples based on the methylation beta values demonstrated that organoids maintained their epigenetic profile after extended passaging (Extended Data Figure 5b), as found previously for colorectal cancer organoids²³.

OC organoids capture tumor heterogeneity

To assess whether organoids capture intra-patient heterogeneity, we compared organoid lines derived from one primary and three metastatic sites of a patient diagnosed with LGSOC (Figure 4a). CNV analysis revealed losses and gains shared by all tumor lesions from the same patient (e.g. loss of chromosome X) as well as copy number changes only present in the metastatic sites (e.g. loss of 17p in LGS-1.2,3,4) (Figure 4a). These CNVs are conserved between tumor tissue and the corresponding organoids (Extended Data Figure 4a) and, therefore, appear to represent genomic changes that occurred at different time points along the course of tumor evolution.

We next tested whether tumor heterogeneity is maintained within an organoid line using a novel single-cell DNA sequencing method (see material and methods) and sequenced 791 cells from 2 recurrent tumor samples (HGS-1-R2, HGS-1-R3, both were derived from a single patient at different time points) and corresponding organoid lines from either one or two time points (HGS-1-R2, passage 5; HGS-1-R3, passage 4 and 12). Calculation of CNV profiles for each cell was followed by independent component analysis that revealed five distinct clusters (Figure 4b). Clusters 1-4 were comprised of aneuploid cells whereas cluster 5 was comprised of diploid cells (Figure 4c). As expected, tumor samples that were obtained from ascites drainage of a single patient within one-month interval, overlapped with each other and did not form separate clusters (Figure 4d), thus validating the robustness of the single-cell DNA sequencing method. Organoid-derived cells overlapped with the same 5 clusters (albeit with low representation in cluster 3) demonstrating both their heterogeneity and resemblance to the original tumor samples (Figure 4d). HGS-1-R3 relative cell abundance in cluster 5 (diploid cells) was dramatically reduced after extended passaging (passage 4 vs. 12), whereas representation of clusters 1, 2 and 4 (aneuploid cells) increased (Figure 4d, e), suggesting that tumor cells overgrew normal cells over time, while maintaining tumor heterogeneity.

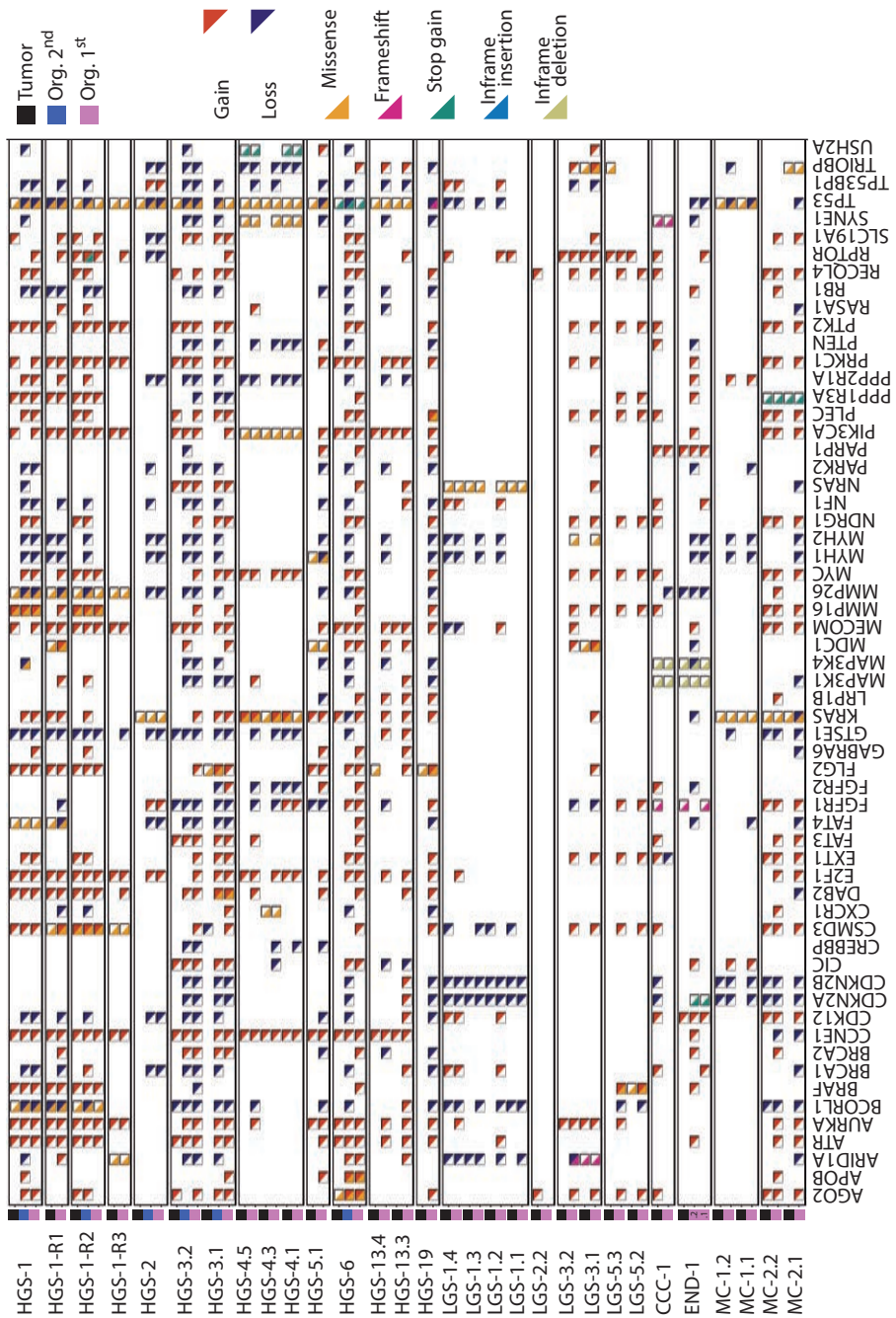


Figure 3. Somatic mutations and amplifications/ deletions in OC organoids. Somatic mutations and amplifications/ deletions in relevant genes of ovarian cancer. For each sample, tumor/ organoid pairs are displayed and indicated by color coding (black- tumors, pink- organoids, blue- organoids re-sequenced and analyzed after extended passaging). Passage number at which organoid lines were sequenced is given in table S7.

1
2
3
4
5
&

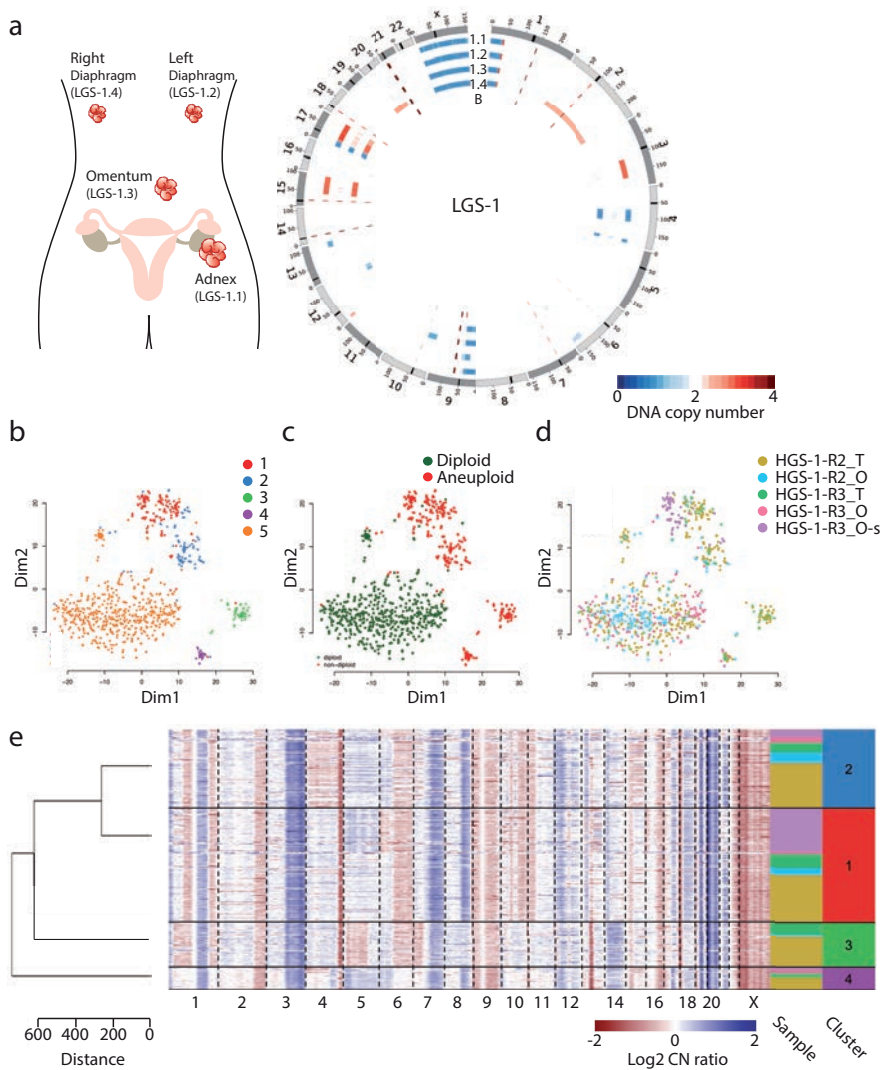


Figure 4. OC organoids capture tumor heterogeneity. (a) Schematic illustration of tumor locations and a circos plot presenting CNV events (red - gain, blue - loss) in the organoid lines derived from a patient diagnosed with LGS OC. Outside to inside: genomic position, LGS-1.1 (adnex tumor), LGS-1.2 (metastasis left diaphragm), LGS-1.3 (metastasis omentum), LGS-1.4 (metastasis right diaphragm), blood germline reference. (b) t-SNE plot of single cell CNV profiles from 2 recurrent tumor samples and corresponding organoid lines (HGS-1-R2, HGS-1-R3) of a single patient. Hierarchical clustering has separated the cells into 5 different clusters (color coded). Total number of analyzed cells = 791. (c) t-SNE plot presenting diploid (green) and aneuploid (red) cells. Total number of analyzed cells = 791. (d) Single cell distribution into the different clusters according to sample of origin. "T"- tumor, "O"- organoid, "-s"- second time point analysis. HGS-1-R2_T, n=351 cells; HGS-1-R2_O, Passage 5, n=159 cells; HGS-1-R3_T, n=93 cells; HGS-1-R3_O, Passage 4, n=122 cells; HGS-1-R3_O, Passage 12, n=66 cells. (e) Clustered CNV heatmap of aneuploid cells presenting gains (blue) and losses (red) across the genome. Sample origin and cluster belonging of each cell is color coded.

Gene expression analysis of OC organoids

To assess organoid gene expression profiles, we performed RNA-seq on 35 OC organoids, and 6 normal OSE and FT organoids. Hierarchical clustering assigned organoids to three independent main groups, representing 1) HGS carcinomas, 2) mucinous and endometrioid tumors and 3) mainly LGS carcinomas, FT and OSE (Figure 5). Organoids derived from multiple tumor lesions of the same patient were transcriptionally more similar to each other than to unrelated organoid lines (e.g. MC-1.1,2 and HGS-3.1,2). In a similar manner, organoids that were sequenced at a second time point after extended passaging clustered with their corresponding samples (HGS-1, P8 vs. P32; HGS-3.1, P4 vs. P32 and HGS-1-R2 P4 vs. P17). Of note, non-malignant MBT and malignant MC organoids clustered together. This was seen in 8 organoid lines derived from 4 different patients (2 MC and 2 MBT) suggesting a biological link between these samples. This finding is in agreement with a causality hypothesis that suggests a stepwise progression from borderline tumors to invasive carcinomas⁴²⁻⁴⁴. Furthermore, OSE(P)7 organoids (derived from a sample collected during risk-reducing salpingo-oophorectomy) clustered together with OC organoids and apart from normal OSE and FT organoid lines. This finding, together with morphological, histological and metaphase spread analysis (Extended Data Figure 3e-f) suggested that OSE(P)7 consists of malignant cells that were not diagnosed by routine pathological examination.

Genetic manipulation and drug screening of OC organoids

To demonstrate the experimental potential of OC organoids, we next adapted genetic manipulation techniques and drug screening methods for normal FT and OC organoids.

Normal FT organoids were electroporated with pSpCas9(BB)-2A-GFP plasmid into which we cloned a guide RNA targeting the *TP53* gene (Extended Data Figure 6a). Thus, we could determine the electroporation efficiency by monitoring GFP expression (Extended Data Figure 6c, d), and target the *TP53* gene, which is believed to be mutated at an early time-point in the course of HGS tumor development. Three days after electroporation, Nutlin3a (which inhibits MDM2-p53 interaction⁴⁵ and, therefore kills *TP53*-wildtype clones) was added to the medium (Extended Data Figure 6a, b). Surviving clones were picked, clonally expanded and analyzed for *TP53* mutations (Extended Data Figure 6e). As a result, multiple clones harboring mutations in *TP53* from carriers of *BRCA* germline mutations were established (Extended Data Figure 6f). In a similar manner, we have electroporated FT organoids with plasmids targeting both *TP53* and *RB1* genes and established clones in which both genes were knocked out (Extended Data Figure 6f). Clone expansion was accompanied with morphological alterations including transition from cystic to denser organoids and increased cell shedding into the organoid lumen (Extended Data Figure 6g). Hierarchical clustering based on RNA-seq assigned the clones into different clusters according to their genetic modifications (Extended Data Figure 6h).

To demonstrate that OC organoids can be genetically modified in a stable manner, they were transduced with a lentiviral-vector driving expression of fluorescently tagged

1

2

3

4

5

&

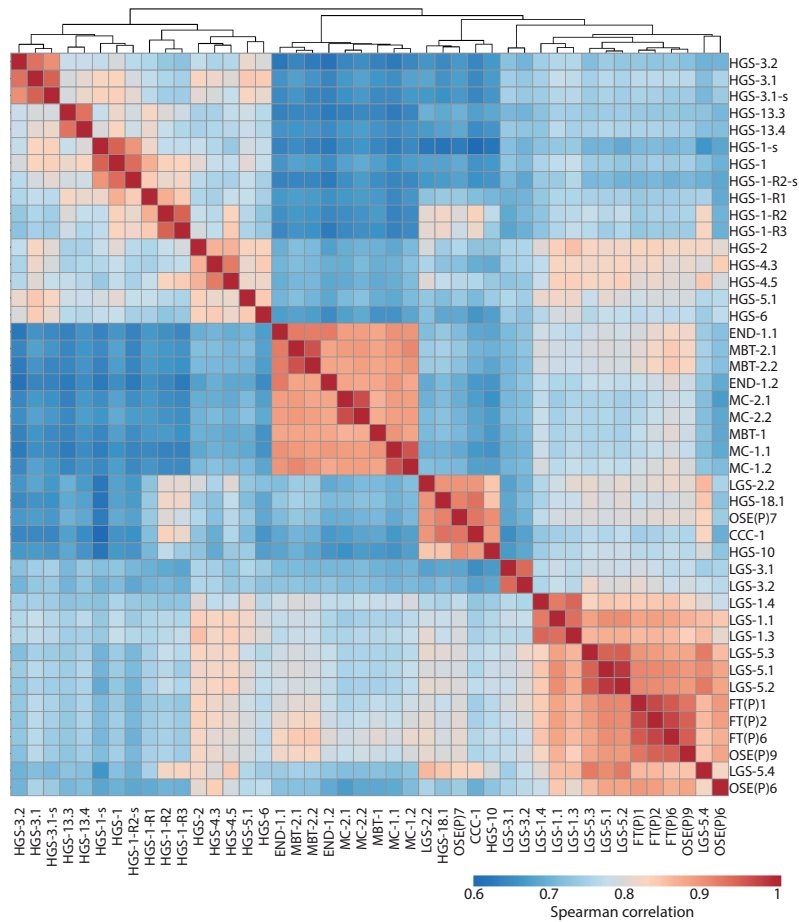


Figure 5. Gene expression analysis of OC organoids. Heatmap of spearman correlation values of normal FT (n=3 independent FT lines), OSE (n=3 independent OSE lines), non-malignant borderline tumors (n=3 independent MBT lines) and malignant organoid lines (n=32 independent malignant lines), based on RNA-Seq expression data. Read counts were normalized for sequencing depth and the 5000 most variable genes were used. For three organoid lines a second time point was analyzed after extended passaging demonstrating high correlation with early passaged organoids. “-s”- second time point analysis. HGS-1: P8 and P32, HGS-3.2: P4 and P32, HGS-1-R2: P4 and P17. Passage number in which all organoid lines were sequenced is given in table S7.

histone-2B (H2B-Neon). H2B-Neon transduced organoids enabled 3D live cell imaging of mitosis, and revealed multiple aberrant chromosomal segregation events (Movie S2-S6).

Next, we tested organoid sensitivity to platinum/taxane drugs that are commonly used in OC treatment protocols, i.e. carboplatin, paclitaxel, as well as non-platinum/taxane drugs that previously were suggested as possible treatments for OC. The drug panel included drugs targeting the PI3K/AKT/mTOR pathway (Alpelisib, Pictilisib, MK2206, AZD8055), PARP (Niraparib), the tyrosine kinase WEE1 (Adavosertib) and gemcitabine.

Organoids were disrupted into small clumps and dispensed into 384-well plates pre-coated with BME. A cell viability assay was performed 5 days after the drugs were added and organoid drug sensitivity was represented by the average area under the dose-response curve (AUC) of two technical replicates⁴⁶. Assay quality was confirmed by calculating plate Z-factor across all plates (Mean=0.61, Extended Data Figure 5e), and by the correlation of AUC between technical and biological replicates (Pearson correlation=0.94, 0.87, respectively Extended Data Figure 5c, d).

Unsupervised hierarchical clustering based on platinum/taxane drug sensitivity divided the organoids into two main clusters: sensitive lines that consisted primarily of HGS organoids, and resistant lines that consisted primarily of non-HGS organoids (Figure 6b). Notably, the HGS-1-R3 line, which was derived from ascites of recurrent disease, clinically resistant to chemotherapy (Table S1), clustered together with the resistant cluster. HGS-1 line, which was derived from the primary, chemotherapy sensitive tumor of the same patient clustered with the sensitive cluster (Figure 6a, b).

Since the *TP53* gene is mutated in the vast majority of OC, we tested whether Nutlin3a can serve to rapidly distinguish between wt and *TP53* mutated OC organoids. In total, 16 organoid lines were tested (3 normal FT lines, 1 genetically modified FT clone and 13 OC lines). As expected, all FT organoid lines were highly sensitive to Nutlin3a treatment whereas the genetically modified clone in which we knocked-out the *TP53* gene and the OC lines (with one exception) were resistant (Figure 6c, d). The only OC line that was sensitive to Nutlin3a, was LGS-1.3 and in this organoid, indeed no point mutation in the *TP53* gene was identified (Table S7).

Drug screening assays demonstrated differential drug responses of individual organoid lines (Figure 6a-e). For example, HGS-3.1 organoid line was highly sensitive to gemcitabine, adavosertib, carboplatin and paclitaxel and resistant to drugs that target the PI3K/AKT/mTOR pathway, whereas HGS-23 line demonstrated the opposite drug sensitivity pattern (Figure 6a-d).

Homologous recombination (HR) deficient cells have been shown to be sensitive to Poly(ADP-ribose)polymerase inhibitors (PARPis)^{47, 48}. To determine whether this correlation is also present in OC organoids, a subset of organoid lines with differential responses to Niraparib (Figure 6e) was tested for HR by using the REcombination CAPacity (RECAP) test, which assess HR capacity using accumulation of RAD51 protein at sites of DNA double strand breaks⁴⁹. Organoids were irradiated with 5Gy X-rays, recovered for 2 hours, fixed and stained with antibodies against RAD51 and Geminin (a marker for S/G2 phases of the cell cycle). The percentage of Geminin⁺ cells with RAD51 foci was scored blinded for sensitivity to Niraparib. Organoids with a low percentage of Geminin⁺ cells with RAD51 foci were more sensitive to Niraparib compared to organoids with a high percentage of Geminin⁺ cells with RAD51 foci (with the exception of MC-2.1) (Figure 6e).

1

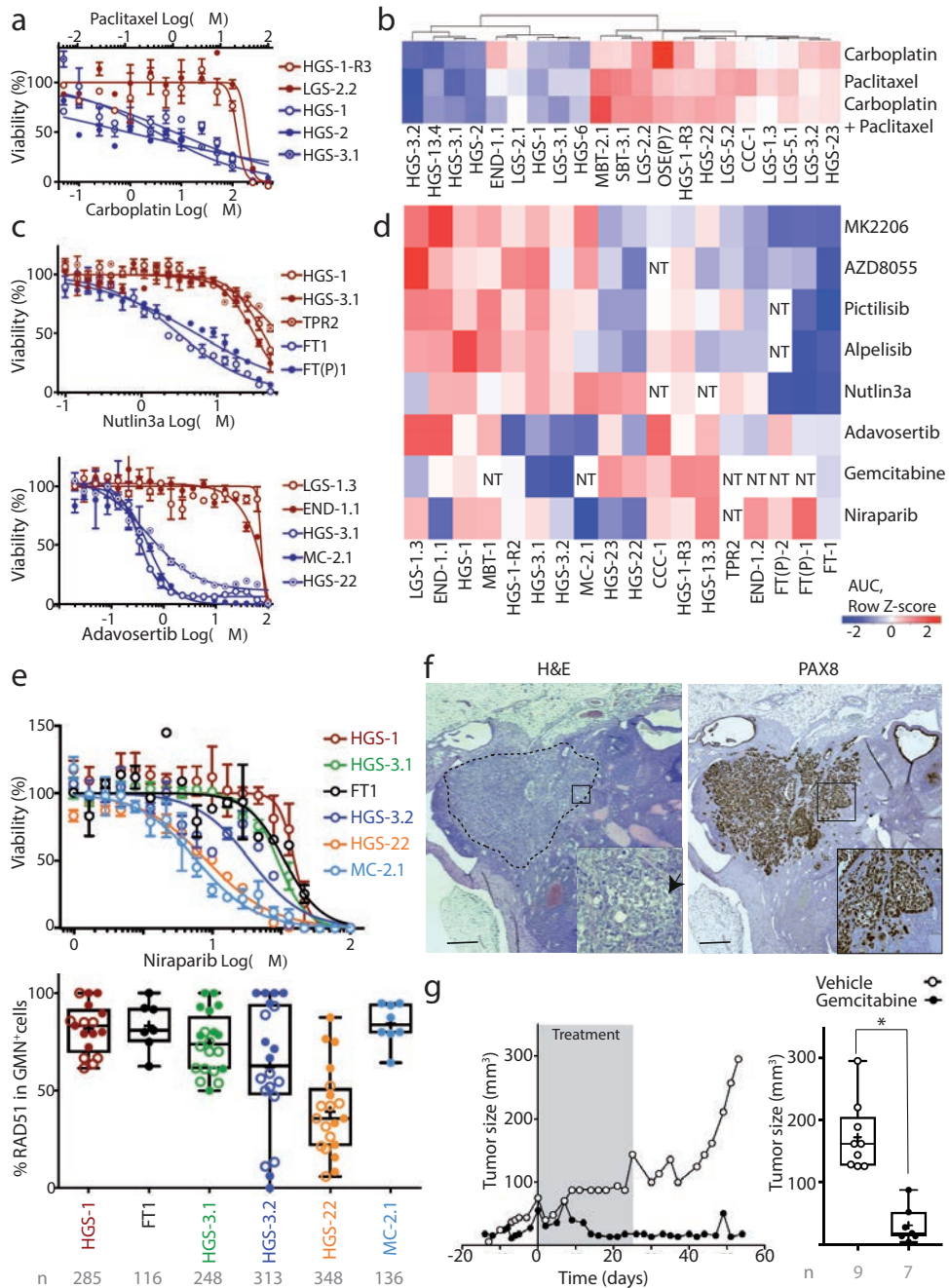
2

3

4

5

&



Xenotransplantation of OC organoids and *in vivo* drug sensitivity

We next tested whether OC organoid can be orthotopically or subcutaneously transplanted into immunodeficient mice. For orthotopic transplantations, organoids were transduced with a lentiviral-vector encoding luciferase and transplanted into the mouse bursa. Bioluminescence imaging was used to validate tumor growth (Extended Data Figure 5f). All three lines that were orthotopically transplanted grew into a tumor (Table S8). Six out of seven lines were successfully transplanted subcutaneously (Table S8). Histological analysis of orthotopically transplanted HGS carcinoma organoid line demonstrated that the tumor invaded the ovary, displayed prominent nuclear atypia, slit-like spaces and maintained PAX8 and p53 staining (Figure 6f, Extended Data Figure 5g). The MC organoid line that was subcutaneously transplanted showed characteristics of a mucinous tumor

◀ **Figure 6. *In vitro* and *in vivo* drug sensitivity assays.** (a) Representative dose response curves of HGS and LGS organoid lines treated with carboplatin/ paclitaxel. Organoid line derived from a recurrent disease (HGS-1-R3) show acquired resistance. Dots represent the mean of technical duplicates. Error bars represent SEM of technical duplicates. (b) Heat-map of euclidean distance of 21 distinct organoid lines, based on AUC row-Z-score values. As expected, most HGSOC organoids (6 out of 9) are more sensitive to carboplatin/ paclitaxel drugs in comparison to non-HGSOC organoids (9 out of 12). HGS-1 organoid line is sensitive to carboplatin/paclitaxel drugs whereas the matching recurrent organoid line (HGS-1-R3) is resistance. (c) Representative dose response curves for Nutlin3a and Adavosertib, upper and lower panels, respectively. Normal FT organoids show high sensitivity for Nutlin3a whereas HGS and genetically modified FT line, which are mutated in the *TP53* gene, are resistant. Dots represent the mean of technical duplicates. Error bars represent SEM of technical duplicates. (d) Heat-map of euclidean distance, based on AUC row-Z-score values, showing organoid response to a panel of drugs, including, PI3K/AKT/mTOR pathway-, PARP- and Wee1- inhibitors. n= 18 distinct organoid lines. (e) Upper panel- dose response curves for Niraparib show differential response between organoid lines. Dots represent the mean of technical duplicates. Error bars represent SEM of technical duplicates. Lower panel- Box and whisker plot (minimum to maximum) presenting RAD51 foci score after radiation. Each point represents percentage of RAD51⁺ cells within GMN⁺ cell population in one organoid. Horizontal bars and “+” represent median and mean of all dots, respectively. Empty and full dots show results of two biologically independent experiments conducted 1-2 passages apart. Total number (n) of analyzed GMN⁺ cells in each organoid line is presented. (f) Histological analysis of organoid derived xenograft (HGS-3.1) upon orthotopic transplantation into the mouse bursa. Tumor cells have invaded into the mouse ovary and H&E staining (left panel) shows solid pattern with indications for slit-like spaces (arrow) as well as pleomorphic cells with prominent nuclear atypia. Xenograft has maintained PAX8 positive staining (right panel). A summary of organoid derived xenograft experiments is presented in Table S8. Scale bar, 0.5mm. (g) Gemcitabine sensitive organoids were subcutaneously injected into immunodeficient mice and tumor size was monitored. Once the tumor reached 50mm³, mice were randomly selected and treated with intraperitoneal injections of Gemcitabine (2mg/kg) (n=7 independent mice) or vehicle (n=9 independent mice), 5 times per week for 4 consecutive weeks (in total 20 injections). Left panel shows an example of tumor growth over time in a vehicle (white dots) and a gemcitabine (black dots) treated mouse. Right panel- box and whisker plot (minimum to maximum) summarizing the results across all vehicle and gemcitabine treated mice, showing tumor size at day 55. Horizontal bars and “+” represent median and mean of all dots, respectively. *P-value< 0.001, t-test.

1

2

3

4

5

&

including goblet cells and haphazardly arranged neoplastic glands lined by columnar cells (Extended Data Figure 5h).

To validate whether *in vitro* drug sensitivity is recapitulated *in vivo*, we chose the HGS-3.1 organoid line that was highly sensitive to gemcitabine (Figure 6c), a nucleoside analog that is in clinical use for HGSOC. Organoids were subcutaneously injected and tumor size was monitored. Once it reached 50mm³, mice were randomly selected and treated with vehicle or gemcitabine. While tumors continued growing in vehicle-treated mice, tumor growth was completely blocked or reduced in gemcitabine treated mice, as indicated by tumor size measured at the end of the experiment (vehicle/ gemcitabine treated mice, N=9/ N=7, respectively) (Figure 6g).

DISCUSSION

Developing reliable experimental models that address clinical challenges, such as early detection, tumor recurrence and acquired chemotherapy resistance, is a high priority in OC research². In this study, we describe an organoid platform that enables long-term *in vitro* expansion, manipulation and analysis of a wide variety of OC subtypes. A comprehensive analysis demonstrates that OC organoids maintain tumor histological characteristics, such as nuclear and cellular atypia, and biomarker expression, such as p53 and PAX8. Organoids and corresponding tumors remained highly similar at the genomic level, even after extended passaging. Furthermore, organoids recapitulated OC hallmarks, such as CNVs, recurrent mutations, and tumor heterogeneity. Finally, unsupervised hierarchical clustering of gene expression data grouped the organoids according to their tumor type and demonstrated that LGS organoids are more similar to normal samples than are HGS lines.

During organoid biobanking of normal FT and OSE samples, obtained from risk-reducing surgeries, we encountered two samples that were apparently malignant: LGS-2 (clinically diagnosed) and OSE(P)7 (indicated by organoid characterization, Extended Data Figure 3e, f). Interestingly, unsupervised hierarchical clustering of gene expression data grouped these organoid lines together, thus implying biological similarity. Both organoid lines were derived from patients at high-risk of developing HGS tumors. Therefore, these samples potentially represent an early time point in HGS development. Establishing and analyzing additional early/pre-malignant organoid lines from pBSO material might substantiate this hypothesis and provide a unique opportunity to study early HGS tumor development.

An additional experimental platform, recently described to model colorectal cancer development⁵⁰⁻⁵³, can be established through CRISPR-mediated mutation of tumor driver genes in normal organoids. Indeed, we demonstrate that normal FT organoids from OC high-risk donors can be efficiently CRISPR-Cas9 genome edited and clonally expanded afterwards, demonstrating the feasibility of such an approach in OC.

HGS tumors are frequently sensitive to platinum-based chemotherapy, whereas non-HGS tumors (such as LGS and mucinous tumors) are characterized by relative

chemoresistance⁵⁴⁻⁵⁷. Consistent with these clinical observations, most HGS organoids were sensitive to platinum-based treatments, whereas non-HGS organoids (i.e. MBT, SBT and LGS) were more resistant (Figure 6b). In one case, we compared drug responses in matched organoid lines derived from primary chemosensitive (HGS-1) and recurrent chemoresistant (HGS-1-R3) tumors of a single patient. This experiment confirmed an increased resistance of the organoid line derived from the recurrent tumor to platinum-based chemotherapy, anecdotally substantiating the clinical relevance of OC organoids. Increasing the number of matched primary-recurrent organoid pairs is currently ongoing. The individual drug responses of OC organoids (e.g. compare HGS-23-and HGS-3.1) illustrates the complexity of choosing the right treatment. We provide proof of concept that *in vitro* drug sensitivity of OC organoid can be tested following xenotransplantation.

In summary, we present a new organoid culture-based platform for the study of OC that supports efficient derivation and long-term *in vitro* expansion of a wide variety of OC subtypes. This living OC organoid biobank -available to the research community-faithfully recapitulates OC hallmarks, can be subjected to genetic manipulations and to drug screening and opens the door to many avenues of OC research.

METHODS

Approval of Studies Involving Humans and Patient Informed Consent

The collection of patient data and tissue for the generation and distribution of normal FT, OSE and OC organoids, has been performed according to the guidelines of the European Network of Research Ethics Committees (EUREC) following European, national, and local law. The medical ethical committee UMC Utrecht (METC UMCU) approved the biobanking protocol: 14-472 HUB-OVI. All patients participating in this study signed informed consent forms and can withdraw their consent at any time.

Available organoids will be catalogued at www.hub4organoids.eu and can be requested at info@hub4organoids.eu. Distribution of organoids to third parties will have to be authorized by the METC UMCU at request of the HUB in order to ensure compliance with the Dutch medical research involving human subjects' act.

OC Tissue Processing

Upon arrival, OC tissues were cut into 3-5 mm³ pieces (Extended Data Figure 1a). 2-3 random pieces were snap frozen and stored at -80°C for DNA isolation, two random pieces were fixed in formalin for histopathological analysis and immunohistochemistry, and the remainder was processed for organoid derivation. For organoid derivation: tissue was minced, washed with 10 ml AdDF+++ (Advanced DMEM/F12 containing 1x Glutamax, 10 mM HEPES, and antibiotics). We let big tissue pieces to sink to tube bottom with gravity (for 2-5min) collect supernatant and centrifuged at 1000 rpm for 5 min. In case of a visible red pellet, erythrocytes were lysed in 2 ml red blood cell lysis buffer (Roche, 11814389001) for 5 min at room temperature followed by additional wash with

1

2

3

4

5

&

10 ml AdDF+++ and centrifugation at 1000 rpm. Remaining big tissue are digested in 5-10 ml AdDF+++ supplemented with 5 μ M RHO/ROCK pathway inhibitor (Abmole bioscience, Y-27632) containing 0.5-1 mg·ml⁻¹ collagenase (Sigma, C9407) on an orbital shaker at 37°C for 0.5-1 hr. The digested tissue suspension was sheared using 5 ml plastic pipettes. Suspension was strained over a 100 μ m filter and large tissue pieces entered a subsequent digestion and shearing step. Suspension was centrifuged at 1000 rpm and the pellet was resuspended in 10 ml AdDF+++ and centrifuged again at 1000 rpm. Once again, in case of a visible red pellet, erythrocytes were lysed in 2 ml red blood cell lysis buffer for 5 min at room temperature followed by additional wash with 10 ml AdDF+++ and centrifugation at 1000 rpm.

Ascites /pleural effusion samples were centrifuged at 1000 rpm and treated with 2 ml red blood cell lysis buffer for 5 min at room temperature. Following erythrocyte lysis 10 ml AdDF+++ was added and suspension was centrifuged at 1000 rpm.

Following removal of large part of the ovarian stroma and the surrounding muscle layers of FT, ovary and FT samples were processed as above.

Organoid Culture

Cell pellet was suspended in 10 mg·ml⁻¹ cold Cultrex growth factor reduced BME type 2 (Trevigen, 3533-010-02) and 40 μ l drops of BME-cell suspension were allowed to solidify on pre-warmed 24-well suspension culture plates (Greiner, M9312) at 37°C for 30 min. Upon BME stabilization, 500 μ l of appropriate organoid medium (OC/OCwnt/ OSE/FT medium, see Table S2) was added and plates transferred to humidified 37°C / 5% CO₂ incubators. In some cases 25 ng/ml HGF (Peprotech) was added to the medium (Table S3). Medium was changed every 3-4 days and organoids were passaged every 1-4 weeks. Organoid passaging: Organoids were mechanically sheared through P1000 pipet tip connected to P200 pipet tip without a filter. Dense organoids that were not easily sheared mechanically were collected with 1 ml pre-warmed (37°C) Accutase solution (A6964, SIGMA), incubated for 1-5 min at room temperature, and mechanically sheared as before. Following the addition of 10 ml AdDF+++ and centrifugation at 1200 rpm, organoid fragments were resuspended in cold BME and reseeded as above at suitable ratios (1:1 to 1:4) allowing the formation of new organoids. In some lines, organoids repeatedly appeared floating in medium. These organoid lines could be transferred to repellent plates (Greiner, 662970) and expanded with medium containing 5% BME (Table S3).

Genetically manipulated FT clones were expanded in OCwnt medium.

Scanning Electron Microscopy (SEM)

To remove BME, organoids were collected with Cell Recovery Solution (Corning) and gently shaken using tube rotator, for 30 min at 4°C. Organoids were allowed to settle down with gravity, the recovery solution was removed and 1 ml of 1% (v/v) glutaraldehyde

(Sigma) in PBS was added. Following an overnight fixation at 4°C, organoids were transferred onto 12 mm poly-L-lysine coated coverslips (Corning). The organoids were serially dehydrated by consecutive 10 min incubations in 2 ml of 10% (v/v), 25% (v/v) and 50% (v/v) ethanol-PBS, 75% (v/v) and 90% (v/v) ethanol-H₂O (2x) followed by 50% ethanol-hexamethyldisilazane (HMDS) and 100% HMDS (Sigma). Coverslips were removed from the 100% HMDS, air-dried overnight at room temperature and mounted onto 12 mm specimen stubs (Agar Scientific). Following gold-coating to 1 nm using a Q150R sputter coater (Quorum Technologies) at 20 mA, samples were examined with a Phenom PRO table-top scanning electron microscope (Phenom-World)

Histology and Imaging

Tissue and organoids were fixed in 4% paraformaldehyde followed by dehydration, paraffin embedding, sectioning, and standard HE staining. For the blind test, sections were randomized and analyzed by an OC pathologist. Immunohistochemistry was performed using antibodies as specified in Table S9.

Images were acquired on a Leica Eclipse E600 microscope and processed using the Adobe Creative Cloud software package.

For time-lapse imaging organoids were plated in BME in glass-bottom 96-well plates and mounted on an inverted confocal laser scanning microscope (Leica SP8X), which was continuously held at 37°C and equipped with a culture chamber for overflow of 6.0% CO₂. Over 16–20 hr, ~10 H2B-mNeon-expressing organoids were imaged simultaneously in XYZT-mode using a ×40 objective (N.A. 1.1), using minimal amounts of 506 nm laser excitation light from a tunable white light laser. Images were taken at 4 min intervals.

Genomic Analysis

For karyotyping, 0.1µg·ml⁻¹ colcemid (Gibco, 15212012) was added to the complete growth medium. About 12 hr later organoids were harvested, trypsinized into single cells, incubated in hypotonic 75mM KCl solution for 10 min, and fixed in methanol:acetic acid solution (3:1). Metaphase spreads were prepared, mounted with DAPI-containing vectashield, imaged on a DM6000 Leica microscope, and quantified by manual chromosome counting. A minimum of 14 spreads was analyzed for each line.

For DNA isolation, library preparation and WGS, organoid and blood samples were processed by using the DNeasy Qiagen kit. DNA from tumor tissue was isolated with the Genomic Tip Qiagen kit, supplemented with RNase treatment. Quality and quantity of samples were checked with Qubit (DNA BR). DNA integrity and RNA contamination was assessed by using TapeStation DNA screens (Genomic screen) and Nanodrop (260/280 ratio).

Per sample 500-1000 ng of DNA was used for DNA library preparation, and whole genome paired-end sequencing (2x150bp) was performed on Illumina HiSeq X Ten and NovaSeq 6000 to an average coverage of 42X.

1

2

3

4

5

&

Table S10 provides a list of all commercial and custom code used for data collection and analysis including: name, version, source, and link.

WGS data was processed using our in-house Illumina Analysis Pipeline (IAP) v. 2.5.1 (<https://github.com/UMCUGenetics/IAP>). Briefly, reads were mapped against the human reference genome GRCh37 using Burrows-Wheeler Alignment with maximal exact matches (BWA-MEM), v. 0.7.5a-r405 (arXiv:1303.3997v1). Read mapping was followed by marking of duplicates, and indel-realignment, according to best practice guidelines⁵⁸ by the Genome Analysis ToolKit (GATK) v.3.4-46⁵⁹.

Normal cell contamination in tumor and organoid samples was estimated in silico using PURPLE v. 2.14³⁷.

Somatic SNVs and indels were called in the tumor and the organoids independently using the corresponding blood sample as a reference and 4 different tools: Strelka, v.1.0.14⁶⁰; VarScan, v.2.4.1⁶¹; Freebayes, v.1.0.2 (arXiv:1207.3907); and Mutect, v.1.1.7⁶². The functional effect of the somatic SNVs and indels were predicted using SnpEff v.4.1⁶³. Tumor-organoid pair VCF files were then merged by selecting high confidence SNVs and indels with a minimum alternative allele read depth of 5 in the tumor or 10 in the organoids and called by at least 2 independent somatic callers in either of the samples. Additionally, high confidence SNVs that were only detected in either the tumor or the organoid sample of a pair, were called in the corresponding sample (tumor or organoid) when supported by more than 5% of the reads covering that position.

Copy number variation was detected for each sample independently using Control-FREEC, v. 7.2⁶⁴ and assuming a ploidy of 2. For sample HGS-6, a ploidy of 3 was assumed for the plots.

Structural variation calling was performed using Manta, v.0.29.5⁶⁵. For increased sensitivity, we ran Manta in the 4 available analysis types: single-sample, multi-sample, tumor-only and tumor-normal. When comparing SVs called in one of the tumor/organoid pairs with the matching sample, we inspected the output of the tumor-normal mode of the pertinent tumor/organoid sample with the results of the four calling modes for the matching tumor/organoid sample.

Somatic variant calling could not be performed for samples without matching reference DNA (CCC-1 and END-1). In these cases, germline variant calling was performed jointly for tumor and organoid samples using GATK's Haplotype Caller, v3.4-46⁵⁹. Germline calls were filtered against the Genome of the Netherlands (GoNL)⁶⁶ and the 1000 Genomes⁶⁷ and only variants with a predicted "moderate" or "high" effect (SnpEff v.4.1⁶³) were kept. For SV calling of the CCC-1 and END-1 samples, the tumor-normal mode of Manta could not be used, but all other Manta variant calling workflows were performed (tumor-only, single-sample, multi-sample). To enrich for somatic SVs, only SVs larger than 10 Kb and not found in the GoNL or 1000 genomes studies were considered for these two samples.

Single Cell Whole Genome Sequencing Library Preparation

Cells were sorted into 384-well plates with 5 ul of mineral oil (Sigma-Aldrich). After sorting cells can be stored at -20C. 500 nl of lysis mix (0.0005 u Qiagen Protease in NEB Buffer 4) was added to each well and lysis was performed at 55C overnight followed by heat inactivation for 20 minutes at 75C and for 5 minutes at 80C. 500nl of Restriction Enzyme mix (0.5 u NLAIII in NEB Cutsmart buffer) was added to each well and restriction was performed for 3 hours at 37C followed by heat inactivation for 20 minutes at 65C. 100 nl of 1 uM barcoded double stranded NLAIII adapter was added to each well. 1100 ul of Ligation mix (200 u T4 DNA Ligase in 1x T4 DNA Ligase buffer supplemented with 3 mM ATP) was added to each well and ligation was performed overnight at 16C. After ligation single cell were pooled and library preparation was performed as described in Muraro et al.⁶⁸. Libraries were sequenced on an Illumina Nextseq500 with 2 x 75 bp paired end sequencing.

Single Cell Whole Genome Sequencing Data Analysis

Reads were aligned to GRCh38 using Burrows Wheeler Aligner v0.7.14 mapping tool with settings 'bwa mem -M'⁶⁹. Data was binned in 1 MB bins and normalized to the expected NLAIII mappability per bin. The expected NLAIII mappability per bin was calculated by generating 10^8 reads from the reference genome, with every read starting at a NLAIII site. These reads were subsequently mapped and binned using the same procedure as for the experimental data. The number of reads per bin was then divided by the average number of reads per bin to acquire the expected NLAIII mappability for each bin. Regions where the expected NLAIII mappability was < 0.9 or > 1.2 were excluded from further analysis. After this the cells were filtered and only cells with > 20000 reads were kept for further analysis. The median read count of each cell was then set to 2 in order to represent a diploid genome. Data was log 2 transformed to obtain log 2 CN ratios and smoothed using a running mean (R package caTools) with a width of 20MB. To remove additional low-quality cells the variance across the genome was calculated for each cell and cells with a variance > 0.3 were removed. For 2D visualization of the data we first performed independent component analysis (ica) (R package fastICA) followed by t-stochastic neighbor embedding (t-SNE) (R package Rtsne). Clustering was performed using ward.D2 hierarchical clustering on the Manhattan distances of the ica transformed data. Subsequently, the average copy number profile per cluster was calculated using the R package DNACopy. Finally, a tree was constructed using ward.D2 hierarchical clustering on the manhattan distances of the DNACopy derived CNV profiles of the non-diploid clusters.

RNA-seq Analysis

RNA was isolated from organoids with Trizol Reagent (Ambion). RNA libraries were generated with the Truseq Stranded Ribo-zero Sample preparation kit. RNA integrity

1

2

3

4

5

&

was assessed by TapeStation (RNA screen) and quantified by Qubit (RNA). Libraries were multiplexed and paired-end sequenced (2x75bp) on Illumina NextSeq.

Table S10 provides a list of all commercial and custom code used for data collection and analysis including: name, version, source, and link.

RNA-seq data was processed with our in-house RNA analysis pipeline (v.2.3.0, <https://github.com/UMCUGenetics/RNASeq>). Reads were aligned to the human reference genome GRCh37 using STAR v. 2.4.2⁷⁰, and then read count was performed with HTSeq-count, v. 0.6.1⁷¹. Features (ENSEMBL definitions GRCh37, release 74) with zero read counts were filtered out (21711 features out of 63677). Gene symbols were mapped to the ENSEMBL features using the biomaRt package v. 2.26.1⁷², and features without corresponding gene symbols and with duplicate mappings were removed. The final count matrix consisted of 30080 rows (genes). The DESeq2 package, v1.10.1⁷³ was then used to normalize the read counts using the median-of-ratios method. Spearman correlation between samples was calculated using the normalized read counts from all 5000 most variable genes and samples were clustered using hierarchical clustering with complete linkage on the correlation matrix. The genetically modified organoid lines were analyzed using the same DESeq2 pipeline.

Methylation Analysis

For methylation analysis 210ng of genomic DNA was used. DNA was sodium bisulfite converted with the Zymo Research EZ DNA methylation kit (Zymo Research, Irvine, CA) and treated with the InfiniumHD FFPE Restore kit (Illumina, San Diego, CA). Next, the DNA was hybridized to the Infinium MethylationEPIC 850K BeadChip (Illumina, San Diego, CA) to analyse the genome-wide methylation status of 865859 methylation sites.

Table S10 provides a list of all commercial and custom code used for data collection and analysis including: name, version, source, and link.

For methylation data analysis, fluorescence intensity data (.IDAT) files were analyzed by using the minfi R package⁷⁴. Beta-values were extracted after applying a normalization step with minfi preprocessFunnorm. Pearson correlation of beta values between samples was calculated, and subsequently unsupervised hierarchical clustering of correlation values was performed on the 11720 most variable probes.

Code Availability

Illumina data processing pipeline v2.2.1 is available under <https://github.com/UMCUGenetics/IAP/releases/tag/v2.2.1>, RNA analysis pipeline v2.3.0 is available under <https://github.com/UMCUGenetics/RNASeq>. All other custom code used for this study is available under <https://github.com/UMCUGenetics/OvCaBiobank>

Gene Editing

Organoids derived from early passaged (P0-P3) FT organoids were dissociated into small clumps using pre-warmed Accutase solution (**A6964**, **SIGMA**), washed once with

AdDF+++ and twice with Opti-MEM (11058021, Life technologies). Cells were suspended with 100 μ l Opti-MEM containing RHO/ROCK pathway inhibitor (10 μ M) and 10 μ g of pSpCas9(BB)-2A-GFP (A gift from Feng Zhang⁷⁵, Addgene plasmid # 48138) with gRNA targeting *TP53* (GACGGAAACCGTAGCTGCC)⁵⁰ or combination of gRNA targeting *TP53* and *RB1* (GTTCGAGGTGAACCATTAAT) genes, and transferred into 2 mm gap NEPA electroporation cuvette (Lot No. 2S1509). For electroporation, we utilized NEPA21 type-II electroporator (Table S11).

Following electroporation, 300 μ l of complete growth medium was added to the cells and they were incubated at room temperature for 15 min. Cells were centrifuged, suspended in 200 μ l BME and plated as previously described. Complete medium was added after cell-BME suspension drops had solidified. 2-3 days after electroporation 10 μ M Nutlin-3 (Cayman Chemical) was added to the growth medium. 2-3 weeks after electroporation, single organoids were picked and transferred into 1.5 ml microcentrifuge tubes containing 200 μ l of pre-warmed Accutase. Following 2-3 min incubation, organoids were sheared into small cell clumps by pipetting, washed with 1ml AdDF+++ and centrifuged for 5 min in 2000 rpm. Cells were resuspended with 40 μ l BME and plated. For genotyping, genomic DNA was isolated using Viagen Direct PCR (Viagen). GoTaq Flexi DNA polymerase (Promega) was used for PCR amplification. Primer sequences: P53_for, 5'-CAGGAAGCCAAAGGGTGAAGA-3' P53_rev, 5'-CCCATCTACAGTCCCCCTTG-3'. RB1_for, 5'-CAGAGTAGAAGAGGGATGGCA-3' RB1_rev, 5'-CAGTGATTCCAGAGTGACGGA-3'. Products were cloned into pGEM-T Easy vector system I (Promega) and sequenced using T7 sequencing primer.

Lentivirus Transduction of Organoids

To visualize mitoses, organoids were infected with lentivirus encoding mNeon-tagged histone 2B and a puromycin-resistance cassette (pLV-H2B-mNeon-ires-Puro⁵⁰) as previously described⁷⁶.

Drug Screen and Viability Assay

1mg/ml dispase II (Invitrogen) was added to the medium of the organoids and these were incubated for 10 min at 37°C to digest the BME. Subsequently, organoids were mechanically dissociated by pipetting and were filtrated using a 70 mm nylon cell strainer (Falcon), resuspended in 2% BME/growth medium (15–20,000 organoids/ml) prior plating in 50 μ l volume (Multi-dropTM Combi Reagent Dispenser) on BME pre-coated 384-well plates.

The drugs and their combinations were added 1 hr after plating the organoids using the Tecan D300e Digital Dispenser. Drugs were dispensed in a randomized manner and DMSO end concentration was 1% in all wells. 120 hr after adding the drugs, ATP levels were measured using the Cell-Titer Glo2.0 (Promega BV) according to the manufacturer's instructions and luminescence was measured using a SpectraMax microplate reader

1

2

3

4

5

&

(Molecular Devices). Results were normalized to vehicle (DMSO = 100%) and baseline control (Navitoclax 20 μ M).

Data was analyzed using GraphPad Prism 6. Using the trapezoid rule for numerical integration, the area under the curve (AUC) is approximated between the lowest and highest concentrations screened in the actual assay. Organoid drug sensitivity was represented by the average AUC of two technical replicates and independent experimental repetitions in a subset of treatments and visualized using RStudio. Experimental repetition with a subset of drugs was performed in the following lines: FT-1, FT(P)-1, END-1.1, END-1.2, MC-2.1, HGS-1, HGS-1-R2, HGS-3.1, HGS-3.2, HGS-22, HGS-23. Euclidean distance between samples was measured using the normalized (Row Z-score) AUC.

Alpelisib (BYL719),	Cat# S2814, Selleckchem
Adavosertib (MK-1775),	Cat# S1525, Selleckchem
AZD8055,	Cat# S1555, Selleckchem
Carboplatin,	Cat# S1215, Selleckchem
Gemcitabine,	Cat# S1714, Selleckchem
MK-2206,	Cat# S1078, Selleckchem
Niraparib (MK-4827),	Cat# S2741, Selleckchem
Nutlin-3,	Cat# 10004372, Cayman Chemical
Paclitaxel,	Cat# S1150, Selleckchem
Pictilisib (GDC-0941),	Cat# S1065, Selleckchem

REcombination CAPacity (RECAP) Assay

Organoids were incubated at 37°C, 5% CO₂ humidified atmosphere and an equal number of organoids were transferred to 3cm petri dishes containing 2ml of medium. One petri dish was irradiated with 5Gy x-rays (200kV, 4mA, YXLON Y.TU 225-D02) and the other petri dish was mock-treated (i.e. not irradiated). 0.02mM of EdU (ThermoFisher Scientific, Click-iT EdU Alexa Fluor 647 Imaging Kit, cat. C10340) was added to the organoids and incubated for two hours at 37°C, 5% CO₂ humidified atmosphere on a 60rpm rotating platform. The organoids were transferred to 15ml falcon tubes and after the organoids were settled down by normal gravity at room temperature, medium was removed and replaced by 10ml buffered formalin (10%). Organoids were fixed for one hour on a rotating device at room temperature, washed twice with PBS and stored in 70% ethanol at 4°C. The organoids were embedded into paraffin, sliced into 5 μ m slices and incubated in 60°C o/n on StarFrost microscope slides (76x26mm, Knittel glass). Immunofluorescence staining was performed to stain for DAPI (ThermoFisher Scientific, cat. P36935,), Geminin (Primary Antibody Rabbit, Proteintech Europe, cat. 10802-1-AP), RAD51 (Primary Antibody Mouse, Gene Tex, GTX70230) and EdU (ThermoFisher Scientific, Click-iT™ EdU Alexa Fluor™ 647 Imaging Kit, cat. C10340). RAD51 foci were scored blindly in ten randomly chosen organoids, counting at least 100 Geminin positive cells in total for both the irradiated and the non-irradiated organoids. Biological repetitions were done as indicated in figure legend (Figure 6). A nucleus was scored as RAD51 positive if

it contained more than five foci. Organoids in which less than 6 cells were counted as Geminin+ were filtered out from analysis.

Organoid Derived Xenograft

Experiments on NSG mice were carried out at the Netherlands Cancer Institute according to local and international regulations and ethical guidelines, and were approved by the local and central animal experimental committee at the Netherlands Cancer Institute (AVD3010020172464; IVD 9.1 EGP 8102) 8102)

Ovarian injection:

Mice are anesthetized with isoflurane (3% induction, and 2% maintenance), a small incision in the flank and peritoneum is made.

Ovary is gently taken from the abdominal cavity and tumor cells are slowly injected with an insulin needle (Terumo 29G x ½, 0.33 x12mm) into the bursa. The ovary is positioned back in the abdominal cavity, and peritoneum and skin are sutured separately.

IVIS-imaging:

Mice were injected with 10 μl/g bodyweight of Beetle luciferin (promega E1605), after 10 minutes bioluminescence was measured on the IVIS Lumina. After sacrifice the ovary was taken out and embedded in paraffin for further analysis.

Intervention study:

Experiments on NSG mice were carried out at the Netherlands Cancer Institute according to local and international regulations and ethical guidelines, and were approved by the local animal experimental committee at the Netherlands Cancer Institute (AVD301002015407; IVD 1.1 EGP 8583).

Subcutaneous injection:

Mice are subcutaneously injected with the organoid lines. Caliper measurements were performed three times per week. When the tumors reached a size of 50 mm³, treatment started with either Vehicle (saline) or Gemcitabine (2 mg/kg), intraperitoneal injection 5 times per week (5 on, 2 off) for 4 consecutive weeks. 10 mice per treatment arm were included. Tumor size was monitored for 55 days, mice that died before that time point (after surgery or Gemcitabine treatment) were excluded from analysis.

Statistical Analyses

Where applicable, statistical methods were outlined in the respective figure legends.

Statistical analysis was performed utilizing Microsoft Excel; GraphPad and R package.

P values were calculated using two-tailed Student's t test. DNA and RNA sequencing analysis details can be found in the relevant methods sections.

For karyotyping a minimum of 14 metaphase spreads was analyzed for each line. For single cell DNA analysis 791 cells from 2 recurrent tumor samples and 3 corresponding organoid lines were analyzed. Drug screen killing curves show the average±SEM of two technical replicates. AUC of independent drug screen repetitions was averaged

1

2

3

4

5

&

and presented in drug sensitivity heatmap (experimental repetitions (n=2) at different passage number in a subset of treatments was carried out in 11 independent organoid lines, Extended Data Figure 5d). For animal intervention experiments 10 mice per treatment arm were included. Mice that died before the experimental end-point were excluded from analysis. In the case of representative results, the number of independent organoid lines or experimental repetitions and their relevant description are indicated in the figure legend.

Clinical Data

Patients agreed with the use of their clinical data by signing informed consent. Clinical data was extracted from the patient file by the Dutch Cancer Registration and included age at diagnosis, patient history, BRCA mutation status, tumor characteristics and treatment modalities.

Reporting Summary

Further information on research design is available in the Life Sciences Reporting Summary linked to this article.

DATA AVAILABILITY STATEMENT

BAM files for DNA and RNA sequencing data are made available through controlled access at the European Genome-phenome Archive (EGA) which is hosted at the EBI and the CRG (<https://ega-archive.org>), under accession number EGA: EGAS00001003073. Data access requests will be evaluated by the UMCU Department of Genetics Data Access Board (EGAC00001000432) and transferred upon completion of a material transfer agreement and authorization by the medical ethical committee UMCU at request of the HUB in order to ensure compliance with the Dutch 'medical research involving human subjects' act.

ACKNOWLEDGEMENTS

We thank T. Bayram for supporting of ethical regulatory affairs. We acknowledge A. Brousalı, P. van der Groep, A. Constantinides, A. Snelting and O. Kranenburg of the Utrecht Platform for Organoid Technology (U-PORT; UMC Utrecht) for patient inclusion and tissue acquisition. We would like to thank the Integraal Kankercentrum Nederland (IKNL) and M. van der Aa for supplying clinical data, and I. Renkens for help with DNA isolations. We would like to acknowledge E. Stelloo for her help with culturing organoids. We would like to thank the people from the Preclinical Intervention Unit of the Mouse Clinic for Cancer and Ageing (MCCA) at the NKI for performing the intervention studies. We would like to thank B. Artegiani and T. Dayton for critically reading the manuscript. O.K. was supported by Marie Skłodowska-Curie IF grant 658933 – HGSOC, This work was funded by the gravitation program CancerGenomiCs.nl from the Netherlands Organisation for Scientific Research (NWO), MKMD grant (114021012) from Netherlands Organization for

Scientific Research (NWO-ZonMw), Stand Up to Cancer International Translational Cancer Research Grant, a program of the Entertainment Industry Foundation administered by the AACR, Dutch Cancer Society (KWF) grant UU2015-7743 and a grant from the Gieskes Strijbis Foundation (1816199). The OncoCode Institute is supported by the Dutch Cancer Society.

AUTHOR CONTRIBUTIONS

Conceptualization, O.K., and H.C.; Methodology, O.K., and H.C.; Software, J.E.V.-I., M.J.V.R., L.K., and W.P.K; Formal Analysis, O.K., K.L., N.H., J.E.V.-I., M.J.V.R., T.J., P.J.V.D., S.A.R., L.K., and W.P.K.; Investigation, O.K., K.L., C.J.D.W., N.H., A.V.B., H.B., J.K., S.A.R., L.K., N.P., R.T., L.M.V.W., and B.P.; Resources, C.J.D.W., L.M.V.W., H.V., M.P.G.V., V.W.H., B.G.N., P.O.W., M.V.D.V., T.B., K.N.G., and R.P.Z.; Data Curation, O.K., C.J.D.W., and J.E.V.-I., Writing – Original Draft, O.K., C.J.D.W., J.E.V.-I., W.P.K., and H.C., Visualization, O.K., C.J.D.W., K.L., J.E.V.-I., W.P.K., L.K., and N.H.; Supervision, M.V.D.V., J.L.B., R.P.Z., H.J.G.S., W.P.K., A.V.O., and H.C.; Project Administration, O.K., C.J.D.W., W.P.K., and H.C.; Funding Acquisition, J.L.B., R.P.Z., P.O.W., W.P.K., and H.C.

COMPETING INTERESTS STATEMENT

We declare that none of the authors have competing financial or non-financial interests as defined by Nature Research.

1

2

3

4

5

&

REFERENCES

1. Vaughan, S. *et al.* Rethinking ovarian cancer: recommendations for improving outcomes. *Nat Rev Cancer* **11**, 719-725 (2011).
2. Bowtell, D.D. *et al.* Rethinking ovarian cancer II: reducing mortality from high-grade serous ovarian cancer. *Nat Rev Cancer* **15**, 668-679 (2015).
3. Fischerova, D., Zikan, M., Dunder, P. & Cibula, D. Diagnosis, treatment, and follow-up of borderline ovarian tumors. *Oncologist* **17**, 1515-1533 (2012).
4. Koshiyama, M., Matsumura, N. & Konishi, I. Recent concepts of ovarian carcinogenesis: type I and type II. *Biomed Res Int* **2014**, 934261 (2014).
5. Cancer Genome Atlas Research, N. Integrated genomic analyses of ovarian carcinoma. *Nature* **474**, 609-615 (2011).
6. Ciriello, G. *et al.* Emerging landscape of oncogenic signatures across human cancers. *Nat Genet* **45**, 1127-1133 (2013).
7. Piek, J.M. *et al.* Dysplastic changes in prophylactically removed Fallopian tubes of women predisposed to developing ovarian cancer. *J Pathol* **195**, 451-456 (2001).
8. Kurman, R.J. & Shih Ie, M. The origin and pathogenesis of epithelial ovarian cancer: a proposed unifying theory. *Am J Surg Pathol* **34**, 433-443 (2010).
9. Thu, K.L. *et al.* A comprehensively characterized cell line panel highly representative of clinical ovarian high-grade serous carcinomas. *Oncotarget* **8**, 50489-50499 (2017).
10. Fleury, H. *et al.* Novel high-grade serous epithelial ovarian cancer cell lines that reflect the molecular diversity of both the sporadic and hereditary disease. *Genes Cancer* **6**, 378-398 (2015).
11. Ince, T.A. *et al.* Characterization of twenty-five ovarian tumour cell lines that phenocopy primary tumours. *Nat Commun* **6**, 7419 (2015).
12. Letourneau, I.J. *et al.* Derivation and characterization of matched cell lines from primary and recurrent serous ovarian cancer. *BMC Cancer* **12**, 379 (2012).
13. Kreuzinger, C. *et al.* Molecular characterization of 7 new established cell lines from high grade serous ovarian cancer. *Cancer Lett* **362**, 218-228 (2015).
14. Sachs, N. & Clevers, H. Organoid cultures for the analysis of cancer phenotypes. *Curr Opin Genet Dev* **24**, 68-73 (2014).
15. Domcke, S., Sinha, R., Levine, D.A., Sander, C. & Schultz, N. Evaluating cell lines as tumour models by comparison of genomic profiles. *Nat Commun* **4**, 2126 (2013).
16. Jones, P.M. & Drapkin, R. Modeling High-Grade Serous Carcinoma: How Converging Insights into Pathogenesis and Genetics are Driving Better Experimental Platforms. *Front Oncol* **3**, 217 (2013).
17. Ben-David, U. *et al.* Patient-derived xenografts undergo mouse-specific tumor evolution. *Nat Genet* **49**, 1567-1575 (2017).
18. Sato, T. *et al.* Long-term expansion of epithelial organoids from human colon, adenoma, adenocarcinoma, and Barrett's epithelium. *Gastroenterology* **141**, 1762-1772 (2011).
19. Gao, D. *et al.* Organoid cultures derived from patients with advanced prostate cancer. *Cell* **159**, 176-187 (2014).

20. Fujii, M. *et al.* A Colorectal Tumor Organoid Library Demonstrates Progressive Loss of Niche Factor Requirements during Tumorigenesis. *Cell Stem Cell* **18**, 827-838 (2016).
21. Boj, S.F. *et al.* Organoid models of human and mouse ductal pancreatic cancer. *Cell* **160**, 324-338 (2015).
22. van de Wetering, M. *et al.* Prospective derivation of a living organoid biobank of colorectal cancer patients. *Cell* **161**, 933-945 (2015).
23. Roerink, S.F. *et al.* Intra-tumour diversification in colorectal cancer at the single-cell level. *Nature* **556**, 457-462 (2018).
24. Vlachogiannis, G. *et al.* Patient-derived organoids model treatment response of metastatic gastrointestinal cancers. *Science* **359**, 920-926 (2018).
25. Sachs, N. *et al.* A Living Biobank of Breast Cancer Organoids Captures Disease Heterogeneity. *Cell* **172**, 373-386 e310 (2018).
26. Verissimo, C.S. *et al.* Targeting mutant RAS in patient-derived colorectal cancer organoids by combinatorial drug screening. *Elife* **5** (2016).
27. Hill, S.J. *et al.* Prediction of DNA Repair Inhibitor Response in Short-Term Patient-Derived Ovarian Cancer Organoids. *Cancer Discov* **8**, 1404-1421 (2018).
28. Kessler, M. *et al.* The Notch and Wnt pathways regulate stemness and differentiation in human fallopian tube organoids. *Nat Commun* **6**, 8989 (2015).
29. Gilmour, L.M. *et al.* Neuregulin expression, function, and signaling in human ovarian cancer cells. *Clin Cancer Res* **8**, 3933-3942 (2002).
30. Aune, G. *et al.* Increased circulating hepatocyte growth factor (HGF): a marker of epithelial ovarian cancer and an indicator of poor prognosis. *Gynecol Oncol* **121**, 402-406 (2011).
31. Sheng, Q. *et al.* An activated ErbB3/NRG1 autocrine loop supports in vivo proliferation in ovarian cancer cells. *Cancer Cell* **17**, 298-310 (2010).
32. Bourgeois, D.L., Kabarowski, K.A., Porubsky, V.L. & Kreeger, P.K. High-grade serous ovarian cancer cell lines exhibit heterogeneous responses to growth factor stimulation. *Cancer Cell Int* **15**, 112 (2015).
33. Antoniou, A. *et al.* Average risks of breast and ovarian cancer associated with BRCA1 or BRCA2 mutations detected in case Series unselected for family history: a combined analysis of 22 studies. *Am J Hum Genet* **72**, 1117-1130 (2003).
34. Gabai-Kapara, E. *et al.* Population-based screening for breast and ovarian cancer risk due to BRCA1 and BRCA2. *Proc Natl Acad Sci U S A* **111**, 14205-14210 (2014).
35. Wang, M. *et al.* PAX2 and PAX8 reliably distinguishes ovarian serous tumors from mucinous tumors. *Appl Immunohistochem Mol Morphol* **23**, 280-287 (2015).
36. Rajagopalan, H. & Lengauer, C. Aneuploidy and cancer. *Nature* **432**, 338-341 (2004).
37. Priestley, P. *et al.* Pan-cancer whole-genome analyses of metastatic solid tumours. *Nature* **575**, 210-216 (2019).
38. Gorringe, K.L. *et al.* High-resolution single nucleotide polymorphism array analysis of epithelial ovarian cancer reveals numerous microdeletions and amplifications. *Clin Cancer Res* **13**, 4731-4739 (2007).

1

2

3

4

5

&

39. Hunter, S.M. *et al.* Pre-invasive ovarian mucinous tumors are characterized by CDKN2A and RAS pathway aberrations. *Clin Cancer Res* **18**, 5267-5277 (2012).
40. Romero, I., Sun, C.C., Wong, K.K., Bast, R.C., Jr. & Gershenson, D.M. Low-grade serous carcinoma: new concepts and emerging therapies. *Gynecol Oncol* **130**, 660-666 (2013).
41. Kuo, K.T. *et al.* Analysis of DNA copy number alterations in ovarian serous tumors identifies new molecular genetic changes in low-grade and high-grade carcinomas. *Cancer Res* **69**, 4036-4042 (2009).
42. Seidman, J.D., Yemelyanova, A., Zaino, R.J. & Kurman, R.J. The fallopian tube-peritoneal junction: a potential site of carcinogenesis. *Int J Gynecol Pathol* **30**, 4-11 (2011).
43. Kurman, R.J. & Shih le, M. Molecular pathogenesis and extraovarian origin of epithelial ovarian cancer--shifting the paradigm. *Hum Pathol* **42**, 918-931 (2011).
44. Seidman, J.D. & Khedmati, F. Exploring the histogenesis of ovarian mucinous and transitional cell (Brenner) neoplasms and their relationship with Walthard cell nests: a study of 120 tumors. *Arch Pathol Lab Med* **132**, 1753-1760 (2008).
45. Vassilev, L.T. *et al.* In vivo activation of the p53 pathway by small-molecule antagonists of MDM2. *Science* **303**, 844-848 (2004).
46. Yadav, B. *et al.* Quantitative scoring of differential drug sensitivity for individually optimized anticancer therapies. *Sci Rep* **4**, 5193 (2014).
47. Lord, C.J. & Ashworth, A. PARP inhibitors: Synthetic lethality in the clinic. *Science* **355**, 1152-1158 (2017).
48. Murai, J. Targeting DNA repair and replication stress in the treatment of ovarian cancer. *Int J Clin Oncol* **22**, 619-628 (2017).
49. Meijer, T.G. *et al.* Functional Ex Vivo Assay Reveals Homologous Recombination Deficiency in Breast Cancer Beyond BRCA Gene Defects. *Clin Cancer Res* **24**, 6277-6287 (2018).
50. Drost, J. *et al.* Sequential cancer mutations in cultured human intestinal stem cells. *Nature* **521**, 43-47 (2015).
51. Matano, M. *et al.* Modeling colorectal cancer using CRISPR-Cas9-mediated engineering of human intestinal organoids. *Nat Med* **21**, 256-262 (2015).
52. Drost, J. *et al.* Use of CRISPR-modified human stem cell organoids to study the origin of mutational signatures in cancer. *Science* **358**, 234-238 (2017).
53. Fumagalli, A. *et al.* Genetic dissection of colorectal cancer progression by orthotopic transplantation of engineered cancer organoids. *Proc Natl Acad Sci U S A* **114**, E2357-E2364 (2017).
54. Schmeler, K.M. *et al.* Neoadjuvant chemotherapy for low-grade serous carcinoma of the ovary or peritoneum. *Gynecol Oncol* **108**, 510-514 (2008).
55. Gershenson, D.M. *et al.* Recurrent low-grade serous ovarian carcinoma is relatively chemoresistant. *Gynecol Oncol* **114**, 48-52 (2009).
56. Pectasides, D. *et al.* Advanced stage mucinous epithelial ovarian cancer: the Hellenic Cooperative Oncology Group experience. *Gynecol Oncol* **97**, 436-441 (2005).
57. Brown, J. & Frumovitz, M. Mucinous tumors of the ovary: current thoughts on diagnosis and management. *Curr Oncol Rep* **16**, 389 (2014).

58. Van der Auwera, G.A. *et al.* From FastQ data to high confidence variant calls: the Genome Analysis Toolkit best practices pipeline. *Curr Protoc Bioinformatics* **43**, 11 10 11-11 10 33 (2013).
59. McKenna, A. *et al.* The Genome Analysis Toolkit: a MapReduce framework for analyzing next-generation DNA sequencing data. *Genome Res* **20**, 1297-1303 (2010).
60. Saunders, C.T. *et al.* Strelka: accurate somatic small-variant calling from sequenced tumor-normal sample pairs. *Bioinformatics* **28**, 1811-1817 (2012).
61. Koboldt, D.C. *et al.* VarScan 2: somatic mutation and copy number alteration discovery in cancer by exome sequencing. *Genome Res* **22**, 568-576 (2012).
62. Cibulskis, K. *et al.* Sensitive detection of somatic point mutations in impure and heterogeneous cancer samples. *Nat Biotechnol* **31**, 213-219 (2013).
63. Cingolani, P. *et al.* A program for annotating and predicting the effects of single nucleotide polymorphisms, SnpEff: SNPs in the genome of *Drosophila melanogaster* strain w1118; iso-2; iso-3. *Fly (Austin)* **6**, 80-92 (2012).
64. Boeva, V. *et al.* Control-FREEC: a tool for assessing copy number and allelic content using next-generation sequencing data. *Bioinformatics* **28**, 423-425 (2012).
65. Chen, X. *et al.* Manta: rapid detection of structural variants and indels for germline and cancer sequencing applications. *Bioinformatics* **32**, 1220-1222 (2016).
66. Genome of the Netherlands, C. Whole-genome sequence variation, population structure and demographic history of the Dutch population. *Nat Genet* **46**, 818-825 (2014).
67. Genomes Project, C. *et al.* A global reference for human genetic variation. *Nature* **526**, 68-74 (2015).
68. Muraro, M.J. *et al.* A Single-Cell Transcriptome Atlas of the Human Pancreas. *Cell Syst* **3**, 385-394 e383 (2016).
69. Li, H. & Durbin, R. Fast and accurate short read alignment with Burrows-Wheeler transform. *Bioinformatics* **25**, 1754-1760 (2009).
70. Dobin, A. *et al.* STAR: ultrafast universal RNA-seq aligner. *Bioinformatics* **29**, 15-21 (2013).
71. Anders, S., Pyl, P.T. & Huber, W. HTSeq--a Python framework to work with high-throughput sequencing data. *Bioinformatics* **31**, 166-169 (2015).
72. Durinck, S., Spellman, P.T., Birney, E. & Huber, W. Mapping identifiers for the integration of genomic datasets with the R/Bioconductor package biomaRt. *Nat Protoc* **4**, 1184-1191 (2009).
73. Love, M.I., Huber, W. & Anders, S. Moderated estimation of fold change and dispersion for RNA-seq data with DESeq2. *Genome Biol* **15**, 550 (2014).
74. Aryee, M.J. *et al.* Minfi: a flexible and comprehensive Bioconductor package for the analysis of Infinium DNA methylation microarrays. *Bioinformatics* **30**, 1363-1369 (2014).
75. Ran, F.A. *et al.* Genome engineering using the CRISPR-Cas9 system. *Nat Protoc* **8**, 2281-2308 (2013).
76. Koo, B.K. *et al.* Controlled gene expression in primary Lgr5 organoid cultures. *Nat Methods* **9**, 81-83 (2011).

1

2

3

4

5

&

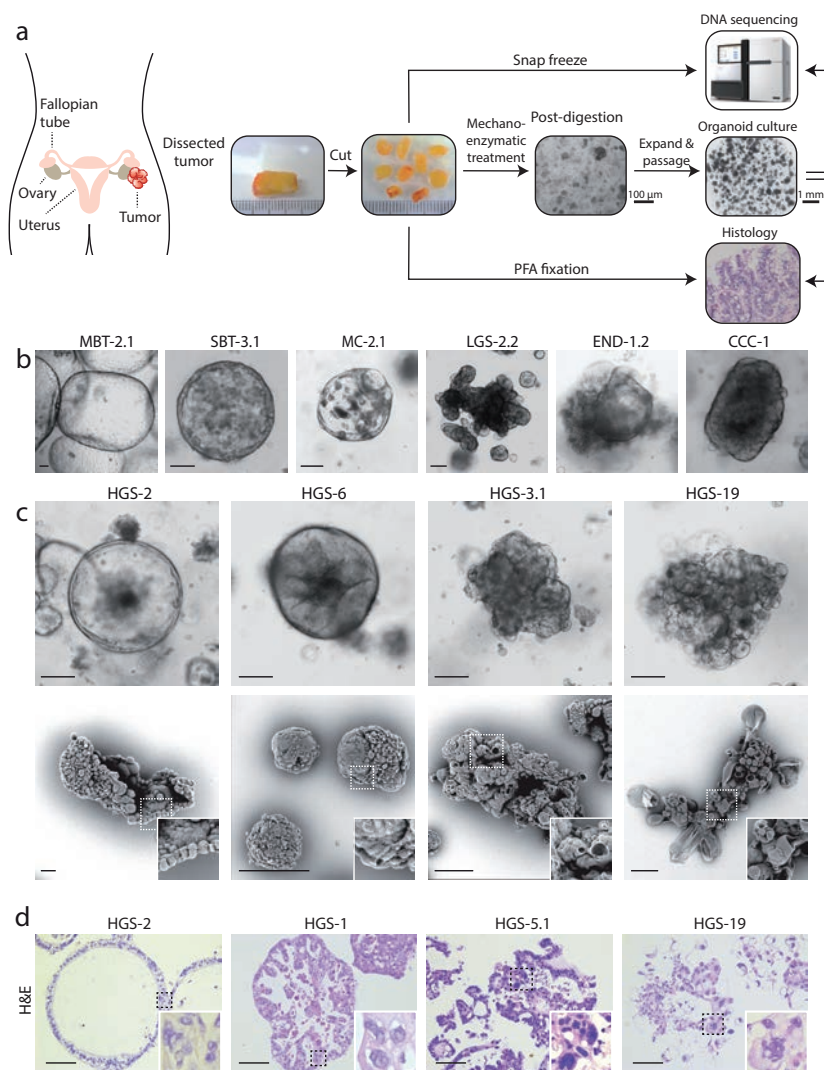
LIST OF SUPPLEMENTARY DATA

Extended Data Figure (ED):

ED Figure 1	Derivation and morphological differences of OC organoids
ED Figure 2	Organoid passage number overview and normal cell contamination in tumors and organoids
ED Figure 3	FT and OSE organoids
ED Figure 4	Genome-wide tumor and organoid pair comparison
ED Figure 5	Molecular characterization, drug screening and xenografts of OC organoids
ED Figure 6	CRISPR-Cas9 mediated genetic manipulation in FT organoids
Table S1*	Patient clinical data
Table S2*	Medium recipe
Table S3*	OC organoid line information
Table S4*	Organoid subtype diversity and derivation efficiency
Table S5*	FT and OSE organoid information
Table S6*	OC organoid histological analysis
Table S7*	RNA and DNA sequencing related information of OC organoids
Table S8*	Organoid derived xenografts
Table S9*	Antibody list
Table S10*	Code availability
Table S11*	Electroporation setup
Video S1*	High-speed time-lapse imaging of normal FT line with beating cilia
Video S2-6*	Live cell imaging of chromosomal segregation in OC organoids

*Tables S1-11 and videos S1-S6 are available online at doi: 10.1038/s41591-019-0422-6.

EXTENDED DATA FIGURES



Extended Data Figure Figure 1. Derivation and morphological differences of OC organoids. (a) Schematic of OC organoid derivation. (b) Bright-field images of MBT, SBT, MC, LGS, END and CCC organoids (left to right), depicting different organoid morphologies. Morphological description of 50 independent organoid lines is provided in Supplementary Table 6. Scale bar, 100 μm. (c) Bright-field (top) and SEM (bottom) images demonstrating main morphologies among different HGS organoid lines. Starting with cystic and well-organized cellular polarity, where microvilli are directed toward the organoid lumen (most left) to dense organoids that gradually (from left to right) show reduced circularity and cellular cohesiveness up to a grape-like shape morphology (most right). Scale bar, 100 μm. (d) High-magnification H&E staining images displaying representative examples of HGS organoid morphologies as well as nuclear and cellular atypia, typically displayed by HGS tumors. Histological description of 50 independent organoid lines is provided in Supplementary Table 6. Scale bar, 100 μm.

1

2

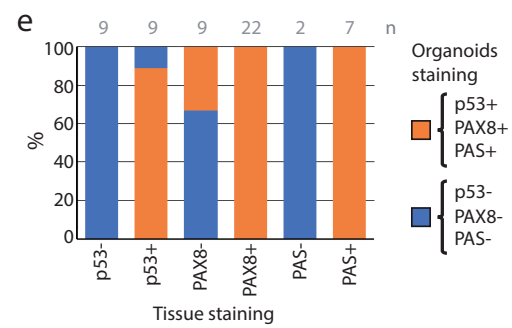
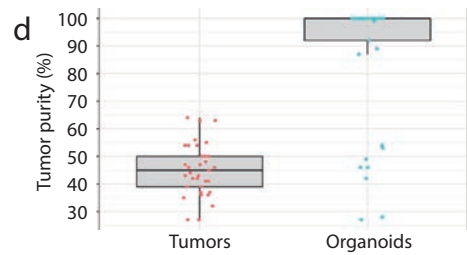
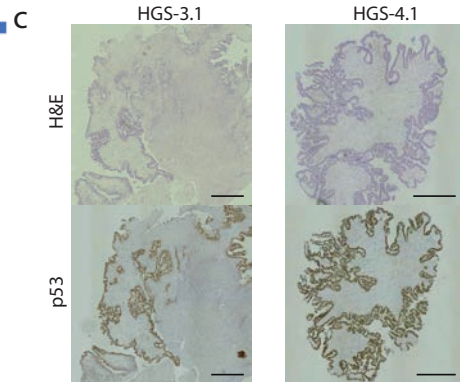
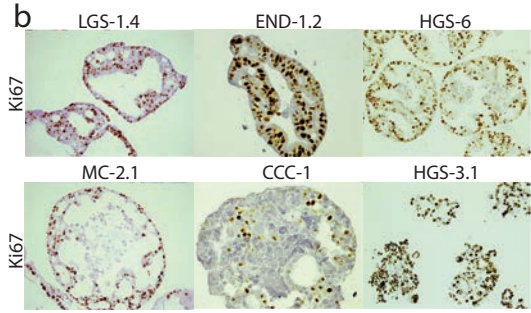
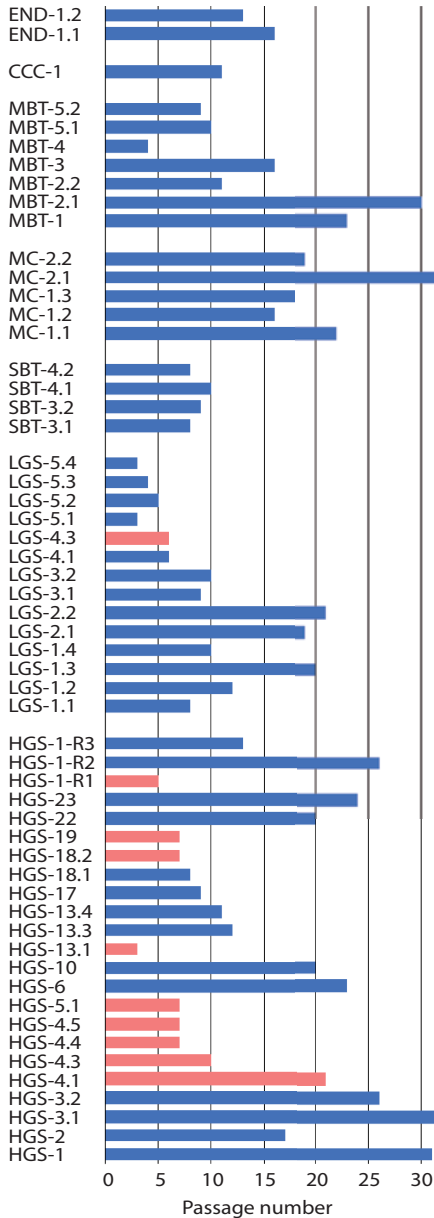
3

4

5

&

a ■ Normal growth
 ■ Reduced growth at indicated passage #



◀ **Extended Data Figure Figure 2.** (a) Column bar graph depicting organoid maximum passage number up until the moment of submission. Organoids that stopped/slowed down their growth are indicated in orange. (b) Representative images of Ki67 staining of six independent organoid lines show a high percentage of ki67-positive proliferating cells. (c) Histological and immunohistochemical images of tumor tissue (derived from two independent patients) showing tumor cell purity within different samples, based on H&E and p53 staining. Scale bar, 0.5 mm. (d) Tukey box-and-whisker plot (1.5× interquartile range) presenting bioinformatic estimation of tumor cell purity percentage of both tissue ($n=35$) and organoid ($n=36$) based on WGS data using PURPLE. Horizontal bars represent median of all dots. Mean and standard deviation across all samples are as follows: $45 \pm 9.2\%$ (tissue) and $88.1 \pm 23\%$ (organoids). (e) Stacked bar chart showing the percentage of organoid lines that are positive for p53, PAX8 and periodic acid–Schiff (PAS) staining (orange) and negative (blue) grouped per original tumor staining status (see also Supplementary Table 6). Total number (n) of tissues stained per group are indicated.

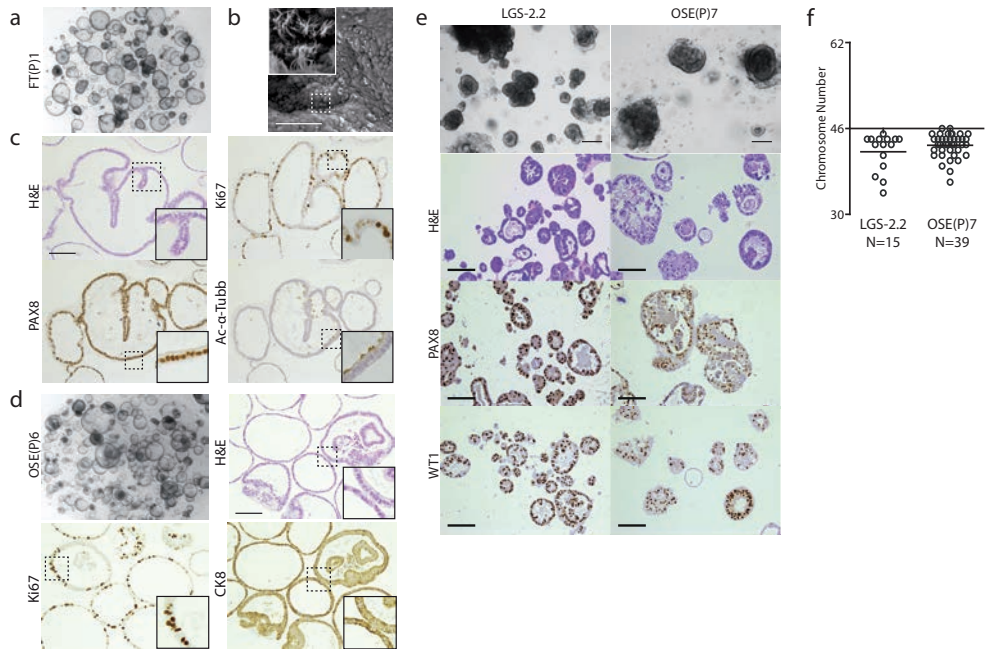
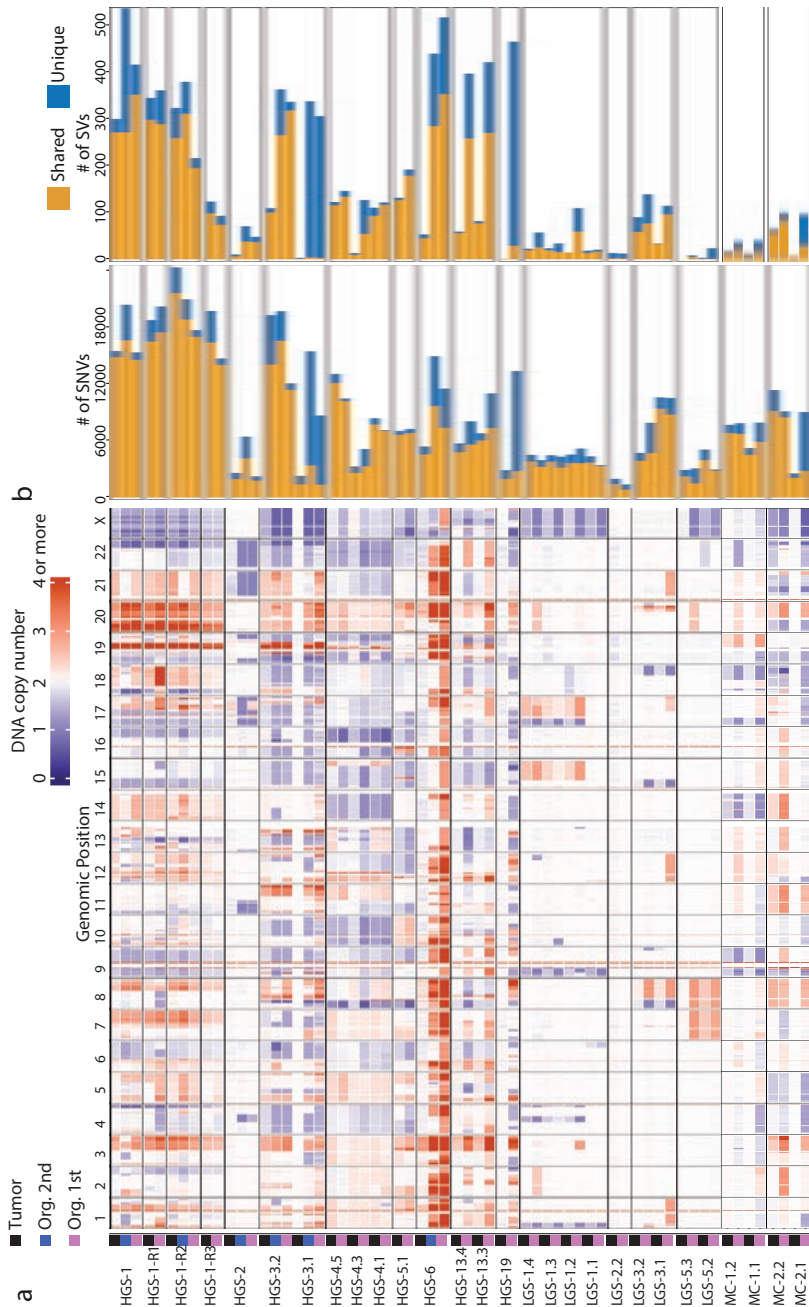


Figure 3. Somatic mutations and amplifications/ deletions in OC organoids. Somatic mutations and amplifications/ deletions in relevant genes of ovarian cancer. For each sample, tumor/ organoid pairs are displayed and indicated by color coding (black- tumors, pink- organoids, blue- organoids re-sequenced and analyzed after extended passaging). Passage number at which organoid lines were sequenced is given in table S7.



Extended Data Figure Figure 4. Genome-wide tumor and organoid pair comparison. (a) Genome-wide CNVs in tumor/organoid pairs (black, tumors; pink, organoids early passage; blue, organoids late passage) depicting gains (red) and losses (blue). (b) Number of shared (yellow) and unique (blue) SNVs (on the left) and SVs (on the right) between tumor/organoid pairs. Shared variants are those that can be found in the corresponding paired sample. Passage number at which organoid lines were sequenced is given in Supplementary Table 7.

1

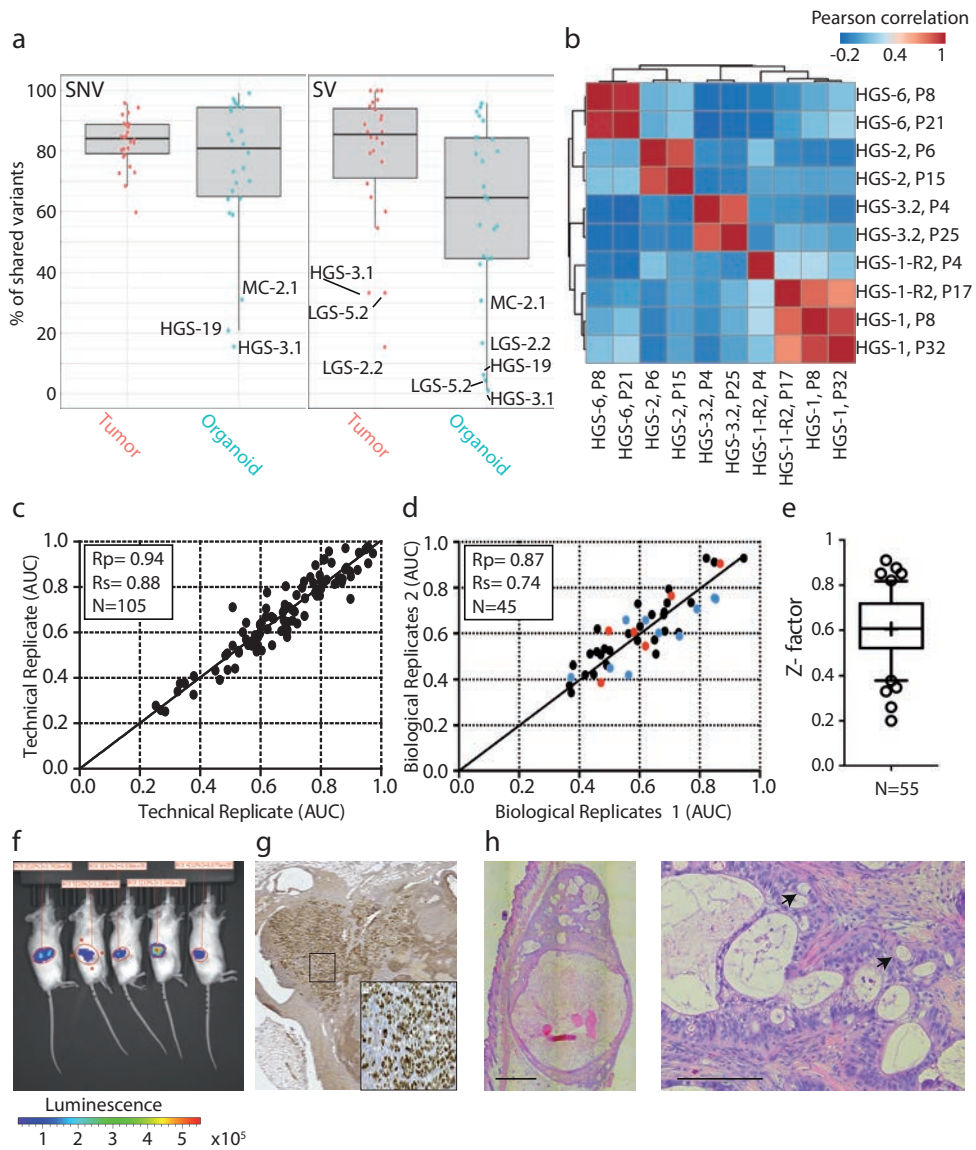
2

3

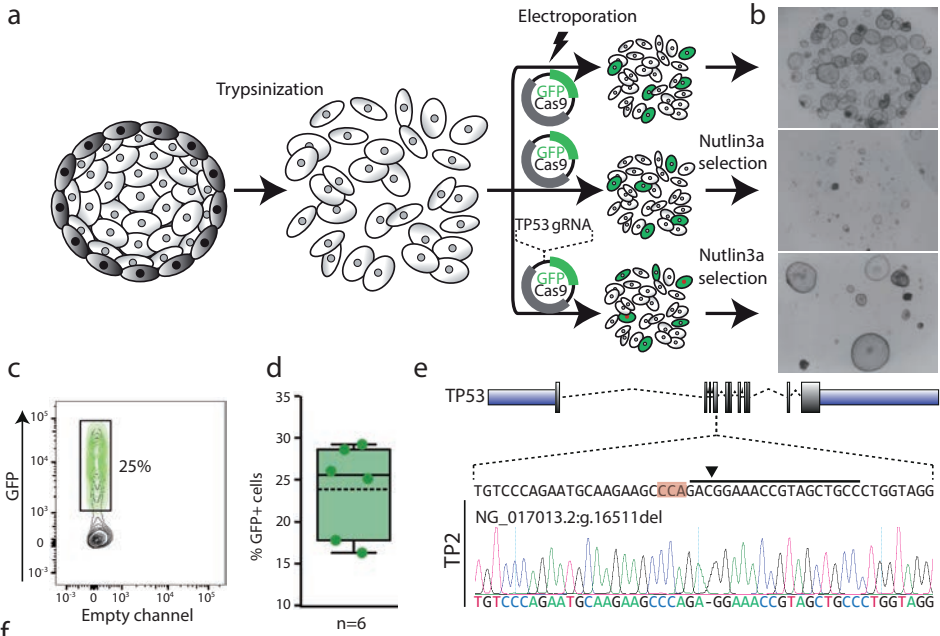
4

5

&

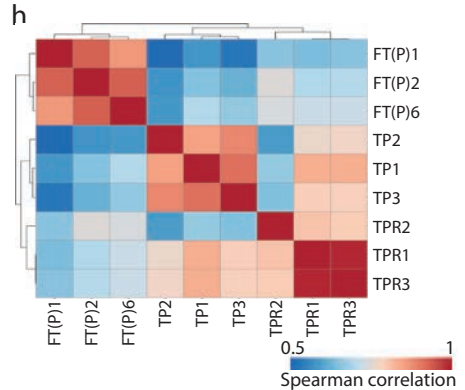
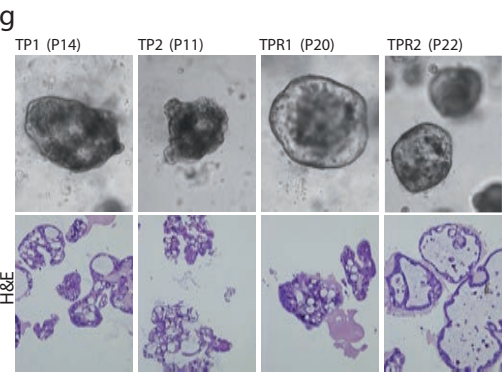


◀ **Extended Data Figure Figure 5. Molecular characterization, drug screening and xenografts of OC organoids.** (a) Tukey box and whisker plot (1.5× interquartile range) summarizing the percentage of shared variants across all tumor (red) and organoid (green) samples. Right and left panels display SNVs and SVs, respectively. Horizontal bars represent median of all dots. Mean and standard deviation across all samples are as follows: SNVs, $82.95 \pm 8.18\%$ (tissue, $n=31$) and $75.62 \pm 23.13\%$ (organoids, $n=31$); SVs, $78.14 \pm 22.11\%$ (tissue, $n=31$) and $60.47 \pm 29.13\%$ (organoids, $n=31$). Samples with a low percentage of shared variants are indicated. (b) Heat map of five independent organoid lines from both early and late passages based on 11,720 methylation probes. The heat map colors represent Pearson correlation values, as calculated from the methylation beta-values. Clustering of the correlation values was performed using hierarchical clustering based on complete linkage. (c) Scatter plot of AUC values across all drug screening data, displaying high correlation between technical replicates (Pearson correlation=0.94, $R^2=0.88$, $n=105$). (d) Scatter plot of AUC values of biological replicates, displaying high correlation (Pearson correlation=0.87, $R^2=0.74$, $n=45$). Colored dots represent biological replicates in which passage differences between experimental repetition is as follows: 1–2 passages, $n=29$ (black); 3–5 passages, $n=10$ (blue) and 13–22 passages, $n=6$, (red), demonstrating stable drug sensitivity even after prolonged passaging. (e) Box-and-whisker plot (10th–90th percentile) showing Z-factor distribution and mean across all drug screening plates. Mean=0.61, ranging between 0.2 and 0.91, $n=55$. (f) Bioluminescence imaging of mice, orthotopically transplanted with luciferase expressing organoid lines depicting tumor growth. A summary of organoid-derived xenograft experiments is presented in Supplementary Table 8. (g) p53 staining of organoid-derived xenograft (HGS-3.1) on orthotopic transplantation into the mouse bursa shows p53 overexpression in tumor cells. (h) Histological analysis of an organoid-derived xenograft (MC-2.1) on subcutaneous transplantation. H&E staining shows haphazardly arranged neoplastic glands lined by columnar cells with variable numbers of goblet cells (arrows), which are specific features of MC. A summary of organoid-derived xenograft experiments is presented in Supplementary Table 8. Left image scale bar, 1 mm. Right image scale bar, 200 μm .



f

FT line- Clone #	Targeted genes		
	TP53 gene		RB1 gene
FT(P)1- TP1	NG_017013.2:g.16499_16523del NG_017013.2:g.16503_16540del	HET -25/-28bp	Not mutated
FT(P)2- TP2	NG_017013.2:g.16511del	HOM -1bp	Not mutated
FT(P)2- TP3	NG_017013.2:g.16512del	HOM -1bp	Not mutated
FT(P)1- TPR1	NG_017013.2:g.16508_16511del NG_017013.2:g.16505_16511del	HET -4/-7bp	NG_0009009.1:g.64106del HOM -1bp
FT(P)2- TPR2	NG_017013.2:g.16511del NG_017013.2:g.16505_16511del	HET -1/-7bp	NG_0009009.1:g.64106_64107insA HOM +1bp
FT(P)2- TPR3	NG_017013.2:g.16508_16509del	HOM -2bp	NG_0009009.1:g.64106_64107insA HOM +1bp



◀ **Extended Data Figure Figure 6. CRISPR-Cas9 mediated genetic manipulation in FT organoids.** (a) Schematic of normal FT organoid electroporation. FT organoids were dissociated into small cell clumps and electroporated with either an empty vector or a vector containing a gRNA directed against *TP53*. Cells were plated and after 2 d of recovery nutlin3a was added. (b) Overview images of organoids 2 weeks after electroporation. Organoids that were electroporated with an empty vector and not treated with nutlin3a showed nice recovery following electroporation (top), whereas the growth of organoids electroporated in a similar manner was dramatically inhibited when nutlin3a was added (middle). Surviving clones that are not inhibited by nutlin3a treatment are visible only when organoids were electroporated with a vector containing *TP53* gRNA (bottom). Four independent electroporation experiments followed by nutlin3A treatment were conducted giving rise to multiple Nutlin3A resistant clones. (c) A representative flow cytometry analysis of organoids 48 h following electroporation demonstrating 25% of the cell express GFP. Summary of six independent repetitions of this experiment are presented in (d). (d) Box-and-whisker plot (minimum to maximum) showing the percentage of GFP positive cells following electroporation. Horizontal bars and dashed horizontal bars represent median and mean of all dots, respectively. Mean \pm s.d. = $23.8 \pm 5.5\%$, median = 25.5%. Six independent experiments that were conducted with three different FT organoid lines are presented, demonstrating high and robust electroporation efficiency. (e) An example of CRISPR–Cas9 mediated editing of *TP53* gene in FT organoids. Targeted locus is presented and gRNA (solid line), PAM sequence (red highlight) and cut point (arrow head) are indicated. Sequencing results revealed out-of-frame deletions induced by CRISPR–Cas9 editing. (f) Table presenting six FT genetically engineered clones derived from two independent donors (FT(P)1 and FT(P)2). For each clone, targeted gene description (in both *TP53* and *RB1* genes) including HGVS nomenclature is presented. (HET, heterozygous; HOM, homozygous). (g) BF images (top) and H&E staining (bottom) of four independent clones show deviation from cystic and well-organized normal FT organoid morphology. Passage number is indicated. This analysis was conducted on three independent TP clones (loss-of-function mutations in the *TP53* gene) and three independent TPR clones (loss-of-function mutations in the *TP53* and *RB1* genes) with similar results. (h) Heat map of Spearman correlation values of three independent normal FT organoid lines (derived from different donors) and genetically engineered clones ($n=3$ independent TP clones (loss-of-function mutations in the *TP53* gene) and 3 independent TPR clones (loss-of-function mutations in the *TP53* and *RB1* genes)), using RNA-seq expression data. Read counts were normalized for sequencing depth and the 1,000 most-variable genes were used. Clones were assigned into different groups according to their mutational profile.



CHAPTER

PATIENT-DERIVED ORGANOID AS A NOVEL TOOL TO STUDY CERVICAL CANCER

4

Kadi Löhmuusaar^{1,2}, Rurika Oka^{2,8}, Jose Espejo Valle-Inclan^{2,3},
Hila Wardak¹, Jeroen Korving^{1,2}, Harry Begthel^{1,2},
Onno W. Kranenburg⁴, Trudy G. N. Jonges⁵,
Ronald P. Zweemer⁶, Sebastiaan Veersema⁷,
Ruben van Boxtel^{2,8}, Hans Clevers^{1,2,8,9}

¹Hubrecht Institute, Royal Netherlands Academy of Arts and Sciences (KNAW) and University Medical Center (UMC) Utrecht, Uppsalalaan 8, 3584 CT Utrecht, the Netherlands

²Oncode Institute, Jaarbeursplein 6, 3521 AL Utrecht, the Netherlands

³Center for Molecular Medicine, UMC Utrecht, Utrecht University, Heidelberglaan 100, 3584 CX Utrecht, the Netherlands

⁴Utrecht Platform for Organoid Technology (U-PORT), UMC Utrecht, Utrecht University, Heidelberglaan 100, 3584 CX Utrecht, the Netherlands

⁵Department of Pathology, UMC Utrecht, Utrecht University, Heidelberglaan 100, 3584 CX Utrecht, the Netherlands

⁶Department of Gynaecological Oncology, Cancer Center, UMC Utrecht, Utrecht University, Heidelberglaan 100, 3584 CX Utrecht, the Netherlands

⁷Department of Reproductive Medicine and Gynaecology, Division Woman and Baby, UMC Utrecht, Heidelberglaan 100, 3584 CX Utrecht, the Netherlands

⁸Princess Máxima Center for Pediatric Oncology, Heidelberglaan 25, 3584 CS Utrecht, the Netherlands

SUMMARY

Cervical cancer is the most prevalent gynecological malignancy, often caused by high-risk human papillomavirus. There is a paucity of human-derived culture systems to study cervical epithelium and the cancers derived thereof. Here, we describe a long-term culturing protocol for ecto- and endocervical epithelia, which generates 3D organoids that closely recapitulate the two tissues of origin by histology and gene expression. Starting from Pap-brush material, a small biobank of patient-derived tumoroids was established that retained the causative HPV genomes. One of these uniquely carried the poorly characterized HPV30 subtype, implying its direct role in carcinogenesis. The tumoroids displayed differential responses to common chemotherapeutics. This study provides a promising platform for cervical (cancer) research and for future personalized medicine approaches.

SIGNIFICANCE

There are currently no untransformed *in vitro* culture systems available that can simultaneously mimic the squamous differentiation of the susceptible tissue and be expanded long-term, prerequisites for enabling virus infection and tracking the progression of transformation, respectively. While the causative link between human papillomavirus infection and cervical cancer is well established, human-based model systems that faithfully recapitulate this disease are scarce and often inadequate. Additionally, conventional cervical cancer cell lines fail to recapitulate the heterogeneity and genomic landscape of the disease, rendering them largely useless for directing therapy response. Here, we establish a new patient-derived organoid platform for healthy endo- and ectocervix as well as for associated malignancies to facilitate cervical cancer research.

INTRODUCTION

Once the deadliest cancer in the world, cervical cancer mortality rates have significantly declined since the discovery of the role of human papillomavirus (HPV) infection in the cancer pathogenesis and development of successful screening strategies¹⁻³. Preventive care via vaccination at a young age, regular Papanicolaou (Pap) tests and additional HPV DNA testing has shown a reduction in the incidence of cervical cancer. However, in low-income countries with limited access to high-quality healthcare, cervical cancer remains the leading cause of death from cancer among women^{4, 5}. Additionally, prophylactic vaccination is not mandatory, only effective when administered at a young age and does not protect against all oncogenic strains of the virus. Thus, challenges for better understanding the pathogenesis of cervical cancer and finding effective treatment strategies still remain.

The most common cervical cancer subtypes are squamous cell carcinoma (SqCa) and adenocarcinoma (AdCa) that account for up to 70% and 25% of all cases respectively⁶. These tumors arise from distinct regions of the uterine cervix: the outer ectocervical, inner endocervical canal and the transformation zone inbetween. The ectocervix is lined with stratified squamous epithelium and is the origin of SqCa-s, whereas the endocervix is composed of glandular columnar cells that can give rise to AdCa-s. The majority of SqCa-s are caused by sexually acquired infection with high-risk HPVs, such as HPV16 and HPV18⁷. The viral tropism towards the ectocervix is associated with the dynamic life cycle of HPVs. The virus infects the proliferating basal cells of the stratified epithelium and requires the host cell's squamous differentiation for the completion of its own life cycle⁸. During productive infection in the host cells, the virus expresses specific oncogenes (E6 and E7) that deregulate the cell cycle, and thus, promotes tumorigenesis⁹⁻¹².

To date, cervical cancer studies have relied on a limited number of cell lines, xenograft and transgenic mouse models¹³. Most of the broadly used cell lines, such as HeLa or CaSki, were established decades ago and have gone through extensive passaging. Therefore, their value for preclinical testing is limited. Additionally, the studies of cancer initiation and progression have been hampered by the difficulty to study HPV in culture, mostly due to the strict viral tropism towards stratified epithelia – a feature that immortalized monolayer cultures fail to recapitulate. On the other hand, organotypic raft cultures are able to support the viral life cycle but cannot be maintained beyond 2-3 weeks¹⁴. Xenograft models represent yet another approach to study the human disease, however, the generation of such models for cervical cancer have been reported to be of low efficiency¹⁵. Infection of experimental animals with HPV is not directly possible. However, engineered mouse models that express viral oncogenes under basal cell-specific reporters do exist, and have greatly enhanced our understanding of the role of the viral oncogenes in cervical tumorigenesis^{16, 17}. The development of novel human-based model systems is anticipated to further increase our understanding of this unique disease.

In the past decade, much progress has been made in culturing adult stem cell-based organoids, organ-like structures that self-organize in 3D culture¹⁸⁻²⁰. Following

1

2

3

4

5

&

similar strategies, tumors from individual patients can also be grown as 3D organoids²¹, while normal organoids can be driven into malignant transformation by the sequential introduction of oncogenic mutations using CRISPR^{22, 23}. Organoid technology has now been extended to a variety of gynecological tissues and tumors, including normal fallopian tubes^{24, 25}, ovarian surface epithelium²⁵, endometrium^{26, 27} and associated cancers^{25, 28, 29}. Here, we report on establishment of long-term human organoid cultures from both healthy ecto- and endocervical tissue as well as associated malignancies.

RESULTS

Derivation of healthy cervical organoids

For organoid establishment, healthy endo- and ectocervical tissues were carefully dissected from the cervical canal of patients undergoing total hysterectomy. The tissues were subjected to different enzymatic treatments using collagenase (endocervix) or dispase-trypsin (ectocervix) (see Methods for more details; Figure 1a). After digestion, the cells were embedded into basement membrane extract (BME) matrix and covered with culture medium. Medium composition of both cultures was optimized for long-term expansion. Our initial basal medium (M1) contained 5 components: Noggin, Nicotinamide (NIC) and p38 inhibitor (p38i), B27 supplement and Rho kinase (ROCK) inhibitor (Y27632) (Figure 1b). Noggin was selected to inhibit differentiation cues from BMP signals and generally facilitates expansion of stem cells¹⁸. Addition of NIC and p38i was previously reported to be important for long-term organoid maintenance¹⁹. The supplement B27 is commonly used in various organoid media to increase sphere-forming efficiency. Y27632 was added to increase proliferation and prevent cell death through anoikis. We observed emergence of small organoids from the both lineages. Addition of FGF7 (M2) was required to significantly increase the outgrowth rate of the organoids (Figures 1b-c). As organoid growth and maintenance were still limited under these basic conditions, we tested additional factors used in other 3D culture systems: N-acetyl cysteine (NAC), TGF- β inhibitor A83, Forskolin (FSK), FGF10 and the Wnt signaling potentiator RSPO1 (Figure 1b). Stepwise addition of these growth factors improved organoid outgrowth efficiency, most notably in ectocervical cultures for which the full medium (M7) yielded the highest organoid outgrowth number (Figures 1b-c). The outgrowth efficiency of endocervical organoids was found to be comparable for the media M2-M6, but slightly increased in the complete medium (M7) (Figure 1b-c). Although, the M7 medium for endocervical cultures was initially promising, we observed more collapsing and differentiated structures after 5-8 passages in culture (Figure 1d). To improve the long-term maintenance, we tested supplementation of additional factors, such as epithelial growth factor (EGF), hormone β -Estradiol (β -Est) and WNT activators (i.e. WNT surrogate and CHIR), which – together – rescued the lines from the growth arrest (Figure 1d).

Under the respective optimized medium conditions, organoids from both lineages emerge within 7 days and within 14 days fully expand (Figure 1e). The endocervical

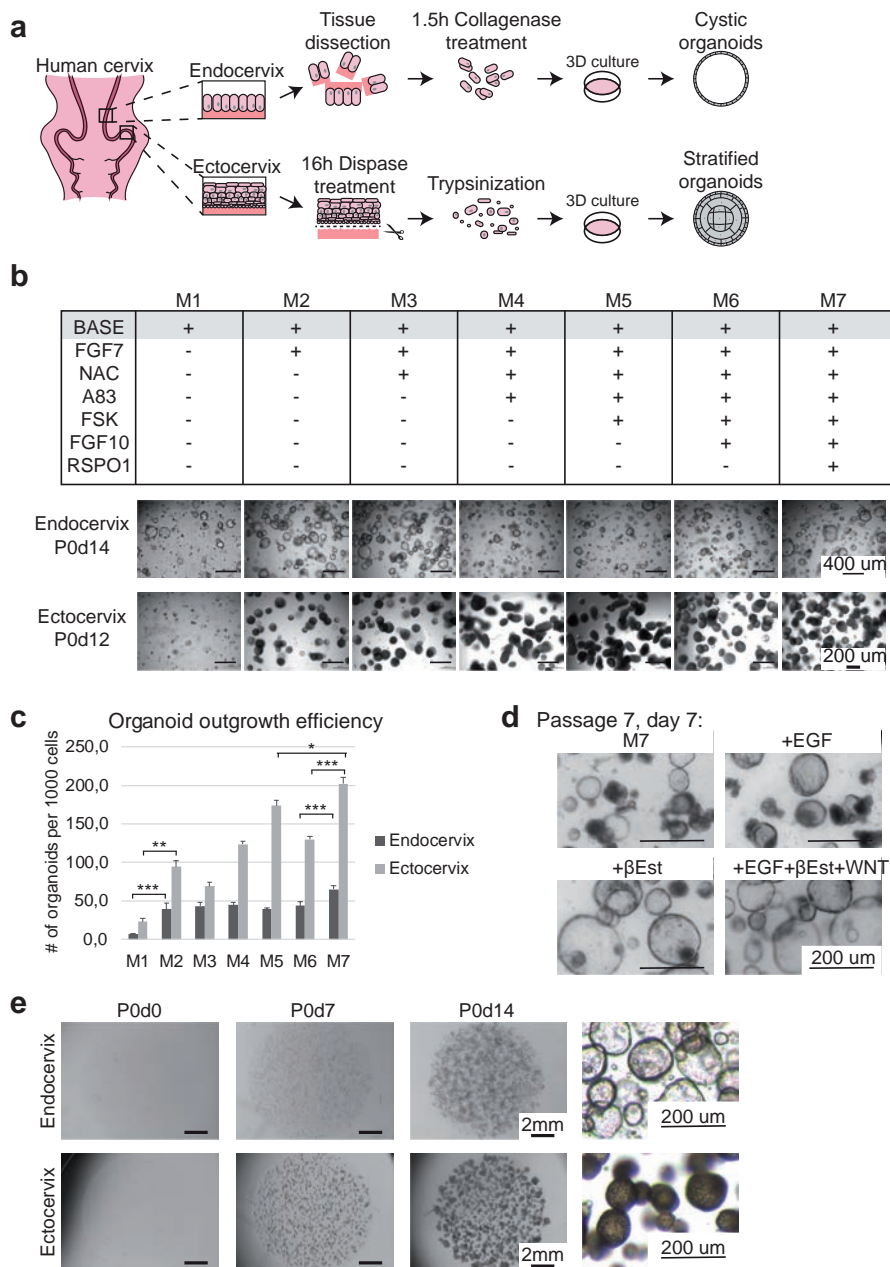


Figure 1. Establishment of organoids from endo- and ectocervix. (a) Schematic overview of tissue processing. Separate biopsies from endo- and ectocervix were dissected, endocervix was treated with collagenase treatment, whereas ectocervix dissociated via dispase-trypsin method. The cellular fragments were seeded into basement membrane matrix extract (BME) and cultured in appropriate medium. Following this protocol, organoids could be derived with 82% and 93% success rate in endo- and ectocervical lineage, respectively. (b) Medium component withdrawal assay and representative images of cultures from both lineages under specified conditions. P-numbers ▶

► indicate the passage numbers and days (d). (c) Number of organoids developed per 1000 seeded cells (i.e. P0) from human endo- and ectocervix under specified culture media after 10 days in culture. Error bars represent SEM of the technical replicates (2 biological replicates with at least 2 technical replicates each, $n \geq 4$). Statistical significance were calculated by two-sided Student's t-test ($*p < 0.05$, $**p < 0.01$, $***p < 0.001$). (d) Representative brightfield images of endocervical organoids after extended time in culture (passage 7, day 7) in full medium (M7) and media with specified supplements. (e) Representative brightfield images of both cultures in their respective medium over two week time course. Endocervical cultures show cystic, whereas ectocervical cultures more dense organoid phenotype. P-numbers indicate the passage numbers and days (d).

organoids form hollow cystic structures, whereas ectocervical organoids show a dense phenotype (Figure 1e). On average, organoids could be passaged each 10-14 days, diluting the organoids 1:4 or 1:10 in endo- and ectocervical cultures, respectively. Established organoid lines could be expanded long-term (up to date, endocervical lines over 10 and ectocervical lines over 20 passages), cryopreserved and successfully recovered upon thawing. Following this protocol, healthy endo- and ectocervical organoids could be derived with a high success rate (82% and 93%, respectively). Normal organoid nomenclature and patient information data for 8 thoroughly characterized healthy organoid lines are presented in Table S1.

Endo- and ectocervical organoids represent miniature replicas of the originating tissues

Endo- and ectocervical epithelia display distinct morphological and transcriptional profiles. Endocervix is a glandular monolayered epithelium with pronounced secretory properties. The epithelium is characterized by expression of the well-known secretory cell transcription factor *PAX8* and its main function is to lubricate the cervical canal by supplying mucus. In contrast, ectocervix is comprised of *P63*-positive basal cells that undergo proliferation and differentiation to form the dynamic multilayered squamous epithelium, which is predominantly protective in function. In order to better characterize the established culture systems, gene expression profiles and histological properties of both organoid lineages were analysed and compared to their respective origins (Figure 2a-d).

Reverse transcription-quantitative PCR (RT-qPCR) analysis of known tissue-specific markers revealed comparable gene expression patterns between the endocervical organoids and the tissue of origin (Figure 2a). Similarly to the originating tissue, endocervical organoids express high levels of the secretory cell marker *PAX8* as well as the generic epithelial markers *KRT7* and *KRT8* (Figure 2a). In concordance with the secretory function of this epithelium, the tissue as well as the organoids express a variety of different mucins, such as *MUC5AC* and *MUC5B* (Figure 2a). This expression profile was validated by immunohistochemical analysis (Figure 2b). A standard haematoxylin and eosin (H&E) staining revealed a fine polarized monolayered architecture of the endocervical organoids, reminiscent of the native tissue (Figure 2b). Under homeostatic conditions,

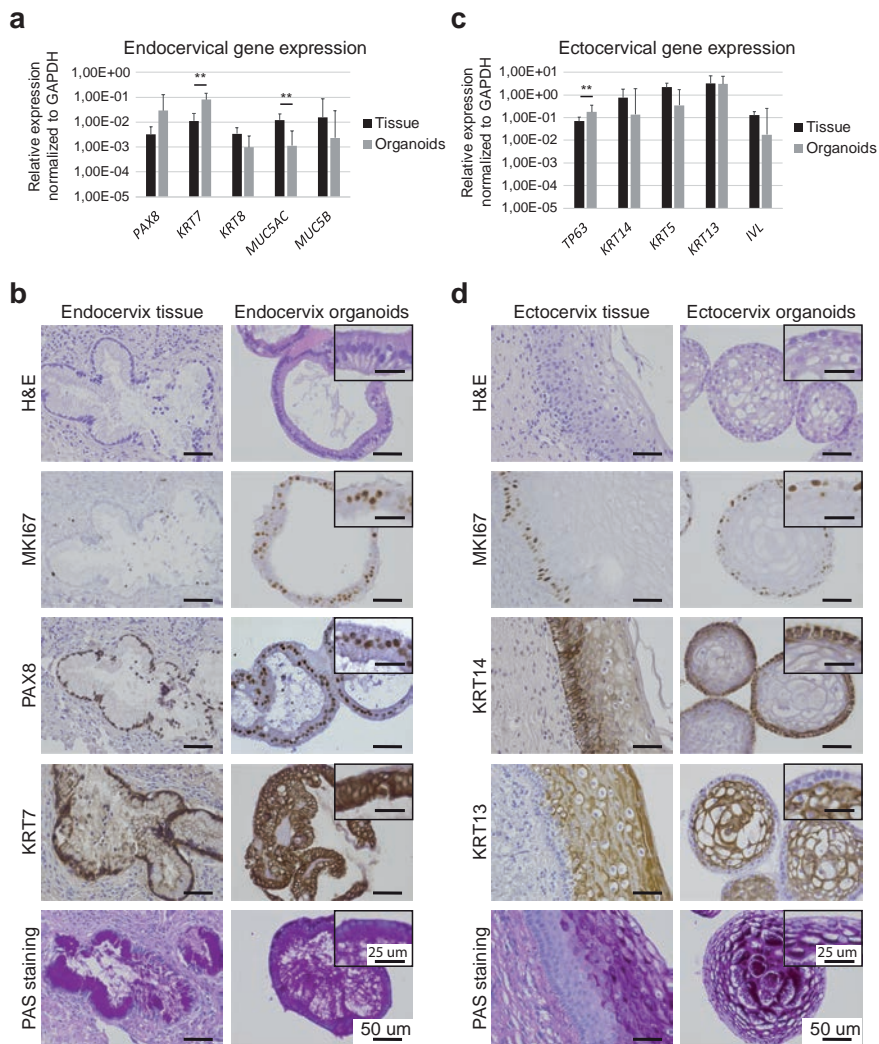


Figure 2. Marker characterization in endo- and ectocervical organoids. (a) RT-qPCR of a normal endocervical tissue and the tissue-derived organoids for glandular epithelium marker *PAX8*, simple columnar epithelium-specific keratins *KRT7/KRT8*, and secreted mucins *MUC5AC/MUC5B*. Error bars represent the 95% confidence interval ($n \geq 3$). Statistical significance was calculated by two-sided Student's t-test ($**p < 0.01$). (b) Haematoxylin and eosin (H&E), Periodic Acid-Schiff (PAS) staining and positive immunostaining for MKI67, *PAX8* and *KRT7* of paraffin-embedded endocervical tissue and corresponding organoids. Scale bars, 50 μm . (c) RT-qPCR of a normal ectocervical tissue and the tissue derived organoids for basal cell markers *TP63/ KRT14*, squamous epithelium-specific keratins *KRT5/KRT13* and terminal differentiation marker *IVL*. Error bars represent the 95% confidence interval ($n \geq 3$). Statistical significance was calculated by two-sided Student's t-test ($**p < 0.01$). (d) H&E and PAS stainings and immunostaining for MKI67, *KRT14* and *KRT13* of paraffin-embedded ectocervical tissue and corresponding organoids. As can be seen, proliferating basal cells (MKI67- and *KRT14*-positive) reside in the periphery of the organoids, whereas the more differentiated keratinocytes (*KRT13*- and PAS-positive) reside in the center of the organoid. Scale bars, 50 μm .

the KRT7-positive endocervix exhibits little capacity to proliferate. However, in our culture system many cells are proliferative, which was confirmed by staining for the common proliferation marker MKI67 (Figure 2b). The secretory products of the glandular cells were also visible in the cultures as revealed by Periodic Acid-Schiff (PAS)-positive stain, which confirmed the functionality of the organoids (Figure 2b).

The ectocervical organoids were also shown to closely recapitulate their tissue of origin (Figure 2c-d). Organoids and originating tissue expressed comparable levels of basal cell markers, such as *P63* and *KRT14*, the squamous epithelium-specific keratin *KRT5*, and committed cell differentiation markers, such as *KRT13* and *IVL* (Figure 2c). Immunohistochemical analysis of the ectocervical cultures revealed a dynamic stratified architecture of the organoids with proliferative MKI67- and KRT14-positive basal-like cells at the periphery of the organoids (Figure 2d). Upon differentiation, basal cells moved inwards and changed in shape and size, giving rise to terminally differentiated KRT13- and PAS-positive layers in the organoids (Figure 2d).

The extensive transcriptomic differences between endo- and ectocervical organoids were corroborated by bulk RNA-sequencing (RNA-seq) analysis. Differential gene expression analysis clearly separated the cultures into two lineage-specific subgroups (Figure S1a). Detailed analysis of the distinct transcriptomic profile of the ectocervical organoids mainly returned keratinization-associated Gene Ontology (GO)-terms, whereas endocervical organoids showed an enrichment in GO-terms associated with cell motility and cilia (Figure S1b-c). Indeed, in addition to secretory cells, the endocervical lining is known to also accommodate ciliated cells that operate in even distribution of mucus and guiding the sperm movement along the cervical canal. The presence of ciliated cells in our endocervical organoids was further supported by the high expression of ciliogenesis-related genes, including the primary ciliary transcription factor *FOXJ1* (Figure S1d), and validated by positive staining for acetylated α -tubulin that marks primary cilia (Figure S1e). Collectively, these data reveal a high degree of similarity between the established healthy organoid lines and their respective origins in terms of both histologic and transcriptomic profile.

Derivation of cervical tumoroids from Pap-brush material

The introduction of Pap tests into the clinic has been instrumental in rapid early diagnosis of cervical abnormalities. As a result, the mortality rate of cervical cancer has significantly declined over the past few decades, predominantly in economically more developed countries³⁰. As the Pap test method is considered to be a non-invasive strategy for collecting cervical cells, we set out to test the possibility to derive cervical cancer organoids (tumoroids) from patient material collected via the Pap-brush method. Pap tests were obtained from consenting patients prior to the surgery or treatment decision. As the amount of tissue that can be obtained via this method is limited and enriched for blood cells, we developed a rapid digestion protocol to process the collected material, which involved initial treatment with a collagenase solution followed by red blood cell lysis

(see Methods section for more details; Figure 3a). The digested material was subsequently embedded in BME and cultured in complete medium (M7), as optimized for healthy ectocervical cultures. Upon establishment, the growth of tumoroids could be observed within 7 days post-seeding (Figure 3a).

As material collection via the Pap-brush method is largely blinded and might yield insufficient cellular material from the tumor lesion, the success rate of tumoroid derivation using this method was found to be around 50% for both major subtypes of cervical cancer, i.e. squamous cell carcinoma (SqCa: 10/20 were successful) and adenocarcinoma

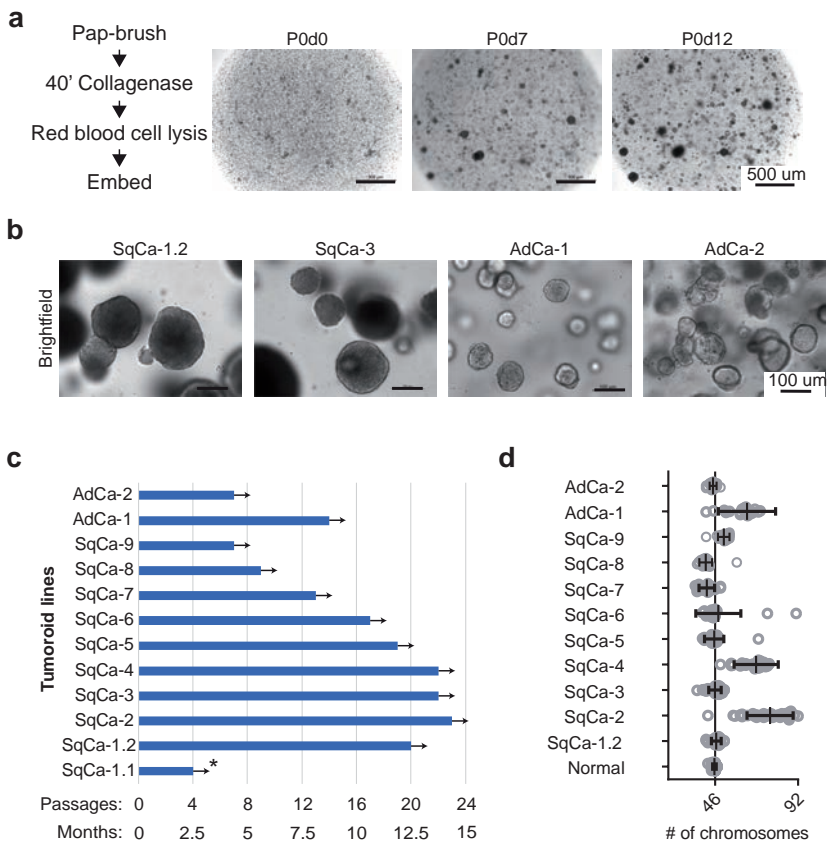


Figure 3. Establishment of patient-derived cervical tumoroids. (a) Schematic pipeline of cancer tissue processing and representative images of the culture over a 12-day time course. P-numbers indicate the passage numbers and days (d). **(b)** Representative images of tumoroid morphologies across the collected subtypes. **(c)** Column bar graph depicting tumoroid maximum passage number up until the moment of submission. **(d)** Scatter plot presenting chromosome number distribution and mean, based on organoid metaphase spreads. In the case of “Normal”, the chromosome numbers were counted in three biological replicates and the results were merged. Asterisk – multiple aliquots of line SqCa-1.1 were frozen in passage 4 and culture was not continued since additional material from the same patient was received later on, labelled as SqCa-1.2. Error bars represent \pm SD (n \geq 16 metaphase spreads counted per line).

(AdCa: 2/4 were successful). Thus, a panel of 12 tumoroid lines was established (Table S1). Cervical cancer predominantly affects pre-menopausal women. Consistently, the majority of the material-donating patients were younger than 50 years of age (average age 47) (Table S1). The derived tumoroid lines showed a variety of morphologies, ranging from dense to cystic (Figure 3b). The tumoroids could be maintained > 1 year (over 20 passages) and showed varying degrees of chromosomal instability (Figures 3c-d). Our tumor organoid nomenclature is based on their histopathological subtype; the numbers refer to patient numbers. Patient clinical data is presented in the Table S1.

Cervical tumoroids recapitulate the disease phenotype

For the majority of the tumoroid lines, direct histological comparison with the matching tumor tissue of origin was not possible due to the low amount and poor integrity of the tissue collected via the Pap-brush method. When the amount of collected material was sufficient, the more intact pieces of the scraped tissue were kept for other purposes, such as histologic or genomic analyses.

Although SqCa-derived tumoroids showed dense morphology in culture, resembling their healthy ectocervical counterparts, histological analysis revealed a striking difference (Figure 4a). In contrast to the healthy ectocervical organoids that showed dynamic squamous differentiation features, the SqCa-derived tumoroid lines displayed less refined structures as evident by the loss of stratification and poor cellular polarity (Figure 4a). The tumoroids featured abundant mitotic figures and atypical, large and hyperchromatic nuclei, suggestive of neoplastic growth (Figure S2). Additionally, tumoroids showed cytoplasmic “halos” – a sign of viral infection (Figure S2).

The abnormal features observed in the histological architecture of the SqCa-derived tumoroids were also evident by the loss of dynamic expression of stratification markers (Figure 4a). Indeed, the basal cell-restrictive marker P63 was abundantly expressed across the entire SqCa tumoroids accompanied by the proliferation biomarker MKI67 (Figure 4a). In addition, tumoroids exhibited decreased expression of the differentiation marker KRT13, indicating a defect in normal squamous differentiation (Figure 4a).

The two AdCa-derived tumoroid lines showed distinct morphologies. While the line AdCa-1 showed denser structures with prominent vacuolization, the line AdCa-2 formed cystic monolayered structures, more reminiscent of healthy endocervical counterparts (Figure 4b). Both AdCa-derived tumoroid lines stained positive for PAX8, confirming their endocervical origin, and showed clear mitotic features (Figure 4b). Of note, PAX8 and MKI67 are commonly used diagnostic markers to confirm the endocervical origin and determine the extent of the disease³¹⁻³⁴.

In addition to the accumulation of pathohistological features, cancer cells often lose their normal growth factor requirement upon transformation^{22, 23}. To test whether this held true for the established cervical tumoroid lines, we performed a set of growth factor withdrawal assays that revealed distinct line-specific patterns in growth factor requirement (Figure S3a-i). Compared to the healthy ectocervical organoids, in which

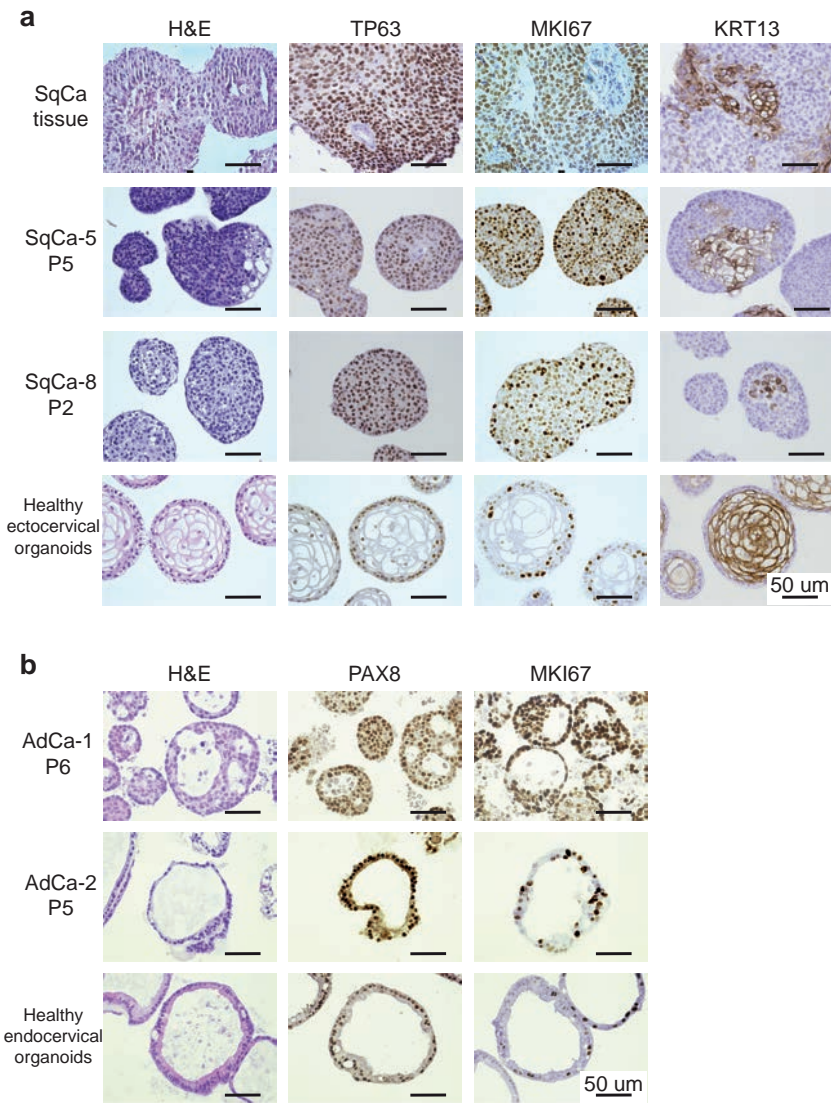


Figure 4. Histological characterization of cervical tumoroids. (a) H&E staining and immunostaining for TP63, MKI67 and KRT13 in SqCa-derived tumoroids and tumor tissue *versus* healthy ectocervical organoids. P-numbers indicate the passage numbers. **(b)** H&E staining and immunostaining for PAX8 and MKI67 in AdCa-derived tumoroids *versus* healthy endocervical organoids. P-numbers indicate the passage numbers.

the cells showed the highest viability in complete medium (M7) (Figure S3a), the tumoroid lines were less dependent on the WNT pathway and mesenchymal niche factors, since RSPO1 and FGF10 could be simultaneously withdrawn (medium M5) from any tested culture without a significant reduction in cell viability (Figure S3b-i). Remarkably, in some cases withdrawal of these factors was even beneficial for growth: four of the SqCa-

derived tumoroid lines, SqCa-1.2, -2, -3 and -4, performed significantly better in medium lacking RSPO1 and FGF10 when compared to the full medium (Figure S3a-e). In contrast, the single tested adenocarcinoma line (AdCa-1) was dependent on all growth factors (Figure S3i). Taken together, these results emphasise patient-dependent differences in tumor cell behaviors that can be captured by patient-derived tumoroid models.

SqCa-derived tumoroids show tumor-associated expression pattern

In concordance with the considerably higher incidence of SqCa compared to AdCa, the former subtype was also overrepresented in our tumoroid panel (10/12, 80%). Therefore, in order to guarantee sufficient statistical power, we limited further transcriptional analysis to SqCa-derived tumoroids. To assess differences in the gene expression profiles between the healthy organoids and SqCa-derived tumoroid lines, the samples were subjected to bulk RNA-seq analysis. Gene expression correlation analysis showed that SqCa-derived tumoroids grouped together into a single branch and apart from healthy ecto- and endocervical organoids (Figure 5a). However, the tumoroid branch clustered closer to healthy ectocervical organoids, reflecting the higher transcriptional similarity to ectocervix, the anticipated origin of SqCa-derived tumoroids (Figure 5a).

Next, differential gene expression analysis was performed between healthy ectocervical and SqCa-derived tumoroids to determine the most significant differentially expressed genes between the two groups. In total, 488 genes were found significantly upregulated ($\log_2FC > 2$, $p_{adj} < 0.05$) and 838 genes significantly downregulated ($\log_2FC < -2$, $p_{adj} < 0.05$) in the SqCa-derived tumoroids compared to the healthy counterparts (Figure 5b). Extraction of the top 20 significantly upregulated genes in the tumoroid group returned a list of genes, which have all been associated with cervical cancer previously (Figure 5c). For instance, a host surrogate marker for viral infection – the tumor suppressor protein p16INK4a – is often used in the clinic to obtain a better indication about viral presence in cervical tissue specimens^{35, 36}. As expected, *CDKN2A* – the gene that encodes for p16INK4a – was seen significantly overexpressed in the SqCa-derived tumoroids compared to the healthy counterparts (Figure 5c). This finding was confirmed by strong immunostaining for p16INK4a in the tumoroids (Figure 5d). Multiple other genes, which have been previously associated with viral infection, were significantly differentially expressed in the tumoroid group. For example, the ubiquitin ligase gene *RNF212*³⁷ and chromosome maintenance gene *SMC1B*³⁸ were found to be upregulated, whereas the low-density lipoprotein receptor gene *LRP1B*³⁹ was found downregulated compared to the healthy ectocervical lines (Figure 5c). In addition, among the top expressed genes, the tyrosine kinase receptor gene *EPHB2*, which has previously been shown to promote cervical cancer progression by inducing epithelial-to-mesenchymal transition⁴⁰, and the tumor-associated antigen *MSLN* were significantly upregulated in the tumoroid group (Figure 5c). Finally, tumoroids displayed significantly higher expression of the *RMI2*, *RPP25* and *RUNX3* genes (Figure 5c). Upregulation of *RMI2* has previously been reported in SqCa-s, and is

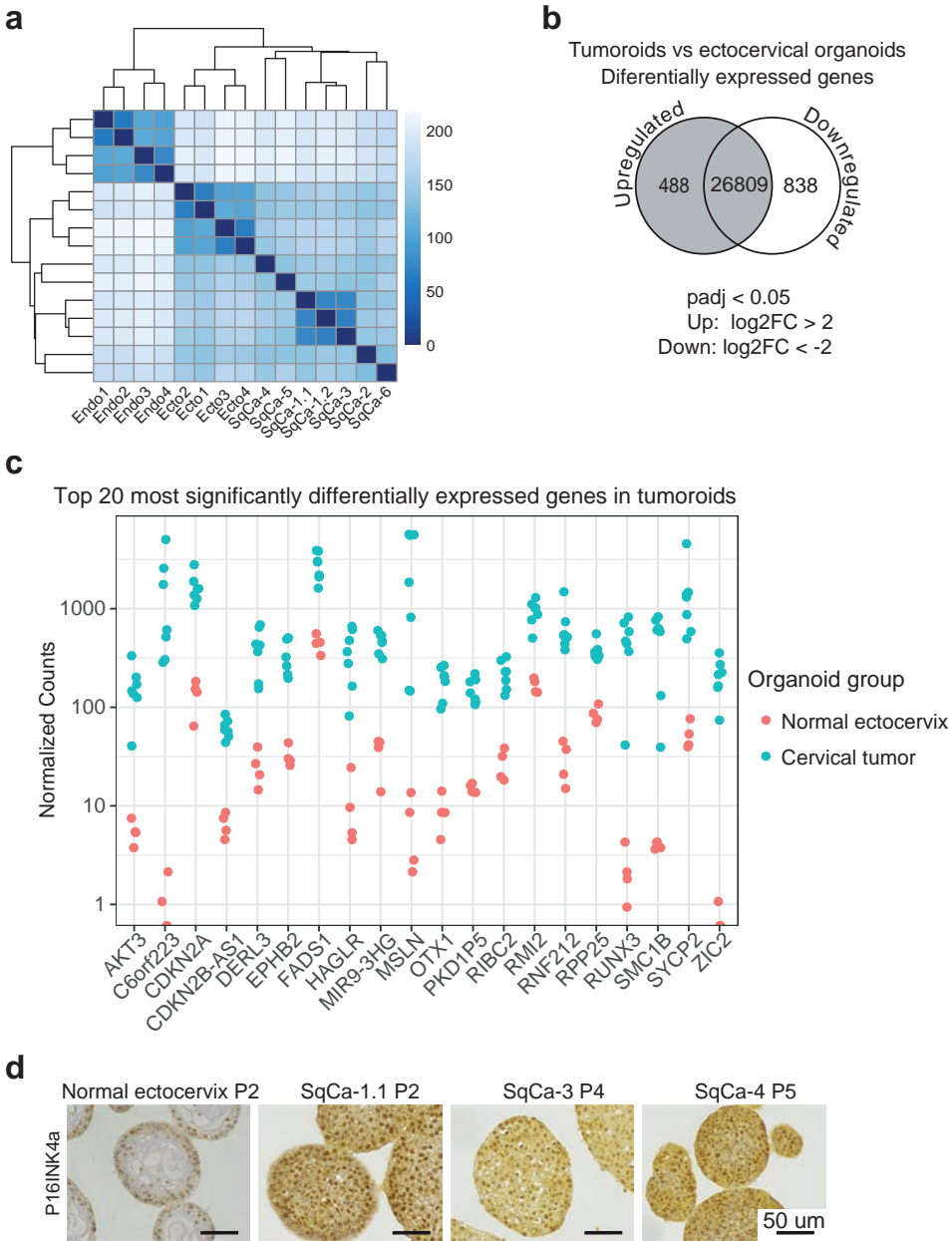


Figure 5. Gene expression profile of cervical tumoroids. (a) Sample-to-sample heatmap showing the Euclidean distances between the healthy ectocervical ($n=4$), healthy endocervical ($n=4$) and tumor-derived ($n=7$) organoid lines. Correlation is based on all the differentially expressed genes in the dataset. (b) Venn diagram of differentially expressed genes in tumoroids. (c) Plot of normalized counts depicting the top 20 most significantly upregulated genes in SqCa-derived tumoroids *versus* healthy ectocervical organoids. (d) Positive immunohistochemical stainings for viral surrogate marker p16INK4a in selection of SqCa-derived tumoroids. P-numbers indicate the passage numbers.

associated with an abnormal DNA methylation profile⁴¹. Overexpression of *RPP25* has been suggested to promote migration, invasion and the EMT process in cervical cancer in a long non-coding RNA-regulated fashion⁴². *RUNX3* is involved in the transforming growth factor β (TGF- β) signaling pathway, which might serve as a tumor suppressor gene in cervical cancer⁴³. Taken together, the tumoroids' gene expression profile closely reflected those observed in cervical cancer.

Tumoroids show common genomic alterations and viral integration

In order to analyse the mutational landscape of the tumoroids, we performed whole exome sequencing (WES) analysis on 7 lines for which we were also able to collect DNA of a small amount of tissue prior to digestion, encompassing 6 SqCa cases and 1 AdCa case. Because we could not obtain matched normal tissue from the patients, it was not possible to differentiate between private germline and somatic variants. Nevertheless, for all lines we identified unique patient-specific mutational profiles that were largely conserved between the tumor tissues and respective tumoroids (Figure 6a, Figure S4). The mutated genes in SqCa-derived tumoroids involved common targets, such as *TP53*, *ARID1B*, *CDKN2A*, *ELF3*, *FAT1* and genes in the DNA repair pathway, such as *BRCA1/2*, *ATM* and *FANCA*, showing high levels of concordance with previously identified recurrently mutated genes^{44, 45} (Figure 6a). In contrast, the AdCa-derived line harbored mutations in a critical tumor suppressor gene *FBXW7* and *CASP8*, which was recently reported to be a mutated gene in cervical cancer⁴⁴ (Figure 6a). Additionally, the AdCa-1 line showed evidence for alterations in NOTCH, TGF- β and epinephrine signaling pathway genes, including *NOTCH3*, *PDGFRB* and *TSC2*, *EPHA2* and *EPHA5*, which are all clinically actionable pathways for cancer therapeutics (Figure 6a). Due to the small panel size, there were only a few common targets that were shared between multiple lines, including *BRCA1*, *FAT1*, *LRP1B* and *ZFH3* (Figure 6a). In the majority of cases the tumoroids displayed higher enrichment in variant allele frequency (VAF) compared to the respective tissues, reflecting the cancer cell purity in our culture system, whereas primary tissue often contains other noncancerous cell types, such as blood cells and/or stromal components (Figure 6a). These results indicated that the tumoroids retained genetic alterations of original tissues and faithfully represented the genomic landscape of clinical disease.

Genomic instability and somatic alterations are usually secondary by-products of cervical cancer development, which is predominantly initiated by viral oncogenesis. We were therefore also interested to determine possible viral integrations and active viral transcripts in the established tumoroid lines. For this, we re-purposed our RNA-seq dataset, containing information about 7 SqCa-derived lines, to search for type-specific viral transcripts and detect unique human-virus fusion mRNAs, the latter indicative of viral integration into the host genome. As expected, multiple unique viral integration sites were detected in all but one line (i.e. SqCa-5), which only showed expression of high-risk HPV16 transcripts, but no fusion-mRNA molecules, indicating the likely episomal maintenance of the viral genome in this line (Figure 6b). In remaining lines, several

unique viral-host mRNA breakpoints were detected, indicating multiple integration sites per line (Figure 6b). In addition to the integration, viral mRNA expression was readily detected in all of the analysed tumoroids (Figure 6b). Of note, no viral transcripts nor

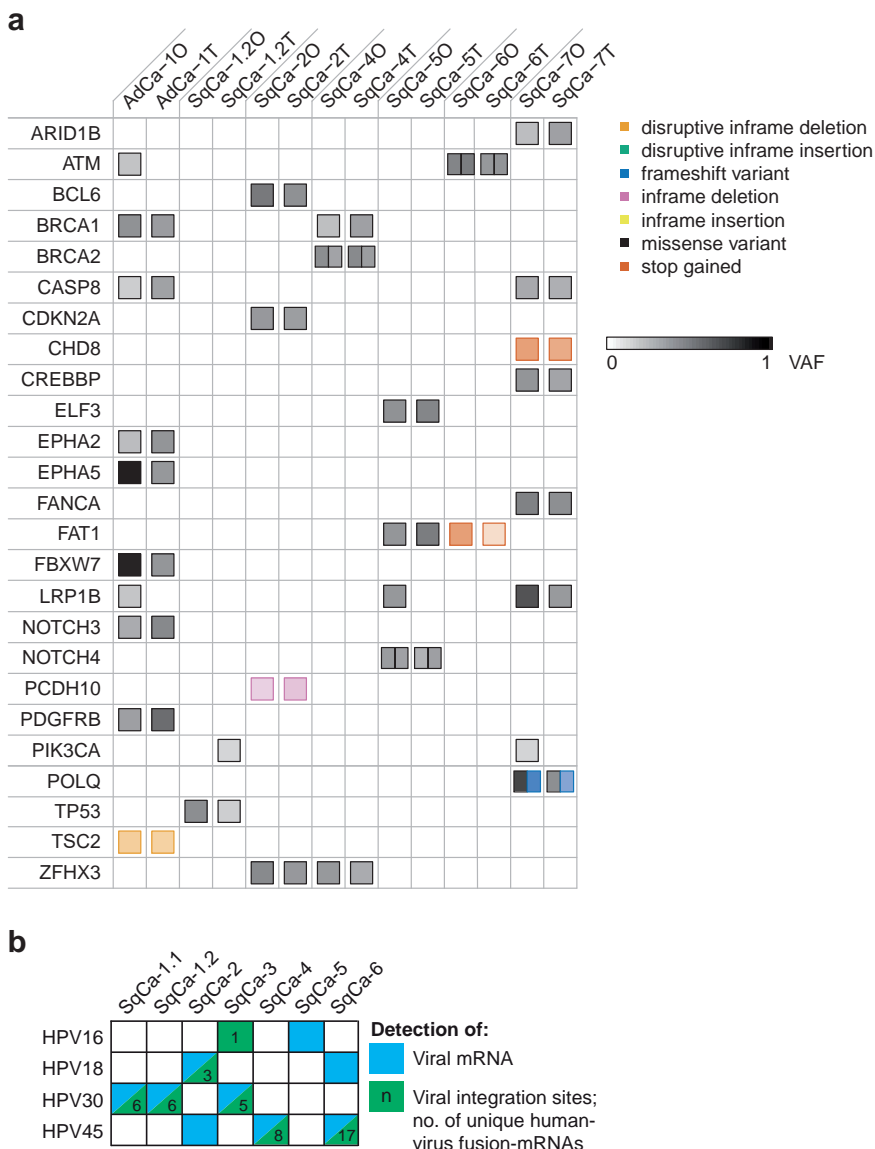


Figure 6. Tumoroids show common genomic alterations and viral integration. (a) Somatic mutations in relevant genes of cervical cancer. For each patient, matched tumor (T) and tumor organoid (O) pairs are displayed. VAF = variant allele frequency. More comprehensive list of genomic alteration can be found in the supplementary Figure S4. **(b)** Results from bulk RNA-seq analysis showing presence of subtype-specific viral transcripts (blue) in SqCa-derived lines and number of detected unique viral-host mRNA-fusion molecules (green) that indicate viral integration sites.

integrations were found in the healthy organoid lines. Most of the tumoroid lines (5/7; 71%) contained viral transcripts from at least one high-risk subtype of HPV, including HPV16, HPV18 and HPV45 (Figure 6b). In two cases active transcripts from more than one viral subtype were detected per line (HPV16/30 in SqCa-3 and HPV18/45 in SqCa-6 lines). Interestingly, two tumoroid lines that were originally derived from the same patient at different time points (labelled as SqCa-1.1 and SqCa-1.2) only showed presence of viral transcripts from a single, relatively poorly characterized HPV30 strain (Figure 6b). According to the International Agency for Research on Cancer (IARC) monograph on human carcinogens⁴⁶, HPV30 is classified under the group 2B carcinogens, i.e. among the agents that are considered potentially carcinogenic. However, without sufficient evidence the actual risk of this HPV subtype is unknown. Our data suggests a plausible direct carcinogenic role for HPV30.

To further validate whether HPV30-infected tumoroids could form tumors upon xenotransplantation into the mice, a pilot assay was performed wherein the SqCa-1.2 tumoroids were subcutaneously injected into left and right flanks of 4 immunodeficient female mice (8 locations/4 mice). Four months following the injections, small palpable tumors were visible in all locations (8/8, 100%) with the average tumor size of 14.4 mm³ (Figure S5a-b). The formed tumors displayed different degrees of squamous differentiation with occasional nests of keratin (keratin pearls) (Figure S5c, asterisk). The latter feature (i.e. keratinization) is commonly absent in the healthy ectocervical tissue, yet often observed in cervical tumors. Superficial extensions into adjacent stromal tissue were observed, suggestive of invasive nature (Figure S5c, black arrowhead). Additionally, the tumors stained positive for the surrogate marker of viral infection (p16INK4a) and showed moderate proliferative capacity (Figure S5c). The human origin of the transplants was confirmed by a specific immunostain for human nuclei (Figure S5c).

Cervical tumoroids show differential drug response

Besides surgical intervention, radiotherapy or its combination with chemotherapy (i.e. chemoradiation) are commonly used for treatment of cervical cancer patients. However, the exact benefit of combining these treatments has remained questionable in the field, and many patients suffer from long-term adverse effects⁴⁷. Multiple studies have recently demonstrated that organoids possess predictive value in cancer therapy⁴⁸⁻⁵². We therefore sought to investigate whether cervical tumoroids could be informative in such assays.

HPV oncogenes target key cell cycle control pathways, such as TP53 signaling⁵³⁻⁵⁵. Concordantly, genomic profiling of the tumoroids showed that while only one line (i.e. SqCa-1.2) harbored a direct mutation in *TP53*, other lines showed evident aberrations in key cell cycle genes, such as *ATM*, *ATR* and *CDKN2A* (Figure 6a, Figure S4). We chose to first assess possible TP53 pathway defects in our tumoroid lines by using the TP53 activating compound Nutlin-3a (Figure 7a). The organoids were dissociated into single cells, suspended in complete medium (M7) containing 5% BME and dispensed into 384-well plates. Two days post plating, the drugs were added, and cell viability was measured 5

days after supplementing the drugs. Staurosporine, a common apoptosis-inducing agent, was used as a baseline control for the assays and the sensitivity of the lines to the drug was visualized via dose-response curves (Figure 7a-b). As expected, the majority of the tested SqCa-tumoroids showed higher resistance to Nutlin-3a as compared to the AdCa-derived and healthy lines, implicating alterations in this key oncogenic pathway in the resistant lines (Figure 7b). In accordance to the genomic data, the TP53-mutated SqCa-1.2 line was among the most resistant lines. The robustness of the drug screening assays was confirmed by the strong correlation of the average area under the dose-response curves (AUC) between biological replicates ($R^2 = 0.74$, Figure 7c).

Next, we tested the tumoroids' sensitivity to several commonly used chemotherapy regimens, including carboplatin, cisplatin and gemcitabine (Figure 7d-f). These assays revealed differential drug responses of individual tumoroid lines. For example, lines SqCa-2 and SqCa-4 showed more resistance towards treatment with the two platinum analogs (Figure 7d-e), whereas the line AdCa-1 showed the highest sensitivity to gemcitabine (Figure 7f). In addition, as the somatic mutation analysis revealed that several lines carried mutations in DNA repair pathways, we were also interested to evaluate the effect of the most commonly used poly(ADP-ribose) polymerase (PARP) inhibitor (i.e. olaparib) that has shown good outcomes on tumors with homologous recombination (HR) repair-deficiency. The results showed differential sensitivity of the lines to this drug (Figure 7g). Surprisingly, the two lines with *BRCA* gene aberrations (i.e. AdCa-1 and SqCa-4) were not among the most sensitive lines (i.e. AdCa-1 line showed the highest resistance to the PARP inhibitor), indicating that the missense variants we detected in the *BRCA* genes of these lines might not be sufficient to induce rigorous homologous recombination deficiency or are passanger mutations.

DISCUSSION

With the emergence of adult stem cell-based organoid technology, novel 3D culture systems have been established from a variety of epithelial tissues, such as intestine¹⁸, liver^{20, 56} and endometrium^{26, 27}. Here, we show that healthy and tumor-derived organoid cultures closely recapitulate the tissues of origin. The precise arrangement of the layers in the ectocervical organoids, where basal cells are positioned in the outermost layer, holds promise for future HPV infection assays, since the stem cells are conveniently accessible for viral entry. Additionally, endocervical organoids could be used to study the development of adenocarcinomas and the biology of a number of sexually transmitted diseases, such as infections with *Chlamydia trachomatis*, *Neisseria gonorrhoea* and herpes simplex virus. Feasibility of organoids to be co-cultured with microorganisms has been demonstrated before⁵⁷⁻⁶². Therefore, the introduced healthy ecto- and endocervical 3D organoid cultures may open new avenues in cervical cancer and infection studies, as well provide new tools to learn more about the natural biology of human cervical epithelium.

Obtaining access to solid tumor material often requires invasive and risk-associated tissue sampling, such as surgical biopsy collection. In this study, we describe derivation

1

2

3

4

5

&

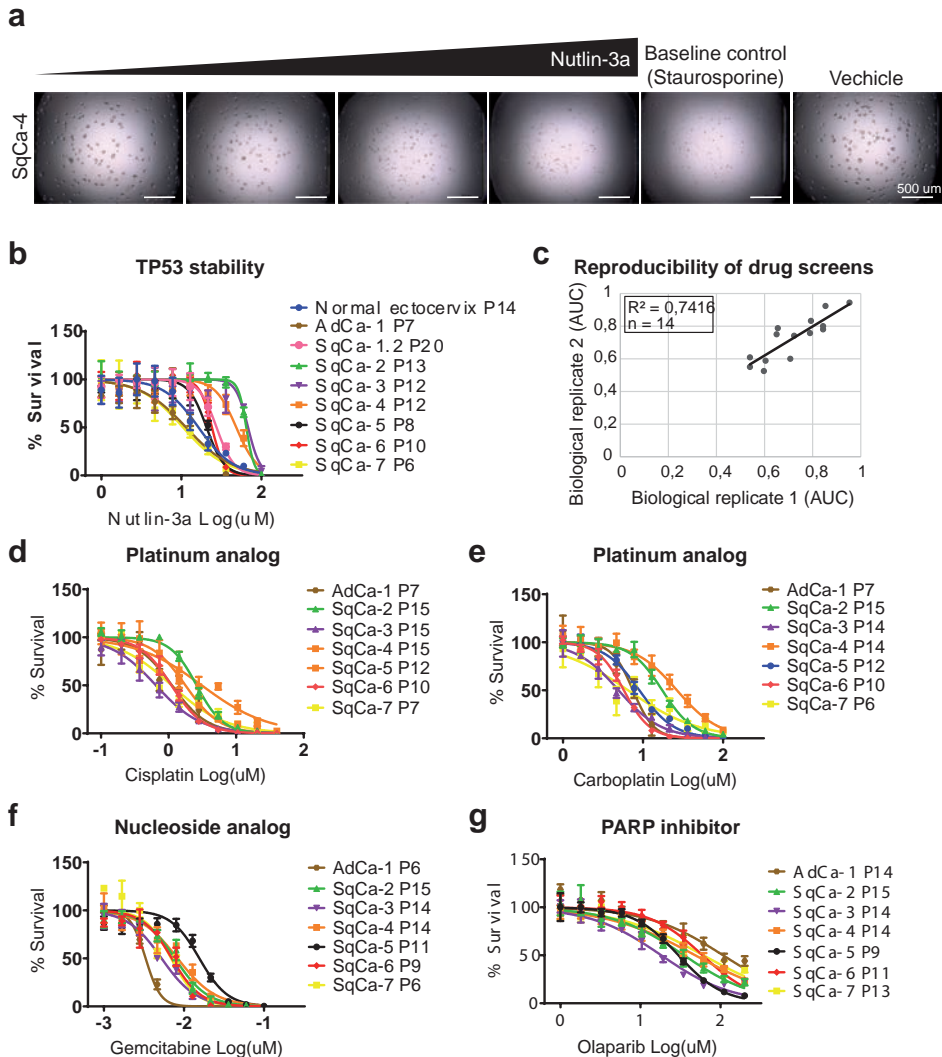


Figure 7. Cervical tumoroids show differential drug responses. (a) Representative brightfield images of Nutlin-3a treated SqCa tumoroids. Scale bar: 500 μ m. (b) Representative dose response curves for Nutlin-3a. SqCa-derived tumoroids are more resistant to Nutlin-3a than AdCa-derived and healthy organoids. Dots and error bars represent the mean and SEM of technical replicates, respectively ($n=3$). P-numbers indicate the passage numbers. (c) Scatter plot of AUC values of biological replicates, displaying high correlation ($R^2 = 0,74$, $n = 14$). (d-g) Representative dose response curves for (d) carboplatin, (e) cisplatin, (f) gemcitabine and (g) olaparib. Dots represent the mean of technical replicates. Error bars represent SEM of technical replicates ($n=3$). P-numbers indicate the passage numbers.

of a panel of 12 cervical tumoroid lines from tumor material collected via the Pap-brush method. The observed tumoroid derivation efficiency from Pap brush material was 50% in both squamous cell and adenocarcinoma subtypes and can likely be improved significantly. The tumoroids can be expanded long-term (> year) and show varied degrees of chromosomal instability, a hallmark of cancer. Comparative gene expression analysis between healthy ectocervical and squamous cell cancer-derived organoids showed evident changes in tumoroid transcriptomes. Among others, the host surrogate marker for viral infection – p16INK4a – was significantly upregulated in the tumoroid group. The tumoroids showed clear evidence for viral carcinogenesis: viral integration and transcripts of high-risk HPV subtypes, including HPV16, HPV18 and HPV45, were readily detected in all the tested lines. Interestingly, transcripts of a single HPV30 subtype were found in two tumoroid lines sampled at different time points from the same donor. Due to insufficient evidence, the exact carcinogenic risk of HPV30 is currently unknown. However, as the role of viral contribution to squamous cell carcinomas is well established and these patient-derived tumoroids formed visible tumors upon subcutaneous xenotransplantation into mice, our data suggests a direct carcinogenic role for HPV30.

As a rewarding outcome of prevention measures, cervical cancer incidence has drastically declined over the years⁶³. Consequently, clinical trials for optimizing treatment regimens for the remaining patients become increasingly challenging. Therefore, new platforms that enable to predict patients' response in a more personalized fashion may be needed. In this manuscript, drug screening assays were performed on a panel of cervical cancer tumoroids which showed differential response to the tested common chemotherapy regimens. While encouraging, observational trials will now be required to determine the predictive value of tumoroid drug screening in a precision medicine setting.

AUTHOR CONTRIBUTIONS

Conceptualization: K.L. and H.C. Methodology: K.L. and H.C. Software: K.L., R.O., J.E.V.-I. Formal analysis and interpretation of data: K.L., R.O., J.E.V.-I., H.W., T.J., R.v.B. Investigation: K.L., R.O., J.E.V.-I., H.W. Technical support: J.K. and H.B. Resources: O.W.K., R.P.Z. and S.V. Data curation: K.L.

ACKNOWLEDGEMENTS

The authors thank A. Brousalı, A. Sneltıng, K. Oostıng and C. Hulsbergen-Veelken of the Utrecht Platform for Organoid Technology (U-PORT; UMC Utrecht) as well as C. de Witte and E. Stello for patient inclusion and tissue acquisition. We acknowledge Anko de Graaff from the Imaging Centre (HIC) of Hubrecht Institute. We thank the Utrecht Sequencing Facility (USEQ) for the library preparations, sequencing and data analysis of cervical organoids. This work is part of the Oncode Institute which is partly financed by the Dutch Cancer Society and was funded by the gravitation program CancerGenomiCs.nl from the Netherlands Organisation for Scientific Research (NWO) and a grant from

1

2

3

4

5

&

the Gieskes-Strijbis Foundation (1816199). R.v.B. was supported by VIDI grant from NWO (no. 016.Vidi.171.023).

DECLARATION OF INTERESTS

H.C. is an inventor on several patents involving adult stem cell-based organoid technology. His full declaration is given at <https://www.uu.nl/staff/JCClevers/>. The remaining authors declare no competing interests.

STAR METHODS

CONTACT FOR REAGENT AND RESOURCES SHARING

Further information and requests for resources and reagents should be directed to and will be fulfilled by the Lead Contact, Hans Clevers (h.clevers@hubrecht.eu). Distribution of organoids to third parties requires completion of a material transfer agreement and will have to be authorised by the Medical Ethical Committee UMCU to ensure compliance with the Dutch medical research involving human subjects' act. Use of organoids is subjected to patient consent; upon consent withdrawal, distributed organoid lines and any derived material will have to be promptly disposed of.

EXPERIMENTAL MODELS AND SUBJECT ANIMALS

Human material for organoid culture

All experiments with human tissue were approved by the medical ethical committee of the UMC Utrecht in accordance with all relevant ethical regulations. For initial establishment of the ectocervical organoid culture system, healthy cervical tissue was obtained anonymously from patients who underwent a hysterectomy performed for benign uterine diseases. Such protocol was valid temporarily for setting up the culture system and approved by the ethics committee (TCBio 17-127) of the Utrecht Medical Center, Utrecht, the Netherlands in compliance with guidelines from Ethical Committee and European Union legislation. Additionally, healthy cervical tissue (TCBio 14-472) and cancer tissue PAP-brushes (TCBio 12-093) were obtained from ovarian and cervical cancer patients, respectively, under the designated ethical protocols. All patients participating in this study under the latter two protocols signed informed consent forms approved by the responsible authority. In all latter cases, patients can withdraw their consent at any time, leading to the prompt disposal of their tissue and any derived material.

Mice

For tumouroid transplantations, *NOD.Cg-Prkdcscid Il2rgtm1Wjl/SzJ* (NSG) female mice were used. Transplantation experiments were performed after institutional review by the Animal Ethics Committee of the Royal Netherlands Academy of Arts and Sciences (KNAW) with project license of AVD8010020151 and research protocol HI19.1004.

METHOD DETAILS

Healthy endo- and ectocervical organoid culture

Distinct digestion treatments were used for healthy endo- and ectocervical tissues. Endocervical tissues were first mechanically minced by scalpels, followed by digestion in collagenase solution (1 mg/mL of collagenase from *Clostridium histolyticum*, Sigma, Cat# C9407) for 1.5 hour at 37°C in a shaker. For ectocervical tissue, a slightly modified version of previously published improved dissociation protocol was used ⁶⁴. Briefly, healthy ectocervical tissue was dissociated with Dispase II solution in AdDF+++ (Advanced DMEM/F12 supplemented with 1x Glutamax, 10 mM HEPES and penicillin-streptomycin, all from Thermo Fisher) with 10 μM ROCK inhibitor (Abmole, Cat# Y-27632) overnight (16 hours) at 4°C on a tube roller. The ectocervical tissues were then incubated for an additional hour at room-temperature (RT) on a tube roller. Subsequently, the intact sheet of epithelium was peeled off from underlying connective tissue. The resulting sheets of ectocervical epithelium were subsequently mechanically minced by scalpels and subjected to dissociation with TrypLE (Gibco, Cat# 12605-010) for 8-10 min at 37°C. After digestion procedure, in both cases resulting cell suspensions were washed three times with AdDF+++ and erythrocytes were lysed in Red Blood Cell Lysis Buffer (Roche, Cat# 11814389001). The cells were filtered through a 70 μm nylon cell strainer (Greiner, Cat# 542070) and collected via centrifugation for 5 min at 1200 rpm. Next, the cells were embedded into Basement Membrane Extract (Cultrex® BME RGF type 2, Trevigen, Cat# 3533-005-02) and plated in 30 μl-volume droplets on a pre-warmed 24-well suspension culture plates (Greiner, Cat# 662102) and allowed to solidify at 37°C for 30 min before addition of medium. The full growth medium (M7) for ectocervical organoids consisted of AdDF+++ supplemented with 1% Noggin conditioned medium (U-Protein Express, Cat# N002), 10% of Rspo1 conditioned medium (made in-house), 1x B27 supplement (Gibco, Cat# 175044), 2.5 mM nicotinamide (Sigma, Cat# N0636), 1.25 mM mM n-Acetylcystein (Sigma, Cat# A9165), 10 μM ROCK inhibitor (Abmole, Cat# Y27632), 500 nM A83-01 (Tocris, Cat# 2939), 10 μM forskolin (Bio-Techne, Cat# 1099), 25 ng/ml FGF7 (Peprotech, Cat# 100-19), 100 ng/ml FGF10 (Peprotech, Cat# 100-26) and 1 μM p38 inhibitor SB202190 (Sigma, Cat# 7067). For endocervical cultures, M7 medium was additionally supplemented with 50 ng/μ EGF (Peprotech, Cat# AF-100-15), 100 nM β-Estradiol (Sigma, Cat# E2257) and two WNT pathway activators, i.e. 0.5 nM WNT surrogate (U-Protein Express, Cat# N001) and 0.3 μM CHIR (Stemgent, Cat# 04-0004-10). During the first 2-3 passages 100 μg/ml Primocin (InvivoGen, Cat# Ant-pm-1) was added to avoid contamination. For splitting, mechanical shearing through fire-polished plugged glass pipettes (Fisher Scientific, Cat# 11506973) can be used for endocervical cultures as the cystic organoids break easily. Due to the dense and hard-to-break properties of the ectocervical organoids, dissociation with TrypLE for 15 min at 37°C is required. After splitting, the plating density for ectocervical lineage should stay between 5000-10000 cells/30 ul drop for optimal outgrowth. The approximate splitting ratio is 1:4 and 1:10 in

1

2

3

4

5

&

every two weeks for endo- and ectocervical lines, respectively. All organoid lines tested negative in the MycoAlert mycoplasma detection kit (Lonza, LT07-318). Following this protocol, organoids could be derived with 82% (10/12) and 93% (25/27) success rate in endo- and ectocervical lineage, respectively. Patient clinical data for 8 more thoroughly characterized lines in this study is presented in Table S1.

Tumor-derived organoid (tumoroid) culture

Cervical tumor tissue were obtained from consenting patients via the Pap-brush method. The Pap-brush was tipped in a tube filled with AdDF+++ to release the tissue fragments from the brush. The tissue fragments were then pelleted and digested in collagenase solution (specified above) for 40 min at 37°C in a shaker. The suspension was then additionally mechanically sheared via a glass-pipet and the cell clumps pelleted via centrifugation for 5 min at 12000 rpm. Before plating the erythrocytes were lysed as described above. The resulting small tissue fragments were then embedded into BME on suspension plates and covered with the full growth medium (specified above). Tumoroid derivation success rate was 50% (12/24 Pap-brushes). Patient clinical data is presented in the Table S1.

Organoid formation efficiency assay

Fresh tissue was digested (see Methods above) and the material dissociated into single cells using TrypLE for 10-15 min at 37°C. Cells were then washed in AdDF+++ and passed through a 70 µm nylon cell strainer to ensure the single-cell suspension. Cells were counted using haemocytometer. For the growth factor requirement experiment (Figure 1b), 5000 cells were plated per 30 µl BME drop into 24-well suspension plate and overlaid with 500 µl of medium. For organoid formation efficiency assay (Figure 1c), 1000 cells were plated into 5 µl BME drops into 48-well suspension plate (Greiner, Cat# 677102) and overlaid with 250 µl of medium. The number of organoids was scored 10 days post-seeding. Data analysis was performed by using ImageJ software and the experiments were performed in at least 2 biological replicates (2 technical replicates per biological replicate, n≥4).

Karyotyping

About 5-6 days after splitting of the organoids, the cultures were treated with 0.1 µg/mL colcemid (Gibco, Cat# 15210-040) in the culture media for 16h at the 37°C cell incubator (with 5% CO₂). Organoids were then collected and dissociated into single-cells using TrypLE. Hypotonic shock was performed by addition of pre-warmed 75 mM KCl and incubated at 37°C for 10 min. The swollen cells were fixed by addition of ice-cold methanol:acetic acid (3:1) while gently tapping the cell suspension. Slides were mounted with DAPI-containing Vectashield (Vector Laboratories, Cat# H-1500-10), imaged on AF7000 microscope (Leica) with a 100x objective, and quantified by manual chromosome counting. At least 15 spreads were analysed per organoid line.

Immunohistochemistry

Tissues were fixed overnight in 4% paraformaldehyde (PFA) at 4°C followed by dehydration and paraffin embedding. To prepare organoids for histological stainings, intact BME-drops containing organoids were collected from the culture plates and incubated in 5 ml Cell Recovery Solution (Corning, Cat# 354253) on ice for 30 min, occasionally inverting the tube, to dissolve BME. Organoids were then allowed to settle to the bottom of the tube by free gravitation, supernatant removed, suspended in 4% PFA at RT for 1h for fixation, washed with PBS, and embedded into paraffin blocks. Sections were cut and hydrated before staining. Sections were subjected to H&E and PAS staining or immunohistochemical staining by using overnight incubation with antibodies raised against TP63 (Abcam, Cat# AB735, 1:800), MKI67 (Monosan, Cat# MONX10283, 1:2000), PAX8 (Proteintech, Cat# 10336-1-AP, 1:2000), KRT7 (Invitrogen, Cat# MA5-11986, 1:500), KRT13 (Progen Biotechnik, Cat# 10523, 1:100), KRT14 (Covance, Cat# 905301, 1:2000), acetylated α Tubulin (Santa-Cruz, Cat# sc-23950, 1:2000), p16INK4a (Abcam, Cat# ab108349, 1:500) and human nuclei (EMD Millipore, Cat# MAB1281, 1:20). For most antibodies, antigen retrieval was performed in citric acid solution (pH 6.0), except for KRT7 and p16INK4a antibodies that required pepsin or TRIS/EDTA (pH 9.0) treatment, respectively. Images were acquired on DM4000 microscope (Leica) and processed using Leica LAS X software.

RNA isolation, cDNA preparation and RT-qPCR

For RT-qPCR analysis, RNA was isolated from cervical organoids and tissues using the RNeasy Mini Kit (Qiagen, Cat# 74104) following the manufacturer's instructions including DNaseI treatment (Qiagen, Cat# 79254). Next, RNA was reverse transcribed from 500 ng of total RNA using GoScript Reverse Transcriptase Kit (Promega, Cat# A5003) and random Oligo(dT)₁₅ Primer (Promega, Cat# C1101). Quantitative PCR was performed with three biological replicates in duplicates using the indicated primers listed in the Table S2, SYBR Green Supermix (Bio-Rad, Cat# 1708887) and Bio-Rad systems. Gene expression was quantified using the delta-delta-Ct method and normalized against GAPDH housekeeping gene.

Bulk RNA-seq analysis

For RNA-seq analysis, RNA was isolated from organoids and tissues using the RNeasy Mini Kit (Qiagen, Cat# 74104) following the manufacturer's instructions including DNaseI treatment. RNA integrity was confirmed by Agilent 2100 bioanalyzer. The libraries were prepared by the Utrecht Sequencing Facility (USEQ) based on polyA enrichment. Sequencing was performed on an Illumina NextSeq500 by using 75-bp paired-end sequencing. Paired-end reads were aligned to the human reference genome (GRCh37) using Burrows-Wheeler Aligner (BWA) (v0.5.9)⁶⁵. DESeq2 (v1.18.0) package⁶⁶ was used to normalize count data and for differential gene expression analysis in Rstudio (R v3.6.2, Bioconductor v3.10 (BiocManager v1.30.10)).

1

2

3

4

5

&

Viral subtype detection and integration analysis

Viral sequences of different HPV subtypes were detected in the RNA-seq data of the different tumoroid lines by using VirusSeq-CLI, a wrapper around the VirusSeq pipeline⁶⁷. VirusSeq-CLI can be accessed through the following website: <https://github.com/UMCUGenetics/VirusSeq-CLI>. For all tumoroid lines, VirusSeq-CLI was used with default parameters and the top hit with more than 1,000 counts was reported. Integration sites were identified by using ViFi⁶⁸. ViFi can be accessed through the following website: <https://github.com/namphuon/ViFi>. For all tumoroid lines, ViFi was used with default parameters.

DNA extraction and whole-exome sequencing analysis

Genomic DNA was isolated from both tissues and tumoroids using Reliaprep gDNA Tissue Miniprep System (Promega, Cat# A2051) according to manufacturer's protocol. The whole exome sequencing (WES) was performed at Macrogen Inc. (Seoul, South Korea) using Agilent SureSelect V7 8Gb 150bp PE Novaseq exome. WES data was mapped against human reference genome GRCh38 by using BWA (v0.7.5) mapping tool⁶⁵ with settings 'bwa mem -c 100 -M'. Sequence reads were marked for duplicates by using Sambamba (v0.6.8) and realigned per donor by using Genome Analysis Toolkit (GATK) IndelRealigner (v3.8.1) Raw variants were multisample-called by using the GATK HaplotypeCaller (v3.8-0) (DePristo et al., 2011) and GATK-Queue (v3.8-0) with default settings and additional option 'EMIT_ALL_CONFIDENT_SITES'. The quality of variant and reference positions was evaluated by using GATK VariantFiltration (v3.8-0) with options '-snpFilterName LowQualityDepth -snpFilterExpression "QD < 2.0" -snpFilterName MappingQuality -snpFilterExpression "MQ < 40.0" -snpFilterName StrandBias -snpFilterExpression "FS > 60.0" -snpFilterName HaplotypeScoreHigh -snpFilterExpression "HaplotypeScore > 13.0" -snpFilterName MQRankSumLow -snpFilterExpression "MQRankSum < -12.5" -snpFilterName ReadPosRankSumLow -snpFilterExpression "ReadPosRankSum < -8.0" -cluster 3 -window 35'. Full pipeline description and settings also available at: <https://github.com/UMCUGenetics/IAP>.

To obtain potential driver mutations and reduce the number of false positive calls, we further filtered with the following criteria: passed by VariantFiltration with a base coverage of at least 10X, HIGH or MODERATE expected effect on the gene reported by SnpEff annotation, no overlap with single nucleotide polymorphisms (SNPs) in the Single Nucleotide Polymorphism Database (v146) nor with the panel of normals (VCF-file available upon request); and absence of the variant in a panel of unmatched normal human genomes (BED-file available upon request) and not RefSNP number has been assigned except for the variants with both RefSNP ID's and COSMIC ID's (well-known drivers). Shared mutations between patients were also excluded as artifacts.

In vitro drug screen

Two days prior to start of the drug screen, organoids were disrupted into single cells using TrypLE and filtered using a 70-mm nylon cell strainer. Cells were counted and resuspended in 5% BME/growth medium (25,000 cells/mL) prior plating in 40 μ L volume in 384-well plates (Corning, Cat# 4588) by using Multi-drop Combi Reagent Dispenser (Thermo Fisher, Cat# 5840300). Two days after plating the cells, the drugs were added using the D300e Digital Dispenser (Tecan). Nutlin-3a (Cayman Chemical, Cat# 10004372), gemcitabine (Selleckchem, Cat# S1714) and olaparib (Selleckchem, Cat# S1060) were dissolved in DMSO. Cisplatin (Sigma, Cat# C2210000) and carboplatin (Selleckchem, Cat# S1215) were dissolved in PBS containing 0.3% Tween-20 (Sigma, Cat# P1379), which was required to dispense these drugs using the HP printer. All wells were normalized for solvent used. DMSO percentage never exceeded 1%, PBS/Tween-20 percentage never exceeded 2%. Drug exposure was performed in triplicates for each concentration shown. Five days (120 hours) after adding the drugs, ATP levels were measured using the CellTiter-Glo 3D Viability Assay (Promega, Cat# G9683) according to the manufacturer's instructions, and luminescence was measured using a Spark multimode microplate reader (Tecan). Results were normalized to vehicle (100%) and baseline control (Staurosporine 1 μ mol/L (Sigma, Cat# 62996-74-1); 0%).

Pilot *in vivo* xeno-transplantation assays

Before transplantations, the tumoroids (SqCa-1.2 line) were trypsinized using TrypLE and dissociated into single-cell suspension. Cells were then counted and approximately 200 000 cells were suspended in 50 μ l of medium mixed with BME at a 1:1 ratio. Subcutaneous injections were performed into opposite flanks of all of the 4 NSG mice (2 flanks per mice, 200 000 cells/50 μ l per location). The mice were sacrificed 4 months (120 days) after injections. Tumor measurements were taken by digital calipers (RS PRO, Cat# 841-2518) and volumes estimated by formula: tumor volume = (length x width²)/2, where length represents the largest tumor diameter and width the perpendicular tumor diameter. All tumors were subjected to immunohistochemical analysis.

QUANTIFICATION AND STATISTICAL ANALYSIS

The experiments described in this study are based on the analysis of at least 3 different organoid lines derived from 3 independent donors. Statistical methods are specified under respective figure legends where applicable. Statistical analyses were performed with MS Excel and GraphPad Prism. P-values were calculated using two-tailed Student's t-test assuming a normal sample distribution, error bars represent either \pm SEM or \pm SD as specified in the legend. RNA-seq and WES data were mapped by BWA method. RNA-seq data was normalized by DESeq2 and analysed in Rstudio. WES data filtering criteria is described in detail under the Methods section. Blinded evaluation of tumoroids and tumors was performed by expert pathologist.

1

2

3

4

5

&

DATA AND SOFTWARE AVAILABILITY

All the raw data (i.e. fastq files for the RNA-seq and WES data) will be deposited on Gene Expression Omnibus (GEO) upon acceptance. However, these data can be made available upon reviewers' request.

REFERENCES

1. Ronco, G. *et al.* Efficacy of HPV-based screening for prevention of invasive cervical cancer: follow-up of four European randomised controlled trials. *Lancet* **383**, 524-532 (2014).
2. Isidean, S.D. *et al.* Human papillomavirus testing versus cytology in primary cervical cancer screening: End-of-study and extended follow-up results from the Canadian cervical cancer screening trial. *Int J Cancer* **139**, 2456-2466 (2016).
3. Horn, J. *et al.* Reduction of cervical cancer incidence within a primary HPV screening pilot project (WOLPHSCREEN) in Wolfsburg, Germany. *Br J Cancer* **120**, 1015-1022 (2019).
4. Shrestha, A.D., Neupane, D., Vedsted, P. & Kallestrup, P. Cervical Cancer Prevalence, Incidence and Mortality in Low and Middle Income Countries: A Systematic Review. *Asian Pac J Cancer Prev* **19**, 319-324 (2018).
5. Randall, T.C. & Ghebre, R. Challenges in Prevention and Care Delivery for Women with Cervical Cancer in Sub-Saharan Africa. *Front Oncol* **6**, 160 (2016).
6. Cohen, P.A., Jhingran, A., Oaknin, A. & Denny, L. Cervical cancer. *Lancet* **393**, 169-182 (2019).
7. Bosch, F.X., Lorincz, A., Munoz, N., Meijer, C.J. & Shah, K.V. The causal relation between human papillomavirus and cervical cancer. *J Clin Pathol* **55**, 244-265 (2002).
8. Kajitani, N., Satsuka, A., Kawate, A. & Sakai, H. Productive Lifecycle of Human Papillomaviruses that Depends Upon Squamous Epithelial Differentiation. *Front Microbiol* **3**, 152 (2012).
9. Schwarz, E. *et al.* Structure and transcription of human papillomavirus sequences in cervical carcinoma cells. *Nature* **314**, 111-114 (1985).
10. Phelps, W.C., Yee, C.L., Munger, K. & Howley, P.M. The human papillomavirus type 16 E7 gene encodes transactivation and transformation functions similar to those of adenovirus E1A. *Cell* **53**, 539-547 (1988).
11. Androphy, E.J., Hubbert, N.L., Schiller, J.T. & Lowy, D.R. Identification of the HPV-16 E6 protein from transformed mouse cells and human cervical carcinoma cell lines. *EMBO J* **6**, 989-992 (1987).
12. Banks, L. *et al.* Identification of human papillomavirus type 18 E6 polypeptide in cells derived from human cervical carcinomas. *J Gen Virol* **68** (Pt 5), 1351-1359 (1987).
13. Larmour, L.I., Jobling, T.W. & Gargett, C.E. A Review of Current Animal Models for the Study of Cervical Dysplasia and Cervical Carcinoma. *Int J Gynecol Cancer* **25**, 1345-1352 (2015).
14. Ozbun, M.A. & Patterson, N.A. Using organotypic (raft) epithelial tissue cultures for the biosynthesis and isolation of infectious human papillomaviruses. *Curr Protoc Microbiol* **34**, 14B 13 11-18 (2014).
15. Hoffmann, C. *et al.* Creation and characterization of a xenograft model for human cervical cancer. *Gynecol Oncol* **118**, 76-80 (2010).
16. Herber, R., Liem, A., Pitot, H. & Lambert, P.F. Squamous epithelial hyperplasia and carcinoma in mice transgenic for the human papillomavirus type 16 E7 oncogene. *J Virol* **70**, 1873-1881 (1996).
17. Song, S., Pitot, H.C. & Lambert, P.F. The human papillomavirus type 16 E6 gene alone is sufficient to induce carcinomas in transgenic animals. *J Virol* **73**, 5887-5893 (1999).
18. Sato, T. *et al.* Single Lgr5 stem cells build crypt-villus structures in vitro without a mesenchymal niche. *Nature* **459**, 262-265 (2009).

1

2

3

4

5

&

19. Sato, T. *et al.* Long-term expansion of epithelial organoids from human colon, adenoma, adenocarcinoma, and Barrett's epithelium. *Gastroenterology* **141**, 1762-1772 (2011).
20. Huch, M. *et al.* Long-term culture of genome-stable bipotent stem cells from adult human liver. *Cell* **160**, 299-312 (2015).
21. van de Wetering, M. *et al.* Prospective derivation of a living organoid biobank of colorectal cancer patients. *Cell* **161**, 933-945 (2015).
22. Matano, M. *et al.* Modeling colorectal cancer using CRISPR-Cas9-mediated engineering of human intestinal organoids. *Nat Med* **21**, 256-262 (2015).
23. Drost, J. *et al.* Sequential cancer mutations in cultured human intestinal stem cells. *Nature* **521**, 43-47 (2015).
24. Kessler, M. *et al.* The Notch and Wnt pathways regulate stemness and differentiation in human fallopian tube organoids. *Nat Commun* **6**, 8989 (2015).
25. Kopper, O. *et al.* An organoid platform for ovarian cancer captures intra- and interpatient heterogeneity. *Nat Med* **25**, 838-849 (2019).
26. Turco, M.Y. *et al.* Long-term, hormone-responsive organoid cultures of human endometrium in a chemically defined medium. *Nat Cell Biol* **19**, 568-577 (2017).
27. Boretto, M. *et al.* Development of organoids from mouse and human endometrium showing endometrial epithelium physiology and long-term expandability. *Development* **144**, 1775-1786 (2017).
28. Hill, S.J. *et al.* Prediction of DNA Repair Inhibitor Response in Short-Term Patient-Derived Ovarian Cancer Organoids. *Cancer Discov* **8**, 1404-1421 (2018).
29. Boretto, M. *et al.* Patient-derived organoids from endometrial disease capture clinical heterogeneity and are amenable to drug screening. *Nat Cell Biol* **21**, 1041-1051 (2019).
30. Meggiolaro, A. *et al.* The role of Pap test screening against cervical cancer: a systematic review and meta-analysis. *Clin Ter* **167**, 124-139 (2016).
31. Cina, S.J., Richardson, M.S., Austin, R.M. & Kurman, R.J. Immunohistochemical staining for Ki-67 antigen, carcinoembryonic antigen, and p53 in the differential diagnosis of glandular lesions of the cervix. *Mod Pathol* **10**, 176-180 (1997).
32. Liang, J. *et al.* Utility of p16INK4a, CEA, Ki67, P53 and ER/PR in the differential diagnosis of benign, premalignant, and malignant glandular lesions of the uterine cervix and their relationship with Silverberg scoring system for endocervical glandular lesions. *Int J Gynecol Pathol* **26**, 71-75 (2007).
33. Tong, G.X. *et al.* Pax8: a marker for carcinoma of Mullerian origin in serous effusions. *Diagn Cytopathol* **39**, 567-574 (2011).
34. Danialan, R. *et al.* The utility of PAX8 and IMP3 immunohistochemical stains in the differential diagnosis of benign, premalignant, and malignant endocervical glandular lesions. *Gynecol Oncol* **130**, 383-388 (2013).
35. Lakshmi, S., Rema, P. & Somanathan, T. p16ink4a is a surrogate marker for high-risk and malignant cervical lesions in the presence of human papillomavirus. *Pathobiology* **76**, 141-148 (2009).
36. Queiroz, C. *et al.* P16(INK4a) expression as a potential prognostic marker in cervical pre-neoplastic and neoplastic lesions. *Pathol Res Pract* **202**, 77-83 (2006).

37. Zhang, L. *et al.* Genomic characterization of cervical cancer based on human papillomavirus status. *Gynecol Oncol* **152**, 629-637 (2019).
38. Degli Esposti, D. *et al.* Unique DNA methylation signature in HPV-positive head and neck squamous cell carcinomas. *Genome Med* **9**, 33 (2017).
39. Liu, L., Ren, M., Han, S., Sun, L. & Zhu, L. Expression level and clinical significance of low-density lipoprotein receptor-related protein 1B gene in cervical squamous cell carcinoma. *Int J Clin Exp Pathol* **11**, 1701-1706 (2018).
40. Gao, Q. *et al.* EphB2 promotes cervical cancer progression by inducing epithelial-mesenchymal transition. *Hum Pathol* **45**, 372-381 (2014).
41. Liu, J. *et al.* Identification of EPHX2 and RMI2 as two novel key genes in cervical squamous cell carcinoma by an integrated bioinformatic analysis. *J Cell Physiol* **234**, 21260-21273 (2019).
42. Yang, J., Hou, S. & Liang, B. LINC00319 promotes migration, invasion and epithelial-mesenchymal transition process in cervical cancer by regulating miR-3127-5p/RPP25 axis. *In Vitro Cell Dev Biol Anim* (2020).
43. Li, Z., Fan, P., Deng, M. & Zeng, C. The roles of RUNX3 in cervical cancer cells in vitro. *Oncol Lett* **15**, 8729-8734 (2018).
44. Cancer Genome Atlas Research, N. *et al.* Integrated genomic and molecular characterization of cervical cancer. *Nature* **543**, 378-384 (2017).
45. Ojesina, A.I. *et al.* Landscape of genomic alterations in cervical carcinomas. *Nature* **506**, 371-375 (2014).
46. IARC Working Group on the Evaluation of Carcinogenic Risks to Humans. Meeting (2008-2009 : Lyon France) & International Agency for Research on Cancer *A review of human carcinogens.* (International Agency for Research on Cancer, Lyon; 2012).
47. Vale, C. *et al.* Late complications from chemoradiotherapy for cervical cancer: reflections from cervical cancer survivors 10 years after the national cancer institute alert. *Clin Oncol (R Coll Radiol)* **22**, 588-589 (2010).
48. Vlachogiannis, G. *et al.* Patient-derived organoids model treatment response of metastatic gastrointestinal cancers. *Science* **359**, 920-926 (2018).
49. Ooft, S.N. *et al.* Patient-derived organoids can predict response to chemotherapy in metastatic colorectal cancer patients. *Sci Transl Med* **11** (2019).
50. Ganesh, K. *et al.* A rectal cancer organoid platform to study individual responses to chemoradiation. *Nat Med* **25**, 1607-1614 (2019).
51. Tiriác, H. *et al.* Organoid Profiling Identifies Common Responders to Chemotherapy in Pancreatic Cancer. *Cancer Discov* **8**, 1112-1129 (2018).
52. Yao, Y. *et al.* Patient-Derived Organoids Predict Chemoradiation Responses of Locally Advanced Rectal Cancer. *Cell Stem Cell* **26**, 17-26 e16 (2020).
53. Huibregtse, J.M., Scheffner, M. & Howley, P.M. A cellular protein mediates association of p53 with the E6 oncoprotein of human papillomavirus types 16 or 18. *EMBO J* **10**, 4129-4135 (1991).
54. Scheffner, M., Huibregtse, J.M., Vierstra, R.D. & Howley, P.M. The HPV-16 E6 and E6-AP complex functions as a ubiquitin-protein ligase in the ubiquitination of p53. *Cell* **75**, 495-505 (1993).

1

2

3

4

5

&

55. Scheffner, M., Werness, B.A., Huibregtse, J.M., Levine, A.J. & Howley, P.M. The E6 oncoprotein encoded by human papillomavirus types 16 and 18 promotes the degradation of p53. *Cell* **63**, 1129-1136 (1990).
56. Hu, H. *et al.* Long-Term Expansion of Functional Mouse and Human Hepatocytes as 3D Organoids. *Cell* **175**, 1591-1606 e1519 (2018).
57. Heo, I. *et al.* Modelling Cryptosporidium infection in human small intestinal and lung organoids. *Nat Microbiol* **3**, 814-823 (2018).
58. Driehuis, E. *et al.* Oral Mucosal Organoids as a Potential Platform for Personalized Cancer Therapy. *Cancer Discov* **9**, 852-871 (2019).
59. Nie, Y.Z. *et al.* Recapitulation of hepatitis B virus-host interactions in liver organoids from human induced pluripotent stem cells. *EBioMedicine* **35**, 114-123 (2018).
60. Pleguezuelos-Manzano, C. *et al.* Mutational signature in colorectal cancer caused by genotoxic pks(+) *E. coli*. *Nature* (2020).
61. Bartfeld, S. *et al.* In vitro expansion of human gastric epithelial stem cells and their responses to bacterial infection. *Gastroenterology* **148**, 126-136 e126 (2015).
62. Lamers, M.M. *et al.* SARS-CoV-2 productively infects human gut enterocytes. *Science* (2020).
63. Yang, D.X., Soulos, P.R., Davis, B., Gross, C.P. & Yu, J.B. Impact of Widespread Cervical Cancer Screening: Number of Cancers Prevented and Changes in Race-specific Incidence. *Am J Clin Oncol* **41**, 289-294 (2018).
64. Fan, T. *et al.* An improved method for primary culture of normal cervical epithelial cells and establishment of cell model in vitro with HPV-16 E6 gene by lentivirus. *J Cell Physiol* **233**, 2773-2780 (2018).
65. Li, H. & Durbin, R. Fast and accurate short read alignment with Burrows-Wheeler transform. *Bioinformatics* **25**, 1754-1760 (2009).
66. Love, M.I., Huber, W. & Anders, S. Moderated estimation of fold change and dispersion for RNA-seq data with DESeq2. *Genome Biol* **15**, 550 (2014).
67. Chen, Y. *et al.* VirusSeq: software to identify viruses and their integration sites using next-generation sequencing of human cancer tissue. *Bioinformatics* **29**, 266-267 (2013).
68. Nguyen, N.D., Deshpande, V., Luebeck, J., Mischel, P.S. & Bafna, V. ViFi: accurate detection of viral integration and mRNA fusion reveals indiscriminate and unregulated transcription in proximal genomic regions in cervical cancer. *Nucleic Acids Res* **46**, 3309-3325 (2018).

SUPPLEMENTARY INFORMATION

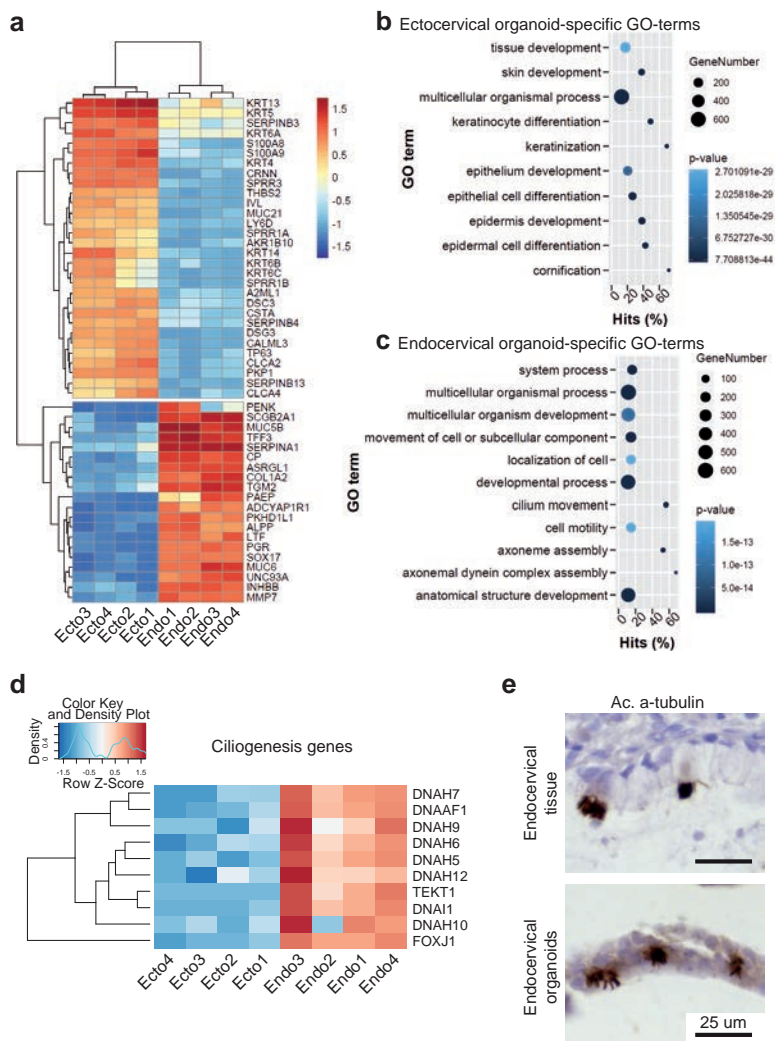


Figure S1. Differential gene expression patterns in healthy endo- and ectocervical organoids (related to Figure 1 and 2). (A) Heatmap of RNA-seq data depicting expression of the 60 differentially expressed genes between normal endo- and ectocervical organoids ($p < 0.01$). Blue indicates low expression, red indicates high expression. Differential expression was calculated as described in DESeq2 package. (B) Bubble plot displaying most significant terms after performing GO enrichment analysis with upregulated genes in ectocervical. Bubble colours represent the corrected p -value. Bubble sizes indicate the number of genes. (C) Bubble plot displaying most significant terms after performing GO enrichment analysis with upregulated genes in endocervical. Bubble colours represent the corrected p -value. Bubble sizes indicate the number of genes. (D) Heatmap depicting the upregulation of ciliogenesis-related genes in normal endocervical organoids compared to ectocervical counterparts. (E) Positive immunohistochemical stainings for acetylated α -tubulin in endocervical tissue and respective organoids, confirming the presence of cilia in this tissue as well as in the respective organoid model.

1
2
3
4
5
&

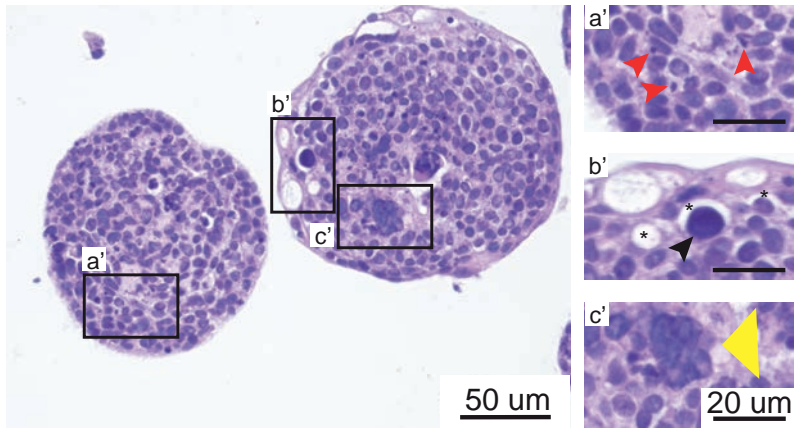


Figure S2. Histopathologies of cervical tumoroids (related to Figure 4). Representative H&E staining of cervical cancer tumoroids (SqCa-3 line) and close-up images of evident histopathologies, including abundant mitotic figures (a', red arrowheads), large and hyperchromatic nuclei (b', black arrowhead), cytoplasmic "halos" (b', asterisks) and multinucleated cells (c', yellow arrowhead).

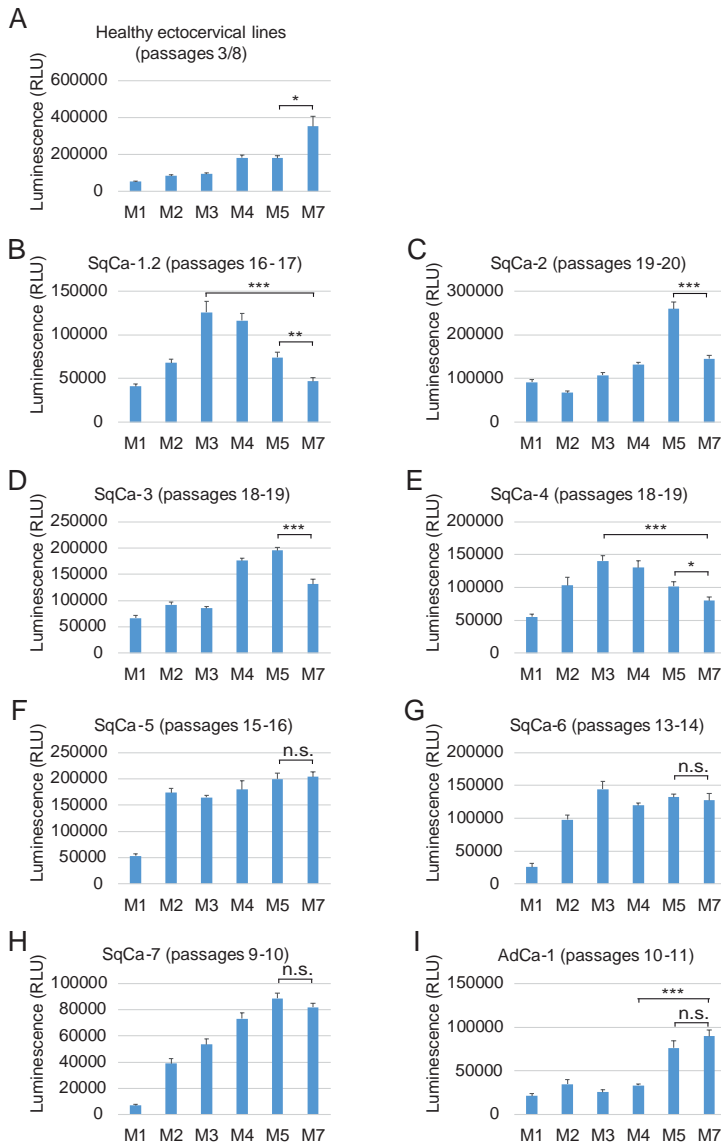
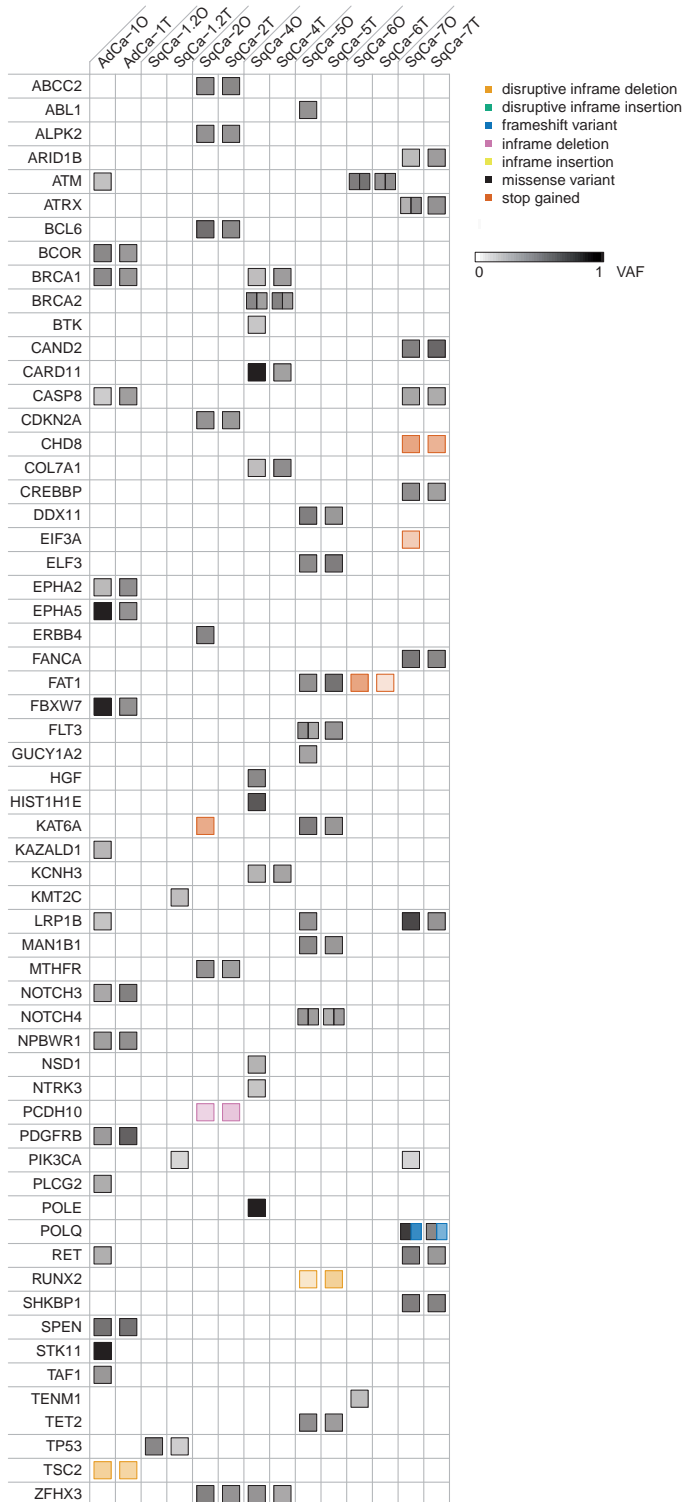


Figure S3. Tumoroid growth factor requirement (related to Figure 3). (A-I) Viability of the (A) healthy ectocervical organoid lines as well as the different tumor lines, including (B) SqCa-1.2, (C) SqCa-2, (D) SqCa-3, (E) SqCa-4, (F) SqCa-5, (G) SqCa-6, (H) SqCa-7 and (I) AdCa-1, measured in different growth factor reduced media 7 days after splitting the cells in comparable densities (1000 cells/40 μ l medium-BME). See detailed media (M1-M7) specifications under Figure 1b. Assay was repeated in two consecutive passages for each line. Error bars represent \pm SEM of 2 biological replicates (lines in different passages) with 4 technical replicates each (n=8). Statistical significance was calculated by two-tailed Student's t-test, p-values were not adjusted to multiple comparisons (* p <0.05, ** p <0.01, *** p <0.001). Cell viability was measured using CellTiter-Glo 3D Viability Assay.



◀ Figure S4. Comprehensive list of somatic alterations detected in analysed samples (related to Figure 6). All somatic mutations detected in matched organoid-tissue pairs using whole exome sequencing analysis.

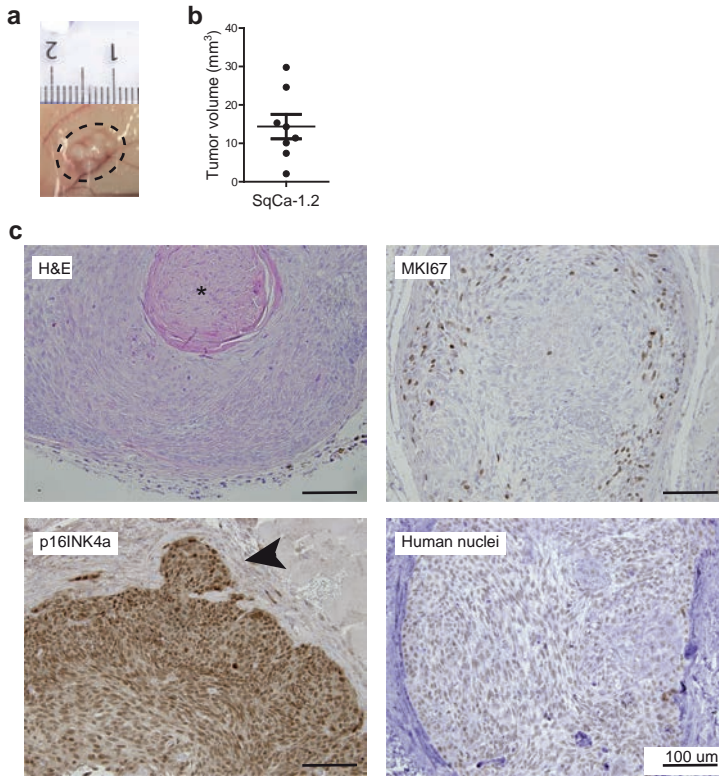


Figure S5. HPV30 infected tumoroids can give rise to tumors after subcutaneous xenotransplantation into mice in a pilot experiment (related to Figures 3-6). (A) Representative image of small subcutaneous papillary tumor (n=8) that was observed 4 months after xenotransplantation with SqCa-1.2 line. (B) The distribution and mean of tumor volumes derived with SqCa-1.2 line (n=8, mean=14 mm³). Error bars represent ±SEM. (C) Representative histological overview images of tumors (n=8) derived from subcutaneous injections with SqCa-1.2 tumoroid line. H&E, MKI67, p16INK4a and human nuclei stainings are shown. Tumors showed occasional keratin pearls (asterisk) and stromal invasion (black arrowhead) – an indication of tumorigenicity.

Table S1. Patient clinical data.

STUDY INFORMATION		SAMPLE INFORMATION							Tumor
No.	Organoid lab name	Line name in manu- script	Patient number	Age	Sampling event	Neo-adjvant chemo-therapy	Sample pathology at diagnosis	Tumor FIGO stage	Tumor grade (code)
Healthy organoid lines									
1	NCX19.1	EctoN1	E18-03875 I	72	Biopsy	Yes	Normal ectocervix from ovarian cancer patient	N/A	N/A
2	NCX19.2	EndoN1	E18-03875 II		Biopsy		Normal endocervix from ovarian cancer patient	N/A	N/A
3	NCX20.1	EctoN2	E18-03932 I	47	Biopsy	Yes	Normal ectocervix from ovarian cancer patient	N/A	N/A
4	NCX20.2	EndoN2	E18-03932 II		Biopsy		Normal endocervix from ovarian cancer patient	N/A	N/A
5	NCX30.1	EctoN3	P19-67412 IV	80	Biopsy	Yes	Normal ectocervix from ovarian cancer patient	N/A	N/A
6	NCX30.2	EndoN3	P19-67412 V		Biopsy		Normal endocervix from ovarian cancer patient	N/A	N/A
7	NCX31.1	EctoN4	P19-67463 IV	46	Biopsy	Yes	Normal ectocervix from ovarian cancer patient	N/A	N/A
8	NCX31.2	EndoN4	P19-67463 III		Biopsy		Normal endocervix from ovarian cancer patient	N/A	N/A
Tumoroid lines									
1	CXC2.1	SqCa-1.1	E18-04009	61	Pap-brush	No	A poorly differentiated cervical squamous cell carcinoma	IIB	3
2	CXC2.2	SqCa-1.2	E18-04042	61	Biopsy	No	A poorly differentiated cervical squamous cell carcinoma	IIB	3
3	CXC6	SqCa-2	P19-52549	37	Pap-brush	No	A SMILE-lesion (in-situ stratified mucin-producing intraepithelial lesion), very strongly suspected for infiltrative growth, CIN1	IA1	N/A
4	CXC7	SqCa-3	P19-53128	62	Pap-brush	No	A well-differentiated cervical squamous cell carcinoma	IB1	1
5	CXC8	SqCa-4	P19-53725	40	Pap-brush	No	A poorly differentiated cervical squamous cell carcinoma	IB2	3
6	CXC15	SqCa-5	P19-61570	49	Pap-brush	No	A moderately differentiated cervical squamous cell carcinoma	IIIB	2

Table S1. (continued)

STUDY INFORMATION				SAMPLE INFORMATION					
No.	Organoid lab name	Line name in manuscript	Patient number	Age	Sampling event	Neo-adjuvant chemo-therapy	Sample pathology at diagnosis	Tumor FIGO stage	Tumor grade (code)
7	CXC20	SqCa-6	P19-66302	40	Pap-brush	No	A poorly differentiated cervical squamous cell carcinoma	IB1	3
8	CXC25	SqCa-7	P19-77226	40	Pap-brush	No	A moderately differentiated cervical squamous cell carcinoma, CIN3	IB1	2
9	CXC27	SqCa-8	P19-78711	44	Pap-brush	No	A moderately differentiated cervical squamous cell carcinoma	IB1	2
10	CXC29	SqCa-9	P19-86345	37	Pap-brush	No	Cervical squamous cell carcinoma (macro-invasive)	1B1	N/A
11	CXC24	AdCa-1	P19-77132	58	Pap-brush	No	A poorly differentiated cervical adenocarcinoma	IB2	3
12	CXC26	AdCa-2	P19-78698	30	Pap-brush	No	A poorly differentiated cervical adenocarcinoma	IB1	3



Table S2. RT-qPCR primer sequences.

No.	Primer	Sequence
1	GAPDH_fw	5'-GTCGGAGTCAACGGATT-3'
2	GAPDH_rev	5'-AAGCTTCCCCGTTCTCAG-3'
3	PAX8_fw	5'-AGCTGCCGACTAAGCATTGA-3'
4	PAX8_rev	5'-GGGTGAGTGAGGATCTGCCA-3'
5	MUC5AC_fw	5'-CTACCAGTGCCAGTGTGTGT-3'
6	MUC5AC_rev	5'-TCTCGTTTGTGCATCACCCCG-3'
7	MUC5B_fw	5'-CAGAACCAAGGCTGACGACTT-3'
8	MUC5B_rev	5'-ATGCAGTTCGAGTGGAAGGG-3'
9	TP63_fw	5'-GACAGGAAGGCGGATGAAGATAG-3'
10	TP63_rev	5'-TGTTTCTGAAGTAAGTCTGGTGC-3'
11	IVL_fw	5'-TGTGAGTCTGGTTGACAGTAGC-3'
12	IVL_rev	5'-GCAGTGGAGTTGGCTGTTTC-3'
13	KRT5_fw	5'-AATGTCAAGAAACAGTGCGCC-3'
14	KRT5_rev	5'-CACTGCTACCTCCGGCAAG-3'
15	KRT7_fw	5'-ACCATGTCCATCCACTTCAGC-3'
16	KRT7_rev	5'-CCAGAAACCGCACCTTGTC-3'
17	KRT8_fw	5'-AGCAAATGTTTGCGGAATGAATG-3'
18	KRT8_rev	5'-GAACCAGGCGGAGATCCCTT-3'
19	KRT13_fw	5'-GACCGCCACCATTGAAAACAA-3'
20	KRT13_rev	5'-TCCAGGTCAGTCTTAGACAGAG-3'
21	KRT14_fw	5'-GCAGCAGAACCAGGAGTACAA-3'
22	KRT14_rev	5'-GAGGAGGTCACATCTCTGGAT-3'



CHAPTER

SUMMARIZING DISCUSSION

5

INTRODUCTION

In this thesis we describe the establishment and characterization of a broad panel of 3D organoid cultures from a variety of epithelial gynecological cancers and respective healthy tissues of origin with the purpose to better understand the heterogeneity and the individual characteristics of these tumors. Gynecological cancers affect different parts of female reproductive tract (FRT) giving rise to a diverse spectrum of epithelial cancers, involving ovaries, fallopian tubes, uterus, cervix and vagina. Although these cancers show distinct molecular profiles and characteristics, not all subtypes are represented by adequate model systems to study the different disease phenotypes. Therefore, independent model systems that represent the inherent disease-specific features are highly anticipated in the field to uncover the best treatment strategies for each type. To date, there are several patient-derived model systems used in gynecological cancer research. These are reviewed in Chapter 1. The invention of organoid technology, in particular, has recently allowed to build highly representative long-term culture systems for human FRT tissues in health¹⁻⁵ and disease^{2,6}. The potential to maintain healthy epithelial cells as a long-term organoid culture without the requirement for transformation, and the compatibility of these models with the state-of-the-art genome editing tools (such as CRISPR-Cas9) has opened up new exciting doors in the human disease modeling strategies. To illustrate such potential, here we demonstrate our work where simple CRISPR-Cas9 genome editing in mouse-derived organoids enables to address the long-standing debate over the possible dual origin of high-grade serous ovarian cancer (Chapter 2). Throughout the subsequent chapters in this work we demonstrate the feasibility to derive patient-derived tumor organoids from different ovarian (Chapter 3) and cervical cancer (Chapter 4) subtypes and respective healthy counterparts that bear remarkable resemblance to their donor tissues of origin.

MODEL SYSTEMS IN GYNECOLOGICAL CANCER RESEARCH

Gynecological cancers constitute a heterogeneous group of malignancies that can arise from different parts of FRT epithelium and display distinct biological behaviours. The cancer studies have traditionally relied on different *in vitro* and *in vivo* model systems that allow investigations on how and why the disease develops, and validation of potential drug candidates. Although the generation of different engineered animal models has greatly benefited our knowledge about the development of these cancers, they can never truly reiterate the entire complexity of human disease phenotype due to the species-related evolutionary divergence. Therefore, patient-derived model systems are required to overcome those differences. In **Chapter 2** we review the currently available human-based model systems for studying the most common gynecological cancers.

Patient-derived material can be used in various ways to generate useful models that better represent the human cell-specific traits and behaviour than any animal model ever could. *In vitro* patient-derived 2D culture systems are often favoured for their easy and economic maintenance. Additionally, the susceptibility of such models to large-scale

1

2

3

4

5

&

screenings and genetic manipulation has made the cell lines extremely useful in dissecting and exploiting different treatment response pathways in cancer cells. For several decades, the US National Cancer Institute (NCI)-60 cancer cell line collection including a 60 thoroughly characterized human cell lines derived from nine tumor types has served the international research community to screen for potential anti-cancer therapeutics⁷⁻⁹. Among the gynecological tumors only a selection of ovarian cancer lines are represented in this panel. Additionally, as cell lines often suffer from strong clonal selection and concurrent loss of tumor cell heterogeneity^{10,11}, there has been a strong push towards the development and integration of more complex models for pre-clinical and clinical screenings that enable to better represent the cellular complexity of tumors.

In order to better retain the heterogeneity, primary tumor cells can be transplanted into mice and the disease development followed *in vivo* in the so-called patient-derived xenograft (PDX) models. This system is particularly suitable for studying intra-tumor heterogeneity, cellular interplay with stromal components and for drug validation. And all the more so that in 2016, encouraged by the better predictive value of PDX models, the United States NCI decided to completely replace the NCI-60 panel with newer PDX models to screen for anti-cancer drugs¹². Despite expensive and labor-intensive, drug validation on PDXs models has now become an indispensable step in just about any drug development pipeline¹³ that help to determine the exact efficacy, metabolic stability and manageable toxicity of a therapeutic candidate in a living system. However, the system lacks compatibility with large-scale screening procedures, which has fueled researchers to look for better high-throughput alternatives.

In a meantime, there has been a significant advance in the *in vitro* culture systems as more complex organotypic models have emerged that better represent the disease characteristics “in a dish”, such as organoid technology. This novel technology has allowed for better preservation of tumor heterogeneity, genomic landscape and medium-throughput assessment of therapy response in the culture settings. Since the invention of the technology¹⁴, the generation of patient-derived organoid cancer biobanks has started to flourish world-wide^{2,6,15-20}, which is predicted to revolutionize the pre-clinical oncology research. Organoids allow more rapid and scalable tool for screening assays and thereby, offer an important new link between clinical practice and translational research. Hence, it can be imagined that in the future such advances will lead to the era of precision medicine, where representative patient-derived cancer model systems allow to determine the right drug for the right patient at the right time.

THE SYMBIOSIS OF ORGANOID TECHNOLOGY AND GENOME EDITING IN DISEASE MODELING

Previously, cancer development studies have largely relied on genetically engineered animal models that allow targeted and conditional transformation of healthy epithelium *in vivo*. Until very recently, such modeling was difficult to carry out and interpret in the *in vitro* systems, since healthy epithelium could not be maintained in conventional cultures

for long-term without necessity for genetical transformation. The invention of organoid technology¹⁴ has offered a new promising breakthrough in the disease modeling “in a dish”, since, apart from tumor cells, the model also supports the growth and stability of healthy epithelial cells in culture. Combining organoid models with yet another state-of-the-art technology, such as CRISPR-Cas9 genome editing, has had a significant impact on overall cancer research, allowing to model the disease from scratch as elegantly demonstrated by multitude of previous studies²¹⁻²³.

In **Chapter 3** we describe our efforts to study the possible dual origin of the most aggressive type of ovarian cancer (OC), namely high-grade serous ovarian cancer (HG-SOC). Despite being the most common type of OC, the exact tissue of origin for HG-SOC is still under debate. It is currently believed that most of the HG-SOCs arise from the fallopian tube epithelium; yet, accumulating evidence also suggests that a smaller percentage of the tumors might have a different origin from the ovarian surface epithelium (OSE)²⁴⁻²⁸. So far, due to technical limitations, no model system has been able to compare the potential of these two epithelia to form OC in parallel. By using organoids derived from mouse tissues, we explore the likelihood of oviduct (the mouse equivalent of the human fallopian tube) and OSE to give rise to HG-SOCs. We exploit CRISPR-Cas9 genome editing tool to build comparative cancer models from both origins by knocking out commonly mutated genes in OC. These genes included *Trp53*, *Brca1*, *Nf1* and *Pten*. The organoids from the two origins and their mutants show distinct lineage-dependent features in terms of gene expression, growth rate and drug response. Our results support the more prevailing view that fallopian tube is the main source of HG-SOCs. However, we observe that smaller percentage of OSE lines carrying similar mutations are able to also form HG-SOC-like tumors, supporting the likely dual origin of these cancers. A parallel organoid-focused study on the origin of HG-SOC reached to the same conclusion²⁹. Follow-up studies are required to more thoroughly determine the differences between the distinct origin-derived tumors in terms of biomarker profile and treatment response that would enable better stratification of patients in the future.

ORGANOID BIOBANKING IN GYNECOLOGICAL CANCER RESEARCH

Apart from building tumor models from healthy epithelia, the organoid technology is now also widely adapted to establish tumor organoid biobanks. The biobank is an expanding resource of highly characterised organoids for different organ systems in health and disease that provides ideal platform for drug screening, target discovery, and genomic and functional studies on a scale beyond what would be feasible in clinical trials or animal models. Including our recent work, several tumoroid biobanks have been already reported from cancers arising in the FRT^{2,6,30}.

In **Chapter 4** we describe our work to establish a novel patient-derived organoid platform for ovarian cancer (OC) research. Epithelial OC has perhaps always been a bit misleading term to characterize the vastly heterogeneous set of tumors that often share

1

2

3

4

5

&

nothing but the same anatomical location. These tumors can range from benign to low- and high-grade forms accompanied with a number of different histological subtypes, including serous, mucinous, clear cell and endometrioid OCs. Considering this complexity, where each of the subtypes represent a distinct disease with unique characteristics, there is a clear need for separate model systems that would enable to capture the whole disease spectrum and allow to advance the studies on each subtype independently. As described earlier, traditional cancer cell lines often fail to capture the tumor heterogeneity and the believed origin for several popular OC lines has recently been found misidentified³¹. Additionally, the success rate of establishing new PDX models is often low, the process considerably time-consuming and shows high inter-subtype variation, the most common high-risk serous histotype showing the highest take-rate^{32,33}.

Since the emergence of organoid cultures, the researchers have also tried to quickly adapt this new technology to OC setting. The first reported effort yielded in short-term cultured HG-SOC organoids that were successfully used to study DNA repair inhibitor response³⁴. Shortly after, we presented a robust protocol that enables efficient derivation and long-term expansion of OC organoids representing all the main subtypes². Following this protocol, we were able to build a comprehensive panel on 56 organoid lines covering the main subtype spectrum of ovarian cancer, and the established lines are readily available for the entire research community. These organoids do not only recapitulate the true intra- and interpatient heterogeneity, but also show differential drug-responses, including acquisition of the chemoresistance in the recurrent disease. Indeed, several more recent follow-up studies on the predictiveness of patient-derived ovarian cancer organoids have found a high correlation between organoid and patient drug response^{30,35}. To conclude, the established OC organoid-derivation protocol provides our field with much-anticipated means to generate long-term organoid models for each subtype depending on the particular research interest and for validating therapeutic response.

In **Chapter 5** we present an organoid-based platform for studying the biology of human cervix and associated malignancies. Previously, there has been a brief report that describes derivation of human organoids from healthy cervical squamocolumnar junction, i.e. the transitional area in between the two cervical histotypes⁵. However, these organoids fail to show healthy polarized histological appearance, likely due to the suboptimal culture conditions, and are overall poorly characterized. Perhaps a more promising preprint can be found on BioRxiv that suggests that endo- and ectocervical epithelium arise from separate stem cell lineages³⁶. Indeed, in this work the authors propose distinct cellular origins for the two cervical histotypes and, supported by organoid derivation assays, delineate the importance of Wnt activation for derivation of columnar lineage of endocervix, while Notch signaling is required for squamous cell stratification of ectocervix. In our work, we have made similar observations and developed a robust protocol to establish long-term organoids from stratified ectocervix and glandular endocervix of healthy patients. These organoids show a remarkable similarity to their respective epithelia of origin in terms of gene expression and histologic appearance. Therefore, this emerging platform offers

a promising tool to further dissect the biology and pathology of cervix, and provides a novel system to investigate different sexually transmitted diseases of cervix via host-pathogen interaction studies, including the high-risk human papillomavirus infection, which is the main cause of cervical cancer.

Like the tissue of origin, cervical malignancies come in two main flavors: squamous cell carcinomas and adenocarcinomas. Organoid models for these main types of cervical cancers have not been reported yet; however, a single case-study has been published that describes organoid derivation and characterization from a rare type of cervical clear cell carcinoma³⁷. In this work, we are the first to describe the establishment of a panel of tumor organoids (tumoroids) from the main cervical cancer subtypes, using material collected via Pap-brush method. These tumoroids show evident cancer-associated mutation profile and gene expression pattern, carry morphological abnormalities and causative viral integration, and display differential response to different chemotherapy regimens. Given the ability to derive tumoroids non-invasively from patients' Pap-brush material, our protocol provides the research community with a relatively easy access to the tissue of interest and a new model system. This, in turn, will hopefully facilitate a rapid generation of additional organoid-based cervical cancer biobanks worldwide, offering new means for advancing the cervical cancer research.

CONCLUDING REMARKS

With the arrival of organoid technology, the gynecological oncology research has been offered a new unprecedented tool to rapidly capture the entire disease spectrum and model the disease from scratch. In this work we illustrate the broad potential of this model system and provide exciting new avenues for the future research. With the advancements in complementary state-of-the-art technologies, such as genome editing and single-cell sequencing, it is now possible to prioritize an individual over the averaged cohort studies and provide customized solutions for each case independently. Indeed, it is particularly important to acknowledge the potential what the organoid technology offers in terms of our efforts to personalize the patient clinical care to individual needs. It is therefore a time to start slowly adapting and integrating this new technology into important ethical and regulatory frameworks that would help bringing the personalized patient care to the next level. The dawn of the precision medicine in cancer research has arrived.

1

2

3

4

5

&

REFERENCES

1. Kessler, M. *et al.* The Notch and Wnt pathways regulate stemness and differentiation in human fallopian tube organoids. *Nat Commun* **6**, 8989, doi:10.1038/ncomms9989 (2015).
2. Kopper, O. *et al.* An organoid platform for ovarian cancer captures intra- and interpatient heterogeneity. *Nat Med* **25**, 838-849, doi:10.1038/s41591-019-0422-6 (2019).
3. Boretto, M. *et al.* Development of organoids from mouse and human endometrium showing endometrial epithelium physiology and long-term expandability. *Development* **144**, 1775-1786, doi:10.1242/dev.148478 (2017).
4. Turco, M. Y. *et al.* Long-term, hormone-responsive organoid cultures of human endometrium in a chemically defined medium. *Nat Cell Biol* **19**, 568-577, doi:10.1038/ncb3516 (2017).
5. Maru, Y. *et al.* Establishment and Molecular Phenotyping of Organoids from the Squamocolumnar Junction Region of the Uterine Cervix. *Cancers (Basel)* **12**, doi:10.3390/cancers12030694 (2020).
6. Boretto, M. *et al.* Patient-derived organoids from endometrial disease capture clinical heterogeneity and are amenable to drug screening. *Nat Cell Biol* **21**, 1041-1051, doi:10.1038/s41556-019-0360-z (2019).
7. Boyd, M. P., KD. Some practical considerations and applications of the National Cancer Institute in vitro anticancer drug discovery screen. *Drug Dev Res*, 91-109 (1995).
8. Weinstein, J. N. & Pommier, Y. Transcriptomic analysis of the NCI-60 cancer cell lines. *C R Biol* **326**, 909-920, doi:10.1016/j.cvi.2003.08.005 (2003).
9. Weinstein, J. N. Integromic analysis of the NCI-60 cancer cell lines. *Breast Dis* **19**, 11-22, doi:10.3233/bd-2004-19103 (2004).
10. Hughes, P., Marshall, D., Reid, Y., Parkes, H. & Gelber, C. The costs of using unauthenticated, over-passaged cell lines: how much more data do we need? *Biotechniques* **43**, 575, 577-578, 581-572 passim, doi:10.2144/000112598 (2007).
11. Ben-David, U. *et al.* Genetic and transcriptional evolution alters cancer cell line drug response. *Nature* **560**, 325-330, doi:10.1038/s41586-018-0409-3 (2018).
12. Ledford, H. US cancer institute to overhaul tumour cell lines. *Nature* **530**, 391, doi:10.1038/nature.2016.19364 (2016).
13. Koga, Y. & Ochiai, A. Systematic Review of Patient-Derived Xenograft Models for Preclinical Studies of Anti-Cancer Drugs in Solid Tumors. *Cells* **8**, doi:10.3390/cells8050418 (2019).
14. Sato, T. *et al.* Single Lgr5 stem cells build crypt-villus structures in vitro without a mesenchymal niche. *Nature* **459**, 262-265, doi:10.1038/nature07935 (2009).
15. van de Wetering, M. *et al.* Prospective derivation of a living organoid biobank of colorectal cancer patients. *Cell* **161**, 933-945, doi:10.1016/j.cell.2015.03.053 (2015).
16. Sachs, N. *et al.* A Living Biobank of Breast Cancer Organoids Captures Disease Heterogeneity. *Cell* **172**, 373-386 e310, doi:10.1016/j.cell.2017.11.010 (2018).
17. Takebe, T., Wells, J. M., Helmrath, M. A. & Zorn, A. M. Organoid Center Strategies for Accelerating Clinical Translation. *Cell Stem Cell* **22**, 806-809, doi:10.1016/j.stem.2018.05.008 (2018).

18. Yan, H. H. N. *et al.* A Comprehensive Human Gastric Cancer Organoid Biobank Captures Tumor Subtype Heterogeneity and Enables Therapeutic Screening. *Cell Stem Cell* **23**, 882-897 e811, doi:10.1016/j.stem.2018.09.016 (2018). -----
1
19. Driehuis, E. *et al.* Oral Mucosal Organoids as a Potential Platform for Personalized Cancer Therapy. *Cancer Discov* **9**, 852-871, doi:10.1158/2159-8290.CD-18-1522 (2019). -----
2
20. Calandrini, C. *et al.* An organoid biobank for childhood kidney cancers that captures disease and tissue heterogeneity. *Nat Commun* **11**, 1310, doi:10.1038/s41467-020-15155-6 (2020). -----
3
21. Drost, J. *et al.* Sequential cancer mutations in cultured human intestinal stem cells. *Nature* **521**, 43-47, doi:10.1038/nature14415 (2015). -----
3
22. Matano, M. *et al.* Modeling colorectal cancer using CRISPR-Cas9-mediated engineering of human intestinal organoids. *Nat Med* **21**, 256-262, doi:10.1038/nm.3802 (2015). -----
4
23. Fessler, E. *et al.* TGFbeta signaling directs serrated adenomas to the mesenchymal colorectal cancer subtype. *EMBO Mol Med* **8**, 745-760, doi:10.15252/emmm.201606184 (2016). 4
24. Ducie, J. *et al.* Molecular analysis of high-grade serous ovarian carcinoma with and without associated serous tubal intra-epithelial carcinoma. *Nat Commun* **8**, 990, doi:10.1038/s41467-017-01217-9 (2017). -----
5
25. Lawrenson, K. *et al.* A Study of High-Grade Serous Ovarian Cancer Origins Implicates the SOX18 Transcription Factor in Tumor Development. *Cell Rep* **29**, 3726-3735 e3724, doi:10.1016/j.celrep.2019.10.122 (2019). -----
&
26. Hao, D. *et al.* Integrated Analysis Reveals Tubal- and Ovarian-Originated Serous Ovarian Cancer and Predicts Differential Therapeutic Responses. *Clin Cancer Res* **23**, 7400-7411, doi:10.1158/1078-0432.CCR-17-0638 (2017). -----
27. Coscia, F. *et al.* Integrative proteomic profiling of ovarian cancer cell lines reveals precursor cell associated proteins and functional status. *Nat Commun* **7**, 12645, doi:10.1038/ncomms12645 (2016).
28. Eckert, M. A. *et al.* Genomics of Ovarian Cancer Progression Reveals Diverse Metastatic Trajectories Including Intraepithelial Metastasis to the Fallopian Tube. *Cancer Discov* **6**, 1342-1351, doi:10.1158/2159-8290.CD-16-0607 (2016).
29. Zhang, S. *et al.* Both fallopian tube and ovarian surface epithelium are cells-of-origin for high-grade serous ovarian carcinoma. *Nat Commun* **10**, 5367, doi:10.1038/s41467-019-13116-2 (2019).
30. Maenhoudt, N. *et al.* Developing Organoids from Ovarian Cancer as Experimental and Preclinical Models. *Stem Cell Reports* **14**, 717-729, doi:10.1016/j.stemcr.2020.03.004 (2020).
31. Domcke, S., Sinha, R., Levine, D. A., Sander, C. & Schultz, N. Evaluating cell lines as tumour models by comparison of genomic profiles. *Nat Commun* **4**, 2126, doi:10.1038/ncomms3126 (2013).
32. Heo, E. J. *et al.* Patient-Derived Xenograft Models of Epithelial Ovarian Cancer for Preclinical Studies. *Cancer Res Treat* **49**, 915-926, doi:10.4143/crt.2016.322 (2017).
33. Liu, J. F. *et al.* Establishment of Patient-Derived Tumor Xenograft Models of Epithelial Ovarian Cancer for Preclinical Evaluation of Novel Therapeutics. *Clin Cancer Res* **23**, 1263-1273, doi:10.1158/1078-0432.CCR-16-1237 (2017).
34. Hill, S. J. *et al.* Prediction of DNA Repair Inhibitor Response in Short-Term Patient-Derived Ovarian Cancer Organoids. *Cancer Discov* **8**, 1404-1421, doi:10.1158/2159-8290.CD-18-0474 (2018).

35. de Witte, C. J. *et al.* Patient-Derived Ovarian Cancer Organoids Mimic Clinical Response and Exhibit Heterogeneous Inter- and Inpatient Drug Responses. *Cell Rep* **31**, 107762, doi:10.1016/j.celrep.2020.107762 (2020).
36. Chumduri, C. G., R.K.; Berger, H.; Koster, S.; Brinkmann, V.; Klemm, U.; Mollenkopf, H.-J.; Herbst, H.; Mangler, M.; Meyer, T.F. Transition of Wnt signaling microenvironment delineates the squamo-columnar junction and emergence of squamous metaplasia of the cervix. . *BioRxiv* (2018).
37. Maru, Y. *et al.* Establishment and characterization of patient-derived organoids from a young patient with cervical clear cell carcinoma. *Cancer Sci* **110**, 2992-3005, doi:10.1111/cas.14119 (2019).



ADDENDUM

ENGLISH SUMMARY

NEDERLANDSE SAMENVATTING

EESTIKEELNE KOKKUVÕTE
(ESTONIAN SUMMARY)

LIST OF PUBLICATIONS

ACKNOWLEDGEMENTS

CURRICULUM VITAE



ENGLISH SUMMARY

In this thesis we describe the establishment and characterization of a broad panel of 3D organoid cultures from a variety of epithelial gynecological cancers and respective healthy tissues of origin with the purpose to better understand the heterogeneity and the individual characteristics of these tumors. Gynecological cancers affect different parts of female reproductive tract (FRT) giving rise to a diverse spectrum of epithelial cancers, involving ovaries, fallopian tubes, uterus, cervix, vagina and vulva. Although these cancers show distinct molecular profiles and characteristics, the current model systems often fail to represent the entire disease spectrum.. Therefore, independent model systems that represent the inherent disease-specific features are highly anticipated in the field to uncover best treatment strategies for each type. Different human-derived model systems used for gynecological cancer research are summarized in the introductory **Chapter 1**. The emergence of organoid technology has recently allowed to build highly representative long-term culture systems for human tissues in health and disease. The potential to maintain healthy epithelial cells as a long-term organoid culture without the requirement for transformation and the compatibility of these models with the state-of-the-art genome editing tools (such as CRISPR-Cas9) has opened up new exciting doors in the human disease modeling. This thesis presents three research projects in which we use organoid technology to study different gynecological cancers.

In the **Chapter 2** we describe our efforts to dissect the origin of the most aggressive type of ovarian cancer, namely high-grade serous ovarian cancer (HG-SOC). Despite being the most common type of ovarian cancer, the exact tissue of origin for HG-SOC is still under debate. It is currently believed that most of the HG-SOCs arise from fallopian tube epithelium; yet, accumulating evidence suggests that a smaller percentage of the tumors might have a different origin, most likely from the ovarian surface epithelium (OSE). So far, no model system has been able to compare the potential of these two epithelia to form ovarian cancers in parallel. By using organoids derived from mouse tissues, we explore the likelihood of fallopian tube (murine oviduct) and OSE to give rise to HG-SOCs. We exploit CRISPR-Cas9 genome editing tool to build comparative cancer models from both origins by knocking out commonly mutated genes in ovarian cancer. Our results support the more prevailing view that fallopian tube is the main source of HG-SOCs. However, we observe that smaller percentage of similar mutants from OSE are also able to form HG-SOC-like tumors, demonstrating the potential dual origin of these cancers. Follow-up studies are required to determine the marker and treatment-response differences between the tumors derived from these distinct origins that would enable better stratification of patients.

In the **Chapter 3** we describe our work to establish a novel patient-derived organoid-based platform for ovarian cancer research. Epithelial ovarian cancer has perhaps always been a bit misleading term to characterize the vastly heterogeneous set of tumors that share nothing but the same anatomical location. These tumors can range from benign to

1

2

3

4

5

&

low- and high-grade forms accompanied with a number of different histological subtypes, including serous, mucinous, clear cell and endometrioid ovarian cancers. Considering this complexity, where each of the subtypes represent a distinct disease with unique characteristics, there is a clear need for separate model systems that would enable to capture the whole disease spectrum and allow to advance the studies on each subtype independently. In this work we present a robust protocol that enables efficient derivation and long-term expansion of ovarian cancer organoids representing all the main subtypes of this cancer. These organoids do not only recapitulate the true intra- and interpatient heterogeneity, but also show differential drug-responses, including acquisition of the chemoresistance in recurrent disease. The established protocol provides our research field with much-anticipated means to generate long-term organoid models for each subtype of ovarian cancer depending on the particular research interest. Following this protocol, we were able to build a comprehensive panel on 56 organoid lines covering the main subtype spectrum and the established lines are readily available for the use to the entire research community.

In the **Chapter 4** we present an organoid-based platform for studying the biology of human cervix and associated malignancies. In this work we develop a robust protocol to establish long-term organoids from stratified ectocervix and glandular endocervix of healthy patients that closely recapitulate the original tissues. Cervical canal is a frequent site of different sexually transmitted infections, including human papillomavirus (HPV) infection which is the main cause of cervical cancers, for which the new organoid-based models offer a great tool to study host-pathogen interaction in human cells. In addition to the healthy lines, an additional isolation method was established to allow tumor organoid (tumoroid) derivation from cervical cancer material collected via Pap-brush method. These tumoroids show evident cancer-associated mutation profile and gene expression pattern, carry morphological abnormalities and causative viral integration, and display differential response to different gold standard chemotherapy regimens. Given the ability to derive tumoroids non-invasively from patients' Pap-brush material, it provides the scientific community with a relatively easy access to the tissue of interest and a new model system. This, in turn, would facilitate rapid generation of organoid-based cervical cancer biobanks worldwide, offering highly anticipated new means for advancing the cervical cancer research.

In summary, the work in this thesis explores the potential of organoid models to be an accurate model for gynecological cancer development studies and drug screening applications.

NEDERLANDSE SAMENVATTING

In deze thesis beschrijven wij het opzetten en de karakterisatie van een groot panel van driedimensionale (3D) organoïde culturen van verschillende epitheliale gynaecologische kankersoorten alsmede van de bijbehorende gezonde weefsels met als doel om de heterogeniteit en individuele eigenschappen van deze kankers beter te begrijpen. Gynaecologische kankers tasten verschillende delen van het vrouwelijk voortplantingsstelsel aan, waaronder de eierstokken, eileiders, baarmoeder, baarmoederhals, vagina, en vulva. Alhoewel deze kankersoorten ieder gekenmerkt worden door specifieke moleculaire profielen en karakteristieken, slagen de huidige modelsystemen er vaak niet in om het hele ziektespectrum na te bootsen. Om deze reden is er een dringende vraag naar onafhankelijke modelsystemen die de eigenschappen van de verschillende kankersoorten kunnen nabootsen om zo de beste specifieke therapeutische aanpak te kunnen bepalen. Organoïde technologie heeft het recentelijk mogelijk gemaakt om zeer representatieve, en langdurig stabiele, kweekmodellen te creëren van zowel ziek als gezond humaan weefsel. De mogelijkheid om gezonde epitheliale cellen (zonder transformatie) gedurende lange tijd stabiel als organoïde cultuur te kunnen behouden, gecombineerd met de toepassing van nieuwe genetische modificatie technieken (zoals CRISPR-Cas9), breidt aanzienlijk de mogelijkheid uit om humane ziektes na te bootsen. Deze thesis beschrijft drie onderzoeksprojecten waarin wij organoïde technologie gebruiken om verschillende gynaecologische kankersoorten te bestuderen.

In **hoofdstuk 2** beschrijven wij ons onderzoek naar de oorsprong van de meest agressieve vorm van eierstokkanker, het hooggradig sereus ovariumcarcinoom (HG-SOC). Ondanks dat het de meest voorkomende vorm van eierstokkanker is, is het exacte type weefsel waaruit deze kankersoort ontstaat nog steeds onduidelijk. Momenteel is de consensus dat HG-SOC in het epitheel van de eierleiders begint; echter duidt steeds meer onderzoek erop dat een klein percentage van deze kankers een andere herkomst heeft, waarschijnlijk het oppervlakte-epitheel van de eierstokken. Tot op heden is het niet mogelijk geweest om met de huidige modelsystemen de potentie van deze twee weefsels om eierstokkankers te kunnen vormen te vergelijken. Door gebruik te maken van organoïden van weefsels van muizen, vergelijken wij de potentie van de eileiders en het oppervlakte-epitheel om HG-SOC te vormen. Wij maken gebruik van de CRISPR-Cas9 technologie om representatieve kankermodellen vanuit deze twee weefsels te bouwen, door genen uit te schakelen die vaak gemuteerd zijn in eierstokkanker. Onze resultaten stemmen overeen met de overheersende gedachte dat HG-SOC het voornaamst in de eileiders ontstaat. Echter, wij laten ook zien dat een klein percentage van dezelfde mutanten van het oppervlakte-epitheel ook HG-SOC kunnen vormen, wat de dubbele oorsprong van deze kankers aantoont. Er is aanvullend onderzoek nodig om de biomarker en therapie respons verschillen tussen de tumoren die ontstaan zijn uit de twee weefsels in kaart te brengen, met als doel de patiënten beter te kunnen stratificeren.

1

2

3

4

5

&

In **hoofdstuk 3** beschrijven wij ons werk waarin wij een nieuw organoïde model voor eierstokkankeronderzoek hebben opgezet. De naam epitheliale eierstokkanker is wellicht altijd al wat misleidend geweest voor deze sterk heterogene set van tumoren die niets anders gemeen hebben dan hun anatomische locatie. Deze tumoren kunnen variëren van goedaardig tot laag- en hooggradige vormen die onder te verdelen zijn in een aantal verschillende histologische subtypen, waaronder sereus, mucineus, heldercellig, en endometrioid eierstokkankers. Gezien deze complexiteit, waarbij elk subtype een verschillende ziekte is met unieke eigenschappen, is er duidelijk behoefte aan losstaande modelsystemen om het hele ziektespectrum te kunnen weergeven en zo ook het onderzoek naar elk subtype verder te helpen. In dit hoofdstuk presenteren wij een robuust protocol om efficiënt eierstokkanker organoïden van de meest voorkomende subtypen van deze kanker te genereren en langdurig te kweken. Deze organoïden reflecteren niet alleen de heterogeniteit binnen en tussen patiënten op weefselniveau, maar laten ook verschil in de werking van geneesmiddelen zien, alsmede ontwikkelde geneesmiddelenresistentie in terugkerende kanker. Het opgezette protocol geeft het onderzoeksveld langverwachte middelen om langdurig stabiele organoïde modellen te genereren voor elk subtype van eierstokkanker, afhankelijk van het specifieke onderzoeksdoel. Met dit protocol hebben wij in totaal een panel van 56 organoïde lijnen op kunnen zetten die de belangrijkste subtypes bevatten en deze opgezette lijnen zijn algemeen beschikbaar voor gebruik in de gehele wetenschappelijke gemeenschap.

In **hoofdstuk 4** presenteren wij een organoïde-gebaseerd platform om de biologie van de baarmoederhals en geassocieerde kanker te bestuderen. In dit werk beschrijven wij een robuust protocol om langdurig stabiele organoïden te genereren van gestratificeerde ectocervix en glandulaire endocervix van gezonde patiënten die grote overeenkomsten met het afkomstige weefsel vertonen. Het cervicaal kanaal is een veelvoorkomende plek van verschillende seksueel overdraagbare infecties, waaronder het humaan papillomavirus (HPV) dat de hoofdoorzaak is van baarmoederhalskankers. De nieuwe organoïde-gebaseerde modellen zijn waardevol om gastheer-pathogeen interacties te bestuderen in humane cellen. In aanvulling op de gezonde lijnen is een andere isoleermethode ontwikkeld om tumor organoïden (tumoroïden) te genereren van baarmoederhalskankermateriaal verkregen door middel van een uitstrijkje. Deze tumoroïden laten duidelijke kankergerelateerde mutatieprofielen en genexpressie patronen zien, bezitten morfologische afwijkingen, en de oorzakelijke virale integratie, en laten verschillen in de werking van chemotherapieën zien. Doordat het mogelijk is om deze tumoroïden op een niet-invasieve manier te verkrijgen via een uitstrijkje van de patiënt, geeft dit het onderzoeksveld een relatief makkelijke manier om specifiek materiaal te verkrijgen alsmede een nieuw modelsysteem. Hierdoor kan vervolgens het opzetten van een biobank van organoïde-gebaseerde baarmoederhalskanker kweken versneld worden, wat de lang verwachte mogelijkheid geeft om baarmoederhalskankeronderzoek verder vooruit te helpen.

Samenvattend heeft het werk in deze thesis de potentie onderzocht van organoïde modellen als accuraat model voor onderzoek naar het ontstaan van gynaecologische kankers en het testen van geneesmiddelen.

1

2

3

4

5

&

EESTIKEELNE KOKKUVÕTE

Käesolevas doktoritöös me kasutame uudset 3D koekultuuri süsteemi – organoidide tehnoloogiat –, et efektiivselt kehaväliselt kasvatada ja uurida rakupopulatsioone. Rakud on isoleeritud nii erinevatest epiteliaalsetest günekoloogilistest kasvajatest kui ka vastavatest normaalsetest kudedest. Doktoritöö eesmärgiks on paremini kirjeldada naiste suguorganite kasvajate mitmekülgsid ja individuaalseid omadusi.

Günekoloogilised kasvajad võivad areneda erinevatest reproduktiivtrakti epiteeli piirkondadest, võimaldades tekkida suurel hulgal iseäralike tunnustega alatüüpidel, sealhulgas erinevatel munasarja-, emakakeha-, emakakaela-, häbeme- ja tupevähi tüüpidel. Hoolimata asjaolust, et antud vähitüübid ja nende alavormid on üksteisest väga erinevad, ei ole seni kasutuses olevad koekultuuri mudelsüsteemid võimaldanud usaldusväärselt esindada kogu vähitüüpide spektrimit. Erinevatest naiste reproduktiivtrakti vähitüüpidest ja nende mudelsüsteemidest oleme andnud laiaulatusliku ülevaate **esimeses sissejuhatavas peatükis**. Seetõttu on teadusmaailmas jätkuv nõudlus üha paremate mudelsüsteemide järele, mis võimaldaksid uurida iga vähivormi individuaalseid omadusi eraldi ja leida optimaalseim tüübipõhine ravistrateegia. Organoidide tehnoloogia hiljutine väljatöötamine, mis põhineb rakkude kasvatamisel toetava rakuvälise maatriksi sees ja optimaalset kasvufaktorite kokteili sisaldavas söötmekeskkonnas, on pakkunud konkurentsivõimelise uue lahendi, kuidas luua uusi rakukultuuri mudeleid, mis esindaksid tunduvalt paremini kudede arhitektuuri ja rakutüüpide dünaamikat. Võimalus kasvatada pikaajalisi organoide normaalse elujõudlusega rakkudest, mis ei ole vastupidavuse saavutamiseks geneetiliselt transformeeritud, kuid mida on kergesti võimalik kaasaegsete geneetika tööriistatega (nagu CRISPR-Cas9 DNA-lõike tehnoloogia) modifitseerida, on avanud uusi paljulubavaid võimalusi inimhaiguste modelleerimiseks rakukultuuris. Käesolev doktoritöö toob teieni kolme laiahaardelise uurimustöö tulemused, kus me oleme rakendanud just organoidide tehnoloogiat, et modelleerida erinevaid günekoloogilisi vähitüüpe koekultuuris.

Teises peatükis me uurime kõige levinuma ja agressiivsema munasarjavähi alatüübi (nn kõrgelt diferentseerunud seroosse munasarjavähi) päritolu. Haiguse kõrgest esinemissagedusest hoolimata ei ole antud alatüübi päritolu küsimust veel endiselt täielikult lahendatud ja teadlaste hulgas puudub konsensuslik üksmeel. Kõige laialdasemalt aktsepteeritud hüpoteesi kohaselt ei arene antud vähitüüp sugugi mitte munasarjast, vaid hoopiski läheduses paikneva munajuha epiteelist. Samas on viimastel aastatel ilmunud üha rohkem alternatiivset tõendusmaterjali, mis justkui viitaks, et arvestuslik osakaal kõnealusel seroosel vähivormil võib areneda ka otseselt munasarja katvast epiteelist. Seniajani pole aga ükski laboratoorne mudelsüsteem võimaldanud paralleelselt uurida munasarjavähi teket mõlemast kandidaatkoest korruga, et hinnata nende suhtelist panust haiguse tekkesse. Organoidide kultuursüsteemi kiire areng on lahendanud senise koekultuuri üldlevinud probleemi säilitada ja paljundada terve elujõudlusega rakke pikaajaseks laboratoorses tingimustes ilma vajaduseta rakkude

eluiga geneetiliselt pikendada. Antud töös me kasutame hiire organeid ja loome erinevad organoidide rakuliinid mõlemast munasarjavähi kandidaat-alkoest – munajuhast ja munasarja katvast epiteelist. Me kirjeldame loodud uute mudelsüsteemide omadusi nii geeniekspressiooni kui histoloogilise analüüsi alusel ning kasutame populaarset CRISPR-Cas9 geenimuundamise tehnoloogiat, et sarnaselt modifitseerida haigusega assotseeruvaid geene mõlemas süsteemis ja võrrelda kummagi epiteeli panust pahaloomuliste munasarja kasvajate moodustumisse. Meie uurimustöö tulemused toetavad hetkel levinud teooriat, et munajuha epiteel on agressiivsete seroosete munasarjakasvajate peamine päritolu allikas. Siiski annavad meie tulemused mõista, et ka munasarja kattev epiteel võib sarnaste mutatsioonide koostoimel anda aluse väiksemale protsendile kasvajatele, demonstreerides haiguse võimalikku kahepoolset päritolu. Edaspidised eksperimendid on vajalikud, et täpsemalt selgitada, kas erinevast koostisest saanud munasarja vähkkasvajaid on võimalik mõne universaalse markergeeni alusel eristada ning kuidas võib kasvaja päritolu mõjutada rakkude tundlikkust keemiaravile.

Kolmandas peatükis me kirjeldame enda pikaajast uurimustööd, mille eesmärgiks oli luua patsientide kasvajakarudest loodud organoidi kultuuridel põhinev platvorm munasarjavähi teadustöök. Epiteeliaalse munasarjavähi termin võib olla kohati eksitav, kuna antud mõiste alla langeb terve hulk erinevate omadustega vähkkasvaja tüüpe, mida ei ühenda peale sarnase anatoomilise leiukoha munasarja piirkonnas suures osas miski. Antud kasvajad võivad varieeruda nii diferentseerumise astmelt kui ka alatüübilt, mille hulgast võib leida nii seroosseid, mutsinoosseid, heledarakulisi kui ka endometrioidseid histoloogilisi alavorme. Arvestades sellist kompleksust, kus iga alagrupp võib kujutada endast täiesti erinevate omadustega haigust, on oluline luua igale tüübile esinduslik mudelsüsteem, mis kannaks edasi antud haigusvormile spetsiifilisi tunnuseid ja võimaldaks läheneda igale alagrupile individuaalselt. Oma kauakestvate katsetuste tulemusel oleme me välja töötanud töökindla protokoll, mis võimaldab efektiivselt luua ja paljundada organoidide patsientidelt kogutud erinevate munasarjavähitüüpide rakkudest. Meie organoidide kultuurid mitte üksnes ei kannu edasi originaalsete vähkkasvajate rakupopulatsioonide- ja patsiendispetsiifilisi omadusi, vaid võimaldavad samuti hinnata kasvajakarude tundlikkust keemiaravile, esindades hästi ka keemiaravi resistentsed vorme. Seega on meie koostatud protokoll suureks sammuks edasi, et soodustada tüübipõhiseid avastusi ja arendada spetsiifilisest haigusvormist lähtuvaid uusi ravistrateegiaid. Esitletud protokoll järgides oleme me loonud laiahaardelise munasarja vähkkasvajate näidispaneeli, mille kogumahus sisaldub 56 uut organoidi liini, esindades kõiki munasarjakasvajate põhitüüpe. Antud paneel on kasutamiseks kättesaadav kogu teaduskogukonnale.

Sarnaselt kolmanda peatükiga, on **neljanda peatüki** keskmes organoididel põhinevad mudelsüsteemid, mis on sel korral orienteeritud emakakaela bioloogia ja selleseoseliste vähkkasvajate teadusalaseks uurimiseks. Selle töö raames esitleme samuti uut protokoll, mis võimaldab pikaajalist organoidi kultuuride loomist nii tervete naispatsientide

1

2

3

4

5

&

näärmeepiteeli kui ka mitmekihilise lameepiteeliga kaetud emakakaela koest. Emakakaela epiteel on väga vastuvõtlik piirkond suguhaiguste tekkeks, sealhulgas papilloomiviiruse infektsiooniks, mis on emakakaelavähi kujunemise üks peamisi põhjuseid. Meie töö tulemusel loodud organoidide kultuurid pakuvad uue mudelsüsteemi peremeesrakkude ja sugulisel teel levivate patogeenide interaktsiooni uurimiseks inimlähedastes tingimustes. Lisaks terve indiviidi kudede baasil ehitatud organoidide kultuuridele olime edukad ka lisaprotokolliga välja töötamisel, mis võimaldab emakakaela vähirakkude propageerimist organoididena (nn tuumoroididena), kusjuures algmaterjaliks piisab vaid Pap-testi harja abil kogutud vähesest rakkude hulgast. Sarnaselt teistele vähitüüpidele, suudavad ka emakakaelavähi tuumoroidid kanda edasi kasvajatele iseloomulikku mutatsiooniprofiili, geeniekspressiooni ja morfoloogilisi iseärasusi. Samuti säilitavad antud tuumoroidid tekkepõhjusliku viiruse DNA-d oma genoomis ja näitavad liinilt varieeruvat tundlikkust erinevate keemiaravi komponentide suhtes. Võttes arvesse asjaolu, et tuumoroidide kasvatamiseks vajalikku koematerjali on võimalik kergesti kokku koguda regulaarselt günekoloogiliste analüüside käigus kasutatava Pap-testi abil, pakub meie uudne protokoll suhteliselt kiire ja valutu meetodi uue mudelsüsteemi laialevikuliseks kasutuselevõtuks. Organoidide tehnoloogial põhinevate üleilmsete emakakaelavähi biopankade loomine võib pakkuda tulevikus uusi seni olematuid võimalusi teadustöö edendamiseks antud vähitüübi valdkonnas.

Kokkuvõtlikult annab käesolev doktoritöö suuremahulise ülevaate organoidide tehnoloogia erinevatest rakendamisevõimalustest günekoloogiliste kasvajate tekke uurimisel ja uute ravistrateegiade arendamisel.

LIST OF PUBLICATIONS

Published

Viil, J., Maasalu, K., Mäemets-Allas, K., Tamming, L., **Löhmussaar, K.**, Tooming, M., Ingerpuu, S., Märtson, A. and Jaks, V. Laminin-rich blood vessels display activated growth factor signaling and act as the proliferation centers in Dupuytren's contracture. *Arthritis Research & Therapy*, 17: 144 (2015).

Kopper, O., De Witte, C.J.* , **Löhmussaar, K.*** , Espejo Valle-Inclan, J.* , Hami, N., Kester, L., Balgobind, A., Korving, J., Proost, N., Begthel, H., van Wijk, L.M., Aristón Revilla, S., Theeuwssen, R., van de Ven, M., van Roosmalen, M.J., Ponsioen, B., Ho, V.W.H., Neel, B.G., Bosse, T., Gaarenstroom, K., Vrieling, H., Vreeswijk, M.P.G., van Diest, P., Witteveen, P.O., Jonges, T., Bos, J.L., van Oudenaarden, A., Zweemer, R.P., Snippert, H., Kloosterman, W.P., Clevers, H.C. An organoid platform for ovarian cancer captures inter- and inpatient heterogeneity. *Nature Medicine*, 25(5): 838-849 (2019)

*Equal contribution

Driehuis, E., Kolders, S., Spelier, S. **Löhmussaar, K.**, Willems, S.M., Devriese, L.A., de Bree, R., de Ruiter, E.J., Korving, J., Begthel, H., van Es, J.H., Geurts V, He, G.W., van Jaarsveld, R.H., Oka, R., Muraro, M.J., Vivié, J., Zandvliet, M.M.J.M., Hendrickx, A.P.A., Iakobachvili, N., Sridevi, P., Kranenburg, O., van Boxtel, R., Kops, G.J.P.L., Tuveson, D.A., Peters, P.J., van Oudenaarden, A., Clevers, H. Oral Mucosal Organoids as a Potential Platform for Personalized Cancer Therapy. *Cancer Discoveries*, 9(7): 852-871 (2019).

Klaas, M.* , Mäemets-Allas, K.* , **Löhmussaar, K.*** , Tooming, M., Viil, J., Jaks, V. Endogenous beta-galactosidase activity marks a TREM2-expressing Kupffer cell population in injured livers of Lgr5-LacZ and wild-type mice. *FEBS Letters*, 594(5): 958-970 (2020).

*Equal contribution

Löhmussaar, K.* , Kopper, O.* , Korving, J., Begthel, H., Vreuls, C.P.H., van Es, J., Clevers, H. Assessing the origin of high-grade serous ovarian cancer using CRISPR-modification of mouse organoids. *Nature Communications*, 11: p. 2660 (2020).

*Equal contribution

Löhmussaar, K., Boretto, M., Clevers, H. Human-Derived Model Systems in Gynecological Cancer Research. *Trends in Cancer*, S2405-8033(20)30215-6 (2020).

De Witte, C.J., Espejo Valle-Inclan, J., Hami, N., **Löhmussaar, K.**, Kopper, O., Vreuls, C.P.H., Jonges, G.N., van Diest, P., Nguyen, L., Clevers, H., Kloosterman, W.P., Cuppen, E., Snippert, H.J.G., Zweemer, R.P., Witteveen, P.O., Stello, E. Patient-Derived Ovarian Cancer Organoids Mimic Clinical Response and Exhibit Heterogeneous Inter- and Inpatient Drug Responses. *Cell Rep.*, 31(11): 107762.

1

2

3

4

5

&

Under revision

Löhmußaar, K., Ora, R., Espejo Valle-Inclan, J., Wardak, H., Korving, J., Begthel, H., Jonges, T., Zweemer, R.P., Veersema, S., van Boxtel, R., Clevers, H. Patient-derived organoids as a novel tool to study cervical cancer. *Cell Stem Cell*

ACKNOWLEDGEMENTS

It's been 5 wonderful years since I first set my foot in the Clevers' lab at the Hubrecht Institute, initially to undertake my 9-month-long internship, and later to proceed on a PhD track in the same lab. Coming from a small and fairly unfamiliar country like Estonia, I'm very grateful and happy that I was given a chance to prove myself, and was accepted into the ranks of the talented scientists of the lab. Despite my initial concerns that a PhD position in such a top-performing lab, as the one of Clevers', might perhaps be too ambitious for me, I am very proud that I decided to still take on this challenge, and thoroughly relieved, that I also managed to make it through in the end. There are many people who have been instrumental in making this journey a successful one, and I hope I'm able to express my sincere gratitude to all of you in this "brief" closing chapter.

First and foremost, I would like to thank my promotor. **Hans**, I'm very grateful for giving me the opportunity to pursue my PhD in your lab. Thank you for seeing a potential in me, and giving me an opportunity to prove myself. Thank you for all the time and guidance you've given me, and for your firm patience with me. Thank you for all the occasions, when I was in doubt about some parts of my projects, and you showed me the confident ways around them. Thanks for pushing my projects forward, and for always pulling the smartest strings to keep everything on track. Your professional skill to delve into just about any project within minutes, and your wisdom to ask critical questions, or provide further insight into versatile topics, continues to amaze and motivate me! The vast amount of scientific breakthroughs the lab has made over the last three decades, your seemingly effortless ways of keeping track of all the many ongoing projects while also busy elsewhere, and your incredible speed in replying to e-mails are truly remarkable. Thank you for the extent of freedom you have given me to reach my own stubborn goals, and for your support in my wishes to attend several scientific meetings abroad to present my work. Your way of treating all the PhD students and postdocs with the same equality as well as the level of independence I've acquired in managing my own projects during the PhD have given me more confidence about my abilities to further pursue my career in academia. Also, thanks for your support and constructive advice about my potential postdoctoral outlooks. My PhD journey has been incredible and, quite surely, it's sad to leave, but it's time to move forward and develop further. I'm sure that your dedication together with the excellence of the entire lab will lead to many more great discoveries in the future, and you will keep moving scientific boundaries. I wish you all the best with guiding both labs (Hubrecht/PMC) forward and dividing your time efficiently in between the two. I'll definitely try to keep track on all the future output of the lab, and hope we'll have occasions to meet again (perhaps a big Clevers' lab reunion in the future!?).

In addition to my promotor, I would also like to thank the other two members of my supervisory board committee: **Dr. Wigard Kloosterman** and **Prof. Hans Bos**. Despite

1

2

3

4

5

&

we only managed to arrange two official committee meetings in the end, I am still very grateful to both of you for your time and commitment during the meetings. Thank you for all the critical questions you asked, and ideas you shared to promote my projects. It was great to receive external feedback on my work, and hold interesting discussions that led to several actionable ideas. Also, thank you for the fruitful collaboration on the ovarian cancer biobank project. It was a great success!

I would like to take my time to also thank the excellent PI of my Estonian lab, **Dr. Viljar Jaks**, for supporting and guiding my post-graduate internship abroad, which later led me to applying for a PhD position in the Clevers' lab. Thank you for your helpful suggestions about the potential labs to consider for my internship, for your generous recommendation letter (that I did not have to write myself!), and for your selfless act of support throughout the entire process. Working in your lab under the joint supervision of you and **Janeli** prepared me well for my PhD endeavour abroad. Teie nähtud vaevaga on minust ka natuke asja saanud, te olete mul jätkuvalt südames ning hindan teie antud panust kõrgelt!

One of my biggest debts of gratitude I owe to my great daily supervisor and long-term colleague, **Oded**. I might have not been the easiest student to start with, but thank you for not giving up on me, and supporting my way throughout the PhD. Despite your initial opinion that it would not be the best idea to pursue a PhD in such a postdoc-oriented lab as the Clevers', thanks for still respecting my ambition to try, and supporting my effort to get Hans' approval whenever possible. I think it was a dynamic interaction as, at first, I worked under your supervision, but later you worked under my pressure. :) From time to time, it might have been stressful, but you survived my personality as well as the postdoc in the Clevers' lab, so, I think, all considered, you would've done an excellent job in becoming a pilot as well (still amazed by that fact!!) I also think that as an intern supervisor you gave me the best possible training and great amount of independence to prepare me for my subsequent PhD endeavour. Thank you for staying involved with my PhD projects until the very end of your postdoc, and even beyond. I quite honestly couldn't have done it without your continuous support and guidance! Your ability to always come up with new ways, even when I thought there were no other ways, is impressive. I liked the manner you always gave sufficient structure to your thoughts ("There are several things to consider. First, ..., second, ... ") but never to your lab bench, which was perhaps always a bit too disorganized to find anything, even after labelling all your stuff. However, your scientific excellence was well-founded, and I think I would still have a lot to learn from you about the project management and the handling of one too many collaborations at once. I'm slightly disappointed that I don't see you working at the Weizmann Institute like we firmly agreed on prior to your departure, but it's great that you're enjoying your much-less-stressful-course-of-life now, and I have much less competition! :) Your humble personality and clearly set priorities (YP: "What's

the (project) status?" -OK: "Married, with two kids") was a delight, and it was my great pleasure to work alongside you, and share projects together with you. You will always be my favourite Jew (sorry, Yotam, but you saw it coming!), and you can be confident that you'll never lose this title (Yotam already has a new favourite Estonian at his new work place anyways, so that's settled)! In addition to the many work-related qualities you enforced, thanks for also keeping me updated about the most relevant series, educating me about the ancient music classics (R.E.M.!!), and recruiting me to your late lunch group. I hope we'll have chances of meeting again in the future, perhaps when I decide to move to Israel and demand to work in the Team Kopper again! Yalla bai! ;)

Up next, I want to thank my fellow Master's students together with who I started my journey at the Hubrecht Institute: **Margit, Jelte, Pieter, Philip, Aletta, Joanne, Seana, Dennis, Jeroen, Astrid, Lina** and **Ton**. We had such a great time in our small students' corner, and we definitely made the most out of it with our seasonal decorations (current students don't even know half of the struggle we went through in that tiny space!). It was great to support each other along the way to the successful finish. **Margit**, with your forever so infectious laughter; **Jelte**, with your forever so delicate taste in music; **Pieter**, with your forever so skillful puns; **Mr. Hubbard**, with your forever so British mannerism (if you like); **Aletta**, with your forever so adventurous travel spirit; **Joanne**, with your forever so patient discussions with Wim; **Seana**, with your forever so authentic excitement; **Dennis**, with your forever so open personality; **Jeroen**, with your forever so Dutch directness; **Astrid**, with your forever so charming smile; **Lina** with your forever so humble (Scandinavian!) nature; and **Ton**, with your forever so deep curiosity. It was a delight to share a studentship together with you, full of hard work and great commitment, fun students' activities, Sinterklaas traditions, borrels and parties. It's great to know that everyone of you have followed your own unique paths, and I'd be happy to catch up with every single one of you in just about anytime! I'm also very happy that two of you (**Margit** and **Jelte**) decided to not leave me hanging alone, as one way or another, we reunited under the Clevers' banner once again. More importantly, you two have also kindly agreed to take on the supportive duties as **my paranymphs** to mark a great ending for my Clevers' lab era!

Margit, although you decided to join the PMC-version of the Clevers' lab, I'm still glad you didn't abandon us completely, and always tried to participate in our PhD activities, and with you there, there always came the laughter! I had a super enjoyable time with you in Athens/Hydra summer school, and I wish we had hanged out more during our PhDs. I love your fun and easy-going attitude, and your courage to always stand by your rights. Thank you for all the loud laughs and crazy jokes about fish without "i's". I admire your original song-writing & organizational skills that led to the Hubrecht's one-and-only-karaoke-borrel-to-date and successful reunion of the party crew in Ardennes. I hope your magnificent ride on a white horse (I have evidence!) will lead you to the awaited altar as

1

2

3

4

5

&

promised! :) I also hope you'll find your motivation to surpass some of the difficulties of the PhD track, and I expect to receive an official invitation letter to your thesis defence in a few years! Thanks for your company & friendship, and for making many ordinary moments extraordinary! Also, thanks for having faith in me by agreeing to support me as my paranymph! Good luck to both you & Bas, and I'm sure we'll keep in touch! :)

Jelte, it was great to have you back in the lab as my fellow PhD-student and a bench-side neighbour. With your amazing return, I loved my newly opened opportunity to always borrow your stuff as my "what-you-own-I-own-policy" was working pretty efficiently for both sides. It's great that you're so RSPOnsible, and have always taken the initiative in organizing multiple PhD activities, including starting the Urban Trail tradition in the lab. Despite I was about to die in every minute throughout those runs, I still joined, and thanks for never leaving me behind the crew! Sadly, we never made it to your home & pride – Rotterdam! But then I've already seen those Feyenoord fans on the public transport, looks quite crazy! :) I think you have a great deal of commitment and compassion in your character that will always make you a good friend to have. Many projects ongoing and coronavirus paper in *Science* – niet slecht, helemaal niet slecht! Gonna give a great start to your academic career, but then we also know all about your fine ketchup production skills, so you clearly have other options! :) Thank you for all the great times we had, and for your full devotion as my paranymph. Good luck in both your professional and personal life, hope you can keep them separate! :)

From the administrative point of view, I have several people to thank for. **Janny**, thank you for organizing all the Erasmus paperwork for my internship prior to my arrival to the lab. Also, thanks for putting together my PhD supervisory committee and for your help with scheduling direct meetings with Hans. I also think you gave me one of the warmest welcomes to the lab with your big hug when I first received an official PhD offer from Hans. It was very heart-warming to see someone as excited as myself! Thanks a lot for that! :) A huge thanks goes also to the two amazing subsequent personal assistants of Hans, **Mascha** and **Annemieke**. Thank you both for effectively managing Hans's timetable, and always finding or introducing availabilities to his calendar in order to keep his time also accessible for lab members. **Mascha**, thank you for your efforts in organizing the first and only Clevers' retreat during my PhD. It was a pity you couldn't join and enjoy the outcome yourself. It was a great success! **Annemieke**, apart from efficiently managing Hans's schedule, thanks for arranging me several flights to the conferences abroad with my own special requests. There were never delays in those flights! :) Also, thanks for holding a firm grip on my promotion schedule. **Wim**, thanks for organizing the student co-ordination and recruiting Oded to supervise me during my internship in the lab. Thanks for sharing a lot of nice stories, and for always being easily approachable and a great chaperon when needed. As a fresh undergraduate student in Estonia, your pioneering study about Lgr5-Rspo1 interaction in 2011 was the first Clevers' paper I

ever read. Therefore, thanks for being my first influence and paving my way to join the Clevers' lab! Also, thanks for allowing me to recruit Milou to my revision works to push the publication forward. I'll be grateful to your kindness forever! **Johan**, thanks for arranging all the formalities and a budget for my PhD, and always being reachable when I have needed help with writing IvD forms. Although sometimes fearsome, I appreciate your blunt directness and personality, and thanks for all your time and effort you have devoted in keeping the lab on a sustainable financial track. All the best! **Stieneke**, thanks for being the fairy godmother of the lab and always keeping a watchful eye over the balance and sustainability in the lab. Thanks for all the miraculous restockings of the Wnt and Rspo conditioned media, reliable behind-the-scenes quality controls and efficient management of the culture media supplements. You truly are the major thriving force behind the effectiveness of the lab. Thanks for always being there to inspect when something was broken or not working, and quick to arrange the repair works. Thanks for introducing many new (tough but fair) regulations to our works that helped to better keep the lab in check. I feel a great deal of gratitude and respect towards your contribution in helping the lab reach its full potential. I wish you all the best, and continued patience in managing all the regulatory affairs within such a gigantic research group as the Clevers'. **Laura**, in my eyes you're the most kind and helpful person in the lab. Always reachable, always accountable and always supportive. Thanks for all the introductory meetings you gave to familiarize me with the lab regulations in the beginning, thanks for all the many polite "Good mornings!" within one day, and thanks for your genuine day-to-day interest in my well-being by always asking how am I doing or how was the vacation/weekend. Also, thanks for always taking a moment to share some encouraging words after my lab presentations to show your support. Thanks for all the reminder e-mails about lab cleaning duties, and sorry for the few times that I totally forgot about them. I love that you're always very considerate about other people's work, and never touch or trash anything before double-checking with the owner. I thoroughly enjoyed working with you, and organizing the catering together for the lab retreat was a great success! I wish you all the strength in handling all the many requests of the people in the lab! **Karien**, with your long-term experience and senior authority in the lab, you were always there to make sure that people are following the rules and fill their duties according to the schedule. Thanks for enforcing responsibility around the lab to ensure the order in the lab. Also, thanks for always sharing your properly validated qPCR primers when I expressed my interest in testing some. I wish you all the best! **Maaïke**, thanks for taking care of the management in the mouse facility, and for your quick notifications when the new antibodies arrived. All the best!

My further gratitude and respect goes to all my wonderful current (**Benedetta** and **Delilah** (*aka Bendela*), **Joep**, **Lulu**, **Daniel**) and former (**Norman**, **Inha**, **Oded**, **Yotam**, **Kai**) office members. **Bene**, in my eyes you are an outstanding person, and you've had quite a remarkable influence over multitude of my decisions during my PhD for which

1

2

3

4

5

&

I'm very grateful for. Your skill to never let anyone take an advantage of you by always standing by your rights, and rightfully enforcing your own terms and conditions, is quite admirable. And one does not simply want to disagree with Bene and deal with an instant Italian-style destruction! :) You're definitely a passionate debater and, therefore, I see your engagement towards politics. But then there are also many other inspiring qualities in you that give you a competitive advantage in research; that you have, of course, exploited to the fullest! For instance, your scientific ability to critically see when things are not working and make swift adjustments to stay on track or decisively drop the interest if found faulty, is something I wish I could be as good at as you. You're quick to grasp new opportunities and use them to your advantage, which is also evident from your successful track record. You're good at discussing science and giving your honest and constructive feedback from which I've benefited a lot. I would like to thank you for all the help you've given me (on your own terms and conditions), and for your consistent effort to make me see things more brighter, and direct me to use my potential to the fullest. In your own unique argumentative way, you've managed to make me more flexible towards some outlooks, and I hope I've managed to teach you that some extent of neutrality is good to have. Thanks for all the caring gestures and always trying to resolve the what-little-disagreements-we've-had. I do not think I need to wish you good luck with your new endeavour as an independent group leader, as I'm pretty confident you're going to become the next Outstanding Young Investigator in a few years to come. Best wishes to both you and Carmine, and don't forget to make babies, otherwise you'll need to adopt one, and who knows with who you might end up then! :) **Delilah**, I find it quite impressive that you're younger than me, but already a postdoc for a year and off to a great start. Your style of tough supervision and strict project management is definitely something from a different league; however, I do see your standpoint that scientific excellence doesn't prosper without a hard work and a strong mentality. And you are a great example of the essence of it yourself! Your thorough attention to details and stubborn perfectionism are definitely features that make you more effective in science. I love your half-Scandinavian more tacit and observational character as it feels a lot like home when you're around. But then there are also those sudden impulsive and impatient surges that give away your Dutch routes... :) Sometimes you're perhaps too quick to judge, without giving a fair chance to prove you wrong, but thanks for always respecting other standpoints as well, and for accepting me to your inner circle. I would also like to thank you for your thorough support and sincere care about my progress, and for translating my thesis summary into fluent Dutch. I wish you all the patience and continuation of clever ideas in completing a successful postdoc in the Clevers' lab. **Bendela**, my CRISPR-HOT duo of effectiveness and efficiency. Although sometimes impossibly annoying, thanks a lot for energizing the office atmosphere and bringing a degree of joyful kindergarten back to the lab. Your collaboration was perhaps even too entertaining to watch. Thanks for always enforcing our late-lunch-group tradition, and for your constant unsuccessful efforts to defeat me on a squash court, despite the bruise

in the face. Thanks for the weekly Zoom-briefings during the quarantine, and for your many good suggestions, ideas & continuous support in regards to the next step in my career. You're like the two adorable little intrigue-weaving step-sisters I never had! And you're welcome for all the effort I put into restraining the intrigues you caused. Idiotas! :) I hope you'll keep up your good work & goal-driven attitude, and you'll add squash into your weekly practice routine, as "the queen of the court" expects to get challenged again in the future. Otherwise, I'll start calling you a CRISPR-FAT duo instead! Ha-haa! Also, I'm looking forward to celebrate the opening of the Bendela's lab! All the best & I'm sure we'll keep in touch! :) **Joep**, I might have been slightly sceptical about your scientific ingenuity at first, but over time I've started to acknowledge it more and more. Your excitement and motivation about science, enteroendocrine cells in particular, is quite remarkable. Your skills to always go in-depth, while also seeing the larger picture, quickly spot new opportunities and formulate new research questions has not only given you the impressive publication record, but has also brought the Clevers' lab to the level it is now, making you, rightfully, the most successful Clevers' PhD of time (*cum laude* for sure!). I want to thank you for all the insight you've given me, for your one too many questions about oviductal secretory cells (that I was never able to properly answer), and for your great (but sometimes perhaps too loud) company in our small office. It was a pleasure to always have you as my back-to-back office mate along our smooth door-to-window trajectory, and to hear all about those random everyday Joepie-facts you felt like sharing. I'm sure that I will continue to hear about your scientific breakthroughs in the future, despite your industrial detour. All the best to you and Joyce, and good luck with everything! :) **Lulu**, you were the sweetest and the most innocent little thing when you first joined our office, but little did we know what was waiting us ahead... :) I find your courage to leave your family far behind, and move over to the Netherlands to start a PhD on your own particularly impressive. Your no-filter way of communication and fun personality has definitely sparkled up our office atmosphere, some say you've even brought a new "office era", but one for sure: with no time you've managed to make yourself an irreplaceable member of the office by earning our thorough appreciation. Thank you for bringing such a nice diversity to our lab, and for your sincere interest and care about the people. Thank you for always making sure we had food in the office, and for your funny and peculiar habits (sleeping in the office, warm water is healthier than cold, taking secret photos, "no need to reply" messages, etc.). I wish you the very best of luck with completing a successful PhD in the lab, and squeezing every bit of possible information out of these intriguing tuft cells. Although I'm moving, I'm sure Bendela will hold a firm grip on you and guide you well to the successful finish, and we'll definitely stay in touch! You know you're always welcome in Copenhagen, but I also hope we'll manage to arrange this Lulu-guided trip to China one day. Keep being brave & amazing! All the best! :) And our latest addition to the office, **Daniel**. I hope everything goes well for you with setting up your projects in the lab and applying for grants. I think you have quite a distinctive previous experience and possess very exciting new expertise, that in

1

2

3

4

5

&

combination with organoid technology will definitely allow you to answer many great biological questions. All the best with everything! :)

That brings me to my former office members in the order of departure. **Norman**, I didn't get the chance to be your office mate for too long, but thank you for always being very acceptive towards me. Your capacity to handle many hardcore projects at once, without any reduction in quality, as well as your vast technological knowledge about biomatrices and microscopy were thoroughly impressive. Also, the way you managed to so casually put together the Development paper about the tube-forming organoids within such a short notice from Hans, was downright remarkable. Thanks for setting such a great example of a hard-working & mature postdoc in the lab, you set this bar real high! Also, thanks for remaining reachable via e-mail whenever I've needed some extra input. All the best to you and your family in San Diego! When are you taking over Vertex? :) **Inha**, thank you for welcoming me to your office and for all the good suggestions in regards to my projects, especially for your help with the RNA-seq library preparations. I adored your humble nature and your great contribution to the quiet office. I think you were one of the most organized & efficient persons in the lab and, therefore, I'm confident that you're seen as a great asset in Johnson & Johnson. You were also one of the founders of the microbiota co-cultures in the lab, and this direction is really picking up fast now thanks to your pioneering work! :) All the best to your family, and I hope Nova keeps being as cute and happy child as I remember. **Oded**, I already devoted an entire paragraph to you to express my gratitude (please see above), but it wouldn't take me much to add that it was also great to share an office with you. **Yotam**, my dear second favourite Jew! :) Your loud voice and turbulent movements caused a great deal of disturbance in our otherwise tranquil office. Nevertheless, your sincere attitude and caring family-guy-persona made you well-received. It was lovely to have someone to always pick on around the lab with my forever-so-sarcastic-style, and I'm glad you always saw through it, and was never offended. Thanks for allowing me to read your grant proposal to refine my critical reading skills, and for all your professional input whenever I needed to understand something better about immunology. Your competitive spirit as a football fan (Ajax forever, uh?) and your well-founded knowledge in PHD (politics, history & democracy) is definitely a virtue to respect. You might also have a talent in baking, but you brought far too little chocolate-chip cookies to the office to tell for certain. I hope you enjoy your new career path, and good luck with your family, including all the many Yotam-juniors. Hope we'll meet again as I'd be happy to polish my sarcasm on you just about anytime! :) **Kai**, thanks for being such a responsible person in the lab, always looking for ways to improve the lab environment and trying to resolve the little troubles within the lab. It was great that you decided to join our office, which helped us to get to know you better. Your vast and detailed knowledge together with your British politeness were well appreciated around the lab. Thanks for the numerous times mapping my data and sharing your suggestions about my work. Thanks for arranging all the paperwork for sequencing submissions,

guest arrivals and student recruitments – you were always on top of the regulatory affairs in the lab! :) I wish you all the best of luck with managing your own lab, and looking forward to reading work done under your correspondence.

My sincere gratitude goes also to my other fellow current (**Jens, Maarten, Cayetano, Marie, Fjodor, Carla, Adriana**), former (**Luc, Frans, Else, Yorick, Kim, Dymph**) and guest-PhD students (**guest-Ludovica, guest-Ana, guest-José, guest-Sara, guest-Maria**) who I haven't mentioned yet. **Jens**, your addition to the group can be truly seen as a game-changer as your particular love towards teamwork has initiated many good collaborative projects with great outcomes. You really are the key contributor to the Clevers' productive paper factory, and I think BIF made a mistake of their lifetime by not granting you the fellowship. Thanks a lot for all the help and politeness, even during the times of the quarantine when you kindly opened up your garden-office to help me with my data transfer quest. Thanks for the many times we organized borrels together and put up the posters, you manage to always perk up the social events with your crazy games and ideas ("what's your favourite protein?"). I acknowledge your particular sense of meme-humor, even though you sometimes cross the line. I also appreciate your extremely competitive spirit in just about any sports, great pianist talent and social networking skills, being the most interactive member of the Clevers' lab. All the best to both you and Maria, and I wish you a lot of wisdom in choosing your next career path as you're up next. No pressure! :) And then there's you, **Martinus Hermanus Geurts!** I was thinking a lot whether to be thoroughly sarcastic here, but I went for the combined version with a touch of niceness added. But, hey, you have to figure out which one is which! It has been truly a pleasure (really?) to have you as a colleague, and to have someone around to constantly annoy. Clearly, I put just a right amount of pressure on you, because look at you now: not even half way through the PhD, but already a great CSC paper published. Needless to say, accomplishing this would've been impossible without me! :) Being so ruthless with you can only mean just one thing: you were always my favorite PhD from the bunch (but only until you forgot my birthday! Now I have a new favourite!). Because, how can you not enjoy the company of an old-school Jesus-looking disco-fan!? Quite clearly, a Bible Belt and church choir influence there! But don't get all flattered now, your brother was still more handsome than you! Ha-haa... didn't know it's gonna be so fun to write! :) To get back to the work-related matters, it was a great decision to join the Clevers' lab. Had you chosen the AvO lab instead, you would've been too many meters away from the best influence you could ever have. Continuing your research on CRISP(e)Rfect line was yet another great decision you made. All these fast and promising developments in the genome editing field is just stupid to not take an advantage of. I heard the next hot thing in the field is *in vivo* CRISPR, how about starting those mouse experiments that you've clearly avoided so far? Anyways, Maarten, thanks for being yourself and letting me have my fun! Thanks for all the professional advice and input in my CRISPR-related questions, and sorry that I pulled breaks on the Brca-project

1

2

3

4

5

&

due to the direct competitive reasons. And don't get all lazy now with me gone as I hope you'll have a few more excellent papers in the bag prior to the grand finish. All the best to you and your hard-working fabulous trophy-wife Laura, and good luck with picking all your organoids from alle welletjes. And remember, if you find yourself too exhausted at times, you can always draw some more energy from a kaas-station. :) **Cayetano**, your ability to thoroughly focus on your research and your high motivation was already well recognized when you first joined the lab as an intern. It was great that you decided to apply for a PhD position and, to no surprise, have made it quite a successful one already with a superb *Nature* paper in the bag. I enjoyed having you as a colleague and thanks a lot for sharing your ideas and thoughts about my projects in the lab. Also, thanks for the surprisingly limited number of times we actually managed to succeed in playing tennis. I admit, you were always better! Your authentic Spanish character (ei!), oftentimes overgrown hair and great percussion skills were definitely a fun sight around the lab. All the best! :) **Marie**, I guess your particularly unique and infectious laughter has not left anyone untouched. I loved your sincere morning grumpiness and your general "cool, but not amused" attitude. I think we have a bit similar taste for sarcasm, which is great to have, isn't it? I will never forget the sight of fun-but-drunk-too-much-Marie! Glad that you made it home that time! :) Thanks for always being very helpful and reachable via text messages over Western blots when needed. I wish you all the best with your many ongoing projects. Gonna be a great publication record in the end! Good luck! :) **Fjodor**, you've also been a particularly great addition to the lab with your prominent medical background and accompanying charismatic character. It's great that you're so enthusiastic and excited about the wet lab work to complement and challenge some of your more theoretical knowledge. With your splendid skill to facilitate discussions and engage everyone to participate in them, you have definitely made yourself an invaluable member of the group. Also, it was always mind-blowing to receive this a-little-bit-extra about cooking and fine-dining from you as your passion for food was widely recognized. I highly recommend!!! Thanks for being such an intellectual person around the lab and bringing some more diversity to the group. Good luck with your PhD and integrating the academic disciplines into the medical curriculum! :) **Carla**, it's great that you joined the Clevers' lab and have found your own cozy niche among the Three Muskeniers. I love your humble and reserved character, and how it utterly changes when your favourite tune comes on (i.e. Britney Spears, Backstreet Boys...)! :) All the best with everything, and hope you'll have a great PhD! **Adriana**, our latest addition to the PhD-crew. I haven't had enough time to get to know you properly, but nevertheless, I can tell that you're a hard-working and well-focused person, and, also, an incredible Illustrator-artist. Thanks for your company and good luck with the PhD-track in the Clevers' lab, don't forget to enjoy the ride! :)

Luc, it was such a pity we only got to spend so little time together during our PhD. You were a great listener and thank you for your fun and down-to-earth personality.

I hope your sudden change in direction brought more satisfaction and happiness into your life! :) **Frans**, it was great to have you as a colleague and it was nice that you already made it very clear during our very first chat that you're not from France. Thanks for fulfilling the DJ role in our culture room for years, and for your friendly personality that was always easily approachable. Good luck with your goal of becoming an expert in organoid pathology! The lab really needs one! All the best! :) **Else**, thanks a lot for all the help and input you gave during the lab meetings. Your ability to effectively organize the collaborations and manage the projects is quite impressive. Also, thanks for the help with setting up the HPV production, it would've taken me much longer without your effective and goal-oriented management. Thank you also for arranging many of the PhD outings, and for all the invitations to the Dekoor concerts, which were always fun to attend. So, when you plan to get married with Frans, please also invite! :) **Yorick**, thanks a lot for being the most mature PhD student from the bunch, and for always staying helpful and down-to-earth as a person. I liked your innovative and risky research ideas, especially the new direction that you led with the snake venom gland organoid project in the lab, which definitely brought more out-of-the-box thinking and excitement to the lab. I hope Surrozen is sufficiently creative and flexible to suit your taste! All the best to you and Lina in chasing your Californian dream! :) **Kim**, thanks for always taking charge and helping with the general lab management works. Thanks for leading the troubleshoot meeting initiative that was very useful and popular (cake time!) among all of us. Your very open and determined personality was great to have in the lab. Thanks for the fun stroll around Lisbon and memorable ride with the Tuk-Tuk! :) And sorry, when sometimes my cultural differences didn't allow me to be so frank and open with you as you would've liked. I wish you all the best with your postdoctoral endeavour in Heidelberg and hope it's rewarding. Good luck! :) **Dymph**, you've had very versatile experiences during your PhD working in different labs, and I hope it will benefit your future in research. Thanks for hanging out with us for some time!

Guest-Ludovica, thanks for joining our lab for a short while and being an easy person to talk to. **Guest-Ana**, thanks for being such a fabulous and eccentric addition to our otherwise ordinary lab environment. Thanks for your genuine excitement and sparkling humor. And when you become a millionaire (like you promised), don't forget about my free flight ticket to Australia, will you? Hope you're doing well! :) **Guest-José**, it was great to welcome you in our small office and during our occasional late lunches. Sorry for confusing you with the cycling directions! I hope you had a great experience in the lab and good memories! **Guest-Sara**, I hope you had a nice stay in our lab, and thank you for your many nice cakes! :) **Guest-Maria**, you were very sweet and it was nice to meet you. Hope you enjoyed your stay in the lab!

The Clevers' lab has always been a strong hub of excellent postdocs. I would also like to thank all the current (**Matteo, Talya, Marrit, Quiwei, Georg, Jochem, Sangho,**

1

2

3

4

5

&

Amanda, Rosie) and former (Nobuo, Jarno, Onur, Yoshi, Tomo, Huili, Angelos, Dominique, Jasper, Lena, DJ, Florijn, Helmuth) postdocs in the lab that I haven't mentioned yet. **Matteo**, in my opinion, you were such a spot-on addition to the lab as I was working pretty much alone in my field of FRT oncology in the lab after Oded left and prior you joined. Therefore, it was great to finally experience some genuine fresh interest, and receive expert advice from a motivated colleague like you. I think you have a super efficient way of managing your projects, often coming up with new ideas and starting collaborations within a group. I feel like I'm always a bit less informed about all those molecular details of reproductive tract biology and hormonal network than you, which makes you such a great colleague to have as I often learned something new from you. Thanks for holding a firm grip on the Wnt project, and for your willingness to help with the joint review during the quarantine. I wish you all the best & great success with your many projects in the Clevers' lab. **Talya**, I have genuinely appreciated your modest, yet strong and outspoken personality, and your great advice on my projects. Thanks a lot for all your unbiased input and suggestions to my ovarian cancer manuscript, it was great to have someone so thorough and focused to perform a critical proofreading on my work. You have a very forceful and influential way of giving advice, and making your opinion heard and understood among others, which I think is such a strong feature to have. I've always admired your patience with the challenging neuroendocrine tumor project and growing those stubborn lines. I hope your next step in career will be taking on a PI position as I think the position would suit you well. I hope your dedication pays off and you'll have several great papers published by the end of your postdoc in the lab. It was super nice to be your colleague, be your tail-runner at the urban trails, and I'm sad that I almost never managed to get you join our lunches (but I guess here I mostly have your husband to blame for, send my regards!). Best of luck with all the continuing work in the lab, and keep up your influential charisma! :) **Marrit**, thanks for the many times you have taken charge and improved our lab environment by doing so, like re-introducing and hosting the (bi)weekly journal clubs, for one (even during the quarantine!), and always being there to organize and manage the Clevers' borrels, for two. I think you have a great deal of authority, and you use it very wisely to give a good influence and direct rational thinking in your own skillful way. Thank you very much for all your input into my projects, and for your help with optimizing the cell viability assays. Also, thanks for encouraging our squash work-outs and keeping us culturally educated by always welcoming us to your concerts. It was very unexpected and surprising to find an Estonian composer in your program. Good luck with your new job, and all the best to Janne and your family! :) **Quiwei**, your relaxed and curious personality has been a great addition to the lab. It's good to have an apoptosis expert in the lab at last, and thanks for all your advice about the relevant assays, and for always generously sharing your primers. Good luck with the joint work with Matteo, and culturing my Fallopian tube organoid lines, I'm sure they're in good hands. Also, all the best with raising your daughter, you definitely need to learn some Dutch to keep up with her in the future! :) **Georg**, thanks for being the type

that is always very helpful and approachable around the lab, and always kindly providing the trial drugs I needed for my screening assays. Thanks for giving me your advice and support about the potential institutes to look out for in order to find a suitable lab for a postdoc. You were often looking super busy and committed to your work, often running late to your own orchestra practice on Fridays due to forgetting that there are always two rounds of bead clean-ups at the end of the library prep protocol! I hope you weren't late to your wedding! :) It was nice that, compared to other postdocs, you were often there to join the cultural events of the lab, be it the football match or some other event (concert/urban trail). It's a pity I never saw you perform with your orchestra. I wish you all the best, and hope you will make the most out of the new PI position! **Jochem**, thanks a lot for your vast knowledge in immunology, and your help with the FACS sorting. It was my pleasure to do some initial RNA-seq analysis on your data. Your enthusiasm as well as your unhurried and discussive way of processing new data was always fun to watch. You must be a great storyteller to your kids! I hope the tuft cells will guide you (and Lulu) to many new discoveries in the field. All the best with everything! :) **Sangho**, I think you are a very humble and nice person. Thank you for showing your interest and co-culture ideas about the cervical organoids, and sorry that we never actually managed to work them out as I was growing very self-doubtful about the efficiency of the HPV-infection in the organoids that would have been a first requirement for the project to succeed. But I think you have picked up a good pace in the lab and running many good projects now, which will definitely lead to great publications in the end. Thanks for welcoming me to your own private culture room and making room for me there during the restauration works at the old culture room. Good luck with your postdoc, and all the best to you and your family! **Amanda**, your open and enthusiastic way to break ice and find excitement in the smallest details is quite extraordinary. It's a great skill to quickly find a common ground in any interaction, and you have your own special way of overflowing every person with nice compliments. Considering we both have some "northern" roots, I found your overjoyed excitement sometimes perhaps too overwhelming and bizarre, but it's great that you're breaking stereotypes, and, please, always stay true to your own unique self. Thanks for your caring personality and always leading us to the finish line at the urban trails. I wish you all the best! **Rosie**, our latest great postdoctoral addition to the group! With the little that I know you, I can tell that you're a super humble and caring colleague, and always in the sparkling mood. Thanks for bringing all the sun from Australia to our moody lab in the gloomy Netherlands. I wish you all the best with your projects and hope your good spirits will not be dampened by heavy rain, rough wind and Dutch cuisine. Good luck! :)

Also the list of our great former postdocs is rather long, but you gotta thank who you gotta thank! :) **Nobuo**, thanks for your friendly nature, and for telling me about PhD options in Japan. **Jarno**, although our time in the lab didn't overlap much, it was sufficient to acknowledge your great wisdom and hard-working spirit. I think you were

1

2

3

4

5

&

one of the most successful postdocs in the lab back then and, to no surprise, with your great precision you've kept up the high standards as a junior PI with many excellent papers published. I want to thank you for always being helpful and supportive during my lab meetings, and for introducing the "Jarno's Friday music" sessions to our culture room. Also, thanks for staying reachable, always willing to share your *TP53* gRNAs and *LGR5* primers, and for always being meticulously right, even when I thought I found a mistake in your work. Oded thought it would've been a great idea for me to apply for a PhD at your lab, and it was actually my genuine Plan B that I never got to use. Too bad! But good luck with securing the tenure track and keep up the good work! All the best! :) **Onur**, thanks for breaking the hierarchy in the lab and for the occasional hang-outs at the students' corner. Thanks for all your efforts with setting up our sequencing pipeline, as I benefited greatly from the working system once you had already left the lab. Also, thanks for showing me a faster route home from the lab. Hope you're doing well and good luck with your lab! :) **Yoshi**, thanks so much for your genuine politeness and respectful manners. Thanks for encouraging my fascination about Japan, and providing me with helpful information during my visits to Japan. I really enjoyed having you as a colleague in the lab and your cheerful spirit. Thanks for staying in touch, and also encouraging your student Mika to come and visit our lab to learn organoid culturing from the true "founding source". Also, thanks a lot for always giving me this extra meter to pass you in hallways, the corridors never looked so spacious before! :) Good luck with your work in Japan, hope the conditioned medium worked out! **Tomo**, my second strong Japan-enthusiasm-supporter! :) It was great being your colleague and see your thorough Japanese-style efficiency with managing all those clonal lines for your massive project. Truly motivational! It was also very nice to share a culture room with you, and I appreciated your contribution to the quiet and focused atmosphere, always wearing your earphones to keep the rhythm. I often found myself wondering what you were listening, but never got a chance to ask!? Anyways, thanks a lot for your input in my work and explaining everything in detail about the WES submission, and for your constant reminder to add the hard-drive to the envelope. It was much appreciated and everything worked out very nicely in the end! Also, thanks for the drive to the Clevers' retreat, I felt very safe in the car despite your right-hand-drive, and I appreciated your calm and steady driving skills. Additionally, thanks for all your help and advice with planning my Japan trips and booking cheaper tickets on fully Japanese websites. I still receive spam letters from those websites! :) You have a great country and hope you and your family have adjusted to the return. All the best! :) **Huili**, I think I had a super nice friendship with you in the lab, and I really enjoyed having you as a colleague. It was very brave of you to come and join the Clevers' lab only so shortly after giving birth. It was also nice to say hi to your cute little princess daughter during your occasional video-chats with family in the lab. I heard a new baby has born, congratulations! :) It was a quick two years for you in the lab, and, with a great amount of dedication, you also made it incredibly successful one. Thanks a lot for your kindness, and for proofreading my liver work back from my Master's studies.

I hope your reunion with the family was amazing, and you keep up the good work! All the best! :) **Angelos**, thanks for letting me read your grant proposal and work. It's a pity that the things went as they went, but I enjoyed the occasional dinners and your relaxed attitude. Hope you're doing well! **Dominique**, thanks for bringing some versatility to the lab with the dog skin organoids. It was slightly less ambitious than snake, but I think the project had great prospects. Hope everything is well! **Jasper**, thanks for your support during my aspire to pursue a PhD in the lab. Your frequent cheerful "Good mornings!" and "How's life?" questions brought a lot of liveliness and great spirit to the lab. Our lab really needed your kind of open-minded and talkative postdoc type to perk up the atmosphere! Thanks for your senior insight into the DNA extraction and virus production, it was well appreciated! Also, thanks for your frequent company at the long microwave queues, time went much faster with you chatting around. Hope the HUB is treating you well! Best wishes! :) **Lena**, thanks for all your help with using the old-school fast-speed microscope for cilia detection, and for your input in optimizing the protocol for tubulin stainings. I hope you have a great new position, and all the best with Mia! **DJ**, thanks a lot for bringing some versatility to the lab with your own eccentric ways and authentic Indian character. Hope the malaria project is going to work out, and good luck at the Lutolf's lab! :) **Florijn**, it was nice to have you in the lab as long as it lasted, and thank you for all your genuine interest in the lab projects. Also, thanks for starting the squash enthusiasm in the lab. Hope Nina is growing well, and all the best at the Rios' lab! **Helmuth**, your critical thinking and great suggestions have made you a very well-acknowledged member of the lab. During the lab meetings it was always nice to see that when everybody else seemed to be completely lost, then you were always there, thinking along & giving suggestions. Thanks for your input and sharing good tricks about the RNA-seq data analysis. Also, thanks for your help with my search for the good candidate labs for my postdoc. Good luck with the next step in your career, congrats again for the ERC, and looking forward to reading papers in your correspondence! :)

Next, I want to thank the two incredible golden hands of our lab who are almost always represented on every Clevers' paper ever written: **Jeroen** and **Harry**. **Jeroen**, thank you for always being up for a challenge. Mastering an intra-bursal injection technique – never tried, but consider it done! Teaching an inpatient person how to cut paraffin blocks – sure, lets do this! Using fixed organoids to create mind-blowing paraffin images upon special request – no problem, there you go! You have such a master skill in artistry that it's no wonder that Hubrecht has never needed to do any outsourcing for creative works, because you can do it all! :) Your helpful and easygoing attitude has made many things easier to accomplish in the lab as well. It's been a great pleasure working with you and my transplantation works would've never been so efficient without your assistance. There were perhaps one too many times that I found myself running behind time while preparing the samples for transplantations, yet you never looked impatient or frustrated, always cheerful and patient. Thanks a lot for your generosity and kindness!

1

2

3

4

5

&

I already received my paraffin-star, but can I also get a cheater's Embryo Award for my graduation? :) **Harry**, you're definitely one of the most irreplaceable members of the lab! Managing an uncountable number of orders, restocking rapidly depleting supplies and performing dozens of stainings per week – and everything is done with the high quality and guaranteed precision. Thanks for all the help with orderings and keeping the lab in order. Also, thanks for never losing your head when I once again came to you with multiple staining requests and always got "Is goed!" for a reply. You were always super helpful and gave good advice about antigen retrieval methods. Thank you for being so generous and kind-hearted (and buying your wife expensive shoes during holidays without complaining)! :) It was great to work with you, and I will be forever grateful!

It has also been a great pleasure to always be surrounded by so many young, smart and high-spirited lab technicians, including **Sepide**, **Carola**, **Veerle**, **Sigrid**, **Eveliëne**, **Priyanka**, **Lisanne**, **Mandy**, **Khoulood**, **Milou**, **Gijs** and **Charel**. I want to thank you all for bringing such a youthful and helpful army of expertise to our lab, and making the lab considerably more efficient by contributing to our works. Thanks, **Milou**, for your willingness to make a sudden switch and give me your complete devotion in an attempt to speed up my revision works during the last months. It was nice working with you, but I'm sure Wim is equally happy to have you back working with him now. I wish you all the best! :) I also want to specifically thank **Carola** for her great companionship in the tissue culture room and dedicated music enthusiasm. Thanks for always insisting on the presence of music at our TC, and for always being very considerate about the other people's taste (Bruno Mars, no problem!). Also, thanks for your multitude of unexpected cakes/cookies that were always very tasty and offered at the right moments. I love your precision and devotion to science, and your forever cheerful attitude. With the years, I've seen a lot of personal growth in you, and I'm confident you'll be bold enough to take on many more great challenges in the years to come. All the best! :) Thanks, **Veerle**, for occasionally taking along my samples from the pathology department, for your friendly & helpful personality, and for making Jelte happy! All the best to both of you! :) Thanks, **Gijs**, for your professional and helpful management of the sequencing matters & all the best with the family-life! :) Thanks, **Mandy**, for the always taking care that the ML-II lab is well stocked. It would have been mess without your surveillance! All the best! :)

Hila, thanks for your courage to undertake an internship in the Clevers' lab under my challenging supervision, for being my first Master's student, for never giving up on your goals, and for reaching to the successful finish line. All the best for the future!

During the first years in the lab, the HUB was a big part of our lab community, including **Sylvia**, **Rob**, **Tulay**, **Farzin**, **Tamana**, **Anjali**, **Marvin**, **Emilio**, **Karien**, **Nilofar**, **Joyce**, **Farzin**, **Ricardo**, **Sridevi**, **René** and **Jinyi**. Thank you all for your contribution to the nice lab environment! Thank you, **Sylvia**, for your help and assistance with setting up the new

HUB protocol for inclusion of cervical cancer patients. The heavy workload you carry with managing the HUB in addition to raising your two adorable twin daughters is extremely brave and admirable. All the best with everything! Thank you, **Tamana**, for your great humor and glamorous perfection to detail. I'm still a bit disappointed that you didn't choose Hubrecht over your other work prospects after HUB, but hope you made a right decision. Good luck with the baby! :) **Anjali**, thank you for being such an amazing colleague and helping us out with the ovarian cancer project. Your meticulous way of recording data has posteriorly saved me from many headaches of finding the right cryovials of interest. I think we had a great friendship, and I was honored to witness your spectacularly awesome wedding. I've never seen anything so traditional before! I love your silly humour and your beautiful Surinamese looks. Hope you're doing well, and all the best with the family-life! :) **Emilio**, thanks for your great personality, and for knowing the locations of all the countries on the map, including Estonia. All the best! :) **Marvin**, you are truly one of a kind and amazingly subtle person. You have this crazy philosophical and compassionate vibe going on, combined with your deep and observant eyes, which is very intriguing and sometimes hard to process, unless you are me, who can always outsmart you! :) Thanks for your engaging smiles and always friendly attitude in the lab. I wish you all the best and I hope to visit your beloved home island Curaçao [Kòrsou] one day! When you get married, I look forward for an invite! :)

1

2

3

4

5

&

Big thanks also to the PMC representatives of the Clevers' lab, led by **Marc** and his colleagues, including **Margit**, **Evelyn** and **Karin** for always attending our weekly lab meetings at the Hubrecht Institute, despite the distance, and for your contribution by occasionally presenting the scientific projects you carry out in the hospital. I think such joint lab meetings were beneficial for both sides. All the best!

With that said, I will finally move on from the Clevers' group as I have also a great number of other important groups/facilities and individuals to thank for, who have made my PhD a successful and enjoyable journey. Up first, I would like to thank all the great collaborators that I've personally interacted with, and who have helped me a lot in my projects. Big thanks to **Dr. Wigard Kloosterman** and his amazing PhD-duo – **Chris** and **José** – for the great collaboration on the OC biobank project. Thanks, **Chris** (by now already Dr. de Witte! Yai!), for all your many useful clinical insights into the disease and for always keeping things meticulously structured and well-recorded at our project meetings. I hope you have plenty of exciting new challenges waiting ahead to reach your post-doc goals! Thanks, **José**, for your ingenious bioinformatics skills, and for making every analysis sound so easy and doable. Also, thanks for helping me out even beyond the OC project by agreeing to perform the viral transcriptome analysis for the other project. You are amazing! :) Thank you, **Ellen**, for all your contribution to the OC project, and for keeping the direction alive by your follow-up work on the subject. What a great way to become a PI! Good luck! Big thanks also to **Dr. Hugo Snippert** and his highly motivated team-member **Nizar** for

sharing their advice during our OC biobank project meetings, and for always ensuring the smartest drug screening layouts for our assays. I would like to also thank **Dr. Ruben van Boxtel** and his very skilled team-member **Rurika** for their constructive advice and all the help with the WES analysis for my cervical cancer project. Also, thanks, Ruben, for taking your time and considerably improving my paper manuscript. Highly appreciated! Additionally, I would like to send my warmest gratitude to the two key medical doctors in the campus, **Dr. Ronald Zweemer** and **Dr. Bas Veersema**, who have been instrumental in making my human-participant-oriented projects a success by facilitating the scientific interaction between the hospital and the Hubrecht Institute, and for providing access to the gynecological tissues of interest. It's always very motivational to meet medical doctors who, aside from their own busy and demanding work schedules, have not lost their enthusiasm about the basic science. All the best to both of you! Special thanks to **Dr. Trudy Jonges** and **Dr. Celine Vreuls** for providing their professional expertise on organoid and tumor pathologies. My great appreciation should be also received by the molecular pathology department at the NKI, led by **Dr. Jos Jonkers** and his team, including **Natalie** and **Marieke**, for quickly arranging the transplantation works for my revisions in their facility. The speed by which you managed to put together a totally new work protocol and your courage to experiment with novel intra-cervical orthotopic injections was truly remarkable! Thanks a lot!

I would like to thank the **Hubrecht's FACS facility** for always helping me out with my sortings. **Stefan**, thanks for your patience to always wait until my less-than-100-positive-cells are all sorted, and for frequently entertaining my time during the wait with some great knowledge about FACS equipment or stories from your Japan experiences. **Reinier** and **Tomasz**, thanks for occasionally covering for Stefan, it was highly appreciated!

Special thanks also to the **Hubrecht Imaging Facility**, led by our micro-man **Anko**. Thanks for all the introductory lessons to the microscopes, and for always being reachable if there was any issues with the equipment or software.

Thanks to all the helpful people of the Hubrecht's **personele zaken**, especially to **Yvonne** for arranging my first PhD contract and informing me about all the associated details, and to **Ilonka** for helping me with registering to different external courses. Also, thanks, Yvonne, for involving me to take part in a "Buddy" support group.

Thanks to all the friendly **receptionists at the Hubrecht's front desk**, especially **Thea**, for all the quick & helpful package deliveries and pick ups.

Thanks to the experts from the Hubrecht's **IT department** for always keeping our systems secure & up to date.

Big thanks also to all the helpful people of the Hubrecht's **civiele dienst** for always staying on top of the Magazijn business.

1

Thanks to all the people in the Hubrecht's **media kitchen** that always make sure we have enough Amp plates and LB medium, and that the glassware is always autoclaved.

2

Thanks to all the experts in the Hubrecht's **technische dienst** for always helping with malfunctioning equipment.

3

Thanks to the Hubrecht's **Albron team** for always taking care of the entire institute's lunch table. I mostly had a habit of taking my own food for lunch, but in occasions when I didn't, I liked your risotto dish the best. Thanks for that!

4

Big thanks to **Prof. van Oudenaarden** for the professional leadership of the institute. Thanks for the traditional yearly "PhD lunches with the director" that provided us an opportunity to raise unmet issues, and get a yearly update about the institute's excellent scientific ranking. Thanks for always organizing the most entertaining musical impro borrels, for launching the fun-to-watch 'Hubrecht Got Talent' shows during the lockdown, and for your unforgettable moves on the dance floor at every Hubrecht's christmas party I can remember.

5

&

Melanie, thanks for always doing such a great job with communicating our science to the general public, and sharing the news about our recent publications on relevant institutional social media platforms. Also, thanks for involving me to participate at the "Weekend van de Wetenschap" event. It was very fun to partake, despite I can't speak proper Dutch. "Oh I wish I could, but I don't want to" - quote from "Friends"?

Merlijn, thanks a lot for giving me an introduction to the ultracentrifuge handling and for patiently allowing me to drag you along during my first attempts to use the machine. Also, thanks for your professional advice on available tubes and rotor options for my work, and providing me with relevant material, equipment & follow-up support. All the best!

Marco, thanks a lot for being on top of the biosafety matters around the institute and for quickly arranging all the relevant approvals for my new virus work. It was a pleasure to work together and I truly appreciated your help. All the best!

John, thanks for always sharing your frustration over the malfunctioning equipment all around the institute. Hope there will be a day when everything runs perfectly! All the best!

I would like to thank **de Koning group** (Eelco, Jüri, Antonio, Gita, Karin, Tim, Liam and Peggy) for always accepting me almost like a legal member of your own small lab

family. **Eelco**, thanks a lot for being so friendly and easygoing, and for making great decisions in hiring new people. It was always very entertaining to see how you often managed to mix up the floors, and occasionally spot you lost at our hallways. Also, thanks for the nice dinner in LA! :) **Antonio**, thanks a lot for your family's (**Ilaria** and little **Cloe**) great Italian hospitality and for your relaxed personality, but strong opinions. I think your addition to the de Koning group was sort of a gear-shifting event as everything seemed to start moving in a much more organized and well-guided fashion under your influence. All the best to you & your sweet family, and hope we'll meet again! :) **Tim**, thanks a lot for the occasional chats on our floor, and for the valuable insight into your lab's affairs. It was great to give you advice about Iceland, and that it happened to be the exact place where you upgraded your relationship status. Also, thanks a lot for the invite to your wedding party, it was a pleasure to celebrate this important day with you. All the best to you and your lovely wife **Caroline**. **Peggy**, thank you for your friendly companionship and relaxed attitude. It was always great to have at least one other reasonable mind around.

Big thanks also to my wonderful "Hubrecht Reports" dinner consortium from the AvO lab: **Maya**, **Anna**, **Nico** and **Peter**. **Maya**, it was truly a lucky co-incident that we happened to get a flat tire on the same day, and met on our mutual way to the bike repair shop. Thanks for your American, blunt and outspoken manners and awesomely friendly character. Your sudden departure was perhaps a little too unexpected, but you probably made a right decision as I know how much you missed the States. Thanks for our many nice dinners and lunch-trips, and also for introducing me to the other members of the group. **Anna**, I really admire your vast bioinformatics skills and your sincere enthusiasm for thorough discussions. Knowing how fast you think and talk, your great scientific output doesn't surprise me a bit. Thanks for being so friendly and always insightful with your ideas. And thanks for always helping me with my many mapping-related questions. I hope the new role as a junior PI suits you well! You deserve it! :) **Nico**, it was a pleasure to meet you, and experience how two sarcastic natures can clash in that of a unique way. My competence level highly increased after getting a grip on you. After all, I've learned that you can also be very nice and supportive! :) You do seem like a reliable guy, but I'm pretty sure I'll never get my gin and tonic you promised! Other than that, you're doing a great job, and you finally also made it with your impressive *Science* paper for which I've already thoroughly congratulated you *a priori*. Looking forward to the opening of the Battich lab! Best wishes for the future with climbing even higher mountains! :) **Peter**, thanks for joining our occasional dinners, and it was nice to see that at least one of the members of the group can hold a heated debate with Maya. Your German passion for precision in historic events was fun to watch. It has also reached my ears that your generous help and endless ingenuity has made you well-appreciated around many floors at the institute. That's great! I wish you all the best! :)

Mauro, thanks a lot for always being very friendly and helpful yourself, or directing me to the right people who could help better. Thanks for accompanying my bus ride to the PhD Masterclass once, I always thought you were a post-doc before that. Also, thanks for the invite to your garden-BBQ (you have some great cooking skills!) and entertaining your guests with a great acoustic concert. It's a pity that I never personally had any projects that involved single-cell sequencing, but it's great that your start-up company is off to a great start, and you're providing such an important service to the entire institute, and externally. All the best for the future! :)

1

Aditya, thanks a lot for all the time and assistance you devoted in helping me getting started with the bulk RNA-seq analysis. I couldn't have done it without you! All the best with the work in Novartis!

2

3

Colinda and **Carrie**, thanks for all the help and suggestions you gave me and Jens with revising the BIF applications and tips for the interview. We did not manage to be as successful as you in the end, but still happy we made it through to the second round. Much appreciated!

4

5

Andreia, thanks a lot for your kind friendship and time we spent together. It was a pity that your lab decided to move to the NKI, but I hope the transfer went smoothly and you're doing well! :)

&

Zunamys, thanks for being such a sparkling "mom" personality and surrounding everybody with your unique unicorn energy. Was great to get to know you and Carlos, and I hope you're having a great time in Germany. All the best! :)

Yeszamine, I really love your incredible honesty and directness. It was great fun to spend some spare time with you, and thanks for the invitation to the Hubrecht's secret yoga club. I often experience that many people that I meet & start to instantly like, tend to leave way too early to distant directions. Same with you! I hope Amsterdam treats you well, and I'm wishing you much joy and happiness! :)

Wessel, thanks for your aspiring and teasing companionship. Also, as intimidating as it may have been, thanks for partnering up with me during the R course. We survived in the end! :) Despite your work on stress granules, I hope you won't experience much stress yourself, and will also survive your PhD. I wish you all the best!

Clément, thanks for your forever friendly and chill personality. Was a lot of fun to hang out with you and witness your true joy when France won the World Cup. I wish you all the best with your PhD in the Mattioli's lab and hope you get everything assembled well, even the nucleosomes.

Anne and Roxanne – you always seem to come in a duplicate. Thanks for your great company and for your fun-spreading spirits. Was nice to spend some time with you! :)

Dennis, I was not making it easy for you, but thanks for never giving up. All the best & be nice to Peggy!

Rob, your devotion and care about our entire institute is remarkable, and I admire your effort to befriend everybody on your path, even a difficult Estonian like myself. Sorry that I never made it to any of your birthday parties; apparently, great people are born on the same days!! All the best with your work and learning all about the anaerobic processes in your fish tank! :)

David, thanks for subscribing to the “Cheerleader” channel, and for your ultimate devotion to it during the quarantine times. Good luck with finalizing your PhD in Sweden, and with my great influence & guidance, you’ll hopefully be in my shoes very soon. No pressure! :)

I would also like to thank the members of my “Buddy” support group, including **Christa, Ilia** and **Iris**. I hope that sharing our views and experiences were helpful to all of you in moving forward & coming up with solutions to reach your own personal goals. It was quite an eye-opening experience for me to learn how different can individual PhD tracks be at the same institute. Thank you for your devotion, support and honesty. Good luck with your PhDs, and, no matter what, be proud of what you achieve! All the best! :)

Also, big thanks to many other aspiring PhD students and scientists in the campus that have crossed my path during various meetings, PhD retreats, borrels or other events, including **Maria** and **Koen** from the Snippert’s lab (UMC); **Susanne, Marloes, Maria, Helena, Dylan, Chloé** and **Ábel** from the AvO’s lab; **Samy, Corina, Kim, Silke** and **Franka** from the Kind’s lab; **Erik** and **Annabel** from the Korswagen’s lab; **Sara, Sven, Hessel, Phong** and **Laurence** (yoga!) from the Bakkers’ lab; **Stijn, Deepak, Sanne** and **Tim** from the Tanenbaum’s lab; **Sebastiaan** (or was it Brian?), **Marta, Bas** and **Louk** from the van Rooij’s lab; **Mark** and **Niels** from the de Laat’s lab; **Sasja, Maaïke, Petra, Jelmer, Maja** and **Alex** from the den Hertog’s lab; **Gaby, Reinier** and **Lotte** from the Galli’s lab; **Juliëtte** from the Garaycoechea’s lab, **Wouter** from the Sonnen’s lab; **Alice** and **Wouter** from the Knipscheer’s lab; **Ajit** from the Kops’ lab; **Javi** from the Geijssen’s lab; **Bas, Caroline** and **Maartje** from the Creighton’s lab; **Camilla** and **Lars** from the Drost’s lab (PMC); **Wim, Tito, Saman** and **Jeff** from the Holstege’s lab (PMC); **Lindy, Michael** and **Waleed** from the Molenaar’s lab (PMC); **Sonja** from (team Kopper) the Coffey’s lab (RMC).

My PhD would have also been much less without the true highlight of the journey – the Hydra summer school. I want to thank all the organizers, lecturers and participants who made this experience so memorable, and who restored my excitement to pursue career in academia further. In particular, I would like to thank the members of our thoroughly international and born-to-be-awesome party crew, including **Margit, Alessia, Becky, Elsa, Ben, Kim, Simon** and **Pablo**. You guys are truly inspirational and talented! It was “pretty” fun spending time with you, one more gorgeous than the next, and it’s amazing that we’ve managed to create such a lively group spirit, which has enabled us to keep in touch, and continue to provide each other occasional support & encouragement. Party crew forever! :) Furthermore, I would like to thank **Prof. Jensen** for much inspiration & fun during the summer school, and for taking me onboard for the next big step. Looking forward to the new adventure ahead!

1

2

3

4

Ja lõpetuseks soovin ma tänada ka oma kõige suurimat kodumaist toetajaskonda: oma kallist pikaagest elukaaslast **Jürit**, hoolivat **perekonda** ja kodumaiseid “tuleviku teadlasi”. Mu kallis **Jüri**, sinuga võtsime me selle seikluse ette üheskoos ning, vaatamata mõningatele raskustele, ei oska ma sõnadesse panna, kui oluline on olnud sinu kohalolu ja toetus. See teekond on olnud täis mõlemapoolset akadeemilist kasvu, üksteise innustamist ja iseseisvumist, nii jagatud rõõme kui ka muresid. Ma tahan sind tänada, et oled alati olnud valmis mu ideedega kaasa tulema, kuid samas pakkunud mulle ka väga toetaval määral vabadust, et jõuda iseseisvate otsuste ja tõekspidamisteni. Siiski, ka sinu enda isiklikud arvamused ja soovid on mulle alati olulised, mistõttu ma loodan, et tulevikus kerkivad need veelgi jõulisemalt esile, sest dialoog annab juurde mõtteainet, mida monoloogiga kunagi ei saavuta. Soovin sulle julget pealehakkamist ja edu doktorantuuri lõpetamisel, kuigi olen enamgi kui kindel, et su tuhande projekti ja oskusliku juhendamisoskuse kombinatsioon saab olema efektiivne ja tulemuslik ning üsna peagi saame näha ka sind kraadi võrra rikkamana. Edukat lõpuspurti, kallid! :) Samuti soovin tänada nii enda kui **Jüri** kallist **perekonda** ja **vanavanemaid**, kes on alati mu käekäigu vastu huvi tundnud, mind moraalselt toetanud ning minu mitte-eriti-mõistetavatele-teaduslikele-avastustele ja saavutustele kogu hingest kaasa elanud. Tänan, et toetasite minu rahvusvahelisi õpinguid ning olite alati paraja nõu ja jõuga abiks. Te olete kõik väga kallid! Soovin tänada ka oma suurepäraseid ja edukaid kodumaiseid “tuleviku teadlasi”, kellega oli ikka ja jälle tore jõulude ajal kokku saada, üksteisega vanu aegu meenutada ning värskeimate tegemistega kurssi viia. Sellest kambast aga kohe erilisemalt soovin ma rambivalgusesse tirida oma kalli kursakaaslase ja parima sõbranna **Carolini**, kes on välisõpingute ajal olnud mulle kohe eriliselt pöidlahoidjaks, kuid kes on ise selle aja jooksul kindlasti eluliselt rohkem saavutanud kui minu südikas doktoritöö. Missest, et kaugel, suur aitäh, et oled alati olnud nagu raudrüütel mu kõrval ja et meie taaskohtumised nii sinu kui ka sinu üha paisuva perekonnaga on alati olnud nii soojad ja rõõm nii ehe! Kalli, musi, pai! :)

5

&

CURRICULUM VITAE

Kadi Lõhmussaar was born on the 30th of June 1991 in Pärnu, Estonia. In 2013 she earned Bachelor of Science degree in Genetechnology at the Univesity of Tartu, Estonia. In her final Bachleor thesis she focused on studying *Lgr5* and *Rspo1* interaction in Wnt signaling pathway at the lab of Dr. Viljar Jaks. She then continued to pursue her studies towards Master's degree in Biomedicine at the same university, graduating in 2015 (*cum laude*). Her Master's thesis work was performed at the lab of Dr. Vilja Jaks focusing on stem cell signaling and liver regeneration. After completing her MSc, Kadi applied for an Erasmus fellowship to perform a 9-month post-graduate internship at the lab of Prof. Hans Clevers in the Hubrecht Institute, Utrecht, the Netherlands. During the internship she assisted in establishing mouse organoid models for ovarin cancer research. In July 2016, Kadi received an offer to pursue her studies on a PhD track in the Clevers' lab. Her doctorate research focused on further establishing organoid-based models for different gynecological cancers and the results of these projects are presented in this thesis.

